

LA-UR-07-5324
September 2007
EP2007-0462

Completion Report for Regional Aquifer Wells R-35a and R-35b



Prepared by the Environmental Programs Directorate

Los Alamos National Laboratory, operated by Los Alamos National Security, LLC, for the U.S. Department of Energy under Contract No. DE-AC52-06NA25396, has prepared this document pursuant to the Compliance Order on Consent, signed March 1, 2005. The Compliance Order on Consent contains requirements for the investigation and cleanup, including corrective action, of contamination at Los Alamos National Laboratory. The U.S. government has rights to use, reproduce, and distribute this document. The public may copy and use this document without charge, provided that this notice and any statement of authorship are reproduced on all copies.

Completion Report for Regional Aquifer Wells R-35a and R-35b


September 2007

Responsible project leader:


Responsible project leader:

Mark Everett		Project Leader	Environmental Programs	9-7-07
Printed Name	Signature	Title	Organization	Date

Responsible LANS representative:

Susan G. Stiger		Associate Director	Environmental Programs	9/12/07
Printed Name	Signature	Title	Organization	Date

Responsible DOE representative:

David R. Gregory		Project Director	DOE-LASO	9-14-07
Printed Name	Signature	Title	Organization	Date

EXECUTIVE SUMMARY

This well completion report describes the drilling, installation, and testing of Los Alamos National Laboratory regional aquifer wells R-35a and R-35b located in Sandia Canyon, Los Alamos, New Mexico. These two wells were installed in the vicinity of municipal supply well PM-3 in accordance with the drilling work plan for wells R-35a and R-35b to satisfy a requirement in the New Mexico Environment Department (NMED) letter dated May 5, 2006, "Approval with Modifications for the Interim Measures Work Plan for Chromium Contamination in Groundwater" to evaluate migration of chromium contamination in the regional aquifer. The two single-screen wells at the R-35 location are set at different depths in the regional aquifer to measure water quality and pumping effects from production wells in the vicinity, especially PM-3.

Well R-35a is the deeper of the two wells and was completed with a well screen in the depth interval corresponding to the top of the well screen in PM-3. Well R-35b was completed with a screen near the top of the regional aquifer. The paired-well configuration is intended to determine if chromium contamination is present in regional groundwater near PM-3, and if so, to evaluate if chromium concentrations vary with depth. If chromium contamination is not present, the R-35 wells will serve as sentry wells for PM-3. Sampling of the wells will be performed as part of the facility-wide groundwater monitoring program. Dedicated submersible-pump sampling systems were installed in both wells.

The R-35 wells were instrumented with dedicated transducers to monitor hydraulic responses to pumping at production wells and to evaluate hydraulic connectivity between the top of the regional aquifer and the deeper zone that corresponds to the top of the screen in PM-3. Pumping tests were performed in R-35a and R-35b following well installation and development.

The R-35 wells were drilled using dual-rotary casing-advance air-drilling methods. The only drilling fluid additives used were potable water and foam. Foam-assisted drilling was used only in the vadose zone and was stopped well above the regional saturated zone; no drilling-fluid additives were used within the regional aquifer, except small amounts of potable water added to the air in a fluid-assist fashion. Additive-free drilling provides minimal impacts to the groundwater and aquifer materials. Both boreholes were successfully completed to their planned depths while advancing casing.

A cased-hole suite of geophysical logs was run in R-35a to aid in well design and hydrogeologic characterization. The wells were completed in accordance with NMED-approved well designs. Both wells were thoroughly developed and all target water-quality parameters were achieved. Hydrogeologic testing performed in both wells indicated they are highly productive and will perform effectively to meet their planned objectives.

CONTENTS

1.0 INTRODUCTION 1

2.0 PRELIMINARY ACTIVITIES 1

 2.1 Administrative Preparation 1

 2.2 Site Preparation 2

3.0 DRILLING ACTIVITIES 2

4.0 SAMPLING ACTIVITIES 5

 4.1 Cuttings Sampling and Coring 5

 4.2 Water Sampling 6

5.0 GEOLOGY AND HYDROGEOLOGY 6

 5.1 Stratigraphy 6

 5.2 Groundwater 8

6.0 BOREHOLE LOGGING 8

 6.1 Video Logging 8

 6.2 Geophysical Logging 8

7.0 WELL INSTALLATION 8

 7.1 Well Design 9

 7.2 Well Construction 9

8.0 POSTINSTALLATION ACTIVITIES 10

 8.1 Well Development 10

 8.2 Aquifer Testing 11

 8.3 Dedicated Sampling System Installation 11

 8.4 Wellhead Completion 12

 8.5 Geodetic Survey 12

 8.6 Site Restoration and Waste Management 12

9.0 DEVIATIONS FROM PLANNED ACTIVITIES 12

 9.1 Deviations 13

 9.2 NMED-Approved Modifications to the Work Plan 13

10.0 ACKNOWLEDGMENTS 13

11.0 REFERENCES 14

Figures

Figure 1.0-1	Location of regional aquifer wells R-35a and R-35b with respect to municipal supply well PM-3 and additional surrounding regional well.....	15
Figure 5.1-1	R-35a borehole stratigraphy	16
Figure 5.1-2	R-35b borehole stratigraphy	17
Figure 7.2-1	R-35a well construction diagram.....	18
Figure 7.2-2	R-35b well construction diagram.....	19
Figure 8.1-1	Specific conductance, turbidity, pH, dissolved oxygen, temperature versus purge volumes at R-35a.....	20
Figure 8.1-2	Specific conductance, turbidity, pH, dissolved oxygen, temperature versus purge volumes at R-35b.....	21
Figure 8.3-1a	As-built schematic regional well R-35a	22
Figure 8.3-1b	As-built fact sheet for regional well R-35a	23
Figure 8.3-2a	As-built schematic regional well R-35b	24
Figure 8.3-2b	As-built fact sheet for regional well R-35b	25

Tables

Table 3.0-1	Fluid Quantities Used during Drilling and Well Construction	27
Table 4.2-1	Summary of Groundwater Screening Samples Collected during the Drilling and Development of R-35a and R-35b	29
Table 6.1-1	R-35 Video and Geophysical Logging Runs.....	31
Table 7.2-1	Annular Fill Materials.....	31
Table 8.1-1	Well Development Volumes and Associated Field Water-Quality Parameters for R-35a	32
Table 8.1-2	Well Development Volumes and Associated Field Water-Quality Parameters for R-35b	34
Table 8.5-1	R-35 Survey Coordinates from SW Mountain Surveys, Inc.....	36
Table 8.6-1	Summary of Waste Samples Collected during Drilling and Development of R-35a and R-35b	36

Appendixes

Appendix A	Lithologic Logs
Appendix B	Groundwater Analytical Results
Appendix C	Borehole Video Logs (see enclosed DVDs)
Appendix D	Geophysical Logging Report
Appendix E	Aquifer Testing Report

Attachment

Attachment 1	Appendix Data Files and Images (on enclosed CD)
--------------	---

Acronyms and Abbreviations

AMSL	above mean sea level
APS	array porosity sonde
ASTM	American Society for Testing and Materials
bgs	below ground surface
CHFR	cased hole formation resistivity
CNT	compensated neutron tool
cu	capture unit(s)
DO	dissolved oxygen
DOE	U.S. Department of Energy
DTW	depth to water
ECS	elemental capture spectroscopy
EES-6	Environmental and Earth Sciences
ELAN	Elemental Log Analysis
ENV	Environmental Stewardship
EP	Environmental Programs
gAPI	gamma ray American Petroleum Institute
gc ³	gram(s) per cubic centimeter
HNGS	hostile natural gamma spectroscopy
ICPMS	inductively coupled (argon) plasma mass spectrometry
ICPOES	inductively coupled (argon) plasma optical emission spectroscopy
I.D.	inside diameter
IDW	investigation-derived waste
IWD	integrated work document
JHA	job hazard analysis
LANL	Los Alamos National Laboratory
LANS	Los Alamos National Security
lbf	pound(s) force
mT	milli-Tesla
NMED	New Mexico Environment Department
NTU	nephelometric turbidity unit
O.D.	outside diameter
ohm-m	ohmmeter(s)
ORP	oxygen-reduction potential
ppb	parts per billion
ppm	parts per million
pvc	polyvinyl chloride
Qal	Quaternary alluvium
Qbo	Otowi Member of the Bandelier Tuff
Qbog	Guaje Pumice Bed of Otowi Member of the Bandelier Tuff
QC	quality control
RCRA	Resource Conservation and Recovery Act

RCT	radiation control technician
TA	technical area
Tb 2	Miocene basalt
Tb 4	Cerros del Rio basalt
TD	total depth
TLD	triple lithodensity tool
TOC	total organic carbon
Tpf	tertiary puye formation
Tsfu	tertiary Santa Fe Group undifferentiated
$\mu\text{S/cm}$	microSiemens per centimeter
UTL	upper tolerance limit
WCSF	waste characterization strategy form

1.0 INTRODUCTION

This completion report summarizes the site preparation, drilling, well construction, well development, aquifer testing, and related activities for monitoring wells R-35a and R-35b drilled and completed in April, May, June, and July 2007 at Los Alamos National Laboratory (LANL, or the Laboratory) for the Environmental Programs (EP) Water Stewardship Project.

The R-35 project site is located in Sandia Canyon on the north side of East Jemez Road (the Los Alamos Truck Route) at mile marker 9 in the eastern portion of the Laboratory in Los Alamos, New Mexico (Figure 1.0-1). The paired-well configuration is intended to determine if chromium contamination is present in regional groundwater near PM-3, and if so, to evaluate if chromium concentrations vary with depth. If chromium contamination is not present, the R-35 wells will serve as sentry wells for PM-3. The drilling objectives were to drill and install two separate single-screened regional aquifer-monitoring wells. R-35a is the deeper well; the objectives were to drill the well so it would align stratigraphically with the top of the well screen in PM-3 and with the top of the Miocene basalt unit at 1136 ft below ground surface (bgs) as the lower bound of the stratigraphic target. R-35b is the shallower well; the objective was to monitor the upper portion of the regional aquifer. The wells are approximately 90 ft apart.

The R-35a borehole was successfully drilled to a total depth (TD) of 1143 ft bgs, 2 ft into the Miocene basalt (Tb 2). A well was installed with a screened interval between 1013 and 1062 ft bgs. The depth to water (DTW) after installation and well development was 792.1 ft bgs. Cuttings were collected at 5-ft intervals in the borehole from ground surface to TD. The R-35a borehole served as the location for the primary set of geophysical logs performed by Schlumberger. Postinstallation activities included well development, aquifer testing, surface completion, dedicated sampling system installation, site restoration, and wellhead surveying.

The R-35b borehole was successfully drilled to a TD of 897.6 ft bgs. A well was installed with a screened interval between 825 and 848 ft bgs. The DTW after installation and well development was 786.9 ft bgs. Cuttings samples were collected at 5-ft intervals in the borehole from ground surface to TD. Postinstallation activities included well development, aquifer testing, surface completion, dedicated sampling system installation, site restoration, and wellhead surveying.

The information presented in this report was compiled from field reports and activity summaries. Records, including field reports, field logs, and survey information, are on file at the Laboratory Records Processing Facility. This report contains brief descriptions of all activities associated with R-35 project, as well as supporting figures, tables, and appendixes.

2.0 PRELIMINARY ACTIVITIES

Preliminary activities included preparing administrative planning documents and constructing the drill site.

2.1 Administrative Preparation

The following documents were prepared to guide the implementation of the scope of work for this well: "Drilling Work Plan for Regional Aquifer Wells R35a and R35b" (LANL 2006, 093388); "Integrated Work Document"; and "Storm Water Pollution Prevention Plan" (LANL 2006, 092600).

2.2 Site Preparation

Site preparation was performed from March 20 to 27, 2007, and included clearing and grading the drill pad, excavating and lining the cuttings containment pits, and installing berms and straw wattles to control stormwater runoff and prevent erosion. The drill pad measured approximately 350 ft x 100 ft and was covered with base-coarse gravel. The R-35a cuttings pit measured approximately 100-ft x 40-ft x 8-ft average depth, and the R-35b cuttings pit measured approximately 60-ft x 40-ft x 8-ft average depth. Radiation control technicians (RCTs) from the Laboratory's Radiation Protection Group-1 performed radiological screening of the site and construction equipment as necessary.

Office and supply trailers, generators, and general field equipment were moved to the site during the subsequent mobilization of drilling equipment. Potable water was obtained from the East Jemez Road overhead fill stand and a fire hydrant near the Los Alamos County landfill. Safety barriers and signs were installed around the borehole-cuttings containment pits and at the pad entrance.

3.0 DRILLING ACTIVITIES

The sequence of drilling activities at the R-35 site was guided by an overall strategy to deal with the potential for encountering perched groundwater within the Cerros del Rio basalt. The Cerros del Rio basalt contains variable amounts of perched groundwater at other regional aquifer drilling sites in Sandia Canyon. If perched groundwater was encountered at the R-35 site, the goal was to isolate and seal it off with casing to avoid commingling with groundwater of the regional aquifer. The strategy dictated that the field crew set up and drill first to the bottom of the Cerros del Rio basalt at the R-35b location to determine if perched groundwater was present. The initial drilling activity at R-35b showed that perched groundwater is not present at this location. This information guided the selection of casing sizes for initiating the deeper R-35a borehole, which had to account for casing off any perched waters encountered while still reaching TD with a minimum size casing that would allow for well construction with a suitable filter pack annular thickness. Reaching TD at the deeper location first was desirable, primarily for the ability to run a comprehensive geophysical suite in that borehole to aid in well design for both wells.

Another important factor at the beginning of the R-35 project that guided drilling activities was the ability to drill the R-35 boreholes to TD without the use of mud-rotary methods. At the onset of drilling activities, contingencies were in place to allow the use of mud-rotary techniques, if needed, to finish the boreholes. Although no other regional monitoring wells had been drilled to completion at the Laboratory without drilling fluid additives or mud-rotary methods, the field team was confident that the holes could be completed without using these techniques and additives. Given the uncertainties surrounding drilling methods and the uncertainties about the nature of formations to be encountered at the R-35 site, the selection of equipment and casing sizes erred on the conservative side for successfully finishing each borehole without mud-rotary techniques or drilling fluid additives.

A Foremost DR-24HD drill rig was used to drill the R-35 boreholes. The rig was equipped with conventional drilling rods, tricone bits, hammer bits, under-reaming hammer bits, one deck-mounted 900 ft³/min air compressor, and general drilling support equipment. Two Wagner 1150 ft³/min trailer-mounted auxiliary air compressors were also part of the drilling support equipment. Dual-rotary drilling techniques were used to drill both R-35 boreholes. Dual-rotary drilling has the advantage of simultaneously advancing and casing the borehole. Three sizes of flush-welded mild carbon-steel casing were used on the R-35 project: 16-in.-inside diameter (I.D.), 12-in.-I.D., and 10-in.-I.D. The 12-in. casing was used only at the R-35a borehole to allow an additional step-down in casing size at depth. The dual-rotary method used air and fluid-assisted air to evacuate cuttings from the boreholes. Drilling fluids included municipal water and a mixture of municipal water with Baroid AQF-2 foaming agent. The fluids

were used to cool the bits and to help remove cuttings from the borehole. An approximate tally of the total drilling fluids introduced into the boreholes, as well as the total fluids recovered, is presented in Table 3.0-1. No additives other than municipal water were used within the regional groundwater system.

Between March 27 and 30, 2007, drilling equipment and supplies were mobilized to the site. On March 30, the R-35b borehole was initiated with dual-rotary methods using 16-in. casing and a 15-in. conventional hammer bit. A brief delay occurred on March 30 and 31, 2007, while determining how deep to run the 16-in. casing. Planning documents indicated the 16-in. casing would be a shallow conductor-type casing and would terminate at the base of the alluvium at about 30 ft bgs. However, upon field observation of the borehole stratigraphy, the field team was not confident that the soft Otowi tuffs below the alluvium were competent enough to support the casing. Therefore, to ensure borehole competency and to avoid a potential blowout below the 16-in. casing when drilling at greater depths under much greater air pressures, the field team advanced the 16-in. casing through the tuff and set it at 265 ft bgs, 3 ft into the top of the Cerros del Rio basalt. Drilling continued below the top of the Cerros del Rio basalt using open-hole drilling methods with a 15-in. conventional hammer bit. An 85-ft interval of lost circulation was encountered in the R-35b borehole between 400 ft bgs and 485 ft bgs. The bottom of the Cerros del Rio basalt in R-35b was reached at a depth of 602 ft bgs. The R-35b borehole was advanced 615 ft bgs before pulling out the tools.

On April 11, 2007, the 16-in. casing was pulled up approximately 10 ft to expose the top of the Cerros del Rio basalt at R-35b, and a borehole video log was run using the Laboratory downhole camera to look for evidence of perched water. Drilling foam in the borehole obscured the bottom 32 ft from viewing. Defoamer was added, and the Laboratory downhole camera was rerun on the morning of April 12 along with a natural gamma log and an induction tool. No perched water was observed in the R-35b borehole. The 16-in. casing was rotated back down to 265 ft bgs before the rig and all equipment were moved to the R-35a location.

On April 13, the R-35a borehole was initiated with dual-rotary methods using 16-in. casing and a conventional 15-in. hammer bit. On April 14, the 16-in. casing was set 3 ft into the top of the Cerros del Rio basalt at 259 ft bgs. Drilling continued below the top of the Cerros del Rio basalt with open-hole drilling. No lost circulation intervals were observed in the Cerros del Rio basalt in the R-35a borehole. The bottom of the Cerros del Rio basalt was reached at 603 ft bgs at R-35a. Open-hole drilling methods were terminated at a depth of 675 ft bgs. The borehole did not reliably stay open below 675 ft bgs. The Laboratory downhole camera, natural gamma, and induction tools were run in the open R-35a borehole on April 24. No perched water was observed in the R-35a borehole.

After the Laboratory geophysical suite was completed, the drive shoe was cut off the 16-in. casing, and a 12-in. casing string was welded and hung in the borehole. Dual-rotary drilling resumed on April 28 at 675 ft bgs using 12-in.-I.D. casing and a conventional 12-in. hammer bit. No drilling additives other than municipal water and air were introduced in the R-35a borehole below 675 ft bgs. Problems evacuating the borehole were encountered at 720 ft bgs, and operations moved from conventional dual-rotary to casing advance with an under-reaming hammer bit. The top of the regional aquifer was encountered late in the day on May 1, but the casing advance drilling method obscured exactly at what point it was encountered. Drilling operations advanced the 12-in. casing to 860 ft bgs on May 1. Before activities began on May 2, an electronic water-level meter was used to measure the top of water at 786.3 ft bgs. The 12-in. casing was advanced to and landed at 940 ft bgs on May 2. Subsequent water-level measurements on May 3 and May 4 recorded the top of water at 940.8 ft bgs and 928.9 ft bgs, respectively, indicating a tight formation and low transmissivity in at least the immediate area of the bottom of the 12-in. casing. The target depth of 940 ft bgs for stopping the 12-in. casing string was chosen based on the top of the well louvers in the municipal well PM-3. Acquiring the best possible geophysical suite through a single string

of casing, as opposed to a double string, was the goal associated with landing the 12-in. casing at that depth. The drive shoe was cut off the 12-in. casing on May 4.

On May 5, hanging a string of welded 10-in.-I.D. casing to the bottom of the R-35a borehole was started. Advancing the borehole resumed on May 7 with 10-in. casing, a 10-in. tricone bit, and conventional dual-rotary methods with no drilling fluid additives. TD was reached at 1143 ft bgs on May 9 in the top of the Miocene basalt. The top of the Miocene basalt was encountered during drilling at 1141 ft bgs. The 10-in. drive shoe was cut off on May 10.

Schlumberger ran a geophysical suite in the R-35a borehole on May 11 and May 12. Details of that operation can be found in Section 6.2 below and in Appendix D of this document.

On May 13, the drill rig and all associated drilling equipment were moved back onto the R-35b borehole. The drive shoe on the 16-in. casing was cut off, and a string of welded 10-in. casing was hung to the bottom of the borehole on May 15 and May 16. Advancing the borehole resumed on May 17. No drilling fluids or additives other than municipal water and air were introduced in the R-35b borehole below 615 ft bgs. A 12-in. casing string was not installed in the R-35b borehole. No true under-reaming casing-advance methods were employed at R-35b; all drilling at the R-35b location was accomplished by either conventional dual-rotary or open-hole methods. TD at R-35b was reached at 897.6ft bgs on May 19. The drive shoe was cut off the 10-in. casing on May 19. All drilling tools were pulled out of the R-35b borehole and drilling operations were finished on May 20.

Both R-35 boreholes were successfully drilled in the regional aquifer to TD without the use of mud-rotary drilling methods or additives. The only drilling additive introduced into either borehole, other than municipal water and air, was Baroid's AQF-2 foaming agent, which was terminated in the lower part of the vadose zone at each borehole. Foam was used in the R-35a borehole to a depth of 675 ft bgs and in the R-35b borehole to a depth of 615 ft bgs. The approximate top of the regional aquifer at the R-35 site is 790 ft bgs. The drive shoes on each string of steel casing were cut off and dismembered from the casing to facilitate casing extraction during well construction. While the drive shoes themselves are small pieces of steel, the casing was cut well above each shoe to ensure the dismembered piece remained aligned with the hole. In the R-35a borehole, the drive shoes are located at the following depths: 10-in. shoe at 1133.9 ft to 1141 ft bgs (7.1 ft long), 12-in. shoe at 934 ft to 940.8 ft bgs (6.8 ft long), and the 16-in. shoe at 249.9 ft to 259.3 ft bgs (9.4 ft long). In the R-35b borehole, the drive shoes are located at the following depths: 10-in. shoe at 888.2 ft to 891.9 ft bgs (3.7 ft long) and the 16-in. shoe at 255 ft to 265.1 ft bgs (10.1 ft long). All the drive shoe sections were isolated in bentonite during well construction activities.

The field crew generally worked one 12-h shift per day, 7 d/wk. Field activities were suspended for an Easter weekend break (April 6–April 9, 2007) and a Memorial Day weekend break from May 25 to May 29, 2007. Operations sustained numerous weather delays for thunder, lightning, and high winds throughout the duration of the project. Very few technical delays were incurred, and they were almost exclusively due to running geophysical and/or video logs in the boreholes. Several mechanical delays stalled progress. The rental Wagner compressors were not reliable and had to be frequently replaced. The rig's top head hydraulic cylinder was in the process of bending while set up on the R-35a borehole. To avoid a possible rupture, a preventative stop-work condition was put into place, and several days were lost waiting on the replacement cylinder to arrive from Canada.

4.0 SAMPLING ACTIVITIES

This section describes the cuttings and groundwater sampling activities at R-35.

4.1 Cuttings Sampling and Coring

Cuttings samples were collected from both R-35 boreholes at 5-ft intervals from ground surface to the TD of 1143 ft bgs at R-35a and the TD of 897.6 ft bgs at R-35b. Approximately 500 to 700 mL of bulk cuttings was collected from the discharge hose, sealed in self-sealed plastic bags, labeled, and archived in core boxes. Sieved fractions (>#10 and >#35 mesh) were placed in chip trays along with unsieved (whole rock) cuttings.

Sieved fractions that make up the contents of the chip trays were collected from ground surface to 615 ft bgs in R-35b and from 615 ft bgs to 1143 ft bgs in R-35a. Sieved fractions for the interval of lost circulation in R-35b (400 to 485 ft bgs) were compensated with cuttings from R-35a. Bulk cuttings samples were collected in R-35b from 615 ft bgs to TD at 897.6 ft bgs; likewise, bulk samples were collected in R-35a from ground surface to 615 ft bgs. The Laboratory's RCTs screened all cuttings before they were removed from the site.

Drilling and sample collection methods for the R-35 project tended to lose the fine fraction of the entire borehole stratigraphy. This effect was particularly evident with increasing depth and the unconsolidated nature of the units below the Cerros del Rio basalt. The foaming agent helped to acquire representative samples in the intervals where it was used. Below the points where the foaming agent was used, acquiring representative grain-size distribution samples became problematic. The volume of compressed air that was employed to avoid mud-rotary methods made catching samples difficult. Because the site was set up with large pits to contain discharged water, no cyclone was used on the discharge hose. Site geologists collected samples with a wire mesh basket directly from the discharge hose. Discharge velocities forced the fine fraction of sample through the basket. Despite this, at least the coarse fraction of the cuttings samples was collected in nearly 100% of both boreholes exclusive of the 85-ft interval of lost circulation in R-35b where there were no returns.

The statement of work for the R-35 project specified collecting representative core samples from the saturated zone near the screen intervals from both boreholes. The core run was proposed for approximately 1060 ft bgs at R-35a. Drilling operations at that depth were in unconsolidated deposits of the Santa Fe Group. The formation was too poorly lithified to expect much recovery, but the larger issue was that the loose sediments would flush out of the core barrel during the trip up through the standing water column. To compensate for not coring, bulk cuttings were collected continuously from the discharge through a 5-ft interval in buckets to provide a more representative sample. Cuttings were continually collected from the discharge from the 1060- to 1065-ft-bgs interval in a bucket. At the end of the 5-ft-interval, the sample bucket was full and densely packed with discharged cuttings including the fine fraction. Although this sample is not equivalent to intact core, it is more representative of the formation near the potential screen interval than the cuttings collected during normal drilling operations. No better formation for coring was encountered during the remainder of drilling in the R-35a borehole, and no coring was attempted.

R-35b was also unsuitable for coring within the target screen interval, so a drive sample was attempted in the R-35b borehole using a 2-ft split spoon on a slide hammer at 820 ft bgs. Two attempts were made with cumulative returns of less than 6 in. Conditions at R-35b were the same as R-35a; the formation below the Cerros del Rio basalt was too poorly lithified to core with conventional core tooling. While the split-spoon method was better suited to the formation, the depth and general nature of the formation

prevented good recovery. The bucket method for bulk-sample collection was employed at R-35b, and continuous bulk samples were collected from the following intervals: 800 to 805 ft bgs, 820 to 825 ft bgs, 840 to 845 ft bgs, and 860 to 865 ft bgs.

4.2 Water Sampling

Groundwater screening samples were collected from the drilling discharge at 20-ft intervals below the top of regional groundwater in the R-35a borehole and at 10-ft intervals in the R-35b borehole. Typically, upon reaching the bottom of a 20-ft run of casing, the driller would cut off water circulation (if injecting water) and circulate air to clean out the hole. As the discharge cleared, a water sample was collected directly from the discharge hose. Not all intervals below the top of water could be captured at the end of a casing run. Alternatively, some samples, particularly those near the top of the regional aquifer in the R-35a borehole, were collected upon start-up of the next casing run after the borehole had time to equilibrate. The samples were submitted to the Laboratory's Earth and Environmental Sciences (EES) 6 groundwater chemistry laboratory for analysis of anions, metals, and (in some cases) total organic carbon (TOC). Sampling documentation and containers were provided by the Laboratory and processed through the Laboratory's Sample Management Office.

Groundwater samples were also collected at regular intervals during well development and aquifer testing. The samples were collected from the submersible development pump discharge port and were submitted for TOC, anions, and metals analyses by the EES-6 laboratory. Groundwater analytical results and details of groundwater chemistry are found in Appendix B.

A summary of all groundwater samples collected during drilling and well development activities is presented in Table 4.2-1.

In addition, groundwater field-screening samples were collected during drilling activities for the analysis of chromium. The samples were analyzed using a HACH model DR/2400 instrument following HACH Method 8023. At the onset of drilling activities, only a few screening samples were proposed to be duplicated by the EES-6 laboratory to verify the accuracy of the field-sampling kits. Ultimately, the EES-6 laboratory analyzed all field-screening samples.

5.0 GEOLOGY AND HYDROGEOLOGY

A brief description of the geologic and hydrogeologic features encountered at R-35 is presented below. The Laboratory's geology task leader and site geologists used cuttings examination along with Laboratory and Schlumberger geophysical logs to determine the geologic contacts. Drilling observations, video logging, water-level measurements, and geophysical logs were used to describe groundwater characteristics encountered at R-35.

5.1 Stratigraphy

Borehole stratigraphy for the R-35a borehole is presented below in order of youngest to oldest geologic units. The stratigraphy for R-35b is similar to R-35a, but the contacts vary by a few feet for some units. All lithologic descriptions are based on discharged cuttings descriptions. Figures 5.1-1 and 5.1-2 illustrate the stratigraphy at R-35a and R-35b, respectively. Detailed lithologic logs are presented in Appendix A.

Quaternary Alluvium, Qal (0 to 45 ft bgs)

Quaternary alluvium consisting of poorly to moderately sorted loose sand and gravel consisting of Bandelier Tuff detritus was encountered from 0 to 45 ft bgs. No evidence of alluvial groundwater was observed.

Otowi Member of the Bandelier Tuff, Qbo (45 to 200 ft bgs)

The Otowi Member of the Bandelier Tuff is present in R-35a from 45 to 200 ft bgs. The Otowi Member is a lithic-bearing, partly pumiceous, and poorly welded ash-flow tuff. It contains reddish gray to gray, subangular to subrounded, intermediate composition volcanic rocks up to 15 mm. Pale yellow to white pumice lapilli are vitric and contain conspicuous phenocrysts of quartz and sanidine.

Guaje Pumice Bed of the Otowi Member of the Bandelier Tuff, Qbog (200 to 220 ft bgs)

The Guaje Pumice Bed is present from 200 to 220 ft bgs. Pumice lapilli contain quartz and sanidine phenocrysts and trace mafic minerals.

Upper Puye Formation, Tpf (220 to 256 ft bgs)

The upper Puye Formation consisted of poorly sorted volcanoclastic silty sand and sandy gravel deposits from 220 to 256 ft bgs. Clasts consist of devitrified intermediate lavas with conspicuous felsic and mafic phenocrysts. The formation ranges from light and medium gray to grayish orange pink.

Cerros del Rio Basalt, Tb 4 (256 to 602 ft bgs)

Cerros del Rio basalt, from 256 to 602 ft bgs, consists of fractured to massive basalt with trace to minor olivine and plagioclase phenocrysts. Portions of this unit were variably vesicular. It ranges from dark to medium gray.

Lower Puye Formation, Tpf (602 to 880ft bgs)

The lower Puye Formation consisted of poorly sorted volcanoclastic silty sand and sandy gravel deposits from 602 to 880 ft bgs. Clasts consist of devitrified intermediate lavas with conspicuous felsic and mafic phenocrysts. The formation ranges from light and medium gray to grayish orange pink.

Santa Fe Group, Undivided, Tsfu (880 to 1136 ft bgs)

The Miocene Santa Fe Group was present from 880 to 1136 ft bgs and consisted of medium gray to grayish orange, silty sands, and silty gravels with minor silt. The gravel and sand consisted primarily of felsic to intermediate composition volcanics along with tuff fragments and basalt. At R-35a, an interval of river gravels containing rounded clasts of intermediate volcanics and about 5% Precambrian quartzite was recorded between 900 and 935 ft bgs. The contact between the Puye Formation and Miocene Santa Fe Group sediments is difficult to assign because of their similar lithologies. This contact is presently placed at 880 ft bgs where abundant crystal-poor to aphyric pumice first appear in drill cuttings. In nearby boreholes, these pumice-rich deposits are correlated with the Miocene Peralta Tuff.

Miocene Basalt, Tb 2 (1136 to 1143 ft bgs, Bottom of This Unit Not Recorded)

Miocene basalt, from 1136 to 1143 ft bgs, consisted of massive basalt with trace to minor olivine and plagioclase phenocrysts. It ranged from dark to medium gray. Drilling operations recorded the top of this unit at 1141 ft bgs while geophysical logging recorded the top of this unit at 1136 ft bgs.

5.2 Groundwater

Regional groundwater was first encountered at R-35a during drilling at approximately 800 ft bgs in the Puye Formation sediments. Groundwater screening samples (Section 4.2) were collected in both boreholes during drilling, well development, and aquifer testing. After well development, static water levels were recorded at 792.1 ft bgs in R-35a and 786.9 ft bgs in R-35b. Discussion of groundwater chemistry is in Appendix B, and aquifer testing data and discussion are detailed in Appendix E.

6.0 BOREHOLE LOGGING

Several video logs and a complete suite of cased-hole geophysical logs were run during the R-35 project. A summary of video and geophysical logging runs is presented in Table 6.0-1.

6.1 Video Logging

Video logs were run in the boreholes to check for the presence of perched groundwater in the Cerros del Rio basalt on April 12 in R-35b and April 24 in R-35a. Perched water was not observed entering either borehole in the videos. The video logs from both boreholes are presented on a digital video disk in Appendix C. Additional video logs were collected in the completed wells. The postconstruction videos are not included in this report. Table 6.1-1 details individual video logging runs.

6.2 Geophysical Logging

A suite of Schlumberger geophysical logs was run inside the drill casing on May 11 and 12 at R-35a. At the time of logging, the bottoms of the three casing strings in the R-35a borehole were located at the following depths: 16-in. casing at 265 ft bgs, 12-in. casing at 940 ft bgs, and 10-in. casing at 1141 ft bgs. The geophysical suite included triple detector lithodensity tool, accelerator porosity sonde (APS), compensated neutron tool (CNT), hostile natural gamma spectroscopy (HNGS), elemental capture spectroscopy (ECS), and cased hole formation resistivity. Interpretation and details of the logging are in Appendix D, Geophysical Logging Report.

Additionally, several natural gamma ray and induction tool logs were run in the R-35 boreholes and wells using the Laboratory's geophysical equipment. Details of the logging operations are presented in Table 6.1-1.

7.0 WELL INSTALLATION

R-35a well casing and annular fill were installed between May 23 and June 22, 2007. R-35b well casing and annular fill were installed between June 29 and July 11, 2007.

7.1 Well Design

The R-35 wells were designed in accordance with the Compliance Order on Consent. Individual well designs were approved by NMED before installation. The wells were designed with single-screened intervals to monitor groundwater quality in the regional aquifer within the Puye Formation (R-35b) and the Santa Fe Group (R-35a).

7.2 Well Construction

R-35a and R-35b were constructed of 4.5-in.-I.D./5.0-in.-outside diameter (O.D.) type A304 stainless-steel casing fabricated to American Society for Testing and Materials (ASTM) A312 standards. External couplings, also type A304 stainless steel fabricated to ASTM A312 standards, were used to connect individual casing and screen joints. The well screen components were on average 12.3 ft long with 10-ft lengths of 4.375-in.-I.D. rod-based 0.020-in. wire-wrapped well screen. The coupled union between two threaded pieces was on average 0.7 ft long. The casing and screen were factory cleaned and also steam cleaned on-site.

The screened interval chosen for R-35a was a 40-ft screen with the top of the screen anchored at 1010 ft bgs. The screened interval chosen for R-35b was a 20-ft screen with the top of the screen anchored at 825 ft bgs. A 22-ft long sump of stainless-steel casing was placed below the well screen in each well. Figures 7.2-1 and 7.2-2 are as-built schematics showing construction details for the completed wells. A Semco work-over rig was used for all well construction and development activities.

Both boreholes were drilled beyond the planned TD of the completed wells. Before well casing was placed in either borehole, backfilling in and above the dismembered 10-in. drive shoes was accomplished with bentonite chips. The annular spaces of the dismembered pieces of steel were filled with bentonite chips, and the chips were installed to a level approximately 10 ft above the top of each piece of steel. Backfilling continued to the approximate calculated depth of the wells with a coarse (8/12) filter-grade silica sand. When the level of the backfill sand was close to the calculated depth of the well, backfilling operations were stopped, and the well components were threaded together and hung in the borehole. A 2-in.-I.D.-steel threaded/coupled tremie pipe was used to deliver all backfill and annular fill materials during well construction.

Because each borehole was overdrilled, each well was designed and built with a lower bentonite seal below the well screen. At R-35a, the lower bentonite seal was installed around the well sump from 1072.9 to 1066.4 ft bgs. At R-35b, the lower bentonite seal was installed around the well sump from 863.2 to 854.6 ft bgs. The primary filter pack of 10/20 silica sand was placed across the screened intervals from 1066.4 to 1007.2 ft bgs at R-35a and from 854.6 to 820.1 ft bgs at R-35b. During and after installation of the primary filter pack, the work-over rig was used to swab the screened intervals with a surge block to promote settling and compaction of the filter pack. A transition sand collar of 20/40 silica sand was then placed above the primary filter pack from 1007.2 to 1005.2 ft bgs at R-35a and from 820.1 to 817.2 ft bgs at R-35b. Following placement of the fine sand collar, a bentonite chip seal was installed from 1005.2 to 999.9 ft bgs at R-35a and from 817.2 to 779.1 ft bgs at R-35b.

The annular space between the top of the upper bentonite chip seals and the bottom of the Cerros del Rio basalt in both boreholes was filled with a high-solids bentonite grout. The intervals from the bottom of the Cerros del Rio basalt to the top of the Guaje Pumice Bed were filled with bentonite chips and hydrated with potable water. Above the Guaje Pumice Bed to ground surface, the annular space of both holes was filled with cement grout containing 2% to 5% bentonite. Figures 7.2-1 and 7.2-2 depict depths and volumes used in each interval at each location. Table 7.2-1 details volumes of materials used during well construction at each well.

Well construction operations proceeded in a normal fashion overall at each location. Problems with uncoated bentonite chips clogging the tremie pipe were encountered at both wells. Typically, these problems resulted in time lost from pulling out the tremie pipe to flush out a bridge of chips somewhere in the tremie pipe string. Water from filter pack installation at R-35a came up inside the 10-in. casing almost to ground surface, indicating the formation was not taking water during construction. This formation occurred after the lower bentonite chip seal had been installed. Approximately 1200 gal. of high-solids bentonite grout loss to the formation was recorded at the R-35a location. Although a small amount of bentonite (~2 gal.) was recovered from the well sump, it is assumed that the majority of this lost material entered a permeable zone or zones within the aquifer. These losses are thought to have occurred primarily at or near the depths of 940 ft and 850 ft bgs. Conditions recorded in the field and the Laboratory natural gamma log support this determination.

Some difficulty was encountered at R-35b retracting the 10-in. casing at the beginning of well construction. The 10-in. casing's behavior was indicative that the drive shoe was only partially cut and not detached. The decision was made to rerun the casing cutter before finishing backfilling operations. Rerunning the casing cutter and recutting the casing solved the retraction difficulties.

8.0 POSTINSTALLATION ACTIVITIES

Following well installation, the wells were developed and aquifer pump tests were conducted. A dedicated submersible pump and the wellhead surface pad were installed at each location. A geodetic survey was performed. Site restoration activities will commence once the final disposition of drill cuttings and groundwater is determined in accordance with the NMED-approved waste-decision trees.

8.1 Well Development

Well development was conducted between June 21 and July 13, 2007, at R-35a and July 12 and July 16, 2007, at R-35b. Initially, the screened interval of both wells was bailed and swabbed to remove formation fines in the filter pack. The swabbing tool was a 4.25-in.-O.D. 1-in.-thick nylon disc attached to a steel rod. The swabbing tool was lowered into the well on a wire line and drawn repeatedly across the screened interval. A 7.5 hp 20-gpm. 4-in.-Berkeley submersible pump was used for the final stage of well development.

The objective of well development is to remove suspended sediment from groundwater, clean out and settle the filter pack, and generally improve the performance characteristics of the well. The goal for turbidity at the end of development is less than 5 nephelometric turbidity units (NTUs). Turbidity measurements at the end of development were 0.93 NTUs and 3.84 NTUs for R-35a and R-35b, respectively. Temperature, pH, dissolved oxygen (DO), oxygen-reduction potential (ORP), and specific conductance were also measured during development. Samples for TOC analysis were collected during development. The goal for TOC at the end of development was less than 2.0 parts per million (ppm). The TOC values at the end of well development for both wells were less than 1.0 ppm. Tables 8.1-1 and 8.1-2 show the volume of water removed during well development and aquifer testing and the resultant water-quality parameters for R-35a and R-35b, respectively.

Development started at R-35a on June 21, 2007 while well construction activities were ongoing at R-35b. Initial conditions at R-35a consisted of bentonite blockage at 1059.7 ft bgs near the bottom of the screen interval and an elevated water level of 648.8 ft bgs. The bentonite blockage was removed with a 4-in.-O.D. split-barrel sampler. The total length of the bentonite bridge was difficult to determine because the material was soft and the bottom was undeterminable, but retrieved material suggests the bridge was less than 2 ft in total length. Fluids and sediment below the bridge were typical of undeveloped,

postconstruction wells. The exact route of entry for the bentonite bridge has not been determined. Bailing and swabbing continued at R-35a until returned water started to clear, at which point a submersible pump was utilized to finish development. Approximately 32,000 gal. of groundwater was purged at R-35a during development activities. Nothing unusual was observed during well development at R-35b. Bailing and swabbing methods were used until returned water was clear. The submersible pump was used after bailing and swabbing to finish development. Approximately 21,000 gal. of water was purged at R-35b during development activities. Discussion of analytical results is presented in Appendix B.

8.1.1 Field Parameters

Criteria for well development were based on field water-quality parameters (pH, DO, temperature, specific conductance, and turbidity). To monitor the progress during well development, samples of groundwater were collected, and field parameters were measured and recorded. Figures 8.1-1 and 8.1-2 show plots of field parameters versus cumulative water purged from R-35a and R-35b. Field parameters were measured under environmental surface conditions at R-35a and R-35b with several parameters showing considerable variation during pumping, including DO. Measurements for ORP are not plotted in Figures 8.1-1 and 8.1-2 because of their variability resulting from the water samples coming in contact with atmospheric air. The primary objective of well development was to remove suspended sediment from groundwater until turbidity, measured in NTU, was less than 5 NTUs for three consecutive samples. Most of the turbidity measurements taken at R-35a and R-35b were less than 5 NTUs. A high turbidity value of 557 NTUs, however, was recorded (Figure 8.1-1) when the pump was lowered down the casing at R-35a. During initial pumping at R-35b, several turbidity values exceeded 1000 NTUs (Figure 8.1-2), and turbidity values rapidly decreased to less than 5 NTUs as suspended sediment was removed from the well. Field parameters were required to be stable before terminating development procedures (see Tables 8.1-1 and 8.1-2). Figures 8.1-1 and 8.1-2 show that specific conductance and turbidity were stable during the later period of pumping and that turbidity values had declined to consistently less than 5 NTUs. Wells R-35a and R-35b were considered fully developed when the limiting values of acceptability were met.

8.2 Aquifer Testing

Aquifer pumping tests were conducted at R-35b from July 20 to July 25 and at R-35a from July 27 to July 29, 2007. Several tests were performed at each location. Several short-duration tests with short-duration recovery periods were performed on the first day of testing in each well. Twenty-four-hour tests followed by 24-h recovery periods completed testing. A 48-h background data collection period was conducted at R-35b between the short-duration tests and the 24-h test. During aquifer testing at each well, the companion well was outfitted with a transducer to record water-level data. The 7.5-hp Berkeley pump used during development was used to perform the aquifer testing. The pump was utilized at full capacity in each well. The results of the pump test data are presented in Appendix E and the data files are in Attachment 1, Appendix Data Files and Images on the enclosed CD.

8.3 Dedicated Sampling System Installation

Dedicated 3-hp, 4-in.-O.D. environmentally retrofitted Grundfos submersible pumps were installed in R-35a and R-35b from July 30 to August 3, 2007. The pump intake at R-35a was set at 998.3 ft bgs. The pump intake at R-35b was set at 832.7 ft bgs. Transducer tubes were also installed to a depth of 994.2 ft bgs in R-35a and 828.6 ft bgs in R-35b. The transducer tubes are 1.0-in.-I.D. flush-threaded polyvinyl chloride (PVC) with 6-in. 0.010-in. screen-slot intervals at the bottom of each tube. The transducer tubes are capped on the bottom below the screens. Dedicated in situ transducers were installed in the PVC tubes. Postinstallation construction and sampling component installation details for

R-35a and R-35b are presented in Figures 8.3-1a and 8.3-2a, respectively. Figures 8.3-1b and 8.3-2b are technical notes for R-35a and R-35b, respectively.

8.4 Wellhead Completion

Reinforced concrete surface pads, 5 ft × 5 ft × 6 in. thick, have been installed at R-35a and R-35b. The pads will provide long-term structural integrity for the wells. A brass survey pin was embedded in the northwest corner of each pad. Ten-inch-I.D. steel protective casings with locking lids were installed around the well risers. The concrete pads were slightly elevated above the ground surface, with base-coarse gravel graded up around the edges.

8.5 Geodetic Survey

Geodetic survey data for the well casing top cap, protective casing, brass pin, and ground surface at R-35a and R35-b were collected on August 22, 2007. The survey data are presented in Table 8.5-1.

8.6 Site Restoration and Waste Management

Fluids and cuttings produced during drilling and development were containerized and sampled in accordance with the February 20, 2007, "Waste Characterization Strategy Form for the R-35 Monitoring Well Installation" (LANL 2007, 095170), prepared for the R-35 well drilling at the Laboratory. Fluids produced during drilling and well development are anticipated to be land-applied after review of associated analytical results per the waste characterization strategy form (WCSF) and the Laboratory EP-Directorate Standard Operating Procedure 010.0, Land Application of Groundwater. Solids produced during drilling are anticipated to be buried in the cuttings pit after review of associated analytical results per the WCSF and the land application decision tree for investigated-derived waste (IDW) solids from construction of wells and boreholes. This decision tree is pending NMED's approval. Both liquid and solid land application will be conducted with concurrence from NMED.

Site restoration activities will include removing water from the cuttings containment pits and land-applying it on-site, removing cuttings from the cuttings containment pits, removing the polyethylene liner, removing the containment area berms, and backfilling and regrading the containment area. Cuttings will be used in accordance with governing documents outlined above. The site will be reseeded with a native seed mix consisting of Indian rice grass, mountain broom, blue stem, sand drop, and slender wheat grass seed. The seed mix will be applied at a rate of 20 lb/acre. Biosol fertilizer will be applied at a rate of 80 lb/acre.

Waste generation and characterization for the R-35 project include a small quantity of contact waste, decontamination fluids, cuttings, discharged drilling water, and purged groundwater. Waste characterization samples were collected for the decontamination water. Characterization samples of the cuttings and from discharged and purged waters were collected on August 15 and 17, 2007. A summary of the waste samples collected for the R-35 wells is presented in Table 8.6-1.

9.0 DEVIATIONS FROM PLANNED ACTIVITIES

In general, drilling, sampling, and well construction at R-35 were performed as specified in the "Drilling Work Plan for Regional Aquifer Wells R-35a and R-35b" (LANL 2006, 093388).

9.1 Deviations

The main deviation from planned activities is as follows.

- Core Sampling: A core sample was proposed from a depth at or near the proposed screen interval in the deeper R-35a borehole. No consolidated formation suitable for coring was encountered in the Puye Formation and Santa Fe Group. A split spoon and slide hammer were acquired to attempt sampling in the R-35b borehole, but cumulative returns from two attempts were less than 6 in.

9.2 NMED-Approved Modifications to the Work Plan

The following changes to the original work plan were implemented after discussions with and approval by NMED.

- Well Screen Design: The final design of well screen was 40 ft long (screen slot opening length) in R-35a. The planned design was 10 ft.
- Well Design: The bentonite chip seal at R-35b was extended above the top of the regional aquifer to a depth of 779.1 ft bgs. The planned design was a 5-ft seal above the top of the 20/40 transition sand to a depth of approximately 812 ft bgs.

10.0 ACKNOWLEDGMENTS

D. Schafer of David Schafer and Associates contributed the aquifer testing section of this report (Appendix E).

P. Longmire of Los Alamos National Laboratory contributed the geochemistry section of this report (Appendix B).

N. Clayton of Schlumberger provided processing and interpretation of borehole geophysical data (Appendix D).

Boart Longyear drilled the R-35 boreholes and installed the wells.

Keers Remediation Inc., prepared the site for drilling activities.

TerranearPMC provided oversight on all preparatory and field-related activities.

11.0 REFERENCES

The following list includes all documents cited in the main text of this report. Parenthetical information following each reference provides the author(s), publication date, and ER ID number. This information is also included in text citations. ER ID numbers are assigned by the Environmental Programs Directorate's Records Processing Facility (RPF) and are used to locate the document at the RPF and, where applicable, in the master reference set.

Copies of the master reference set are maintained at the NMED Hazardous Waste Bureau; the U.S. Department of Energy—Los Alamos Site Office; U.S. Environmental Protection Agency, Region 6; and the Directorate. The set was developed to ensure that the administrative authority has all material needed to review this document, and it is updated with every document submitted to the administrative authority. Documents previously submitted to the administrative authority are not included.

LANL (Los Alamos National Laboratory), March 2006. "Storm Water Pollution Prevention Plan for SWMUs and AOCs (Sites) and Storm Water Monitoring Plan," Los Alamos National Laboratory document LA-UR-06-1840, Los Alamos, New Mexico. (LANL 2006, 092600)

LANL (Los Alamos National Laboratory), June 2006. "Drilling Work Plan for Regional Aquifer Wells R-35a and R-35b," Los Alamos National Laboratory document LA-UR-06-3964, Los Alamos, New Mexico. (LANL 2006, 093388)

LANL (Los Alamos National Laboratory), March 22, 2007. "Waste Characterization Strategy Form for the R-35 Monitoring Well Installation," Los Alamos, New Mexico. (LANL 2007, 095170)

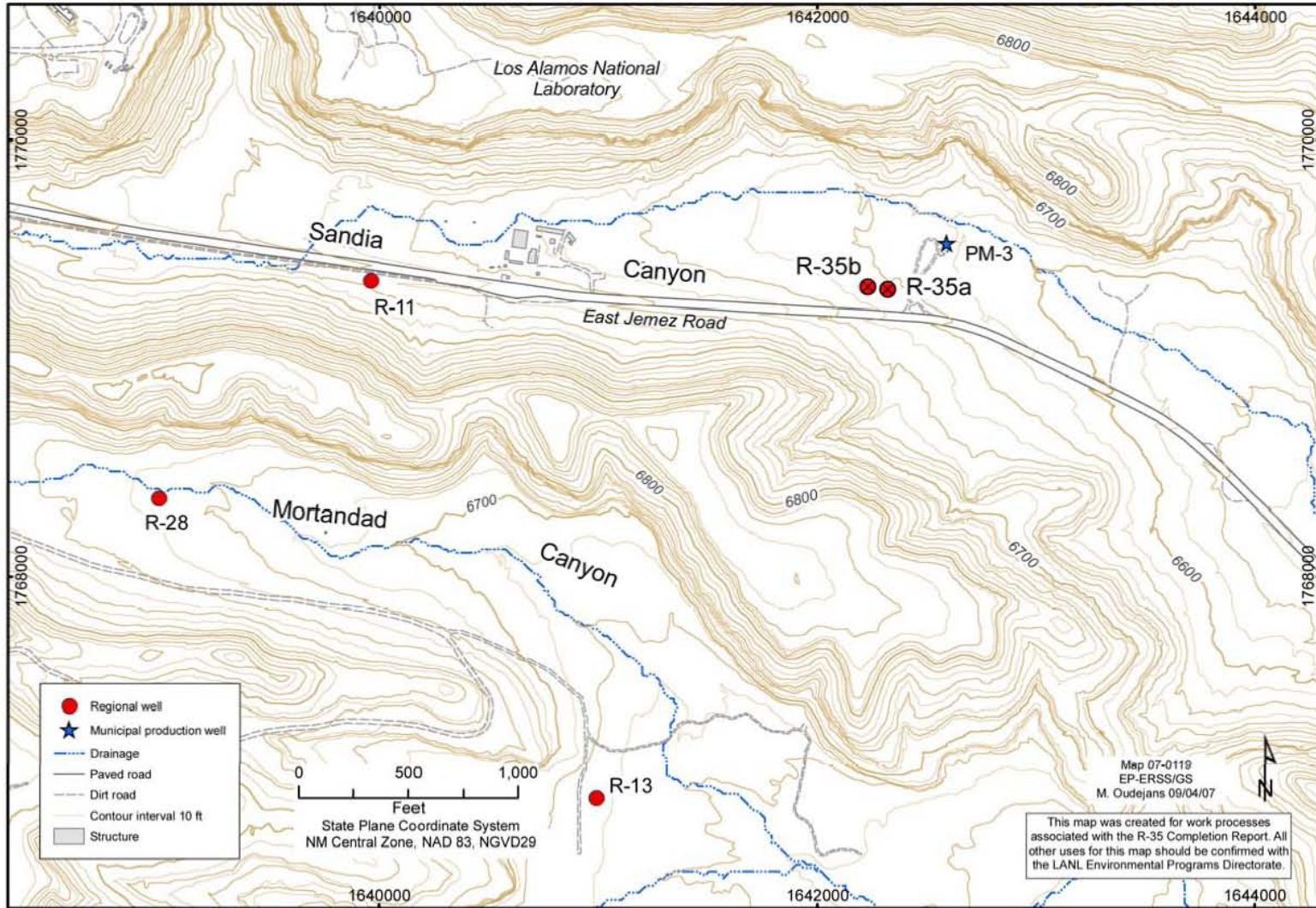


Figure 1.0-1 Location of regional aquifer wells R-35a and R-35b with respect to municipal supply well PM-3 and additional surrounding regional well

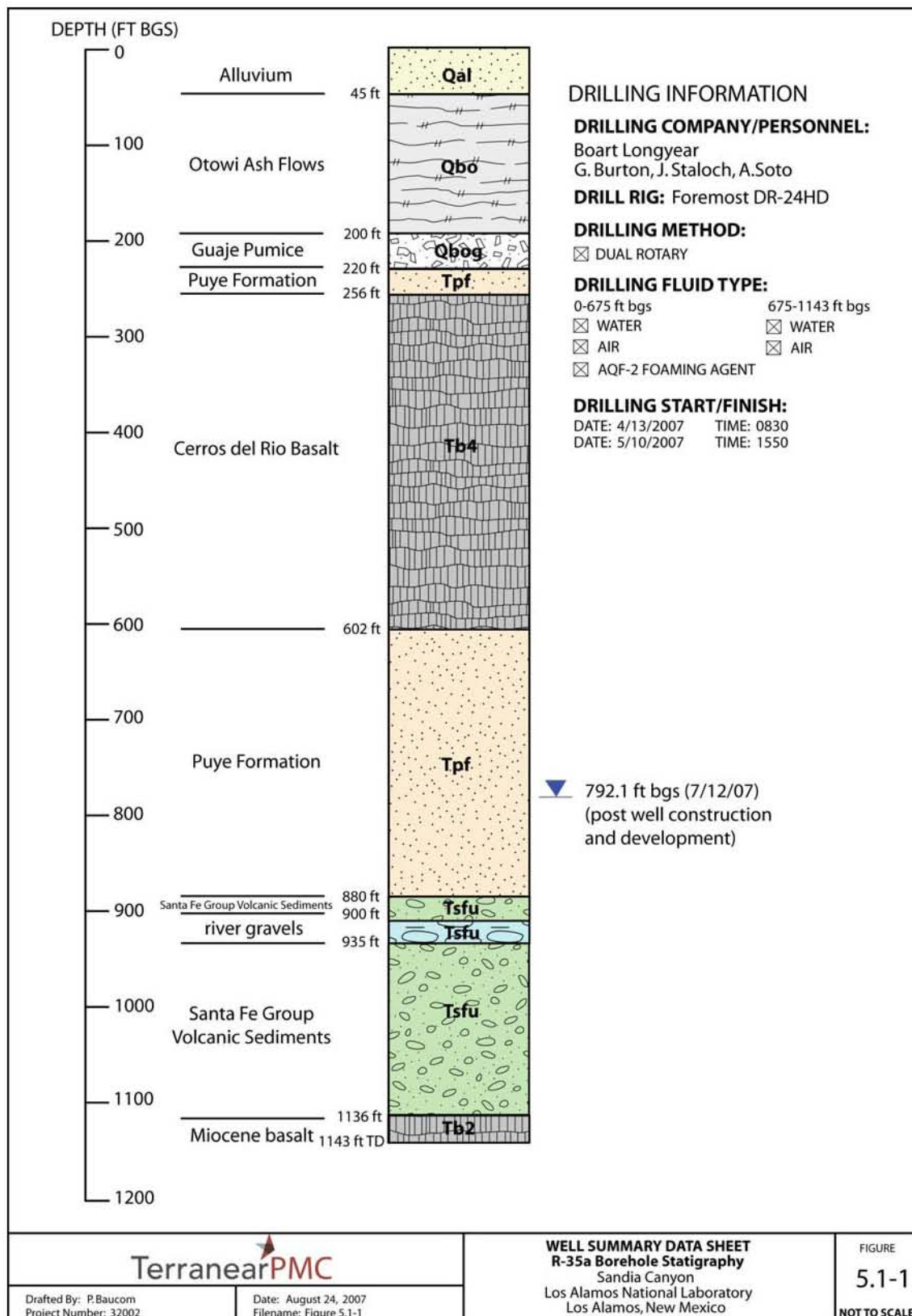


Figure 5.1-1 R-35a borehole stratigraphy

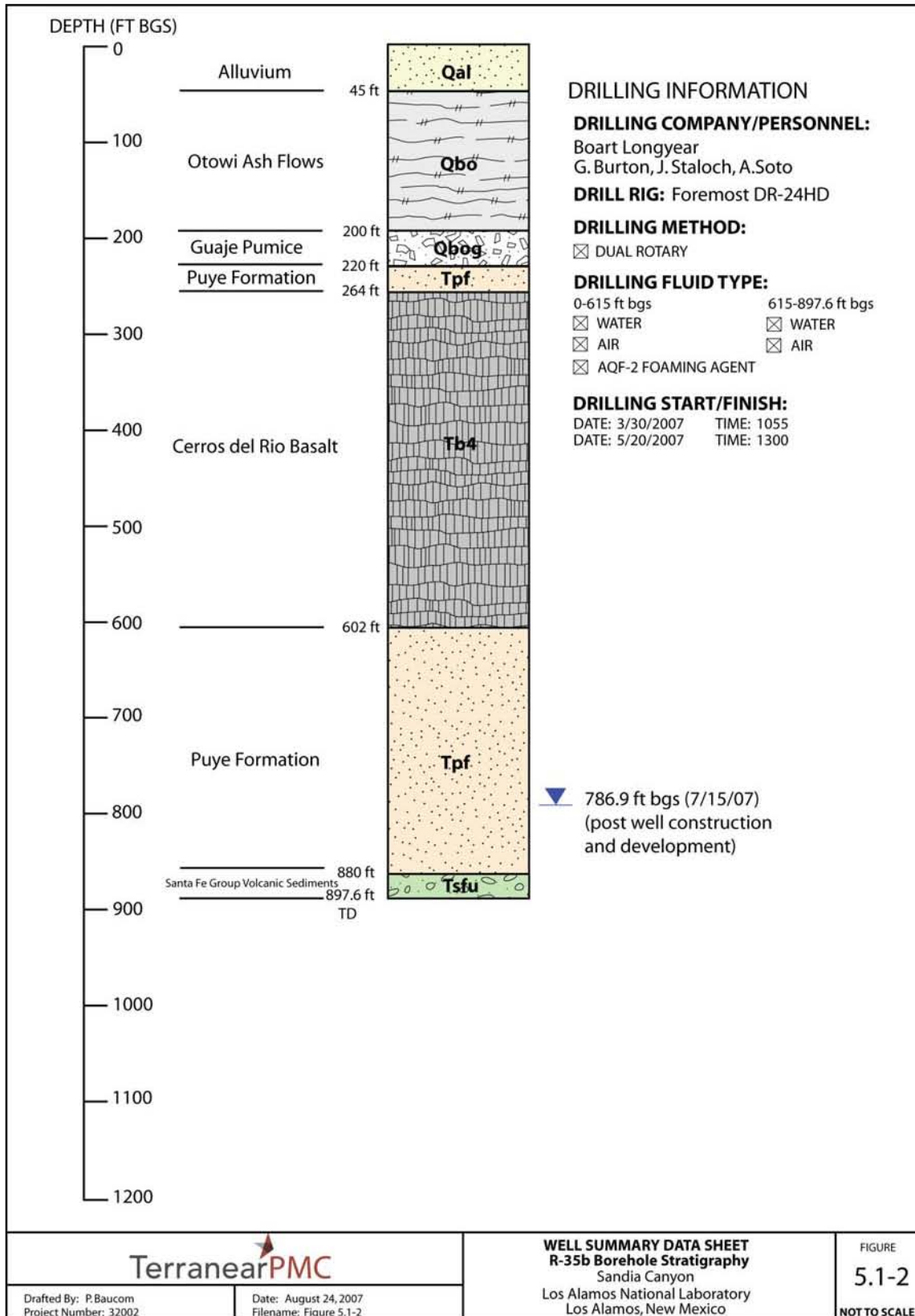


Figure 5.1-2 R-35b borehole stratigraphy

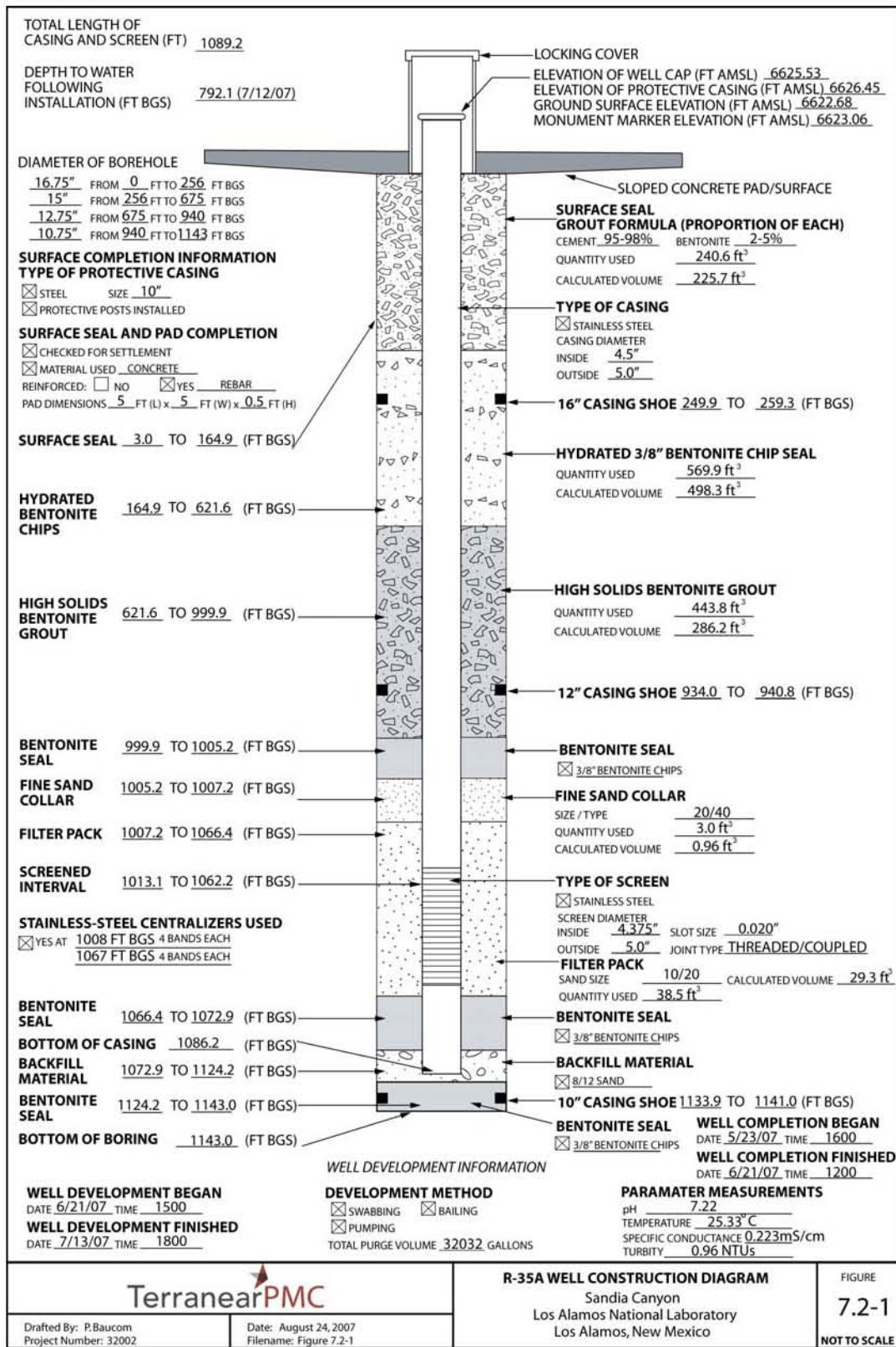


Figure 7.2-1 R-35a well construction diagram

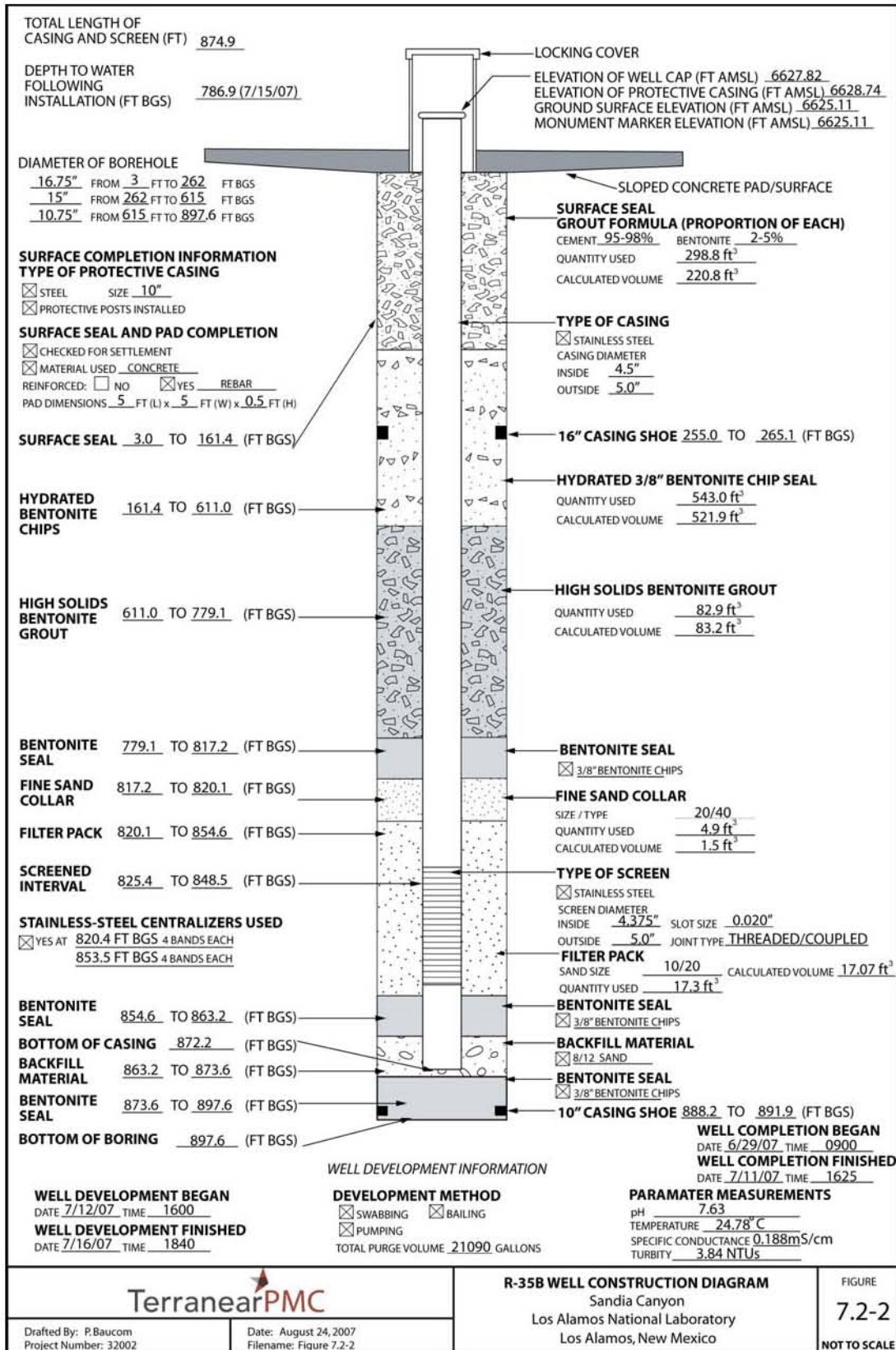


Figure 7.2-2 R-35b well construction diagram

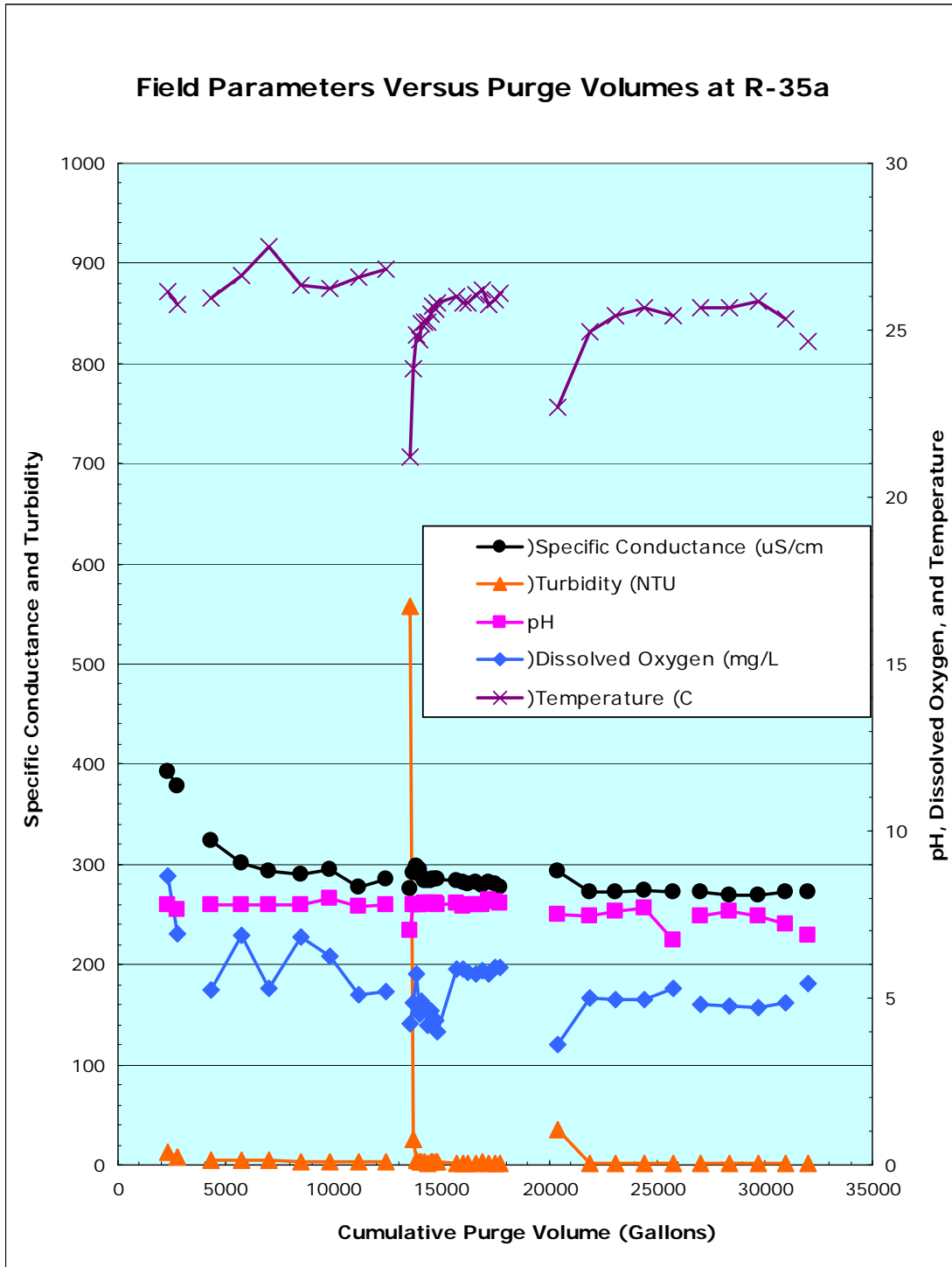


Figure 8.1-1 Specific conductance, turbidity, pH, dissolved oxygen, temperature versus purge volumes at R-35a

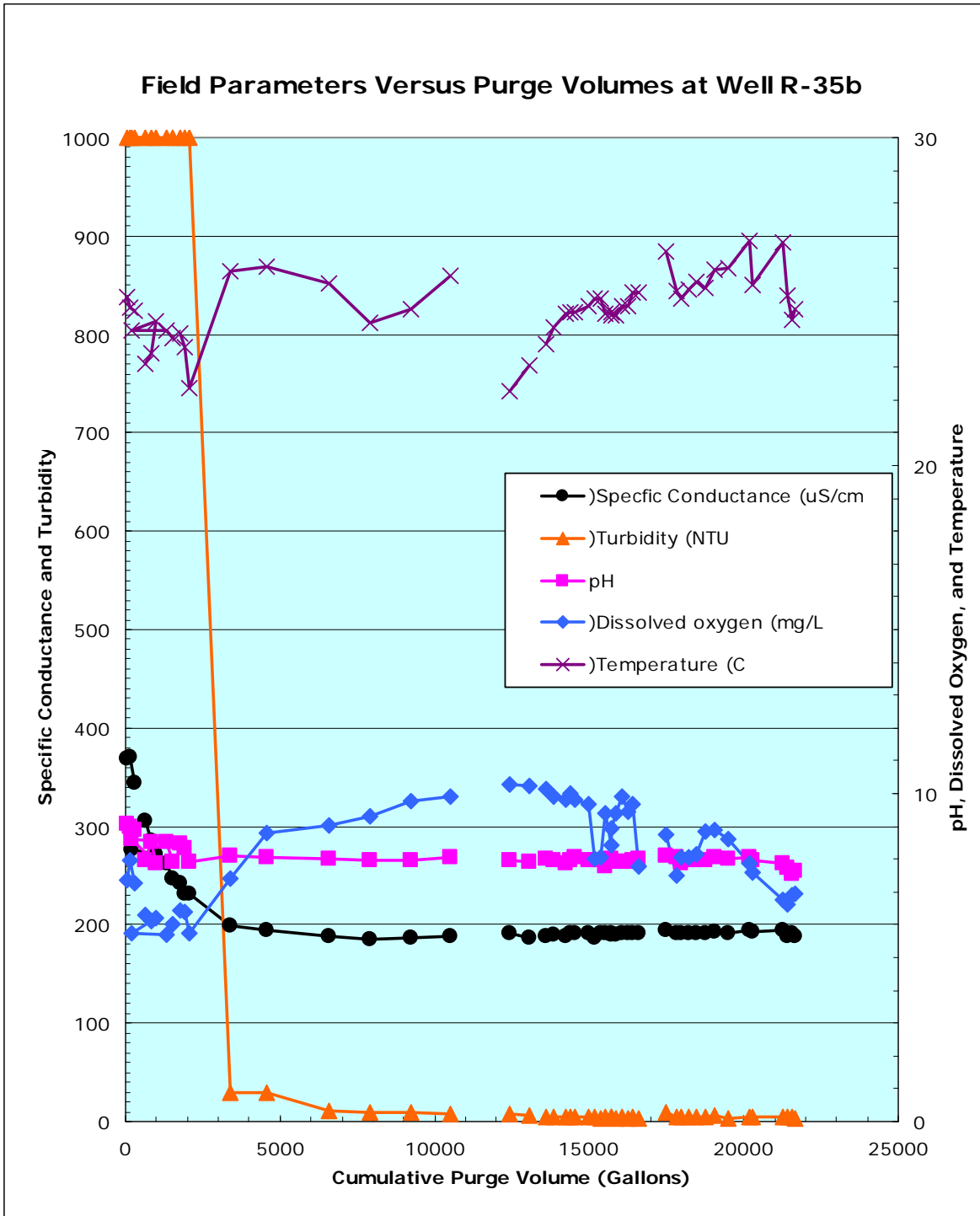


Figure 8.1-2 Specific conductance, turbidity, pH, dissolved oxygen, temperature versus purge volumes at R-35b

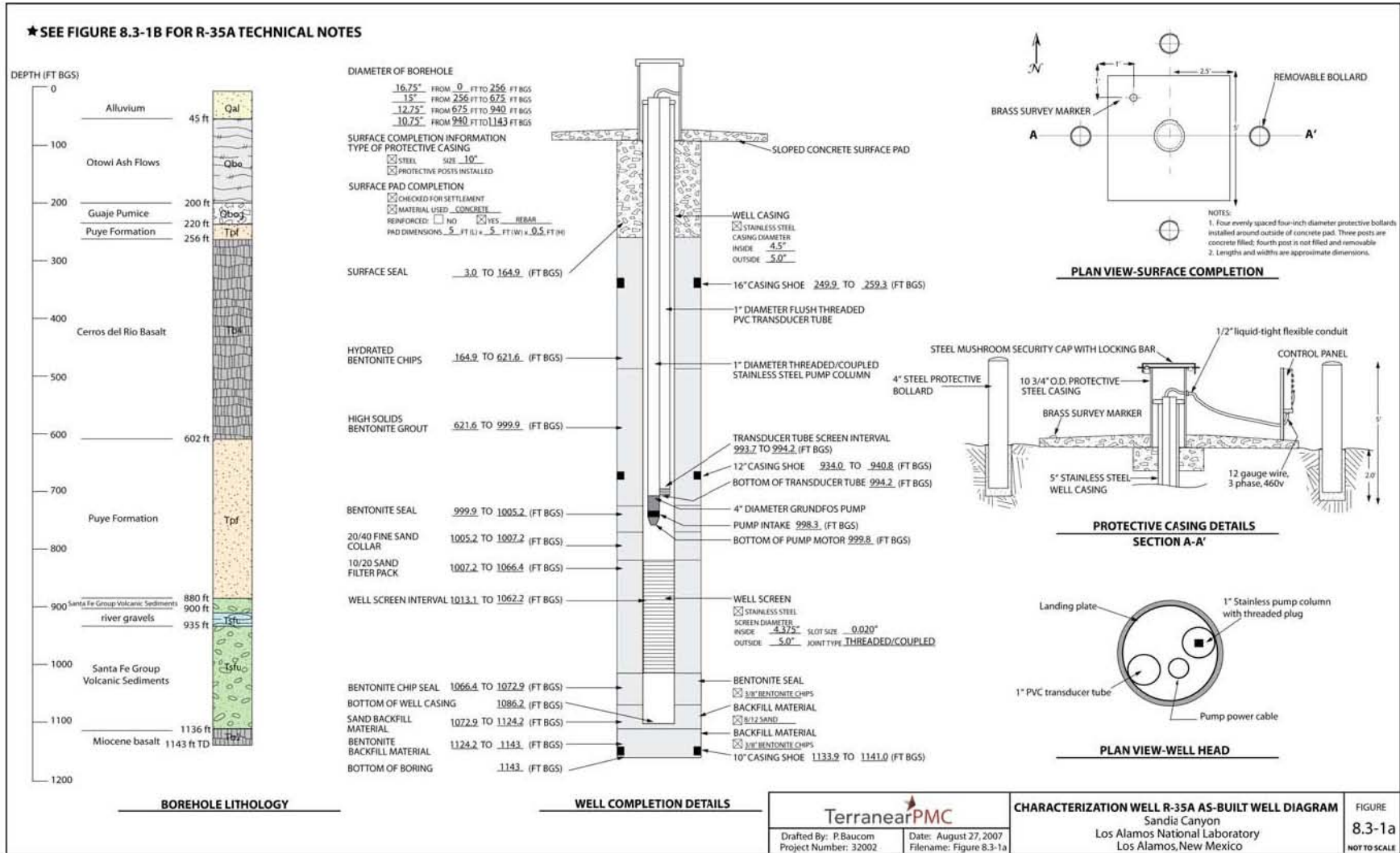


Figure 8.3-1a As-built schematic regional well R-35a



Figure 8.3-1b As-built technical notes for R-35a

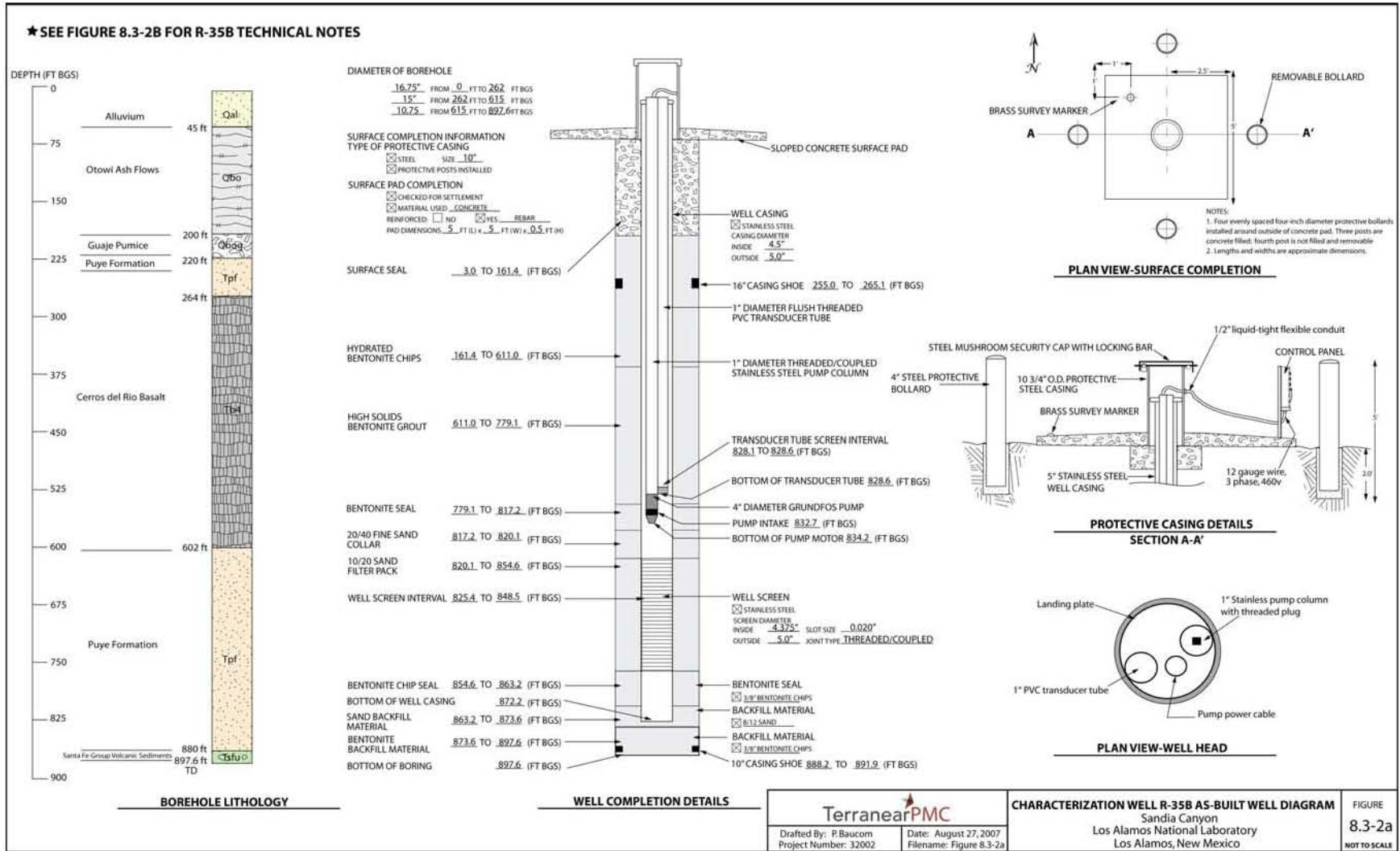


Figure 8.3-2a As-built schematic regional well R-35b


<p>R-35B TECHNICAL NOTES: ¹</p> <p>SURVEY INFORMATION²</p> <p>Brass Marker Northing: 1769316.2317 Easting: 1642321.7013 Elevation: 6623.06</p> <p>Well Casing (top of stainless steel) Northing: 1769314.1646 Easting: 1642323.3674 Elevation: 6625.53</p> <p>BOREHOLE GEOPHYSICAL LOGS Triper Detector Lithodensity, Accelerator Porosity Sonde, Compensated Neutron, Hostile Natural Gamma Spectroscopy, Cased Hole Formation Resistivity</p> <p>DRILLING INFORMATION</p> <p>Drilling Company Boart Longyear</p> <p>Drill Rig DR-24HD</p> <p>Drilling Methods Dual Rotary Fluid-assisted air rotary</p> <p>Drilling Fluids Air, potable water, AQF-2</p> <p>MILESTONE DATES</p> <p>Drilling Start: 3/30/2007 Finished: 5/20/2007</p> <p>Well Completion Start: 6/29/2007 Finished: 7/11/07</p> <p>Well Development Start: 7/12/07 Finished: 7/16/07</p> <p>WELL DEVELOPMENT</p> <p>Development Methods Performed swabbing, bailing, and pumping Total Volume Purged: 21,090 gallons</p> <p>Parameter Measurements (Final) pH: 7.63 Temperature: 24.78 °C Specific Conductance: 0.188 mS/cm Turbidity: 3.84 NTU</p> <p>AQUIFER TESTING Constant Rate Pumping Test Water Produced: 36,000 gallons Average Flow Rate: 22.5 gpm Performed on: 7/24/2007-7/24/2007</p> <p>NOTES 1) Additional information available in "Final Completion Report, Characterization Well R-35, Los Alamos National Laboratory, Los Alamos, New Mexico, August 2007. 2) Coordinates based on New Mexico State Plane Grid Coordinates, Central Zone (NAD83); Elevation expressed in feet above mean sea level using the National Geodetic Vertical Datum of 1929.</p>			
		<p>R-35B TECHNICAL NOTES Sandia Canyon Los Alamos National Laboratory Los Alamos, New Mexico</p>	<p>FIGURE 8.3-2b NOT TO SCALE</p>
Drafted By: P.Baucorn Project Number: 32002	Date: August 24, 2007 Filename: Figure 8.3-2B		

Figure 8.3-2b As-built technical notes for R-35b

**Table 3.0-1
Fluid Quantities Used during Drilling and Well Construction**

Borehole	Date	Water (gal.)	Cumulative Water (gal.)	Foam (gal.)	Cumulative Foam (gal.)	Cumulative Returns in Pit: Fluids (gal.)
Drilling						
R-35a	04/13/07	2000	2000	0	0	100
	04/14/07	1500	3500	15	15	100
	04/15/07	3000	6500	75	90	250
	04/16/07	1500	8000	15	105	400
	04/17/07	4500	12500	50	155	400
	04/18/07	4500	17000	40	195	500
	04/23/07	2000	19000	20	215	550
	04/28/07	1000	20000	0	215	550
	04/29/07	250	20250	0	215	600
	04/30/07	250	20500	0	215	600
	05/01/07	1400	21900	0	215	650
	05/02/07	800	22700	0	215	3000
	05/07/07	500	23200	0	215	3500
	05/08/07	0	23200	0	215	10,000
05/09/07	0	23200	0	215	11,000	
R-35b	03/30/07	700	700	14	14	100
	03/31/07	400	1100	10	24	100
	04/01/07	400	1500	10	34	100
	04/02/07	550	2050	10	44	200
	04/03/07	800	2850	15	59	200
	04/04/07	3000	5850	50	109	200
	04/05/07	2500	8350	45	154	200
	04/10/07	1500	9850	30	184	300
	04/11/07	800	10650	20	204	300
	05/17/07	750	11400	0	204	500
	05/18/07	0	11400	0	204	1300
	05/19/07	0	11400	0	204	2500

Table 3.0-1 (continued)

Borehole	Date	Water (gal.)	Cumulative Water (gal.)	Foam (gal.)	Cumulative Foam (gal.)	Cumulative Returns in Pit: Fluids (gal.)
Well Construction						
R-35a	05/18/07	1000	1000	n/a*	n/a	n/a
	05/19/07	600	1600	n/a	n/a	n/a
	05/20/07	400	2000	n/a	n/a	n/a
	05/21/07	3000	5000	n/a	n/a	n/a
	05/22/07	2500	7500	n/a	n/a	n/a
	05/30/07	100	7600	n/a	n/a	n/a
	05/31/07	600	8200	n/a	n/a	n/a
	06/01/07	2500	10700	n/a	n/a	n/a
	06/02/07	3500	14200	n/a	n/a	n/a
	06/03/07	600	14800	n/a	n/a	n/a
	06/04/07	2000	16800	n/a	n/a	n/a
	06/05/07	1800	18600	n/a	n/a	n/a
06/06/07	400	19000	n/a	n/a	n/a	
R-35b	06/17/07	500	500	n/a	n/a	n/a
	06/25/07	400	900	n/a	n/a	n/a
	07/03/07	3500	4400	n/a	n/a	n/a
	07/04/07	3500	7900	n/a	n/a	n/a
	07/05/07	1500	9400	n/a	n/a	n/a
	07/06/07	2000	11400	n/a	n/a	n/a
Total Volume (gal.)						
R-35a	42200					
R-35b	22800					

*n/a = Not applicable. Foam use and pit use discontinued after drilling activities; therefore, no additional fluids were produced.

Table 4.2-1
Summary of Groundwater Screening Samples Collected during the
Drilling and Development of R-35a and R-35b

Borehole ID	Location ID	Sample ID	Date Collected	Depth (ft)	Sample Type
Drilling					
R-35b	SA-27677	CASA-07-76391	04/10/07	530	Drilling water ^a
R-35a	SA-27676	CASA-07-76392	04/27/07	n/a ^b	Drilling water
R-35a	SA-27676	CASA-07-76393	05/07/07	1000	Groundwater
R-35a	SA-27676	CASA-07-76394	05/07/07	1020	Groundwater
R-35a	SA-27676	CASA-07-76395	05/08/07	1040	Groundwater
R-35a	SA-27676	CASA-07-76396	05/01/07	760	Drilling water
R-35a	SA-27676	CASA-07-76397	05/02/07	900	Groundwater
R-35b	SA-27677	CASA-07-76398	05/18/07	820	Groundwater
R-35b	SA-27677	CASA-07-76399	05/18/07	830	Groundwater
R-35b	SA-27677	CASA-07-76400	05/18/07	840	Groundwater
R-35b	SA-27677	CASA-07-76401	05/19/07	850	Groundwater
R-35b	SA-27677	CASA-07-76402	05/19/07	860	Groundwater
R-35b	SA-27677	CASA-07-76403	05/19/07	870	Groundwater
R-35b	SA-27677	CASA-07-76404	05/19/07	880	Groundwater
R-35b	SA-27677	CASA-07-76405	05/19/07	897	Groundwater
R-35a	SA-27676	CASA-07-76408	05/08/07	1060	Groundwater
R-35a	SA-27676	CASA-07-76514	05/01/07	760	Drilling water
R-35a	SA-27676	CASA-07-76515	05/01/07	800	Groundwater
R-35a	SA-27676	CASA-07-76516	05/01/07	840	Groundwater
R-35a	SA-27676	CASA-07-76517	05/01/07	860	Groundwater
R-35a	SA-27676	CASA-07-76518	05/02/07	880	Groundwater
R-35a	SA-27676	CASA-07-76519	05/02/07	900	Groundwater
R-35a	SA-27676	CASA-07-76520	05/02/07	920	Groundwater
R-35a	SA-27676	CASA-07-76521	05/02/07	940	Groundwater
R-35a	SA-27676	CASA-07-76522	05/07/07	960	Groundwater
R-35a	SA-27676	CASA-07-76523	05/07/07	980	Groundwater
R-35a	SA-27676	CASA-07-76524	05/08/07	1080	Groundwater
R-35a	SA-27676	CASA-07-76525	05/08/07	1100	Groundwater
R-35a	SA-27676	CASA-07-76526	05/08/07	1120	Groundwater
R-35a	SA-27676	CASA-07-76527	05/09/07	1140	Groundwater
R-35b	SA-27677	CASA-07-76528	05/18/07	820	Groundwater
R-35b	SA-27677	CASA-07-76529	05/18/07	830	Groundwater
R-35b	SA-27677	CASA-07-76530	05/18/07	840	Groundwater
R-35b	SA-27677	CASA-07-76531	05/19/07	850	Groundwater
R-35b	SA-27677	CASA-07-76532	05/19/07	860	Groundwater
R-35b	SA-27677	CASA-07-76533	05/19/07	870	Groundwater

Table 4.2-1 (continued)

Borehole ID	Location ID	Sample ID	Date Collected	Depth (ft)	Sample Type
Drilling					
R-35b	SA-27677	CASA-07-76534	05/19/07	880	Groundwater
R-35b	SA-27677	CASA-07-76535	05/19/07	897	Groundwater
Well Development					
R-35a	SA-27676	CASA-07-76673	07/11/07	983.5	Groundwater
R-35a	SA-27676	CASA-07-76674	07/11/07	983.5	Groundwater
R-35a	SA-27676	CASA-07-76675	07/11/07	983.5	Groundwater
R-35a	SA-27676	CASA-07-76676	07/11/07	983.5	Groundwater
R-35a	SA-27676	CASA-07-76677	07/11/07	983.5	Groundwater
R-35a	SA-27676	CASA-07-76678	07/11/07	983.5	Groundwater
R-35a	SA-27676	CASA-07-76679	07/11/07	983.5	Groundwater
R-35a	SA-27676	CASA-07-76680	07/11/07	983.5	Groundwater
R-35a	SA-27676	CASA-07-76681	07/11/07	983.5	Groundwater
R-35a	SA-27676	CASA-07-76682	07/12/07	1004.4	Groundwater
R-35a	SA-27676	CASA-07-76683	07/12/07	1004.4	Groundwater
R-35b	SA-27677	CASA-07-76684	07/12/07	828	Groundwater
R-35a	SA-27676	CASA-07-76685	07/13/07	1004.4	Groundwater
R-35a	SA-27676	CASA-07-76686	07/13/07	1004.4	Groundwater
R-35b	SA-27677	CASA-07-76687	07/13/07	828	Groundwater
R-35a	SA-27676	CASA-07-76688	07/13/07	1004.4	Groundwater
R-35b	SA-27677	CASA-07-76409	07/01/07	n/a ^b	Groundwater bailer ^c
R-35b	SA-27677	CASA-07-76689	07/13/07	828	Groundwater
R-35b	SA-27677	CASA-07-76690	07/15/07	828	Groundwater
R-35b	SA-27677	CASA-07-76691	07/15/07	828	Groundwater
R-35b	SA-27677	CASA-07-76692	07/15/07	828	Groundwater
R-35b	SA-27677	CASA-07-76693	07/15/07	828	Groundwater
R-35b	SA-27677	CASA-07-76694	07/15/07	828	Groundwater
R-35b	SA-27677	CASA-07-76695	07/15/07	828	Groundwater
R-35b	SA-27677	CASA-07-76696	07/16/07	828	Groundwater
R-35b	SA-27677	CASA-07-76697	07/16/07	828	Groundwater
R-35b	SA-27677	CASA-07-76698	07/16/07	828	Groundwater
R-35b	SA-27677	CASA-07-76699	07/16/07	828	Groundwater
R-35b	SA-27677	CASA-07-76700	07/16/07	828	Groundwater

^a Drilling water samples are from municipal water source.

^b n/a = Not applicable.

^c Sample collected during development bailing, as opposed to pumping.

**Table 6.1-1
R-35 Video and Geophysical Logging Runs**

Date	Depth (ft)	Description
R-35a		
4/24/07	107–666	Laboratory video, gamma ray, and induction tools run; 16-in. casing to 258 ft
5/11 and 5/12/07	0–1143	Schlumberger complete geophysical suite including TLD, ACS, CNT, HNGS, ECS, and cased hole formation resistivity.
6/26/07	0–1030	Zeroed at TOC; water level at 630 ft; well casing to TD; screen from 1015 to 1030+ ft.
7/15/07	0–1082	As-built. Laboratory video, gamma ray, and induction tools run. SWL at 791 ft bgs. Postdevelopment/preaquifer test; assess bentonite impact at top of sump.
R-35b		
4/11/07	560–583	Laboratory video run. 16-in. casing to 255 ft; terminated due to foam in borehole at 583 ft.
4/12/07	0–608	Laboratory video, gamma ray, and induction tools run. 16-in. casing to 255 ft; driller's TD at 615 ft; slough at 608 ft.
6/18/07	0–800	Laboratory video run to assess 10-in. casing drive shoe cut. Tremie pipe in hole; ran to 800 ft and lost image. Also ran caliper tool after pulling out tremie pipe; caliper data inconclusive.
7/30/07	0–872	As built. Laboratory video only. Standing water level at 787 ft bgs. Screen at 824 ft to 847 ft bgs. Nothing unusual noted.

**Table 7.2-1
Annular Fill Materials**

Material	Volume R-35a	Volume R-35b
Surface seal: cement slurry	240.6 ft ³	298.8 ft ³
Bentonite seal: bentonite chips	569.9 ft ³	543.0 ft ³
Bentonite seal: high solids bentonite grout	443.8 ft ³	82.9 ft ³
Upper annular seal: bentonite chips	3.34 ft ³	24.0 ft ³
Fine sand collar: 20/40 silica sand	3.0 ft ³	4.9 ft ³
Primary filter: 10/20 silica sand	38.5 ft ³	17.3 ft ³
Lower annular seal: bentonite chips	4.1 ft ³	5.42 ft ³
Backfill material: coarse 8/12 silica sand	32.3 ft ³	6.6 ft ³
Backfill material: bentonite chips	11.8 ft ³	15.1 ft ³
Potable water	19,000 gal.	11,400 gal.

**Table 8.1-1
Well Development Volumes and Associated Field Water-Quality Parameters for R-35a**

Date	pH	Temp (°C)	DO (mg/L)	ORP (mV)	Specific Conductivity (µS/cm)	Turbidity (NTU)	Purge Volume between Samples (gal.)	Cumulative Purge Volume (gal.)
7/10/07	7.79	26.13	8.65	59.2	0.393	12.7	315	2310
	7.63	25.79	6.93	16.6	0.378	7.41	420	2730
	na*	na	na	na	na	na	840	3570
7/11/07	7.8	25.98	5.25	108.6	0.324	4.91	814	4384
	7.77	26.64	6.89	97.5	0.301	4.72	1364	5748
	7.78	27.51	5.28	56.4	0.294	4.03	1276	7024
	7.78	26.37	6.84	176.4	0.29	3.54	1430	8454
	7.97	26.24	6.24	114.7	0.295	3.45	1364	9818
	7.75	26.61	5.09	169.2	0.278	2.43	1320	11138
	7.78	26.83	5.21	108.9	0.285	2.53	1276	12414
	na	na	na	na	na	na	1056	13470
7/12/07	7.02	21.22	4.22	-19.8	0.276	557	120	13590
	7.81	23.84	4.87	-29.5	0.292	25.3	144	13734
	7.81	24.84	5.7	-67.7	0.298	4.53	144	13878
	7.81	24.71	4.53	-46.1	0.295	3.72	96	13974
	7.81	25.18	4.9	-38.8	0.289	2.84	132	14106
	7.83	25.25	4.74	-62.4	0.283	3.42	120	14226
	7.83	25.24	4.2	-30.5	0.283	2.13	156	14382
	7.85	25.49	4.6	-41.1	0.283	2.62	120	14502
	7.84	25.72	4.27	-35.7	0.286	3.4	108	14610
	7.83	25.63	4.32	-26	0.286	3.1	108	14718
	7.8	25.82	4	-14.1	0.286	3.97	132	14850
	7.86	26.02	5.85	-21.5	0.284	2.37	882	15732
	7.75	25.84	5.87	20.3	0.282	1.78	252	15984
	7.8	25.83	5.78	-7.2	0.281	2.14	231	16215
	7.8	26.08	5.72	20.1	0.282	2.22	357	16572
	7.79	26.22	5.81	81.2	0.279	2.53	336	16908
	7.95	25.76	5.71	-26.2	0.282	1.97	315	17223
	7.9	25.9	5.9	-25.6	0.281	1.86	252	17475
	7.86	26.11	5.91	-21.1	0.277	1.59	273	17748
	na	na	na	na	na	na	2452	20200
7/13/07	7.52	22.71	3.6	90.5	0.293	35.6	185	20385
	7.44	24.95	5.02	46.6	0.272	1.2	1496	21881

Table 8.1-1 (continued)

Date	pH	Temp (°C)	DO (mg/L)	ORP (mV)	Specific Conductivity (µS/cm)	Turbidity (NTU)	Purge Volume between Samples (gal.)	Cumulative Purge Volume (gal.)
7/13/07	7.6	25.42	4.97	145.2	0.273	1.02	1210	23091
	7.69	25.67	4.95	96.1	0.274	1.04	1320	24411
	6.72	25.44	5.28	174.9	0.272	0.94	1320	25731
	n/a	n/a	n/a	n/a	n/a	n/a	110	25841
	7.43	25.68	4.79	96.6	0.272	1.25	1210	27051
	7.59	25.66	4.76	93.4	0.269	0.98	1320	28371
	7.46	25.87	4.72	116.8	0.27	1.02	1320	29691
	7.22	25.33	4.86	142.3	0.273	0.96	1320	31011
	na	na	na	na	na	na	220	31231
	6.87	24.67	5.42	170.6	0.272	0.93	801	32032
R-35a aquifer testing purge volumes								
7/26/07	7.66	25.52	4.92	-4.6	0.284	2.51	555	32587
	7.65	26.01	4.43	-14.4	0.281	1.08	1319	33906
	7.78	26.60	3.85	-11.9	0.284	2.91	641	34547
	7.75	25.58	3.75	-13.5	0.283	1.02	1179	35726
7/27/07	8.00	24.05	3.78	10.2	0.294	1.30	645	36371
	7.80	27.44	4.12	-22.0	0.292	0.61	5203	41574
	8.00	26.42	6.29	24.4	0.285	0.55	5160	46734
	8.17	24.53	6.75	122.4	0.283	0.54	4537	51271
	8.02	25.04	5.98	118.2	0.285	0.52	5741	57012
	8.11	22.50	8.69	167.4	0.277	0.59	5203	62215
	8.03	24.78	8.67	121.9	0.280	0.61	3225	65440

*na = Not available.

**Table 8.1-2
Well Development Volumes and Associated Field Water-Quality Parameters for R-35b**

Date	pH	Temp (°C)	DO (mg/L)	ORP (mV)	Specific Conductivity (µS/cm)	Turbidity (NTU)	Purge Volume between Samples (gal.)	Cumulative Purge Volume (gal.)
7/12/07	na ^a	na	na	na	na	na	0	0
	9.09	25.14	7.35	4.1	0.369	V.turb ^b	58	58
	9	24.83	7.95	4.1	0.371	V.turb	83	141
	8.9	24.71	7.28	-10.1	0.344	>1000	151	292
	na	na	na	na	na	na	18	310
7/13/07	7.96	23.12	6.29	127.8	0.305	>1000	341	651
	8.51	23.41	6.09	85.2	0.285	>1000	174	825
	7.88	24.42	6.21	143	0.271	>1000	160	985
	8.59	24.14	5.74	43.1	0.277	>1000	203	1188
	8.54	24.13	5.69	53.9	0.262	>1000	160	1348
	7.91	23.89	6.01	136.6	0.247	>1000	174	1522
	na	na	na	na	na	na	116	1638
	8.46	24.01	6.44	90.6	0.242	>1000	131	1769
	8.34	23.59	6.41	105.9	0.231	>1000	160	1929
	7.93	22.36	5.73	128.4	0.232	>1000	131	2060
7/15/07	8.08	25.94	7.39	115.5	0.199	29.9	1320	3380
	8.06	26.08	8.78	73.3	0.194	29.7	1210	4590
	8.02	25.55	9.05	71.3	0.188	11.2	1980	6570
	7.94	24.36	9.32	97.5	0.185	9.29	1320	7890
	7.96	24.77	9.77	109.4	0.187	8.7	1320	9210
	8.04	25.8	9.89	82.4	0.189	7.14	1320	10530
	na	na	na	na	na	na	670	11200
	7.96	22.28	10.26	137.4	0.191	7.09	1210	12410
7/16/07	7.91	23.07	10.23	120.4	0.186	5.49	660	13070
	na	na	na	na	na	na	330	13400
	8.02	23.69	10.12	112.8	0.189	5.13	225	13625
	7.96	24.23	9.91	118.6	0.19	4.44	225	13850
	7.89	24.61	9.82	114.1	0.188	4.45	375	14225
	7.97	24.68	10.02	109.4	0.191	4.24	150	14375
	8.04	24.67	9.83	100.4	0.192	4.12	150	14525
	7.95	24.86	9.67	101.2	0.191	4.14	150	14675
	7.96	25.07	8.02	101.5	0.186	3.92	300	14975
	7.95	25.09	8.04	98.6	0.191	3.85	225	15200
	7.77	24.64	9.38	106.4	0.191	4.27	150	15350
	7.99	24.68	8.41	93.5	0.191	3.86	150	15500
	7.95	24.57	8.92	97.7	0.19	4.68	195	15695

Table 8.1-2 (continued)

Date	pH	Temp (°C)	DO (mg/L)	ORP (mV)	Specific Conductivity (µS/cm)	Turbidity (NTU)	Purge Volume between Samples (gal.)	Cumulative Purge Volume (gal.)
7/16/07	7.9	24.58	9.38	95.2	0.19	3.54	180	15875
	7.91	24.84	9.92	93.7	0.191	4.36	165	16040
	7.93	24.85	9.45	88.8	0.191	3.41	195	16235
	7.97	25.29	9.66	83.1	0.191	3.89	165	16400
	8.03	25.26	7.76	60	0.191	3.64	225	16625
	na	na	na	na	na	na	195	16820
	na	na	na	na	na	na	300	17120
	8.1	26.53	8.73	4.7	0.195	9.49	352	17472
	8.04	25.32	7.51	46.8	0.191	5.25	352	17824
	7.88	25.07	8.05	60.4	0.192	4.19	132	17956
	7.95	25.36	8.04	59.6	0.191	4.98	286	18242
	7.98	25.58	8.17	58.3	0.191	4.16	242	18484
	7.96	25.41	8.85	62.8	0.191	3.91	286	18770
	8.06	25.96	8.9	56.3	0.193	6.88	264	19034
	7.99	26.01	8.63	54.3	0.192	3.57	484	19518
	8.06	26.84	7.87	36.5	0.194	5.03	660	20178
	7.95	25.49	7.59	56.7	0.193	4.19	110	20288
	7.87	26.8	6.75	44.4	0.195	5.11	990	21278
	7.72	25.17	6.6	51.1	0.188	4.3	154	21432
	7.54	24.44	6.91	66	0.191	4.81	110	21542
7.63	24.78	6.93	60.5	0.188	3.84	110	21652	
na	na	na	na	na	na	616	22268	
R-35b aquifer testing purge volumes								
7/20/07	No parameters collected						4695	26963
7/23/07	7.56	25.68	6.1	98.4	0.191	3.79	3960	30923
	7.48	26.26	5.02	60.4	0.190	1.88	3555	34478
	7.52	27.03	5.0	61.4	0.189	1.73	1102	35580
	7.96	26.55	5.2	38.4	0.190	1.66	1755	37335
	7.90	24.49	5.01	68.1	0.187	1.65	2295	39630
	7.92	23.74	5.75	86.5	0.186	2.00	2723	42353
	8.13	22.93	5.94	86.0	0.186	1.57	2677	45030
7/24/07	8.15	22.22	5.96	95.9	0.185	1.60	2677	47707
	8.16	21.80	6.05	95.8	0.186	1.67	2723	50430
	8.15	21.37	6.24	99.0	0.185	1.52	2723	53153
	8.09	21.37	na	na	0.186	2.01	2700	55853
	8.18	22.68	6.07	97.0	0.195	1.18	2362	58215

^a na = Not available.

^b V.turb = Very turbid (nephelometric reading off-scale).

**Table 8.5-1
R-35 Survey Coordinates from SW Mountain Surveys, Inc.**

North	East	Elevation	Identification
1769316.2317	1642321.7013	6623.06	R-35a brass pin embedded in pad
1769314.6401	1642327.2999	6622.68	R-35a ground surface near pad
1769314.6253	1642323.3416	6626.45	R-35a top of protective casing
1769314.1646	1642323.3674	6625.53	R-35a top of well cap
1769328.3684	1642229.8769	6625.21	R-35b brass pin embedded in pad
1769328.2203	1642228.5786	6625.11	R-35b ground surface near pad
1769326.8621	1642231.3767	6628.74	R-35b top of protective casing
1769326.3277	1642231.5953	6627.82	R-35b top of well cap

Note: Coordinates based on Los Alamos Coordinate System from B0005 and B0006.

**Table 8.6-1
Summary of Waste Samples Collected during Drilling and Development of R-35a and R-35b**

Borehole ID	Location ID	Sample ID	Date Collected	Description	Sample Type
n/a*	n/a	GW35-07-574	5/4/2007	Drum	Decon water
n/a	n/a	GW35-07-575	6/1/2007	Drum	Decon water
R35-b	WST-600902	GW35-07-6075	8/15/2007	Frac tank	Development water
R35-b	WST-600902	GW35-07-6076	8/15/2007	Frac tank	Development water
R35-b	WST-600902	GW35-07-6083	8/15/2007	Pit contents	Drilling water
R35-a	WST-600902	GW35-07-6084	8/15/2007	Pit contents	Drilling water
R35-a	WST-600902	GW35-07-6085	8/15/2007	Frac tank	Development water
R35-a	WST-600902	GW35-07-6086	8/15/2007	Frac tank	Development water
R35-a	WST-600902	GW35-07-6077	8/17/2007	Pit contents	Drill cuttings
R35-a	WST-600902	GW35-07-6078	8/17/2007	Pit contents	Drill cuttings
R35-b	WST-600902	GW35-07-6079	8/17/2007	Pit contents	Drill cuttings
R35-b	WST-600902	GW35-07-6081	8/17/2007	Pit contents	Drill cuttings

*n/a = Not applicable.

Appendix A

Lithologic Logs

Los Alamos National Laboratory
Regional Hydrogeologic Characterization Project
Borehole Lithologic Log

BOREHOLE ID: R-35a		TECHNICAL AREA (TA) 72		PAGE: 1 of 4	
DRILLING COMPANY: Boart Longyear		START DATE/TIME: 4/13/07:0830		END DATE/TIME: 5/10/07:1550	
DRILLING METHOD: Dual Rotary		MACHINE: Foremost DR-24 HD		SAMPLING METHOD: Grab	
GROUND ELEVATION: 6622.68 ft above mean sea level (amsl)				TOTAL DEPTH (TD): 1143 ft below ground surface (bgs)	
DRILLERS: G. Borton/J. Staloch/A. Soto			SITE: S. White/P. Baucom		
DEPTH (ft)	LITHOLOGY		LITHOLOGIC SYMBOL	Notes	
0–20	<p>ALLUVIUM: Pale yellowish brown (10 YR 6/2) Sand and silt. Clasts are moderately rounded to subangular Bandelier Tuff and minor intermediate lavas. Matrix consists of fine-grained ash and silt. Predominately quartz, feldspar, and sanidine grains, ~3%–5% lithics and pumice fragments.</p>		Qal	<p>Quaternary alluvium: (0–45 ft bgs) 15–20 ft bgs: Increase of pumice fragments in 35+ fraction to ~50%</p>	
20–45	<p>Pale yellowish brown to grayish orange pink (10 YR 6/2 to 5 YR 7/2). All other aspects are same as above.</p>				
45–60	<p>OTOWI MEMBER OF BANDELIER TUFF: Grayish orange pink (5 YR 7/2) Poorly welded lithic-rich volcanic tuff. Pumice fragments are up to 10 mm. Lithic fragments are ~35%–45% overall of fines-depleted cuttings, predominantly volcanic clasts. Pumice is vitric. 10+ fraction: Vitric pumice with ~30% lithics 35+ fraction: Vitric pumice with ~50% quartz and sanidine grains and 20%–25% lithics</p>		Qbo	<p>Otowi Member of Bandelier Tuff: (45–200 ft bgs)</p>	
60–80					
80–140	<p>80 ft bgs: Lithic component increases to ~50% of fines-depleted cuttings. Lithics are dark volcanic fragments.</p>				
140–200	<p>140–200 ft bgs: Discoloration is evident. Whole rock color changes to moderate reddish brown (10R 4/6).</p>				
200–220	<p>GUAJE PUMICE BED: Grayish orange pink (5 YR 7/2) Vitric nonwelded tuff with ~85%–90% vitric pumice (up to 15 mm) and ~15% lithics. Lithics are predominately volcanic, including basalt and rhyodacite. Some fine-grained ash matrix was recovered. 35+ fraction: ~12% quartz and sanidine grains were noted in 35+ fraction.</p>		Qbog	<p>Guaje Pumice Bed: (200–220 ft bgs)</p>	

Borehole Lithologic Log (continued)

BOREHOLE ID: R-35a		TA-72		PAGE: 2 of 4	
DEPTH (ft)	LITHOLOGY	LITHOLOGIC SYMBOL	Notes		
220–256	<p>PUYE FORMATION: Grayish orange to moderate yellowish brown (10 YR 7/4 to 10 YR 5/4)</p> <p>Fine-grained ash and silt matrix. Sandy fine-to-coarse volcanoclastics. Larger clasts are subrounded. Volcanic clasts include andesite, dacite, rhyolite, pumice, and basalt, ~4% quartz and sanidine crystals. Some olivine was also noted.</p>	Tpf	Puye Formation: (220–256 ft bgs)		
256–580	<p>CERROS DEL RIO BASALT: Medium dark gray to dark gray (N4 to N3)</p> <p>Numerous dense massive lava flows are separated by (blocky) interflow breccias. Variably vesicular basalt. ~2% olivine, plagioclase and pyroxene phenocrysts. Slight clay coating.</p>	Tb4	Cerros del Rio basalt: (256–602 ft bgs)		
560–602	580 ft bgs: Basalt is slightly vesicular.				
602–685	<p>PUYE FORMATION: Medium light gray to light brownish gray (N6 + 54 R 6/1)</p> <p>Poorly sorted unconsolidated volcanoclastic sediments. Medium- to coarse-grained, subangular to angular sand and gravel pieces with trace silt. Some subrounded sand and gravel are also present. Gravel consists of 95%–100% volcanic lithics including rhyolite, dacite, andesite, minor basalt, pumice, and rhyodacite. Sand is slightly more mafic with minor quartz.</p> <p>35+ fraction: Dacite, rhyodacite, andesite, minor basalt, tuff fragments, and pumice, ~3% quartz</p>	Tpf	Puye Formation: (602–880 ft bgs)		
685–720	685 ft bgs: Sand component is more quartz-rich (<5%) medium to very coarse-grained. Slightly more gravel-sized pumice is present.		More silt was noted during sieving.		

Borehole Lithologic Log (continued)

BOREHOLE ID: R-35a		TA-72		PAGE: 3 of 4	
DEPTH (ft)	LITHOLOGY	LITHOLOGIC SYMBOL	Notes		
720–785	<p>PUYE FORMATION: Medium light gray to light brownish gray (N6 + 54 R 6/1)</p> <p>Pumice increasing: ~15% pumice fragments in whole rock sample</p> <p>10+ fraction: 15%–20% pumice</p> <p>35+ fraction: 20% pumice</p>	Tpf	720–730 ft bgs: Pumiceous interval		
785–830	785 ft bgs: Increase in fine sand and silt in whole rock sample, silt coats larger gravels. Gravels: coarse-grained porphy. Phenocrysts identified in whole rock and 10+ fraction include feldspar, biotite, amphibole, and quartz.				
830–840	830–840 ft bgs: Gravels more rounded to subrounded. Also whole rock color is mottled: light and medium gray to reddish brown.				
840–880	Gravels are angular to subrounded.				
880–900	<p>SANTA FE GROUP VOLCANIC SEDIMENTS: Unconsolidated pumice-rich volcanoclastic sands and gravels</p> <p>Sands: 35%–40% pumice; gravel: 20%–25% pumice</p> <p>Pumice fragments are white, aphyric, <0.5 cm, and subrounded. Whole rock and 10+ fraction: 50%–65% pumice 35+ fraction, 80%–85% pumice.</p> <p>Remaining composition: Intermediate to felsic volcanic lithics included rhyolite, dacite, andesite, and trace basalt.</p> <p>Fines: 2% quartz compared with sand (35+ fraction); trace silt and ash</p>	Tsfu	<p>Santa Fe Group volcanic sediments: (880–900 ft bgs)</p> <p>895 ft bgs: Pumice is less abundant.</p>		
900–935	<p>SANTA FE GROUP RIVER GRAVELS: Unconsolidated gravels and sands</p> <p>Well-rounded to subrounded gravels and sands with trace silt. Gravels consist of 20%–30% volcanic clasts (andesite, basalt, rhyolite, pumice, minor dacite) and 70%–80% other (quartzite [5%], rounded river rock, conglomerate [little], sandstone [trace], siltstone, chert). Sand is very coarse to coarse-grained.</p>	Tsfu	Santa Fe Group river gravels: (900–935 ft bgs)		
935–950	<p>SANTA FE GROUP VOLCANIC SEDIMENTS: Unconsolidated volcanoclastic sands and gravels with minor silt</p> <p>Subangular to subrounded gravels and sands consisting of 80%–90% intermediate to mafic volcanic rock fragments and 10%–20% other (pumice, siltstone [trace]). Sand is poorly sorted. Rounded gravels are rare.</p>	Tsfu	Santa Fe Group volcanic sediments: (935–1136 ft bgs)		

Borehole Lithologic Log (continued)

BOREHOLE ID: R-35a		TA-72		PAGE: 4 of 4	
DEPTH (ft)	LITHOLOGY	LITHOLOGIC SYMBOL	NOTES		
950–965	SANTA FE GROUP VOLCANIC SEDIMENTS: 950 ft bgs: Appearance of rhyolite clasts with white feldspar phenocrysts	Tsfu	Santa Fe Group volcanic sediments: (935–1136 ft bgs)		
965–985	965 ft bgs: Increase in pumice fragments 35+ fraction: 10%. Whole rock and 10+ fraction: 7%.				
985–1000	985 ft bgs: Fines well preserved in whole rock sample (up to 30% silt, fine sand, and clay) 985–990 ft bgs: Abundant white pumice		985–990 ft bgs: Pumiceous interval		
1000–1035	1000 ft bgs: Less silt and fines in whole rock sample. Pumice content is also less (5% overall). 1000–1010 ft bgs: Appearance of gravel-sized red-brown tuffaceous sandstone; abundant in 35+ fraction				
1035–1040	1035 ft bgs: Fines well preserved in whole rock (50% silt and fine sand with minor clay; 50% poorly sorted medium to very coarse sands, pumice [10%], and intermediate volcanic rock fragments [5%]). Pumice and rock fragments appear weathered.				
1040–1045	1040 ft bgs: Interval coarser-grained. Little sand or silt is in whole rock sample.				
1045–1070	1045 ft bgs: Gravels and sands are pumice and tuff-rich. Volcanic lithics are still present but are less abundant than in above sections.		1045–1070 ft bgs: Tuff and pumice-rich interval 1060–1065: Bucket grab sample		
1070–1100	Fines well preserved in whole rock sample (dominantly silt). Sands and gravels include intermediate and felsic volcanic rock fragments, tuffaceous sandstone, and white pumice (10% in 35+ fraction).				
1095–1100	1095 ft bgs: Tuffaceous sandstone clasts dominant		1095–1100 ft bgs: Tuffaceous sandstone clasts dominant		
1100–1136	Increasingly mafic-rich: Subrounded to subangular basalt lithics-dominant volcanic rock fragment. Percentage increases with depth (up to 50%). Andesite and rhyolite fragments are still present; ~5% pumice (35+ fraction).		Potential thin soil (paleosol) horizon between 1135 and 1140 ft bgs		
1136–1143 (TD)	MIOCENE BASALT: Olivine-rich crystalline basalt. Groundmass is coarsely crystalline.	Tb2	Miocene basalt: 1136–1143 ft bgs (TD) Basaltic rubble between 1136 and 1141 ft bgs Top of solid basalt at 1141 ft bgs		

**Los Alamos National Laboratory
Regional Hydrogeologic Characterization Project
Borehole Lithologic Log**

BOREHOLE ID: R-35b		TA-72		PAGE: 1 of 3	
DRILLING COMPANY: Boart Longyear		START DATE/TIME: 3/30/07:1055		END DATE/TIME: 5/20/07:1300	
DRILLING METHOD: Dual Rotary		MACHINE: Foremost DR-24 HD		SAMPLING METHOD: Grab	
GROUND ELEVATION: 6625.11 FT AMSL				TOTAL DEPTH: 897.6 ft bgs	
DRILLERS: G. Borton/J. Staloch/A. Soto			SITE GEOLOGIST: S. White/P. Baucom		
DEPTH (ft)	LITHOLOGY		LITHOLOGIC SYMBOL	Notes	
0–20	<p>ALLUVIUM: Pale yellowish brown (10 YR 6/2) Sand and silt. Clasts moderately rounded to subangular Bandelier Tuff and minor intermediate lavas. Matrix consists of fine-grained ash and silt. Predominately quartz, feldspar, and sanidine grains, ~3%–5% lithics and pumice fragments.</p>		Qal	<p>Quaternary alluvium: (0–45 ft bgs) 15–20 ft bgs: Increase of pumice fragments in 35+ fraction to ~50%</p>	
20–45	<p>Pale yellowish brown to grayish orange pink (10 YR 6/2 to 5 YR 7/2). All other aspects same as above.</p>				
45–80	<p>OTOWI MEMBER OF BANDELIER TUFF: Grayish orange pink (5 YR 7/2) Poorly welded lithic-rich volcanic tuff. Pumice fragments are up to 10 mm. Lithic fragments are ~35%–45% overall of fines-depleted cuttings, predominantly volcanic clasts. Pumice is vitric. 10+ fraction: Vitric pumice with ~30% lithics 35+ fraction: Vitric pumice with~ 50% quartz and sanidine grains and 20%-25% lithics</p>		Qbo	<p>Otowi Member of Bandelier Tuff: (45–200 ft bgs)</p>	
80–140	<p>80 ft bgs: Lithic component increases to ~50% of fines-depleted cuttings. Lithics are dark volcanic fragments.</p>			<p>Little recovery from 135 to 140 ft bgs; whole rock only</p>	
140–200	<p>140–200 ft bgs: Discoloration is evident. Whole rock color changes to moderate reddish brown (10R 4/6).</p>			<p>No recovery from 155 to 160 ft bgs</p>	
200–220	<p>GUAJE PUMICE BED: Grayish orange pink (5 YR 7/2) Vitric nonwelded tuff with ~85%–90% vitric pumice (up to 15 mm) and ~15% lithics. Lithics predominately volcanic, including basalt and rhyodacite. Some fine-grained ash matrix recovered. 35+ fraction: ~12% quartz and sanidine grains were noted in 35+ fraction.</p>		Qbog	<p>Guaje Pumice: (195–220 ft bgs)</p>	

Borehole Lithologic Log (continued)

BOREHOLE ID: R-35b		TA-72	PAGE: 2 of 3	
DEPTH (ft)	LITHOLOGY	LITHOLOGIC SYMBOL	NOTES	
220–264	<p>PUYE FORMATION: Grayish orange to moderate yellowish brown (10 YR 7/4 to 10 YR 5/4)</p> <p>Fine-grained ash and silt matrix. Sandy fine-to-coarse volcanics. Larger clasts are subrounded. Volcanic clasts include andesite, dacite, rhyolite, pumice, basalt, ~4% quartz and sanidine crystals. Some olivine was also noted.</p>	Tpf	Puye Formation: (220–264 ft bgs)	
264–400	<p>CERROS DEL RIO BASALT: Medium dark gray to dark gray (N4 to N3).</p> <p>Numerous dense massive lava flows are separated by (blocky) interflow breccias. Variably vesicular basalt is ~2% olivine, plagioclase, and pyroxene phenocrysts. Slight clay coating.</p>	Tb4	Cerros del Rio basalt: (256–602 ft bgs)	
400–485	<p>380 ft bgs: Basalt is slightly less vesicular than above.</p> <p>No recovery</p>		320–340 ft bgs: Possible iddingsite phenocrysts were noted; possible alteration.	
485–602	<p>485 ft bgs: Basalt massive. Clay coating is heavier than in above sections.</p>		400–485: Interval of lost circulation. Driller reports void between 400 and 402 ft bgs.	
	<p>580 ft bgs: Basalt, slightly vesicular</p>		485–505: Circulation returns sporadically.	
			530–535 ft bgs: Only whole rock recovery	
			No recovery from 600 to 605 ft bgs	
602–680	<p>PUYE FORMATION: Medium light gray to light brownish gray (N6 + 54 R 6/1)</p> <p>Poorly sorted unconsolidated volcanoclastic sediments. Medium- to coarse-grained, subangular to angular sand and gravel pieces with trace silt. Some subrounded sand and gravel also present. Gravel consists of 95%–100% volcanic lithics including rhyolite, dacite, andesite, minor basalt, pumice, and rhyodacite. Sand is slightly more mafic with minor quartz.</p> <p>35+ fraction: Dacite, rhyodacite, andesite, minor basalt, tuff fragments, and pumice ~3% quartz</p>	Tpf	Puye Formation: (602–880 ft bgs)	
680–720	<p>685 ft bgs: Sand component is more quartz-rich (<5%) medium to very coarse-grained. Slightly more gravel-sized pumice is present.</p>		More silt was captured during sampling.	

Borehole Lithologic Log (continued)

BOREHOLE ID: R-35b		TA-72	PAGE: 3 of 3	
DEPTH (ft)	LITHOLOGY	LITHOLOGIC SYMBOL	Notes	
720–730	PUYE FORMATION: Medium light gray to light brownish gray (N6 + 54 R 6/1)	Tpf	720–730 ft bgs: Pumiceous interval	
730–785	Pumice increasing. ~15% pumice fragments in whole rock sample 10+ fraction: 15%–20% pumice 35+ fraction: 20% pumice			
785–830	785 ft bgs: Increase in fine sand and silt in whole rock sample, silt coats larger gravels. Gravels: coarse-grained porphy. Phenocrysts identified in whole rock and 10+ fraction include feldspar, biotite, amphibole, and quartz.		800–805: Bucket grab sample 820–825: Bucket grab sample	
830–880	830–840 ft bgs: Gravels are more rounded to subrounded. Also whole rock color is mottled: light and medium gray to reddish brown.		840–845: Bucket grab sample 860–865: Bucket grab sample	
880–897.6 (TD)	SANTA FE GROUP VOLCANIC SEDIMENTS: Unconsolidated pumice-rich volcanoclastic sands and gravels Sands: 35%–40% pumice. Gravel: 20%–25% pumice. Pumice fragments are white, aphyric, <0.5 cm, and subrounded. Whole rock and 10+ fraction: 50%–65% pumice 35+ fraction: 80%–85% pumice. Remaining composition: Intermediate to felsic volcanic lithics including rhyolite, dacite, andesite, and trace basalt. Fines: 2% quartz (35+ fraction); trace silt and ash	Tsfu	880–897.6: Santa Fe Group volcanic sediments. 897.6: TD	

Appendix B

Groundwater Analytical Results

B-1.0 SAMPLING AND ANALYSIS OF GROUNDWATER AT R-35a AND R-35b

A total of 18 screening samples were collected from the regional aquifer during drilling at R-35a at 40-ft intervals ranging from 760 to 840 ft below ground surface (bgs) (3 samples) and at 20-ft intervals ranging from 840 to 1140 ft bgs (15 samples). Eight screening samples were collected during drilling at R-35b at 10-ft intervals ranging from 815 to 890 ft bgs. The borehole water samples were air-lifted to the surface. At the time of sample collection, the drill casing was positioned at the indicated depth provided in Tables B-1.0 and B-2.0 (see Attachment 1, Appendix Data Files and Images, on enclosed CD), and it is assumed that the water samples obtained came primarily from that depth. Additional screening-groundwater samples were collected during development and pumping at each completed well. The samples were analyzed for cations, anions, perchlorate, and metals. During drilling, 10 water samples were also submitted for total organic carbon (TOC) analyses. During pumping of wells R-35a and R-35b, a total of 29 samples was analyzed for TOC and inorganic chemicals.

B-1.1 Field Preparation and Analytical Techniques

Chemical analyses of screening-groundwater samples were performed at Los Alamos National Laboratory's (LANL's, or the Laboratory's) Earth and Environmental Sciences Group 6. Groundwater samples were filtered before analysis for metals, trace elements, and major cations and anions. Aliquots of samples collected from R-35a and R-35b were filtered through 0.22- μm Millex filters (Tables B-1, B-3, and B-4; see Attachment 1, Appendix Data Files and Images, on enclosed CD). Eight samples collected from borehole R-35b were filtered through 0.02- μm Whatman filters to remove colloidal material (Table B-2; see Attachment 1, Appendix Data Files and Images, on enclosed CD). Samples were acidified with analytical-grade nitric acid to a pH of 2.0 or less for metal and major cation analyses. Total carbonate alkalinity was measured using standard titration techniques. Samples collected for TOC analysis were not filtered.

Groundwater samples were analyzed using techniques specified in the U.S. Environmental Protection Agency SW-846 manual. Ion chromatography was the method used for bromide, chloride, fluoride, nitrate, nitrite, oxalate, chlorate, perchlorate, phosphate, and sulfate analysis. The instrument detection limit for perchlorate was 0.002 parts per million (ppm). Inductively coupled (argon) plasma optical emission spectroscopy (ICPOES) was used for analyses of calcium, magnesium, potassium, silica, and sodium. Aluminum, antimony, arsenic, barium, beryllium, boron, cadmium, cesium, chromium, cobalt, copper, iron, lead, lithium, manganese, mercury, molybdenum, nickel, rubidium, selenium, silver, thallium, thorium, tin, vanadium, uranium, and zinc were analyzed by inductively coupled (argon) plasma mass spectrometry (ICPMS). The precision limits (analytical error) for major ions and trace elements were generally less than $\pm 10\%$ using ICPOES and ICPMS. Charge balance errors for dissolved cations and anions were generally less than $\pm 10\%$ for complete analyses of the above inorganic solutes provided in Tables B-1 through B-4 (see Attachment 1, Appendix Data Files and Images, on enclosed CD).

B-1.2 Analytical Results for Borehole Screening Samples

Analytical results for screening-groundwater samples collected at boreholes R-35a and R-35b are provided in Tables B-1 and B-2, respectively (see Attachment 1, Appendix Data Files and Images, on enclosed CD). Figure B-1.2-1 shows dissolved concentrations of boron, chloride, molybdenum, nitrate(N), sodium, and sulfate versus depth at boreholes R-35a and R-35b. Concentrations of these solutes are far below state and federal regulatory standards for groundwater and drinking water. Concentrations of chloride, molybdenum, nitrate(N), sodium, and sulfate at the two boreholes exceed Laboratory background within the regional aquifer (LANL 2007, 095817). The upper tolerance limits (UTLs) for

chloride, molybdenum, nitrate(N), sodium, and sulfate in the regional aquifer are 3.75 mg/L, 3.82 µg/L, 0.75 mg/L, 28.55 mg/L, and 6.22 mg/L, respectively (LANL 2007, 095817). The highest dissolved concentration of molybdenum (349 µg/L) occurred at a depth of 840 ft bgs at borehole R-35a (Figure B-1.2-1, Table B-1 [table in Attachment 1, Appendix Data Files and Images, on enclosed CD]). At borehole R-35b, the highest dissolved concentration of molybdenum (160 µg/L) occurred at a depth of 830 ft bgs (Figure B-1.2-1, Table B-2 [table in Attachment 1, Appendix Data Files and Images, on enclosed CD]). Concentrations of boron at boreholes R-35a and R-35b are within Laboratory background for the regional aquifer. Total dissolved concentrations of detectable chromium ranged from 0.001 to 0.002 ppm at boreholes R-35a and R-35b (Tables B-1 and B-2; see Attachment 1, Appendix Data Files and Images, on enclosed CD). Concentrations of TOC ranged from 8.17 to 48.2 mg/L and from 8.13 to 43.1 mg/L at boreholes R-35a and R-35b, respectively (Tables B-1 and B-2; see Attachment 1, Appendix Data Files and Images, on enclosed CD). Concentrations of nitrate(N) ranged from 0.445 to 1.288 mg/L and from 0.818 to 1.816 mg/L at boreholes R-35a and R-35b, respectively (Tables B-1 and B-2; see Attachment 1, Appendix Data Files and Images, on enclosed CD). Concentrations of perchlorate were less than detection (<0.002 ppm) at boreholes R-35a and R-35b.

B-1.3 Analytical Results for Screening Samples Collected during Well Development

Analytical results for screening groundwater samples collected during well development at R-35a and R-35b are provided in Tables B-3 and B-4, respectively (see Attachment 1 Appendix Data Files and Images, on enclosed CD). During well development, groundwater-screening samples were collected from a submersible pump consisting of a mild-steel discharge pipe equipped with a standard submersible pump. The discharge rate was approximately 22 gal./min.

B-1.3.1 Well R-35a

During well construction of R-35a, bentonite was discovered in the well at a depth of 1059.7 ft bgs near the bottom of the screen interval. Most of the bentonite was physically removed during well development by using a split-barrel sampler and bailer, allowing extraction of most of the bentonite. Continued well development and aquifer testing at R-35a have enhanced removal of bentonite as evidenced by concentration decreases of exchangeable cations and anions.

Analytical results obtained from pumping well R-35a were evaluated for the presence of residual bentonite, following geochemical protocols established by the Laboratory (LANL 2007, 096330) and approved by the New Mexico Environment Department. Groundwater samples analyzed from well R-35a passed the Laboratory well screen test (a single score of 79.1% for the combined 14 samples), consisting of 28 criteria for this particular test. Based on this evaluation, it is not likely that residual bentonite is impacting the water chemistry at R-35a. Excessive concentrations of barium, total carbonate alkalinity, chloride, iron, and sulfate contributed to 20.9% of the combined 14 samples that failed several criteria of the Laboratory well screen test. All 14 samples failed the dissolved barium criterion; 13 samples failed the dissolved iron criteria; and 12 samples failed the total carbonate alkalinity, chloride, and sulfate criteria. Dissolved concentrations of total carbonate alkalinity, barium, and iron increased during pumping. This increase probably related to in situ groundwater chemistry as fresh groundwater is drawn to the pumping well. Chloride and sulfate are contaminants within Sandia Canyon at R-35a and R-35b.

Sodium and sulfate are the dominant major solutes associated with ion-exchange processes involving bentonite. These two analytes are used to evaluate removal efficiency of bentonite from the filter pack during pumping at well R-35a. Concentrations of these two solutes significantly decreased during well development at R-35a (Table B-3; see Attachment 1, Appendix Data Files and Images, on enclosed CD), suggesting that residual bentonite was removed from the well during pumping. Concentrations of sodium

and sulfate also approached Laboratory background UTL values for the regional aquifer (LANL 2007, 095817). Figure B-1.3-1 shows dissolved concentrations of sodium, sulfate, and silica during pumping of well R-35a. Concentrations of sodium decreased from 41.4 to 20.1 ppm (Table B-3; see Attachment 1, Appendix Data Files and Images, on enclosed CD) and approached the average concentration of 17.05 ppm measured at the borehole from 1000 to 1060 ft bgs before the introduction of bentonite at R-35a. During drilling, concentrations of dissolved sodium ranged from 15.2 to 18.2 ppm within this depth interval during drilling (Table B-1; see enclosed on CD). This depth interval overlaps with the screen interval of 1010 to 1050 ft bgs at well R-35a. During most of the pumping, concentrations of sodium were less than the background UTL of 28.55 mg/L for the regional aquifer (LANL 2007, 095817).

Concentrations of sulfate decreased from 66.9 to 8.17 ppm during pumping of the well (Table B-3; see Attachment 1, Appendix Data Files and Images, on enclosed CD) and approached the average concentration of 6.76 ppm measured at the borehole from 1000 to 1060 ft bgs (Table B-1; see Attachment 1, Appendix Data Files and Images, on enclosed CD). Concentrations of sulfate ranged from 6.04 to 7.34 ppm within this depth interval (Table B-1; see Attachment 1, Appendix Data Files and Images, on enclosed CD). Concentrations of sulfate were slightly greater than the background UTL of 6.22 mg/L for the regional aquifer (LANL 2007, 095817).

The regional aquifer contains varying dissolved concentrations of silica resulting from partial dissolution of volcanic ash (glass) and sedimentary amorphous silica phases. Concentrations of dissolved silica generally increased from 73 to 84.5 ppm during pumping of well R-35a (Table B-2; see Attachment 1, Appendix Data Files and Images, on enclosed CD) and exceeded the average concentration of 44.2 ppm measured at the borehole from 1000 to 1060 ft bgs (Table B-1; see Attachment 1, Appendix Data Files and Images, on enclosed CD). The increase in silica concentrations during pumping is probably representative of in situ conditions within the regional aquifer independent of well construction at R-35a. Concentrations of dissolved silica ranged from 31.7 to 66.4 ppm within this depth interval (Table B-1; see Attachment 1, Appendix Data Files and Images, on enclosed CD). During pumping of well R-35a, concentrations of dissolved silica were less than the background UTL of 98.98 mg/L for the regional aquifer (LANL 2007, 095817) (Figure B-1.3-1).

Figure B-1.3-2 shows dissolved concentrations of vanadium and zinc during pumping of well R-35a. These ions undergo adsorption/desorption reactions with bentonite, and they are also used to evaluate the removal efficiency of bentonite from the filter pack at R-35a. A fraction of vanadium and zinc concentrations measured during pumping probably results from the introduction of bentonite during well construction, in addition to predrilling concentrations. Concentrations of zinc are far below state and federal groundwater and drinking water standards. There are no groundwater and drinking water standards for vanadium. Concentrations of vanadium varied from 0.005 to 0.018 ppm (5 to 18 parts per billion [ppb]) during pumping of the well (Table B-3; see Attachment 1, Appendix Data Files and Images, on enclosed CD) and exceeded the average concentration of 0.00375 ppm (3.75 ppb) measured at borehole R-35a from 1000 to 1060 ft bgs (Table B-1; see Attachment 1 on enclosed CD) before the introduction of bentonite. Concentrations of vanadium ranged from 0.002 to 0.006 ppm (2 to 6 ppb) within this depth interval of the borehole (Table B-1; see Attachment 1, Appendix Data Files and Images, on enclosed CD). During pumping of well R-35a, concentrations of vanadium were less than the background UTL of 25.58 $\mu\text{g/L}$ for the regional aquifer (LANL 2007, 095817). Concentrations of zinc fluctuated between 0.004 and 0.077 ppm (4 and 77 ppb) during pumping (Table B-3; see Attachment 1, Appendix Data Files and Images, on enclosed CD) and exceeded the average concentration of 0.001 ppm (1 ppb) measured at the borehole from 1000 to 1060 ft bgs (Table B-1; see Attachment 1, Appendix Data Files and Images, on enclosed CD) before the introduction of bentonite. Concentrations of zinc ranged from <0.001 to 0.001 ppm (<1 to 1 ppb) within this depth interval (Table B-1; see Attachment 1, Appendix Data Files and Images, on enclosed CD). During pumping of well R-35a, concentrations of zinc exceeded the background median concentration of 1.92 $\mu\text{g/L}$ for the regional aquifer (LANL 2007, 095817).

B-1.3.2 Well R-35b

Because no bentonite was displaced during well construction of R-35b, analytical results from well R-35b were not evaluated for the presence of residual bentonite following geochemical protocols established by the Laboratory (LANL 2007, 096330). Analytical results for R-35b obtained during development generally reflect site conditions during drilling. Turbidity values exceeding 1000 nephelometric turbidity units (NTUs), however, were measured during initial development that decreased to less than 5 NTUs because 13,850 gal. of the total 22,268 gal. was pumped from R-35b. Higher dissolved concentrations of metal-trace elements and major ions were observed in samples associated with early stages of pumping at R-35b. Concentrations of solutes analyzed during mid- to late stages of pumping (Table B-4; see Attachment 1, Appendix Data Files and Images, on enclosed CD) were in agreement with the borehole water samples collected from R-35b (Table B-2; see Attachment 1, Appendix Data Files and Images, on enclosed CD).

Wells R-35a and R-35b are downgradient of treated sewage effluent released from the Laboratory since the early 1950s (LANL 2006, 094161). This effluent contains organic and inorganic carbon, including total carbonate alkalinity in the form of bicarbonate. Concentrations of bicarbonate generally increased from 127 to 150 ppm during pumping of R-35a (Table B-3; see Attachment 1, Appendix Data Files and Images, on enclosed CD) and were greater than the average concentration of 125 ppm measured in borehole R-35a from 1000 to 1060 ft bgs (Table B-1; see Attachment 1). Concentrations of bicarbonate ranged from 109 to 141 ppm within this depth interval (Table B-1; see Attachment 1, Appendix Data Files and Images on enclosed CD). Concentrations of bicarbonate were greater than the UTL (109 mg/L) for the regional aquifer (LANL 2007, 095817) during pumping of well R-35a.

Well development and aquifer testing were conducted at R-35b on July 12–13 and July 15–16, 2007. During initial testing conducted on July 12 and 13, stagnant water was removed from the well, with turbidity values exceeding 1000 NTUs (Table B-4; see Attachment 1, Appendix Data Files and Images, on enclosed CD). Dissolved concentrations of selected major ions and trace elements were the highest during the first 2 d of pumping. These most notably include dissolved concentrations of aluminum, arsenic, bicarbonate, chloride, total chromium, iron, phosphate, sodium, sulfate, and TOC (Table B-4; see Attachment 1, Appendix Data Files and Images, on enclosed CD). After this initial period of pumping, dissolved concentrations of most of the major ions and trace elements decreased and generally were less variable during the remainder of pumping (Table B-4; see Attachment 1, Appendix Data Files and Images, on enclosed CD). Interestingly, dissolved concentrations of barium, calcium, magnesium, manganese, and strontium were lower during initial pumping in comparison to values measured during later periods of pumping (Table B-4; see Attachment 1, Appendix Data Files and Images, on enclosed CD).

B-1.4 Analytical Results for Aquifer Performance Testing at R-35a

Results of chemical analyses for eight groundwater samples collected during the pumping-aquifer performance test at R-35a are provided in Table B-5 (see Attachment 1 enclosed on CD). Cation-anion charge balances ranged from –5% to –1% for the samples, indicating a slight excess of dissolved anions. All groundwater samples were filtered through 0.2- μ m membranes to remove most colloidal material, possibly excluding ferric hydroxide. Concentrations of iron in filtered samples ranged from 0.26 to 0.64 ppm (Table B-5; see Attachment 1, Appendix Data Files and Images, on enclosed CD).

Extraction of groundwater at R-35a during the pumping test enhanced additional removal of any potential residual bentonite from the well. Concentrations of chloride, iron, sodium, and sulfate analyzed during the pumping test (Table B-5; see Attachment 1, Appendix Data Files and Images, on enclosed CD) were less

than those measured during well development at R-35a (Table B-4; see Attachment 1, Appendix Data Files and Images, on enclosed CD). Concentrations of regulated chemicals are far below state and federal groundwater and/or drinking water standards. Dissolved concentrations of chloride and sulfate generally decreased during the pumping test, ranging from 9.83 to 8.55 ppm and from 10 to 7.21 ppm, respectively. Dissolved concentrations of sodium fluctuated between 18.4 and 23.1 ppm (Table B-5; see Attachment 1, Appendix Data Files and Images, on enclosed CD). Dissolved concentrations of vanadium, however, generally increased during the pumping test, ranging from 0.015 to 0.032 ppm. Dissolved concentrations of zinc fluctuated between 0.009 and 0.018 ppm. Total dissolved concentrations of chromium generally increased during pumping, ranging from 0.002 to 0.006 ppm (Table B-5; see Attachment 1, Appendix Data Files and Images, on enclosed CD). Interestingly, dissolved concentrations of detectable molybdenum varied slightly (0.001 to 0.002 ppm) and were much lower than concentrations measured during drilling (0.009 to 0.349 ppm) (Table B-1; see Attachment 1, Appendix Data Files and Images, on enclosed CD). Concentrations of TOC varied between 0.40 and 0.74 ppm. Dissolved concentrations of perchlorate were less than analytical detection (<0.005 ppm) using the ion chromatography method.

B-2.0 REFERENCES

The following list includes all documents cited in this appendix. Parenthetical information following each reference provides the author(s), publication date, and ER ID number. This information is also included in text citations. ER ID numbers are assigned by the Environmental Programs Directorate's Records Processing Facility (RPF) and are used to locate the document at the RPF and, where applicable, in the master reference set.

Copies of the master reference set are maintained at the NMED Hazardous Waste Bureau; the U.S. Department of Energy—Los Alamos Site Office; the U.S. Environmental Protection Agency, Region 6; and the Directorate. The set was developed to ensure that the administrative authority has all material needed to review this document, and it is updated with every document submitted to the administrative authority. Documents previously submitted to the administrative authority are not included.

LANL (Los Alamos National Laboratory), October 2006. "Mortandad Canyon Investigation Report," Los Alamos National Laboratory document LA-UR-06-6752, Los Alamos, New Mexico. (LANL 2006, 094161)

LANL (Los Alamos National Laboratory), May 2007. "Groundwater Background Investigation Report, Revision 3," Los Alamos National Laboratory document LA-UR-07-2853, Los Alamos, New Mexico. (LANL 2007, 095817)

LANL (Los Alamos National Laboratory), May 2007. "Well Screen Analysis Report, Revision 2," Los Alamos National Laboratory document LA-UR-07-2852, Los Alamos, New Mexico. (LANL 2007, 096330)

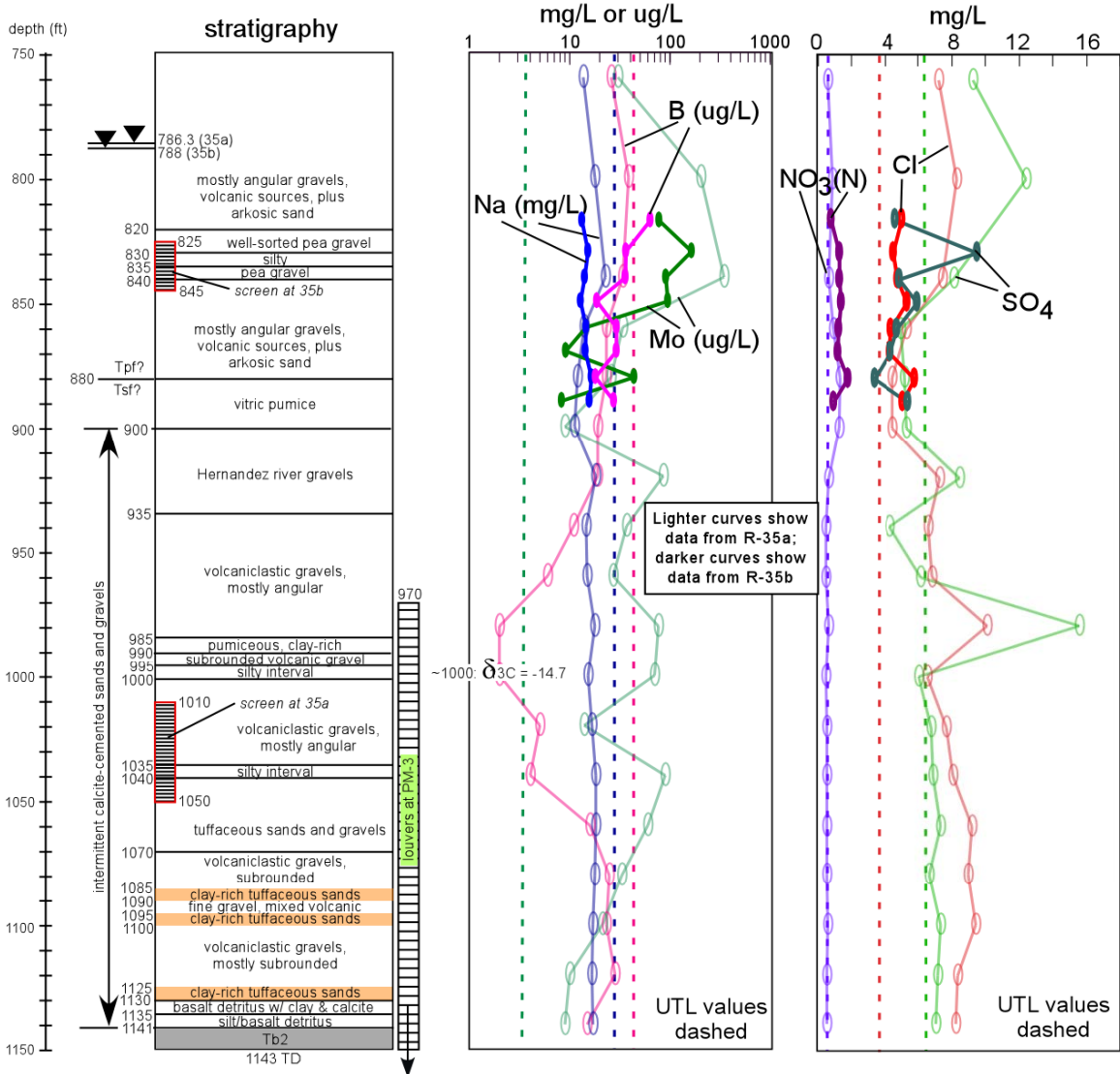


Figure B-1.2-1 Hydrostratigraphy and concentrations of boron (B), chloride (Cl), molybdenum (Mo), nitrate(N) (NO₃(N)), sodium (Na), and sulfate (SO₄) at boreholes R-35a and R-35b, Sandia Canyon, New Mexico. (UTL means upper tolerance limit for background solute concentrations within the regional aquifer.)

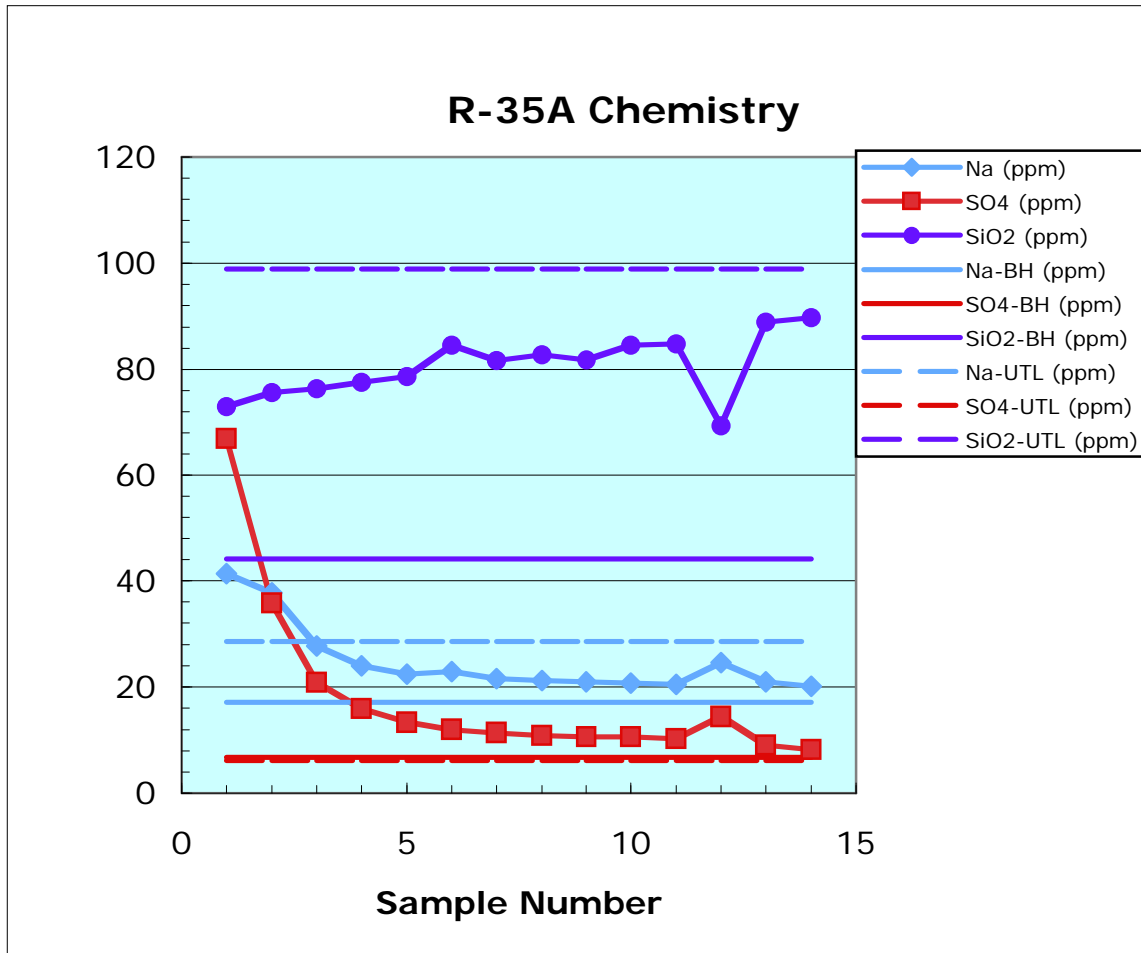


Figure B-1.3-1 Dissolved concentrations of sodium (Na), sulfate (SO₄), and silica (SiO₂) versus sample number collected during development at well R-35a, Sandia Canyon, New Mexico

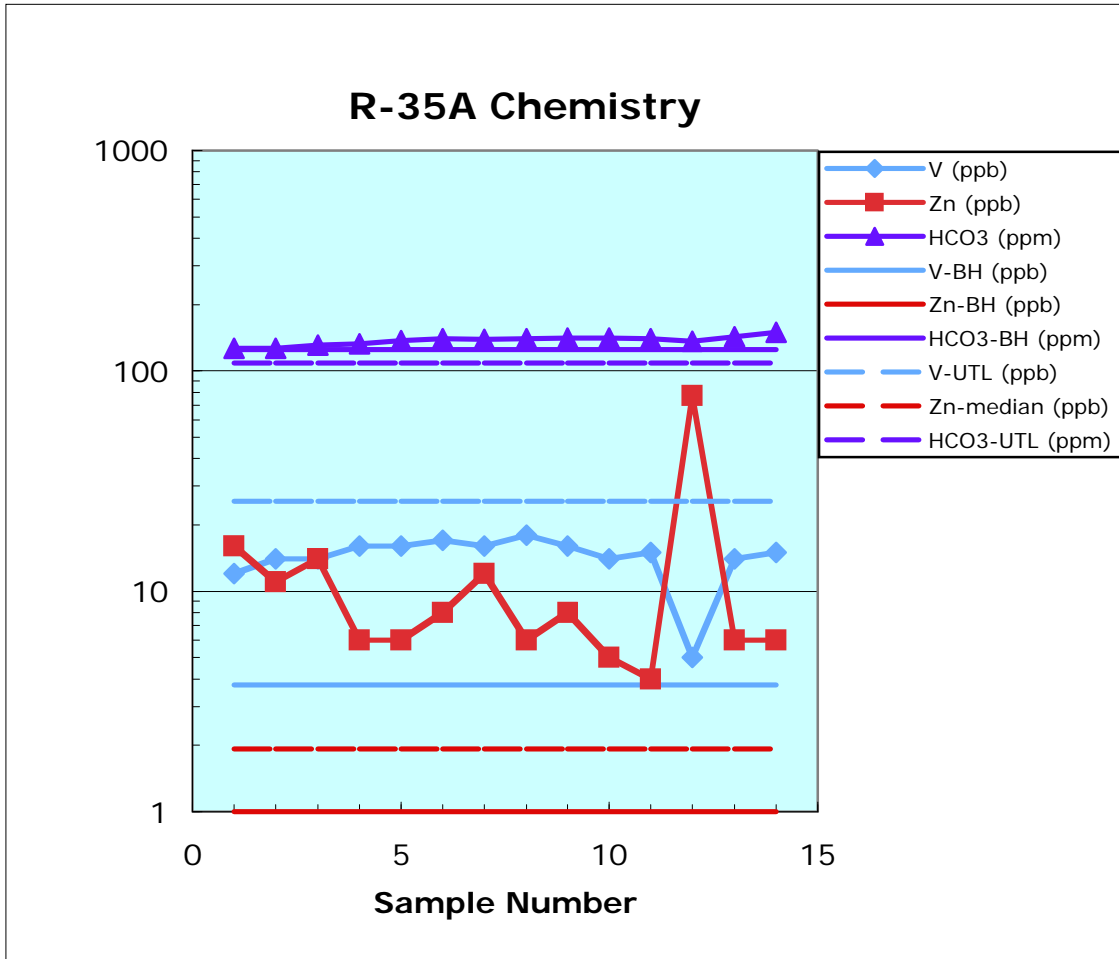


Figure B-1.3-2 Dissolved concentrations of vanadium (V), zinc (Zn), and bicarbonate (HCO₃) versus sample number collected during development at well R-35a, Sandia Canyon, New Mexico

Appendix C

Borehole Video Logs (see enclosed DVDs)

Appendix D

Geophysical Logging Report

D-1.0 INTRODUCTION

This report describes borehole geophysical logging measurements from characterization well R-35a done by Schlumberger Water Services in May 2007 before well completion. The report (1) summarizes the technology, measurements, and procedures employed and (2) presents the processed results from these measurements and discusses their interpretation. The logging measurements were acquired from 89 to 1143 ft below ground surface (bgs) when the borehole contained

- 10 in.- inner diameter (I.D.) freestanding steel casing from ground surface to 1143 ft (bottom of hole, as measured by the logs), drilled with an approximately 10-in.-diameter bit size below approximately 940 ft bgs (single string of casing from 940 to 1143 ft bgs);
- 12 in.-I.D. freestanding steel casing from ground surface to approximately 940 ft, drilled with an approximately 12.25-in.-diameter bit size from approximately 260 to 940 ft bgs (double string of casing from 260 to 940 ft bgs); and
- 16-in.-I.D. freestanding steel casing from ground surface to approximately 260 ft, drilled with an approximately 15-in.-diameter bit size from ground surface to 260 ft bgs (triple string of casing from 0 to 260 ft bgs).

The primary purpose of the geophysical logging was to characterize the geologic/hydrogeologic section intersected by the well, with an emphasis on determining the regional aquifer groundwater level, depth-specific capacity for flow (production capacity), stratigraphy/lithology of geologic units, perched-groundwater zones, and unsaturated zone moisture content. These objectives were accomplished by measuring the following along the length of the well almost continuously: (1) total water-filled porosity from which—in combination with lithologic composition estimated from the other logs—an indirect estimate of hydraulic conductivity (production capacity) was made; (2) bulk density (sensitive to total water plus air-filled porosity and grain density); (3) bulk electrical resistivity (only measurable through a single string of casing); (4) neutron-induced gamma ray spectroscopy, providing bulk concentrations of several important mineral-forming elements, as well as hydrogen; and (5) spectral natural gamma ray, including potassium, thorium, and uranium concentrations.

Preliminary results of these measurements were generated in the logging truck when the geophysical services were performed and are documented in field logs provided on-site. However, the measurements presented in the field results are not fully corrected for borehole conditions (particularly casing) and are provided as separate, individual logs. The field results were reprocessed by Schlumberger to (1) correct/improve the measurements for borehole/formation environmental conditions as best as possible; (2) perform an integrated analysis of the log measurements so that they are all coherent and provide consistent hydrogeologic and geologic results; and (3) combine the logs in a single presentation, enabling integrated interpretation. The reprocessed log results provide better quantitative property estimates that are consistent for all applicable measurements, as well as estimates of properties that otherwise could not be reliably estimated from the single measurements alone (e.g., total porosity inclusive of all water and air present, water saturation, hydraulic conductivity, and lithology).

Overall, the geophysical log measurements from well R-35a provide good quality results that are consistent with each other through most of the borehole, although the log measurements become significantly less reliable at representing true geologic formation conditions where there is more than one casing string due to added (and unknown) distance and amount of steel between the logging tool sensor and formation. The quality of the measurements was degraded across intervals where the borehole likely contained large washouts and/or a rugose hole behind the casing (potentially across the intervals 276–334, 362–412, 574–583, 600–666, 718–730, 760–763, 768–772, 778–781, 798–816, and 866–872 ft bgs in varying degrees of severity). The measurements most affected by the adverse borehole

conditions were ones that have a shallow depth of investigation and that require close contact to the uncased borehole wall—the bulk density and the neutron porosity measurements. The greatest impact on the log processing was erroneously high air-filled and/or water-filled porosity in the problem zones as estimated from the logs. Through the integrated analysis and interpretation of all the logs, it was determined that the individual shortcomings of the specific measurements are reduced. Thus, the results derived from integrated log analysis (e.g., the optimized water-filled porosity log) are the most robust single representation of the geophysical log measurements, providing a wealth of valuable high-resolution information on the geologic and hydrogeologic environment of the R-35a locale.

Important results from the processed geophysical logs in R-35a include the following.

- The standing water level in R-35a was relatively stable throughout the logging acquisition, remaining near 798 ft bgs for logging runs.
- The processed logs indicate that the intersected geologic section is fully saturated with water from the bottom of the log interval (1143 ft bgs) to at least 798 ft bgs (standing water level at the time of logging) and likely to 786.3 ft bgs, which lies within fanglomerate of the Puye Formation. The measured porosity across the saturated log interval (representing the regional aquifer) varies considerably (18%–60% of total rock/sediment volume) but predominantly ranges from 28% to 45%. The highest porosity anomalies are likely associated with voids (borehole washouts) behind the casing or between multiple strings of casing. Overall, the processed logs indicate that much of the saturated interval has high production capacity, except for the intervals 927–1012 and 1133–1143 ft bgs that appear to have lower production capacity. The most productive aquifer zones estimated from the processed logs (based on permeability estimators using total porosity and mineral composition) are the entire 798–927 bgs interval (particularly 798–816, 823–863, 868–876, 886–898, and 902–927 bgs), and 1020–1024, 1039–1052, 1088–1092, and 1120–1130 ft bgs.
- The processed logs indicate that the vadose-zone interval above the regional aquifer (786.3 ft bgs) has generally low water content and water saturation. The following zones have higher water content and water saturation: 208–285, 328–392, 452–494, 573–601, 666–696, and 755–786 ft bgs. Many of these zones coincide with lower total porosity or clay-rich lithology, as estimated from the integrated log analysis. This suggests that the higher water content is associated with lower permeability material, possibly acting as vertical barriers to flow and/or “sponges.” The highest measured volumetric water content is 28% of total rock/sediment volume at 215 and 230 ft bgs.
- The geophysical log results clearly delineate that most of the saturated/water-filled section of the borehole (783 to 1133 ft bgs) consists of alluvium/fanglomerate. Below 1133 ft bgs, the processed logs strongly indicate a lithology change to basaltic lava. The alluvium/fanglomerate sequence extends into the unsaturated section up to 601 ft bgs, although the processed logs show a change in sediment compositions (e.g., higher silicon and potassium, lower iron) and physical property characteristics (lower porosity up to 660 ft). In the interval from 258 to 601 ft bgs, the log results clearly indicate a change in the matrix geochemical makeup from the overlying and underlying fanglomerate deposits, likely representing a sequence of basaltic lavas. Above this sequence, the log results suggest a return to alluvial/fanglomerate deposits up to 217 ft bgs. The geophysical log response in the 200- to 217-ft bgs zone is characteristic of the Guaje Pumice Bed with very high total porosity, high water-filled porosity at the bottom (40%) that decreases in the upward direction, and a large increase in thorium and uranium concentrations. The log results corroborate volcanic tuff overlying the pumice bed and extending to the top of the log interval (89 ft bgs).

D-2.0 GEOPHYSICAL LOGGING SERVICES AND TOOLS

Geophysical logging services were performed in characterization well R-35a by Schlumberger in May 2007 before initial well completion. The purpose of these services was to acquire in situ measurements to help characterize the near-borehole geologic formation environment. The primary objective of the geophysical logging was to provide an in situ evaluation of formation properties (hydrogeologic and geologic) intersected by the well. This information was used by scientists, engineers, and project managers in the Los Alamos Characterization and Monitoring Well Project to design the well completion, to better understand subsurface site conditions, and to assist in overall decision-making.

The following primary geophysical logging tools were used by Schlumberger in well R-35a:

- Array porosity sonde (APS) that measures the volumetric water content of the formation at several depths of investigation through casing and in water or air-filled hole to evaluate moist/porous zones using a pulsed epithermal neutron measurement as well as neutron capture cross section, which is sensitive to water and clay content
- Compensated neutron tool (CNT) that measures volumetric water content of the formation through casing and in water-filled hole using a thermal neutron measurement;
- Triple lithodensity (TLD) tool that measures formation bulk density through casing to estimate total porosity;
- Cased hole formation resistivity (CHFR) tool that measures formation electrical resistivity at a deep depth of investigation to evaluate presence of porous and clay-rich zones;
- Hostile-environment natural gamma spectroscopy (HNGS) tool that measures gross natural gamma and spectral natural gamma ray activity, including potassium, thorium, and uranium concentrations, to evaluate geology/lithology, particularly the amount of clay and potassium-bearing minerals; and
- Elemental capture spectroscopy (ECS) tool that measures neutron-induced spectral gamma ray activity. This determines elemental weight fraction concentrations of a number of key rock-forming elements used to characterize geochemistry, mineralogy, and lithology of the formation, as well as hydrogen content (closely related to water content).

In addition, calibrated gross gamma ray was recorded with every service to correlate depths between the different logging runs. Table D-2.1 summarizes the geophysical logging runs performed in R-35a.

A more detailed description of these geophysical logging tools can be found on the Schlumberger website (<http://www.slb.com/content/services/evaluation/index.asp?>).

D-3.0 METHODOLOGY

This section describes the methods Schlumberger employed for geophysical logging of Well R-35a, including the following stages/tasks:

- Measurement acquisition at the well site
- Quality assessment of logs
- Reprocessing of field data

D-3.1 Acquisition Procedure

Once the well drilling project team notified Schlumberger that R-35a was ready for geophysical well logging, the Schlumberger district in Farmington, New Mexico, mobilized a wireline logging truck, the appropriate wireline logging tools and associated equipment, and crew to the job site. Upon arriving at Los Alamos National Laboratory (the Laboratory) site, the crew completed site-entry paperwork and received a site-specific safety briefing.

After arriving at the well site, the crew proceeded to rig up the wireline logging system, including

- parking and stabilizing the logging truck in a position relative to the borehole that is best for performing the surveys,
- setting up a lower and an upper sheave wheel (the latter attached to and hanging above the borehole from the drilling rig/mast truck),
- threading the wireline cable through the sheaves, and
- attaching the end of the cable to the appropriate sonde(s) for the first run.

Next, prelogging checks and any required calibrations were performed on the logging sondes, and the tool string was lowered into the borehole. If any of the tools required active radioactive sources (in this case, a neutron and gamma source for the CNT/ECS and TLD, respectively), the sources were taken out of their carrying shields and placed in the appropriate tool source-holding locations using special source-handling tools just before the tool string was lowered. The tool string was lowered to the bottom of the borehole and brought up at the appropriate logging speed as measurements were made. At least two logging runs (one main and one repeat) were made with each tool string.

Upon reaching the surface, any radioactive sources were removed from the tools and were returned to their appropriate storage shields, thus eliminating any radiation hazards. Any postlogging measurement checks were performed as part of log quality control (QC) and assurance. The tool string was cleaned as it was pulled out of the hole, separated, and disconnected.

The second tool string was attached to the cable for another logging run, followed by subsequent tool strings and logging runs. After the final logging run was completed, the cable and sheave wheels were rigged down.

Before departure, the logging engineer printed field logs and created a compact disk containing the field log data for on-site distribution and sent the data via satellite to the Schlumberger data storage center. The Schlumberger data processing center was alerted that the data were ready for postacquisition processing.

D-3.2 Log QC and Assessment

Schlumberger has a thorough set of procedures and protocols for ensuring that the geophysical logging measurements are of very high quality. This includes full calibration of tools when they are first built, regular recalibrations and tool measurement/maintenance checks, and real-time monitoring of log quality as measurements are made. One of the primary responsibilities of the logging engineer before and during acquisition is to ensure that the log measurements meet prescribed quality criteria.

All Schlumberger logging tools undergo a tool-specific base calibration that directly relates the tool response to the physical measurement using the designed measurement principle. Calibration occurs when the tools are first assembled in the engineering production centers. Calibration is accomplished through a combination of computer modeling and controlled measurements in calibration models with known chemical and physical properties.

The base calibration for most Schlumberger tools is augmented through regular “master calibrations” typically performed every 1 to 6 months in local Schlumberger shops (such as Farmington, New Mexico), depending on tool design. Master calibrations consist of controlled measurements using specially designed calibration tanks/jigs and internal calibration devices that are built into the tools, both with known physical properties. The measurements are used to fine-tune the tool’s calibration parameters and to verify that the measurements are valid.

In addition, on every logging job, before and after on-site calibrations are executed for most Schlumberger tools directly before and after lowering and removing the tool string from the borehole. For most tools, these represent a measurement verification instead of an actual calibration used to confirm the validity of the measurements directly before acquisition and to ensure that they have not drifted or been corrupted during the logging job.

All Schlumberger logging measurements have several associated depth-dependent QC logs and flags to assist with identifying and determining the magnitude of log quality problems. These QC logs are monitored in real-time by the logging engineer during acquisition and are used in the postacquisition processing of the logs to determine the best processing approach for optimizing the overall validity of the property estimates derived from the logs.

Additional information on specific tool calibration procedures can be found on the Schlumberger web page (<http://www.hub.slb.com/index.cfm?id=id11618>).

D-3.3 Processing Procedure

After the geophysical logging job was completed in the field and the data were archived, the data were downloaded to the Schlumberger processing center. The data were processed there in the following sequence. (1) The measurements were corrected for near-wellbore environmental conditions; the measurement field processing for certain tools (in this case, the ECS) was redone using better processing algorithms and parameters. (2) The log curves from different logging runs were depth matched and spliced. (3) The near-wellbore substrate lithology/mineralogy and pore fluids were modeling through integrated log analysis. Afterward, an integrated log montage was built to combine and compile all the processed log results.

D-3.3.1 Environmental Corrections and Raw Measurement Reprocessing

If required, the field log measurements were processed to correct for conditions in the well, including fluid type (water or air), presence of steel casing, and (to a much lesser extent) pressure, temperature, and fluid salinity. Basically, these environmental corrections entail subtracting from the measurement response the known influences of the set of prescribed borehole conditions. In R-35a, the log measurements requiring these corrections are the CHFR absolute bulk-formation resistivity, APS porosity, neutron capture cross section, CNT porosity, TLD bulk-formation density, ECS elemental concentrations, and HNGS spectral gamma ray logs.

The CHFR cased hole bulk-formation resistivity measurement is highly dependent on the dimensions and properties of the steel casing and cement (the latter is not applicable for well R-35a because the casing was freestanding). This is particularly true for this measurement because the casing is effectively being employed as an electrical current electrode, which is part of the tool in an open hole laterolog resistivity tool (accounted for in the tool "geometric factor" when deriving an absolute formation resistivity measurement). Due to inherent unknowns about casing/well geometry and electrical properties (e.g., influence of multiple strings of casing), which are instrumental to the CHFR cased hole measurement, the raw bulk-formation resistivity is a relative (as opposed to absolute) measurement. As part of the reprocessing, the raw resistivity measurement was linearly scaled using best judgment from experience in the area and corroboration with the other log measurements. This scaling factor is essentially associated with the geometric factor of the laterolog measurement, which is generally considered to be a linear factor for most laterolog geometries, including the CHFR. A reliable formation resistivity measurement is not attainable in multiple strings of casing.

Two neutron porosity measurements are available: one that measures thermal ("slow") neutrons (CNT tool) and one that measures epithermal ("fast") neutrons (the APS tool for R-35a). Measurement of epithermal neutrons is required to make neutron porosity measurements in air-filled holes. In water-, mud-filled holes, both the epithermal and thermal neutron measurements are valid. Both measurements can be fully environmentally corrected for a single string of steel-casing. Both epithermal (APS) and thermal (CNT) neutron porosity measurements were made in R-35a. The CNT thermal neutron porosity was only attainable in the water-filled section of the well (below 798 ft). Both the APS and CNT neutron porosity measurements were reprocessed for casing, borehole fluid type (air versus water), and other environmental conditions. The APS also measures the neutron capture cross section. This measurement was also corrected for well environmental conditions at the time of logging. For further processing and analysis (e.g., integrated log analysis), the reprocessed neutron porosity and neutron capture cross section logs were used.

The raw ECS elemental yield measurements include the contribution of iron from steel casing and hydrogen from fluid in the borehole. The processing consists of subtracting this unwanted contribution from the raw normalized yield then performing the normal elemental yields-to-weight fraction processing. The contribution to subtract is a constant baseline amount (or zoned constant values if there are bit/casing size changes), usually determined by comparing the normalized raw yields in zones directly above and below the borehole casing/fluid change. Casing corrections were applied to the ECS logs across the entire log interval, attempting to account for one string of steel casing below 940 ft, two strings of casing above 940 ft, and three strings above 260 ft. When the ECS logging occurred in R-35a, the borehole contained water from bottom to 798 ft. No hydrogen correction was required in the air-filled section above 798 ft, and the difference between the hydrogen yield above and below this depth was used to determine the baseline borehole hydrogen correction to apply below.

The HNGS spectral gamma ray is affected by the material (fluid, air, and casing) in the borehole because different types and amounts of these materials have different gamma ray shielding properties. The HNGS measures incoming gamma rays emitted by radioactive elements in the formation surrounding the borehole. The processing algorithms try to correct for the damping influence of the borehole material. The HNGS logs from R-35a were reprocessed to account for the environmental effects of the casing, borehole fluid (water below 798 ft and air above), and hole size as best as possible.

The measurements cannot be fully corrected for borehole washouts or rugosity because the specific characteristics (e.g., geometry) of these features are unknown (especially in this scenario where they are hidden by casing), and their effects on the measurements are often too significant to account for. Thus, the compromising effects of these conditions on the measurements should be considered in the interpretation of the log results.

D-3.3.2 Depth-Matching and Splicing

Once the logs were environmentally corrected for the conditions in the borehole and the raw measurement reprocessing was completed, the logs from different tool runs were depth-matched to each other using the HNGS tool run as the base reference. Gross gamma ray was used as the common correlation log measurement for depth-matching the different runs. The depth reference for all the processed logs is ground surface.

D-3.3.3 Integrated Log Analysis

An integrated log analysis, using as many of the processed logs as possible, was performed to model the near-wellbore substrate lithology/mineralogy and pore fluids. This analysis was performed using the Elemental Log Analysis (ELAN) program, a petrophysical interpretation program designed for depth-by-depth quantitative formation evaluation from borehole geophysical logs. ELAN estimates the volumetric fractions of user-defined rock matrix and pore constituents at each depth based on the known log measurement responses to each individual constituent by itself¹. ELAN requires an a priori specification of the volume components present within the formation, namely, fluids, minerals, and rocks. For each component, the relevant response parameters for each measurement are also required. For example, if one assumes that quartz is a volume component within the formation and the bulk density tool is used, then the bulk density parameter for this mineral is well known to be 2.65 g/cm³.

The logging tool measurements, volume components, and measurement response parameters used in the ELAN analysis for R-35a are provided in Table D-3.1. The final results of the analysis—an optimized mineral-fluid volume model—are shown on the integrated log montage (see Attachment 1, Appendix Data Files and Images, on the enclosed CD), third track from the right (inclusive of the depth track). In addition, the ELAN program provides a direct comparison of the modeled versus the actual measured geophysical logs, as well as a composite log of all of the key ELAN-derived results, including geologic/hydrogeologic properties computed from the mineral-fluid volume model (see Attachment 1, Appendix Data Files and Images, on the enclosed CD). To make best use of all the measurement data and to perform the analysis across as much of the well interval as possible (90 to 1143 ft bgs), as many of the processed logs were included in the analysis as possible, with less weighting applied to less robust logs. Not all of the tool measurements shown in Table D-3.1 and the ELAN modeled versus measured log display are used for the entire interval analyzed because not all the measurements are available or of good quality across certain sections of the borehole. To accommodate fewer tool measurements, certain model constituents are removed from the analysis in some intervals.

The ELAN analysis was performed with as few constraints or prior assumptions as possible. Considerable effort was made to choose a set of minerals or mineral types for the model that is representative of

Los Alamos area geology and its volcanic origins. For the ELAN analysis, the log interval from 90 to 217.5 ft bgs was assumed to be tuff or pumice. A mineral suite considered representative of this volcanic tuff, based on Laboratory cuttings mineral analysis, was used (primary “minerals” silica glass/cristobalite/tridymite [indistinguishable from the log measurements], quartz, potassium feldspar, and augite, with accessory minerals calcite and pyrite). The results of laboratory analyses of Bandelier Tuff and Puye Formation samples from around the Laboratory site were also used to constrain the proportion of quartz versus the combination of glass/cristobalite/tridymite in the ELAN analysis. The log intervals 217.5 to 258 ft and 599 to 1,143 ft bgs were assumed to be in the Puye or Santa Fe Formation, or fanglomerate/alluvium with similar composition. Based on Laboratory cuttings mineral analysis, a mineral

¹ Mathematically, this corresponds to an inverse problem—solving for constituent volume fractions from an (over)determined system of equations relating the measured log results to combinations of the tool measurement response to individual constituents.

suite considered representative of this geology was used (primary “minerals” silica glass/cristobalite/tridymite [indistinguishable from the log measurements], plagioclase and potassium feldspar; quartz at a defined small fraction of the silica glass content; variable amounts of montmorillonite clay; with possible accessory/trace minerals biotite, hematite, augite, hypersthene, heavy mafic minerals, and pyrite). The log interval 258 to 599 ft bgs was assumed to be basaltic lava flows/material with a possible mineral suite of plagioclase and potassium feldspar, quartz, augite, hypersthene, heavy mafic minerals (such as magnetite), montmorillonite, hematite, and pyrite

No prior assumption is made about water saturation—where the boundary between saturated and unsaturated zones lies (e.g., the depth to the top of the regional aquifer or perched zones). Thus, the presence and amount of air in the pore space is unconstrained. Total porosity and water-filled porosity are also left unconstrained throughout the analysis interval, despite the obvious influence on the log response of borehole washouts (voids) behind the casing. There is no way to objectively correct for the adverse effect on the log measurements from these borehole conditions; therefore, the decision was made to perform the ELAN analysis to honor the log measurements. Accordingly, interpretations should be made from the ELAN results with the understanding that the mineral-fluid model represents a mathematically optimized solution that is not necessarily a physically accurate representation of the native geologic formation. Within this context, the ELAN model is a robust estimate of the bulk mineral-fluid composition that accounts for the combined response from all the geophysical measurements.

D-4.0 RESULTS

Preliminary results from the wireline geophysical logging measurements acquired by Schlumberger in R-35a were generated in the logging truck at the time the geophysical services were performed and were documented in the field logs provided on-site. However, the measurements presented in the field results are not fully corrected for undesirable influence (from a measurement standpoint) of borehole and geologic conditions and are provided as separate, individual logs. The field log results have been processed (1) to correct/improve the measurements, as best as possible, for borehole/formation environmental conditions and (2) to depth-match the logs from different tool runs in the well. Additional logs were generated from integrated analysis of processed measured logs, providing valuable estimates of key geologic and hydrologic properties.

The processed log results are presented as continuous curves of the processed measurement versus depth and are displayed as (1) a one-page compressed summary log display for selected directly related sets of measurements (see Figures D-4.1-1, D-4.1-2, and D-4.1-3) and (2) an integrated log montage that contains all the key processed log curves, on depth and side by side (see Attachment 1, Appendix Data Files and Images, on the enclosed CD). The summary log displays address specific characterization needs, such as porosity, production capacity, moisture content, water saturation, and lithologic changes. The purpose of the integrated log montage is to present, side by side, all the most salient processed logs and log-derived models, depth-matched to each other, so that correlations and relationships between the logs can be identified. Important results from the processed geophysical logs in R-35a are described below.

D-4.1 Well Fluid Level

The standing water level in R-35a (within the freestanding 10-in.-I-D- casing) was stable during the May 11–12, 2007, logging, remaining between 796 and 798 ft bgs for all four logging runs.

D-4.2 Regional Aquifer

The processed geophysical logs definitively indicate fully water saturated conditions below 798 ft bgs (see porosity summary display in Figure D-4.1 or integrated log montage in Attachment 1, Appendix Data Files and Images, on the enclosed CD). The estimated pore volume water saturation (fraction of the total pore volume containing water) computed from the ELAN analysis is very high (80%–100%, mostly 100%) from 798 ft bgs to the bottom of the log interval (1143 ft bgs). While there is a significant decrease in the ELAN-computed water saturation above 798 ft, there is still a peak in water content and water saturation (reaching 60%) at 786 ft, and the water content derived from the ECS tool indicates high water-filled porosity up to 786 ft where it decreases significantly (the ECS measurement is one of the deeper reading logs). In the interval above 786 ft, all the processed logs and ELAN results indicate low water content and low water saturation.

These overall geophysical log results suggest that at the time of the logging, the regional aquifer groundwater level resided no deeper than 798 ft bgs and likely at a depth close to 786 ft bgs in this location, with the regional aquifer itself below.

The log-derived estimates of water-filled and total porosity², which should be close to the same in the fully water saturated section (and are, except for 786–798 ft bgs, as described above), vary considerably (18%–60%), but predominantly range 28%–45% across the section of the log interval that intersects the apparent regional aquifer (786–1143 ft bgs). The highest porosity anomalies are likely associated with voids (borehole washouts) behind the casing or between multiple strings of casing. There appears to be a baseline porosity increase in the interval 786–945 ft bgs compared with the section below, which corresponds to the location of the two strings of casing during the logging (compared with one below). This concurrence suggests the overall increase in porosity could be due to the influence on the logging measurements of the greater distance between the inner casing and the geologic formation (resulting in higher, nongeologic, water volume in the measurement volume of investigation).

Key hydrogeologic characteristics observed from the processed continuous geophysical logs across the depth section within the apparent regional aquifer (786–1143 ft bgs) are described below and zoned based on intervals that have similar characteristics (referenced to depth below ground surface).

- **786–798 ft bgs:** This zone has total porosity and water-filled porosity ranging 26%–40% and 5%–17% of total rock volume, respectively, as estimated from the ELAN integrated log analysis. This range in porosities and water contents results in low water saturation estimates, ranging 23%–60% of total pore volume. However, as discussed in the beginning of this section, the water content (water-filled porosity) measured from the ECS tool (the deepest reading water content measurement in the logging suite) is much higher than the ELAN estimate and closely matches the total porosity estimate, indicating much higher (full) water saturation. Assuming full water saturation in this interval, the estimated producibility is moderate, highest in the zone 790–793 ft bgs, where the ELAN analysis doesn't indicate presence of clay or calcite. The remainder of the interval is shown from the ELAN analysis to contain calcite and/or clay, which results in lower hydraulic conductivity estimates.
- **798–816 ft bgs:** This zone has very high total and water-filled porosity (44%–70% and 38%–55% of total rock volume, respectively, as estimated from the ELAN integrated log analysis), very likely elevated due to voids behind the casing biasing the fluid-sensitive logs used to measure porosity. The water saturation estimate from the ELAN analysis varies from 60% to 100% of total pore

² Water-filled porosity (synonymous with volumetric water content) is defined in this report as the fraction of the total rock volume occupied by water. Total porosity is defined as fraction of the total rock volume occupied by water plus air, plus any other fluid or gas (non-solid). Water saturation is defined as the fraction of the total porosity that is occupied by water.

volume, likely indicating less than full saturation as a result of the bulk density measurement's greater sensitivity to voids behind casing than the neutron porosity measurements (the bulk density measurement is the primary source of information on total porosity versus water content for the neutron measurements). Notwithstanding possible effects of borehole-to-casing voids, the average water content is around 45% of total rock volume, and the ELAN analysis doesn't indicate the presence of fine-grained material, suggesting this interval contains porous, productive alluvial sediments.

- **816–871 ft bgs:** This interval has very high total and water-filled porosity (40%–52% of total rock volume, averaging about 45%, for both). Water saturation, as estimated from the ELAN analysis, is close to 100% of total pore volume for most of the interval. The ELAN lithology estimate does not indicate the presence of clay. With high porosity and no clay indication, estimated producibility (production capacity) across the interval is high. However, there are zones where the ECS calcium measurement is elevated, indicating the possible presence of calcite (as predicted by the ELAN results), which could represent lower producibility zones due to calcite cementation of the formation matrix. The estimated calcite-rich zones, which correspondingly have lower estimated hydraulic conductivity from the ELAN analysis, are 816–822, 824–826, 830.5–832.5, 834.5–836.5, 843.5–846.5, 852–854.5, and 863–868, and 816–822 ft bgs.
- **871–927 ft bgs:** This zone is characterized by high total and water-filled porosity (32%–45% of total rock volume, averaging about 38%), although the porosity is noticeably lower than the interval above. Water saturation is estimated at 100% across the zone, and the ELAN analysis does not indicate any presence of clay. As a result of lower porosity, the estimated producibility is slightly lower than the interval above but still high. Similar to the interval above, the ELAN results indicate zones with calcite, possibly reducing hydraulic conductivity due to cementation: 872–874, 877–885.5, 887.5–890.5, 899–901, 912–915, 918–920, and 922–924.5 ft bgs.
- **927–1012.5 ft bgs:** This interval has overall reduced porosity compared with the section above and below (18%–50% of total rock volume, averaging around 30%, decreasing significantly below 943 ft bgs), with estimated water saturation near 100%. There is a high porosity anomaly (reaching 55%) at 983.5–988 ft bgs, likely caused by a void (washout) behind the casing. The primary difference between this interval and saturated section above is the presence of clay, as estimated from the ELAN analysis, which results in significantly lower estimated producibility/hydraulic conductivity. In particular, the zones with the highest clay content and, correspondingly, lowest estimated hydraulic conductivity are 927–934, 964–972, 988–992.5, and 1004–1012.5 ft bgs.
- **1012.5–1053 ft bgs:** This interval has varying porosity, generally increasing with depth (28% of total rock volume at top, increasing to 50% at bottom). Estimated water saturation is near 100%, indicating close agreement between the bulk density and neutron-based porosity logs. The ELAN analysis indicates small, varying amounts of clay. Overall, estimated hydraulic conductivity trends higher with the increasing porosity, but the highest estimated producibility is in the zone 1020–1024 ft bgs.
- **1053–1078 ft bgs:** This zone has relatively uniform, moderately high total porosity that generally decreases with depth (38% of total rock volume at top, decreasing to 28% at bottom). Estimated hydraulic conductivity varies considerably across the zone as a result of varying amounts of clay predicted from the ELAN analysis; overall producibility is lower than the section directly above. The following discrete zones have higher estimated clay content and thus lower estimated hydraulic conductivity: 1053–1056, 1065–1068, and 1075–1078 ft bgs.
- **1078–1100 ft bgs:** This zone is characterized by high porosity (27%–43% of total rock volume) and high producibility, particularly in the zone 1088–1092 ft bgs where clay and calcite are not present in the ELAN analysis results.

- **1100–1118 ft bgs:** This zone has lower porosity (ranging 30%–35% of total rock volume) than the surrounding section. Correspondingly, estimated hydraulic conductivity is also lower than the surrounding section, with the lowest values occurring at 1105–1110 ft bgs (where porosity is the lowest and the ELAN analysis indicates the presence of clay), increasing above and below that depth.
- **1118–1132 ft bgs:** This zone is characterized by varying, overall high, porosity (25%–40% of total rock volume). Estimated producibility is high overall, peaking across the interval 1126.5–1132 ft bgs.
- **1132–1143 ft bgs (bottom of logged section):** The processed logs indicate sharply lower porosity in this zone (averaging about 20% of total rock volume), and the ELAN analysis suggests the rock composition could be basaltic. Estimated producibility is quite low across the zone, although possibly relatively higher in the zone 1136–1140 ft bgs.

D-4.3 Vadose-Zone Perched Water

Above 786 ft bgs (the estimated apparent regional aquifer groundwater level from the processed geophysical logs) to the top of the log interval (89 ft bgs), the processed geophysical logs indicate highly variable total and water-filled porosity, ranging from 10% to 80% and 2% to 30%, respectively, of total rock volume. Most of the zones that have unrealistically high porosity values (above 50% of total rock volume) likely contain voids (possibly borehole washouts) behind the multiple strings of casing in the borehole at the time of logging, where the porosity measurements are severely influenced by the large volume of air-filled borehole surrounding the sensors on the logging tools. The estimated water saturation, computed from the processed geophysical logs based on the total and water-filled porosity estimates, is highly variable, ranging from negligible to 100% of total pore volume.

Described below are the key hydrogeologic characteristics from the water table upwards (referenced to depth below ground surface) that were observed from the processed continuous geophysical logs across the logged depth section within the apparent vadose zone above the regional aquifer (89–786 ft bgs)

- **727–786 ft bgs:** Water content and, correspondingly, water saturation (as estimated from the ELAN analysis) generally increase from top to bottom, ranging from 0 at 727 ft bgs to 18% of total rock volume (water content) and 60% of total pore volume (water saturation) at 786 ft. The total porosity estimate from the ELAN analysis ranges 20%–40%, with a number of anomalously and unrealistically high-porosity peaks (reaching greater than 50% of total rock volume), where the log measurements are obviously affected by air-filled voids (possibly borehole washouts) behind the casing. Not surprisingly, where the ELAN results indicate unrealistically high total porosity, water content and water saturation are very low, including at 727 ft where these property logs are zero. The ELAN analysis results indicate that the estimated clay content trends with the water content, increasing from top to bottom.
- **682–727 ft bgs:** Water saturation consistently increases in the uphole direction, especially above 696 ft bgs, ranging from 0% of total pore volume at the bottom to 100% at the top. Correspondingly, water-filled porosity (volumetric water content) increases from bottom to top, from 0% of total rock volume at 727 ft bgs to a peak of 12% at 684 ft bgs. Total porosity generally has the opposite trend, averaging about 25% of total rock volume from 698 to 727 ft bgs, decreasing to 20% from 685 to 698 ft then sharply decreasing to 12% at 682 ft. The ELAN analysis results indicate the presence of clay above 698 ft bgs, increasing in content to the top of the interval. The ELAN results also indicate varying amounts of calcite. The overall geologic conceptual model from these ELAN porosity and lithology results is that there is a very tight, possibly well-cemented (with clay and/or calcite), low-permeability layer at 678–682 ft bgs, which

is acting to increase moisture content and thus water saturation. It is also possible, although not considered likely, that the significant decrease in estimated total porosity, resulting mostly due to a high bulk density measurement in zone, is caused by something different in the casing configuration at this depth (e.g., geometry of the two concentric casing strings).

- **601–682 ft bgs:** Water saturation and water content are generally very low across this interval, mostly below 7% of total pore volume and 3% of total rock volume, respectively, except at the bottom, where water saturation sharply increases to 100% and water content rises to 12%. The increase in water saturation and water content starts at 664 ft bgs, increasing with depth, coinciding with a corresponding rapid decrease in total porosity (decreasing from over 50% of total rock volume, obviously erroneously high, to 12% at 682 ft bgs). Total porosity, derived from the ELAN analysis primarily as a function of the bulk density measurement, is very high (40% and higher) across most of the interval, indicating the measurement is being affected by voids between the casing the borehole wall. Estimated clay content from the ELAN results is generally low, except below 666 ft bgs.
- **573–601 ft bgs:** Water saturation and water content is slightly higher in this zone compared with the directly adjacent sections, reaching a high of 20% of total pore volume and 7% of total rock volume, respectively. The total porosity derived from the ELAN analysis is very high (over 48% of total rock volume), which is geologically unrealistic and likely the result of the air-filled void between the inner casing and borehole wall, biasing the bulk density measurement low. The ELAN analysis lithology results indicate that this zone is at the bottom of a sequence of basaltic lavas; possibly, water is accumulating at the bottom of the volcanic sequence on top of the underlying formation.
- **494–573 ft bgs:** Water saturation and water content are very low across this interval, consistently about 5% of total pore volume and 3% of total rock volume, respectively. The total porosity is also quite consistent but very high, averaging about 45% of total rock volume, likely elevated due to the influence of air-filled annular space between the inner casing and borehole wall. The ELAN analysis lithology results indicate that this zone is a continuation of the basaltic lavas from below.
- **452–494 ft bgs:** Water saturation increases significantly in this zone (reaching a high of 42% of total pore volume) as a result of higher water content (high of 7% of total rock volume) and much lower total porosity (low of 15% of total rock volume). The ELAN analysis results indicate the lithology is a continuation of the basaltic lavas from below and above, although it does indicate a higher silica content (modeled unrealistically as quartz). Conceptually, the high water content and water saturation could be the result of water accumulation in the tighter, lower permeability section.
- **392–452 ft bgs:** Water content is very low across this interval, consistently about 3% of total rock volume. Total porosity generally increases in the uphole direction from about 25% of total rock volume at the bottom to close to 80% at the top, undoubtedly adversely affected by air-filled annular void behind the inner casing. Correspondingly, water saturation decreases in the uphole direction from a high of 13% at the bottom to less than 5% at the top. The ELAN analysis lithology results indicate that this zone is a continuation of the basaltic lavas from below.

- **328–392 ft bgs:** Water saturation increases significantly in this zone (reaching a high of 39% of total pore volume) as a result of higher water content (high of 6% of total rock volume) and much lower total porosity (low of 12% of total rock volume). The ELAN analysis results indicate the lithology is a continuation of the basaltic lavas from below and above. Conceptually, the high water content and water saturation could be the result of water accumulation in the tighter, lower permeability section.
- **285–328 ft bgs:** Water content is very low across this interval, averaging about 4% of total rock volume. Total porosity is very high (mostly above 43% of total rock volume with peaks above 70%), which is geologically unrealistic and likely the result of the air-filled void between the inner casing and borehole wall, biasing the bulk density measurement low and thus the total porosity high. Correspondingly, estimated water saturation is very low (2%–8% of total pore volume). The ELAN analysis lithology results indicate that this zone is a continuation of the basaltic lavas from below.
- **258–285 ft bgs:** Water content is higher than the section below (averaging about 10% of total rock volume, highest in the section), increasing the water content results in a higher water saturation as well (reaching 25% of total pore volume). Total porosity is very high, averaging about 45% of total rock volume, with a peak over 70%, likely elevated due to air-filled annular space behind the casing. The ELAN analysis lithology results indicate a continuation of the basaltic lavas from below.
- **217–258 ft bgs:** Total water content increases significantly in this interval compared with the section below reaching 29% of total rock volume. Total porosity varies from 40% to over 50% of total rock volume, likely biased high due to air-filled voids behind the casing. These porosities translate into an estimated water saturation ranging 18%–58% of total pore volume, with peaks at 254–257, 228–233, and 217–223 ft bgs. The ELAN analysis results indicate a change in lithology from the basaltic lavas below to clastic, alluvial sediments; the results also suggest the presence of clay, especially at the top (217–223 ft bgs). One possible explanation for increased water content in this zone is the presence of clay, acting as a low-permeability sponge that retains water infiltrating from above.
- **210–217 ft bgs:** This zone contains the highest water content in the vadose zone, with a peak of 29% of total rock volume at 216 ft bgs, decreasing to 12% at 210 ft. Water saturation peaks at 60% of total pore volume and decreases to 30% at the top. Estimated total porosity is close to 50% of total rock volume, which, although very high, may be representative of formation conditions, considering that all indications from the ELAN analysis results are that this zone is the Guaje Pumice Bed.
- **89–210 ft bgs:** Water content and water saturation generally decrease in the uphole direction, from about 12% to 7% of total rock volume (water content) and 35% to 10% of total pore volume (water saturation). Estimated total porosity ranges 36%–50% of total rock volume. Although these ranges are high, they may be representative of formation conditions, considering that the ELAN analysis lithology results indicate that this zone is likely composed of volcanic tuff.

D-4.4 Geology

The processed geophysical log results, particularly the matrix geochemistry logs, provide information on lithology and formation contacts intersected by R-35a across the log interval (from 89 to 1143 ft bgs). The generalized geologic stratigraphy observed from the logs across the measured interval is as follows (depth below ground surface):

- **89–210 ft bgs (top of processed log interval): Very high porosity silicon, potassium, and thorium rich material (likely volcanic tuff or derived from volcanic tuff)**—Characterized by very high total porosity (36%–50% of total rock volume); high silica glass/tridymite/cristobalite content; moderate potassium feldspar or augite content; and minor amounts of quartz and calcite (or other calcium-bearing minerals)
- **210–217 ft bgs: Very high-porosity silicon rich volcanic tuff/pumice**—Characterized by very high total porosity (50% of total rock volume); high silica glass/tridymite/cristobalite content; moderate potassium feldspar and augite (or similar minerals) content; and minor amounts of quartz and calcite (or other calcium-bearing minerals)
- **217–258 ft bgs: Heterogeneous alluvium/fanglomerate containing clay**—Characterized by potentially very high total porosity (over 40% of total rock volume, but highest porosity is likely associated with voids behind casing); high silica glass/tridymite/cristobalite and plagioclase feldspar content; variably small to moderate amounts of clay, potassium feldspar and calcite; variably trace to minor amounts of biotite, hematite, pyrite and/or heavy mafic minerals
- **258–334 ft bgs: Plagioclase feldspar rich volcanics (likely basalt)**—Characterized by unrealistically very high total porosity (greater than 50% of total rock volume), likely elevated due to voids behind the casing; high plagioclase feldspar; variably minor to moderate silica minerals or alkali feldspars and augite (or similar mineral) content; and variably small amounts of heavy mafic minerals
- **334–358 ft bgs: Lower porosity plagioclase feldspar rich volcanics (likely basalt)**—Characterized by relatively low total porosity (low of 12% of total rock volume); high plagioclase feldspar; variably minor to moderate silica minerals or alkali feldspars and augite (or similar mineral) content; and variably small amounts of heavy mafic minerals
- **358–424 ft bgs: Plagioclase feldspar rich volcanics (likely basalt)**—Characterized by unrealistically very high total porosity (mostly greater than 50% of total rock volume), likely elevated due to voids behind the casing; high plagioclase feldspar; variably minor to moderate silica minerals or alkali feldspars and augite (or similar mineral) content; and variably small amounts of heavy mafic minerals
- **424–487 ft bgs: Low to moderate porosity plagioclase feldspar rich volcanics (likely basalt)**—Characterized by relatively low to moderate total porosity (high of 35% of total rock volume at top decreasing to a low of 15%); high plagioclase feldspar; variably minor to moderate silica minerals or alkali feldspars and augite (or similar mineral) content; and variably small amounts of heavy mafic minerals, and potentially pyrite
- **487–601 ft bgs: Plagioclase feldspar rich volcanics (likely basalt)**—Characterized by potentially very high total porosity (averaging about 45% of total rock volume, but porosity could very well be elevated due to the annular space between the inner casing and formation); high plagioclase feldspar; variably minor to moderate silica minerals or alkali feldspars and augite (or similar mineral) content; and variably small amounts of heavy mafic minerals, and potentially pyrite
- **601–675 ft bgs: Potentially very high porosity, heterogeneous alluvium/fanglomerate, possibly containing calcite**—Characterized by potentially very high total porosity (over 40% of total rock volume, but highest porosity is likely associated with voids behind casing); high silica glass/tridymite/cristobalite or quartz content; variably small to moderate amounts of potassium and plagioclase feldspar and calcite; variably trace to minor amounts of clay, hypersthene, augite, biotite, hematite, pyrite and/or heavy mafic minerals

- **675–752 ft bgs: Relatively low porosity alluvium/fanglomerate containing varying amounts of clay**—Characterized by low total porosity (12%–27% of total rock volume, except for anomalous peaks reaching greater than 50% likely associated with voids behind casing); high silica glass/tridymite/cristobalite or quartz content; variably small to moderate amounts of potassium and plagioclase feldspar and calcite; variably trace to minor amounts of clay, hypersthene, augite, biotite, hematite, pyrite and/or heavy mafic minerals
- **752–798 ft bgs: Moderate porosity, heterogeneous alluvium/fanglomerate containing varying amounts of clay**—Characterized by moderate total porosity (25%–40% of total rock volume, except for anomalous peaks reaching greater than 40% likely associated with voids behind casing); high silica glass/tridymite/cristobalite or quartz content; variably small to moderate amounts of potassium and plagioclase feldspar and calcite; variably trace to minor amounts of clay, hypersthene, augite, biotite, hematite, pyrite and/or heavy mafic minerals
- **798–871 ft bgs: Very high-porosity alluvium/fanglomerate**—Characterized by very high total porosity (38%–55% of total rock volume, very likely the highest porosities are elevated due to annular space behind the casing); high plagioclase feldspar content; variably minor to moderate silica glass/tridymite/cristobalite, potassium feldspar, augite, hypersthene, and calcite content; and variably trace to minor amounts of quartz, augite, biotite, hematite, pyrite and/or heavy mafic minerals
- **871–927 ft bgs: High porosity alluvium/fanglomerate**—Characterized by high total porosity (32%–45% of total rock volume, averaging about 38%); high plagioclase feldspar content; variably minor to moderate silica glass/tridymite/cristobalite, potassium feldspar, augite, hypersthene, and calcite content; and variably trace to minor amounts of quartz, augite, biotite, hematite, pyrite and/or heavy mafic minerals
- **927–943 ft bgs: High porosity alluvium/fanglomerate containing clay**—Characterized by high total porosity (40%–47% of total rock volume); high plagioclase feldspar content; variably minor to moderate hypersthene, clay, and calcite content; and variably trace to minor amounts of silica glass/tridymite/cristobalite, quartz, augite, biotite, hematite, pyrite and/or heavy mafic minerals
- **937–1012.5 ft bgs: Moderate porosity alluvium/fanglomerate containing varying amounts of clay**—Characterized by variable moderate total porosity (18%–50% of total rock volume, averaging around 30%, very likely the highest porosities are elevated due to voids behind casing); high plagioclase feldspar content; variably minor to moderate silica glass/tridymite/cristobalite, potassium feldspar, augite, clay and calcite content; and variably trace to minor amounts of quartz, hypersthene, biotite, hematite, pyrite and/or heavy mafic minerals
- **1012.5–1133 ft bgs: Variably moderate to high porosity alluvium/fanglomerate**—Characterized by variably moderate to high total porosity (25%–50% of total rock volume); high plagioclase feldspar content; moderate silica glass/tridymite/cristobalite; variably minor to moderate potassium feldspar, hypersthene, augite, and calcite content; and variably trace to minor amounts of quartz, clay, biotite, hematite, pyrite and/or heavy mafic minerals
- **1133–1143 ft bgs (bottom of log interval): Low porosity volcanics (likely basalt)**—Characterized by low total porosity (average about 20% of total rock volume); high plagioclase feldspar content; moderate augite content; variably minor to moderate calcite content; variably trace to minor silica minerals or alkali feldspars, hypersthene, biotite, hematite, pyrite and/or heavy mafic minerals

D-4.5 Summary Logs

Three summary log displays have been generated for R-35a to highlight the key hydrogeologic and geologic information provided by the processed geophysical log results:

- Porosity and hydrogeologic properties summary log showing continuous hydrogeologic property logs, including total porosity (water and air), water-filled porosity, water saturation, estimated hydraulic conductivity, transmissivity, and relative producibility (production capacity); highlights key derived hydrologic information obtained from the integrated log results, including (Figure D-4.1)
- Density and clay content summary showing a continuous logs of formation bulk density and estimated grain density, as well as estimated clay volume, highlights key geologic rock matrix information obtained from the log results (Figure D-4.2)
- Spectral natural gamma ray and lithology summary showing a high vertical resolution, continuous volumetric analysis of formation mineral and pore fluid composition (based on an integrated analysis of the logs), and key lithologic/stratigraphic correlation logs from the spectral gamma ray measurement (concentrations of gamma-emitting elements); highlights the geologic lithology, stratigraphy, and correlation information obtained from the log results (Figure D-4.3)

D-4.6 Integrated Log Montage

This section summarizes the integrated geophysical log montage for R-35a. The montage is provided in Attachment 1, Appendix Data Files and Images (on enclosed CD). A description of each log curve in the montage follows, organized under the heading of each track, starting from track 1 on the left-hand side of the montage. Note that the descriptions in this section focus on what the curves are and how they are displayed; the specific characteristics and interpretations of the R-35a geophysical logs are provided in the previous section

D-4.6.1 Track 1—Depth

The first track on the left contains the depth below ground surface in units of feet, as measured by the geophysical logging system during the HNGS logging run. All the geophysical logs are depth-matched to the gross gamma log acquired with this logging run.

D-4.6.2 Track 2—Basic Logs

The second track on the left (inclusive of the depth track) presents basic curves:

- Gamma ray (thick black), recorded in gamma ray American Petroleum Institute (gAPI) standard units and displayed on a scale of 0 to 125 gAPI units
- Neutron capture cross-section from the APS tool (long-dashed olive green), which is sensitive to water content and lithology, recorded in capture units (cu) and displayed on a scale of 0 to 25 cu
- Single arm caliper from the TLD (thin solid pink) with nominal bit size as a reference (dashed-dotted black) to show nominal annular distance between inside of inner casing to borehole wall (pink shading), recorded as hole diameter in inches and displayed on a scale of 8 to 18 in.

Two gamma ray curves from the HNGS are displayed:

- Total gross gamma (thick solid black curve)

- Gross gamma minus the contribution of uranium (dashed black)
- Yellow shading between the two curves to show uranium contribution to the total gamma ray response.

D-4.6.3 Track 3—Resistivity

The third track displays the resistivity measurement from the CHFR tool, spanning the section of the well that had a single string of casing at the time of the logging (the measurement is not possible in more than one string of steel casing). The resistivity logs are recorded in units of ohmmeters (ohm-m) and are displayed on a logarithmic scale of 2 to 2000 ohm-m.

The two resistivity logs from the CHFR that are displayed are

- bulk electrical resistivity measured at depth stations (black circles connected by black straight line segments), a deep reading relative resistivity measurement recorded at stations while the tool is “clamped” to the inner wall of the casing that is scaled afterwards, and
- resampled and box-car averaged bulk electrical resistivity computed from the station measurements (solid purple curve) to provide a continuous, smoothed curve.

D-4.6.4 Track 4—Porosity

The fourth track displays the primary porosity log results. All the porosity logs are recorded in units of volumetric fraction and are displayed on a linear scale of 0.75 (left side) to -0.1 (right side). Specifically, these logs consist of

- APS epithermal neutron porosity derived from near-far detector pairing (bold solid dark blue curve)—deepest reading epithermal neutron porosity from APS tool, processed for zoned air-filled and water-filled cased hole;
- APS epithermal neutron porosity derived from near-array detector pairing (solid sky blue curve)—medium depth of investigation epithermal neutron porosity from APS tool, processed for zoned air-filled and water-filled cased hole;
- APS slowing down time porosity derived from pulsed neutron time series in the array detectors (thin dotted cyan curve)—shallowest reading epithermal neutron porosity from APS tool, processed for zoned air-filled and water-filled cased hole;
- CNT water-filled resolution enhanced thermal neutron porosity (thin solid light blue curve)—thermal neutron porosity valid only in the fluid-filled borehole;
- ECS bulk volumetric water content derived from hydrogen weight concentration measurement, corrected for water in casing and converted to volume fraction (short-dashed pink);
- Total porosity derived from bulk density and ELAN water-filled porosity using a grain density of 2.35/2.55/2.65 g/cc (dashed red curve), 2.45/2.65/2.75 g/cc (long-dashed red curve), and 2.55/2.75/2.85 g/cc (dotted red curve) with red shading between the 2.35/2.45/2.65 g/cc and 2.55/2.75/2.85 g/cc porosity curves to show the range (the lowest grain density range used across the tuff/pumice interval [89–217 ft], the middle grain density range used across the alluvium/fanglomerate intervals [217–258 and 601–1132 ft], and the highest grain density range used across the basalt/dacite intervals [258–601 and 1132–1143 ft]); and
- ELAN total water and air-filled porosity (bold dashed-dotted cyan)—derived from the ELAN integrated analysis of all log curves to estimate optimized matrix and pore volume constituents.

D-4.6.5 Track 5—Density

The fifth track displays the

- bulk density, corrected for single string of steel casing (thick solid maroon curve) on a wrapping scale of 1 to 3 g/cm³, and
- apparent grain density (dashed brown curve), derived from the ELAN analysis, on a scale of 2.4 to 3.2 g/cc.

D-4.6.6 Track 6—HNGS Spectral Gamma

The sixth track from the left displays the following spectral components of the HNGS measurement results as wet weight concentrations, corrected as best as possible for casing and borehole size and fluid:

- Potassium (solid green curve) in units of percent weight fraction and on a scale of -2.5% to 2.5%
- Thorium (dashed brown) in units of parts per million (ppm) and on a scale of 20 to -20 ppm; and
- Uranium (dotted blue) in units of parts ppm and on a scale of 20 to 0 ppm.

D-4.6.7 Tracks 7 to 12—Geochemical Elemental Measurements

The narrow tracks 7 to 12 present the geochemical measurements, along with their estimated 1 standard deviation uncertainty range: iron (Fe) and silicon (Si), sulfur (S) and calcium (Ca), estimated aluminum (Al) and potassium (K), titanium (Ti), and gadolinium (Gd), hydrogen (H), and apparent relative bulk chlorinity (Rela. Cl), and uranium (U) and carbon yield (C Yield) from left to right, respectively, in units of dry matrix weight fraction (except K and H in wet-weight fraction, Rela. Cl in ppk, U in wet-weight ppm, and C yield in relative yield units).

D-4.6.8 Track 13—ELAN Mineralogy Model Results (Dry-Weight Fraction)

Track 13 displays the results from the ELAN integrated log analysis (the matrix portion)—presented as dry-weight fraction of mineral types chosen in the model:

- Montmorillonite clay (brown/tan)
- Hematite (orange with small black dots)
- Quartz (yellow with closely spaced small black dots)
- Combined silica glass, tridymite, and cristobalite (yellow with widely spaced large black dots)
- Orthoclase or other potassium feldspar (lavender)
- Labradorite or similar plagioclase feldspar (pink)
- Biotite (light green)
- Pyrite (orange-tan with black squares)
- Hypersthene (purple)
- Augite (maroon)
- Heavy mafic/ultramafic minerals, such as magnetite or olivine (dark green)
- Calcite (cyan)

D-4.6.9 Track 14—ELAN Mineralogy and Pore Space Model Results (Wet-Volume Fraction)

Track 14 displays the results from the ELAN integrated log analysis presented as wet mineral and pore fluid volume fractions:

- Montmorillonite clay (brown/tan)
- Clay-bound water (checkered gray-black)
- Hematite (orange with small black dots)
- Quartz (yellow with closely spaced small black dots)
- Combined silica glass, tridymite, and cristobalite (yellow with widely spaced large black dots)
- Orthoclase or other potassium feldspar (lavender)
- Labradorite or similar plagioclase feldspar (pink)
- Biotite (light green)
- Pyrite (orange-tan with black squares)
- Hypersthene (purple)
- Augite (maroon)
- Heavy mafic/ultramafic minerals, such as magnetite or olivine (dark green)
- Calcite (cyan)
- Air (red)
- Intergranular (nonclay) water (white)
- Moved air (orange)
- Moved water (blue)

D-4.6.10 Track 15—Water Saturation

Track 15 displays the continuous-in-depth water saturation logs estimated from the processed logs, recorded in units of volumetric fraction of pore space filled with water (ratio of cubic feet per cubic feet and presented on a scale of 0 to 1 ft³/ft³ (left to right).

Optimized estimate of water saturation (volumetric fraction of pore space filled with water) from the ELAN analysis (bold dashed-dotted purple curve with blue shading to the right and red shading to the left, corresponding to water-filled and air-filled pore space, respectively)

Water saturation as calculated directly from the bulk density and ELAN-estimated porosity using a grain density of 2.35/2.55/2.65 g/cm³ (dashed cyan curve), 2.45/2.65/2.75 g/cm³ (solid cyan curve), and 2.55/2.75/2.85 g/cm³ (dotted cyan curve) with stippled cyan shading between the 2.35/2.55/2.65 g/cm³ and 2.55/2.75/2.85 g/cm³ water saturation curves to show the range (the lowest grain density range used across the tuff/pumice interval [89–217 ft], the middle grain density range used across the alluvium/fanglomerate intervals [217–258 and 601–1132 ft], and the highest grain density range used across the basalt/dacite intervals [258–601 and 1132–1143 ft]).

D-4.6.11 Track 16—Hydraulic Conductivity

Track 16 displays the following estimates of hydraulic conductivity (K) derived from the ELAN integrated log analysis (sensitive to the estimated porosities and mineral composition), presented on a logarithmic scale of 10^{-5} to 105 ft/d:

- A K-versus-depth estimate derived from using the k-lambda permeability equation with water-filled porosity and matrix mineral weight fraction values derived from the ELAN analysis, converted to hydraulic conductivity (bold solid blue curve with gradational coloring to represent the range of hydraulic conductivity relative to standard unconsolidated clastic sediments)
- An intrinsic K-versus-depth estimate (assuming full saturation) using the K-lambda permeability equation with total porosity and matrix mineral weight fraction values derived from the ELAN analysis, converted to hydraulic conductivity (dotted cyan)
- An intrinsic K-versus-depth estimate (assuming full saturation) using the ELAN total porosity and mineral-based permeability equation with total porosity and matrix mineral weight fraction values derived from the ELAN analysis, converted to hydraulic conductivity (dotted purple)
- In addition, estimates of cumulative transmissivity from the bottom of the log interval are displayed for the K-lambda estimator (bold dashed-dotted bright green curve) and the ELAN mineral-based estimator (dashed dark green curve) computed by integrating from bottom to top the hydraulic conductivity estimates, presented on a logarithmic scale of 10^{-5} to 10^5 ft²/d.

D-4.6.12 Track 17—Predicted Flow (Production Potential) Profile

Track 17 displays the integrated predicted relative flow (production potential) profile from the permeability (hydraulic conductivity) logs that mimics a flow meter (spinner) acquired under flowing conditions:

- Predicted relative water flow profile derived from the k-lambda water permeability log (bold solid blue curve), displayed on a unitless linear scale of 0 to 1 relative volumetric flow rate (ratio of flow rate to flow rate)
- Predicted relative water flow profile derived from the ELAN water permeability log(long-dashed blue), displayed on a unitless linear scale of 0 to 1 relative volumetric flow rate
- Relative integrated intrinsic permeability profile derived by integrating the k-lambda intrinsic permeability log(dashed-dotted brown), displayed on a unitless linear scale of 0 to 1
- Relative integrated intrinsic permeability profile derived by integrating the ELAN intrinsic permeability log(dashed brown)), displayed on a unitless linear scale of 0 to 1
- Predicted hypothetical well water flow versus depth profile for the entire log interval (dotted green), assuming a well radius of 4 in., entirely open to flow, and pumping is occurring under steady state conditions with a drawdown of 25 ft (incremental flow computed using the Theis steady state flow equation)—derived from the K-lambda water permeability log (bold solid blue), displayed on a scale of 0 to 1.5 million gpd.

D-4.6.13 Track 18—Summary Logs

Track 18, the second track from the right, displays the following summary logs that describe the fluid and air-filled volume measured by the geophysical tools.

- Optimized estimate of total volume fraction water from the ELAN analysis (solid blue curve and blue plus cyan area shading)

- Optimized estimate of volume fraction intergranular water (nonclay bound water-filled porosity) from the ELAN analysis (dashed cyan curve and cyan area shading)
- Optimized estimate of total volume fraction of air-filled porosity from the ELAN analysis (solid red curve and dotted red area shading)
- Estimate of bulk volumetric water content from the ECS tool (thin dashed dark blue curve)
- The porosity and volumetric water content scales shown from 0 to 1 total volume fraction, left to right.

D-4.6.14 Track 19–Depth

The final track on the right, the same as the first track on the left, displays the depth below ground surface in units of feet, as measured by the geophysical logging system during the HNGS logging run.

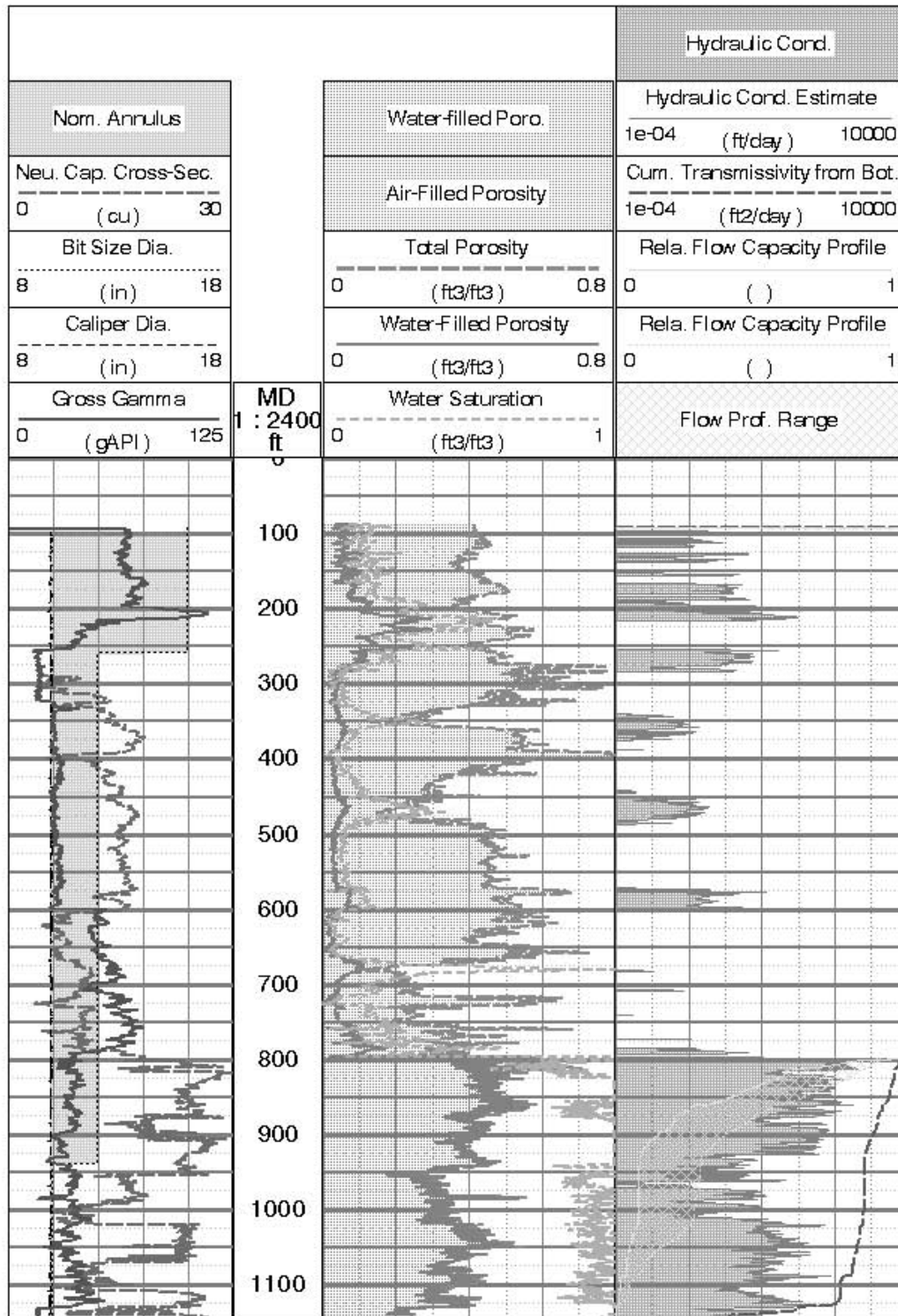


Figure D-4.1-1 Summary of porosity logs in R-35a borehole from processed geophysical logs, interval of 97 to 1143 ft bgs, with caliper, gross gamma, neutron capture cross section, water saturation, estimated relative flow capacity profile, hydraulic conductivity, and transmissivity logs also displayed. Porosity, water saturation, and hydraulic conductivity logs are derived from the ELAN integrated log analysis.

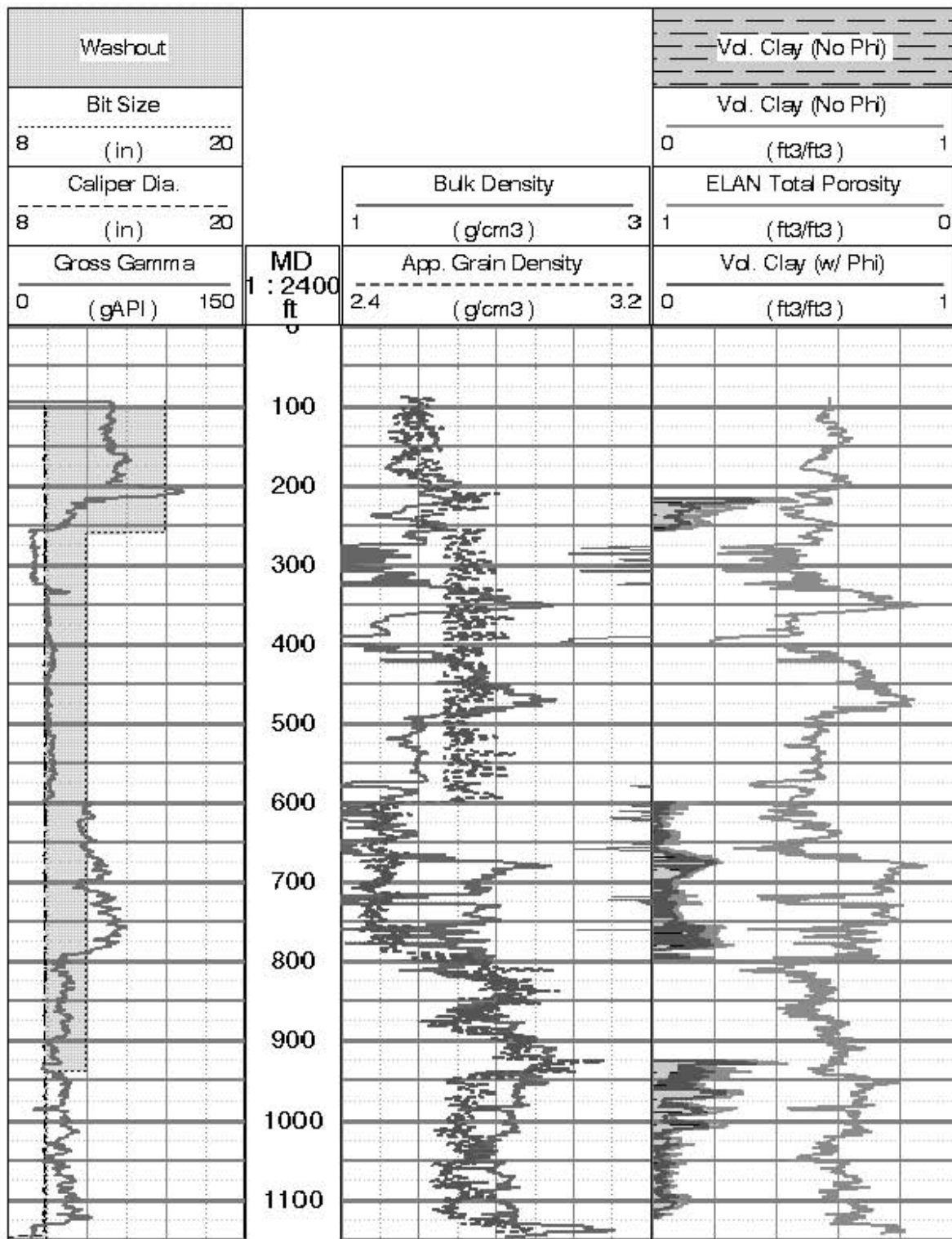


Figure D-4.1-2 Summary of bulk density and volume clay logs in R-35a borehole from processed geophysical logs, interval of 97 to 1143 ft bgs. Also shown are caliper, gross gamma, apparent grain density, and total porosity logs (the latter two derived from the ELAN analysis).

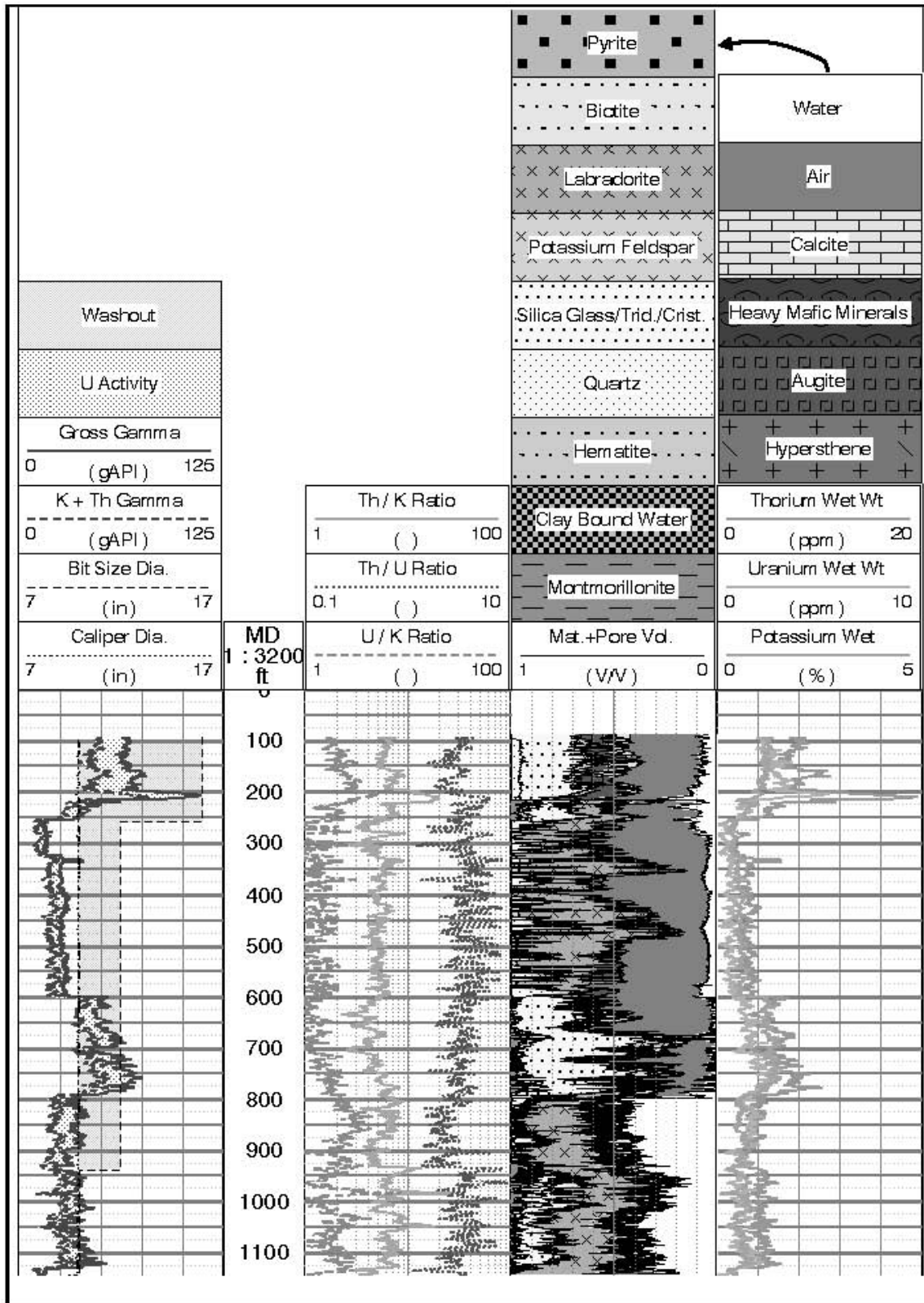


Figure D-4.1-3 Summary of spectral natural gamma ray logs and ELAN mineralogy/lithology and pore fluid model volumes derived from the ELAN integrated log analysis for R-35a borehole, interval 65 to 1143 ft bgs. Caliper log is also shown.

**Table D-2.1
Geophysical Logging Services, Their Combined Tool Runs and Intervals Logged,
As Performed by Schlumberger In Borehole R-35a**

Date of Logging	Borehole Status	Run #	Tool 1	Tool 2	Tool 3	Tool 4	Depth Interval
11 May-2007	Steel free-standing casing from surface to bottom. Single string of 10-in.-I.D.-casing from 940 to 1143 ft, with bit size of ~10.25 in. Double string of 12 in.-I.D.-casing from 260 to 940 ft, with bit size of ~12.25 in. Double string of 16-in.-I.D.-casing from 0 to 260 ft, with bit size of ~16.25 in.	1	TLD (bottom)	CNT	GR (top)		TLD: 104–1-142 ft CNT: 798–1-136 ft
Same	Same	2	CHFR	GR			924–1-124 ft
12 May-2007	Same	3	ECS	GR			96–1-141 ft
Same	Same	4	HNGS				96–1-137 ft

Table D-3.1
Tool Measurements, Volumes, and Respective Parameters Used in the R-35a ELAN Analysis

Volume Tool Measurement	Air	Water	Hypersthene	Hematite	Labradorite	Silica Glass, Cristo., Tridy.	Heavy Mafic Minerals	Augite	Montmorillonite	Biotite	Pyrite	Orthoclase	Calcite	Quartz
Bulk density (g/c ³) ^a	-0.19	1.00	3.55	5.161	2.68	2.33	5.08	3.08	2.02	3.04	4.99	2.54	2.71	2.64
Thermal neutron porosity. (nonlinear) (ft ³ /ft ³) ^b	0	1.00	0.036	0.126	-0.01	-0.03	0.07	0.015	0.65	0.15	0.01	-0.01	0.0	-0.07
Epithermal neutron porosity. (ft ³ /ft ³)	0	1.00	0.012	0.0556	-0.01	0.0	0.022	-0.01	0.6	0.14	0.165	-0.01	0.0	-0.05
Resistivity (ohm-m)	Very high	28.19	Very high	Very high	Very high	Very high	Very high	Very high	Computed	Very high	Very high	Very high	Very high	Very high
Dry weight silicon (lbf/lbf) ^c	0.0	0.0	0.24	0.0	0.247	0.468	0.184	0.225	0.242	0.178	0.0	0.3	0.0	0.468
Dry weight calcium (lbf/lbf)	0.0	0.0	0.0	0.0	0.09	0.0	0.0	0.10	0.012	0.007	0.0	0.0	0.405	0.0
Dry weight iron (lbf/lbf)	0.0	0.0	0.20	0.699	0.023	0.0	0.22	0.112	0.02	0.199	0.466	0.015	0.0	0.0
Dry weight aluminum (lbf/lbf)	0.0	0.0	0.0	0.0	0.162	0.0	0.0	0.018	0.103	0.081	0.0	0.104	0.0	0.0
Dry weight sulfur (lbf/lbf)	0.0	0.0	0.0	0.0	0.0	0.0	0.0	0.0	0.0	0.0	0.535	0.0	0.0	0.0
Dry weight titanium (lbf/lbf)	0.0	0.0	0.01	0.01	0.0	0.0	0.0	0.048	0.001	0.016	0.0	0.0	0.0	0.0
Wet weight potassium (lbf/lbf)	0.0	0.0	0.0	0.0	0.0	0.0	0.0	0.003	0.004	0.070	0.0	0.12	0.0	0.0
Weight hydrogen (lbf/lbf)	0.0	0.111	0.0	0.0	0.0	0.01	0.0	0.0	0.022	0.003	0.0	0.0	0.0	0.0
Wet weight thorium (ppm)	0	0	13.5	0	1.75	2	4	13.5	24	25	0	5	0	0
Neutron capture (cu)	0	22.21	18.9	101.4	7.87	4	103	25.66	20	54.1	90	15.82	7.4	4.7

^a gc³ = Gram(s) per cubic centimeter.

^b ft³/ft³ = Cubic foot per cubic foot.

^c lbf = Pound(s) force.

Appendix E

R-35 and PM-3 Pumping Test Analyses

E-1.0 INTRODUCTION

This report describes the hydraulic analysis of formation sediments at wells R-35a and R-35b located in Sandia Canyon adjacent to Los Alamos County supply well PM-3. The primary objective of the analysis was to determine the hydraulic properties of the zones screened by R-35a and R-35b, as well as the intervening aquitard between the two screen zones. Testing consisted primarily of constant-rate pumping tests conducted on R-35a and R-35b. During the tests, water levels were monitored in the two R-35 wells, several Los Alamos County supply wells, and several other R wells in the area. Monitored zones included PM-1, PM-3, PM-4, PM-5, R-5 Screens 3 and 4, R-8 Screens 1 and 2, R-9, R-11, R-13, and R-28.

Because of the proximity of PM-3 to the tested wells, PM-3 was shut down on July 2, 2007, 2.5 wk before running the R-35 tests to minimize its effect on local water levels. Once the R-35 well tests were completed and PM-3 was put back online, the restart provided an opportunity to obtain pumping test data from the PM-3 startup cycle and subsequent recovery. During this period, water levels were measured in the same group of wells that had been monitored as part of the R-35 testing effort.

Consistent with most of the R-well pumping tests conducted on the plateau, an inflatable packer system was used in wells R-35a and R-35b to eliminate the effects of casing storage on the test data.

E-1.1 Conceptual Hydrogeology

R-35a is completed within Santa Fe Group sediments, with 49.1 ft of screen from 1013.1 to 1062.2 ft below ground surface (bgs). The static water level at the time of testing was 791.0 ft. R-35b is completed within the Puye Formation, with 23.1 ft of screen set from 825.4 to 848.5 ft. During testing, the static water level was 787.1 ft. The ground surface elevation at R-35b is 2.3 ft higher than that at R-35a and thus the static water levels between the two wells differed by 6.2 ft (elevation 5837.8 ft in R-35b and 5831.6 ft R-35a). The 6.2 ft higher water level in R-35b implied a strong downward gradient between the Puye Formation and Santa Fe Group sediments, with a layer of tight material lying between the two permeable aquifers. Table E-1 summarizes the ground surface elevations of the R-35 wells, along with depths and elevations of the screen zones and water levels. The data presented in Table E-1 were based on a preliminary survey conducted to support this pumping test analysis and were adequate for the purposes of this report. A final, formal survey was planned to be conducted subsequently.

Table E-1
Water Levels and Screen Depths

Well	Depth (ft)	Elevation (ft above mean sea level [amsl])
R-35a		
Land surface	0.0	6622.6
Water level	791.0	5831.6
Screen top	1013.1	5609.5
Screen bottom	1062.2	5560.4
R-35b		
Land surface	0.0	6624.9
Water level	787.1	5837.8
Screen top	825.4	5799.5
Screen bottom	848.5	5776.4

Observations made during the drilling of R-35a identified a tight zone around 900 ft. The transition from the Puye to the Santa Fe Group occurs at 880 ft, with a 20-ft section of volcanic sediments from 880 to 900 ft, underlain by river gravels. It was assumed that this 20-ft interval might comprise, or at least be a component of, the aquitard separating the two permeable formations. In the hydraulic analysis of the pumping data, the upper aquifer was considered to be a 93-ft-thick unconfined zone, extending from the static water level of about 787 ft to the top of the Santa Fe Group sediments at 880 ft. The deeper aquifer was considered to be 236 ft thick, extending from the top of the river gravels at 900 ft to the top of a Miocene Basalt layer encountered at 1136 ft.

This conceptual interpretation is not certain, and other alternative descriptions of the aquifer makeup are possible. Based on the available data, it is not possible to know the aquifer demarcations with certainty. Nevertheless, the proposed interpretation seems reasonable based on the available evidence.

R-35b Testing

R-35b was tested from July 19 to 25, 2007. Testing consisted of background data collection, brief trial pumping on July 20, followed by a 24-h constant-rate pumping test that was begun on July 23.

Three trial tests were conducted. Trial 1 was conducted at a discharge rate of 22.5 gpm for 60 min from 9:45 a.m. until 10:45 a.m. and was followed by 75 min. of recovery until 12:00 p.m. Trial 2 was conducted for 60 min. from 12:00 p.m. until 1:00 p.m. at a discharge rate of 22.3 gpm. Following shutdown, recovery was monitored for 90 min until 2:30 p.m. Trial 3 was conducted for 90 min from 2:30 p.m. to 4:00 p.m. at a discharge rate of 22.5 gpm. Following shutdown, recovery/background was monitored for 3960 min until 10:00 a.m. on July 23.

At 10:00 a.m. on July 23, the 24-h pumping test was begun at a rate of 22.6 gpm. Pumping continued until 10:00 a.m. on July 24. Following shutdown, recovery/background measurements were recorded for 24 h. until 10:00 a.m. on July 25.

R-35a Testing

R-35a was tested from July 25 to 29. Testing consisted of background data collection, brief trial pumping on July 26, a 24-h. constant-rate pumping test that was begun on July 27, and finally a sampling event on July 29.

Two trial tests were conducted. Trial 1 was conducted at a discharge rate of 22.0 gpm for 75 min from 9:45 a.m. until 11:00 a.m. and was followed by 120 min. of recovery until 1:00 p.m. Trial 2 was conducted for 75 min. from 1:00 p.m. until 2:15 p.m. at a discharge rate of 21.5 gpm. Following shutdown, recovery/background was monitored for 1185 min until 10:00 am on July 27.

At 10:00 a.m. on July 27, the 24-h pumping test was begun at a rate of 21.4 gpm. Pumping continued until 10:00 a.m. on July 28. Following shutdown, recovery/background measurements were recorded for 24 h. until 10:00 am on July 29.

Before pulling the pump, water samples were taken from R-35a on July 29 by pumping the well for 130 min from 10:00 a.m. until 12:10 p.m. The initial pumping rate was more than 20 gpm but was adjusted quickly to 4.4 gpm where it was maintained for the bulk of the sampling period. Following shutdown, recovery data were recorded for 65 min until 1:15 p.m.

PM-3 Testing

After a shutdown period of 35 d for the R-35 testing from July 2 until August 6, PM-3 was restarted and put back online. The initial pumping cycle consisted of pumping the well at a rate of 1450 gpm for 1460 min from 9:30 a.m. on August 6 until 9:50 a.m. on August 7. Following shutdown, recovery was monitored in PM-3 for 1346 min. until 8:16 a.m. on August 8 and in R-35a for 2011 min. until 7:21 p.m. on August 8.

During the PM-3 pumping test, despite the high pumping rate, several of the shallow R wells showed limited response to pumping, on the order of a couple hundredths of a foot, consistent with the presence of an aquitard separating the shallow aquifer from the deeper sediments. In addition to conventional pumping test analysis methods, computer modeling was used to examine the shallow aquifer response in R-35b to quantify the leakance of the aquitard.

E-2.0 BACKGROUND DATA

The background water-level data collected in conjunction with running the pumping tests allow the analyst to see what water-level fluctuations occur naturally in the aquifer and help distinguish between water-level changes caused by conducting the pumping test and changes associated with other causes.

Background water-level fluctuations have several causes, among them barometric pressure changes, operation of other wells in the aquifer, earth tides and long-term trends related to weather patterns. The background data hydrographs from the monitored wells were compared with barometric pressure data from the area to determine if a correlation existed.

Previous pumping tests on the plateau have demonstrated a barometric efficiency for most wells of between 90% and 100%. Barometric efficiency is defined as the ratio of water-level change divided by barometric pressure change, expressed as a percentage. In the initial pumping tests conducted on the early R wells, downhole pressure was monitored using a vented pressure transducer. This equipment measures the difference between the total pressure applied to the transducer and the barometric pressure, this difference being the true height of water above the transducer.

Subsequent pumping tests, including R-35, have utilized nonvented transducers. These devices simply record the total pressure on the transducer, that is, the sum of the water height plus the barometric pressure. This results in an attenuated "apparent" hydrograph in a barometrically efficient well. Take as an example a 90% barometrically efficient well. When monitored using a vented transducer, an increase in barometric pressure of 1 unit causes a decrease in recorded downhole pressure of 0.9 unit because the water level is forced downward 0.9 unit by the barometric pressure change. However, using a nonvented transducer, the total measured pressure increases by 0.1 unit (the combination of the barometric pressure increase and the water-level decrease). Thus, the resulting apparent hydrograph changes by a factor of 100 minus the barometric efficiency and in the same direction as the barometric pressure change, rather than in the opposite direction.

Barometric pressure data were obtained from the Los Alamos National Laboratory Technical Area (TA) 54 tower site from the Environmental Division—Meteorology and Air Quality (ENV-MAQ). The TA-54 measurement location is at an elevation of 6548 ft amsl, whereas the wellhead elevations average approximately 6624 ft amsl. The static water levels averaged about 789 ft below land surface, making the water-table elevations an average of 5835 ft amsl. Therefore, the measured barometric pressure data from TA-54 had to be adjusted to reflect the pressure at the elevation of the water table within the R-35 wells.

The following formula was used to adjust the measured barometric pressure data:

$$P_{WT} = P_{TA54} \exp \left[-\frac{g}{3.281R} \left(\frac{E_{R35} - E_{TA54}}{T_{TA54}} + \frac{E_{WT} - E_{R35}}{T_{WELL}} \right) \right]$$

Equation 1

Where P_{WT} = barometric pressure at the water table inside R-35a or R-35b,

P_{TA54} = barometric pressure measured at TA-54,

g = acceleration of gravity, in m/sec² (9.80665 m/sec²),

R = gas constant, in J/Kg/degree Kelvin (287.04 J/Kg/degree Kelvin),

E_{R35} = land surface elevation at R-35 site, in feet (6624 feet average),

E_{TA54} = elevation of barometric pressure measuring point at TA-54, in feet (6548 ft)

E_{WT} = elevation of the water level in R-35a and R-35b, in feet (approximately 5835 ft average),

T_{TA54} = air temperature near TA-54 in degrees Kelvin (assigned a value of 68.2 degrees Fahrenheit, or 293.3 degrees Kelvin), and

T_{WELL} = air temperature inside R-35a and R-35b in degrees Kelvin (assigned a value of 73.4 degrees Fahrenheit, or 296.2 degrees Kelvin).

This formula is an adaptation of an equation provided by ENV-MAQ. It can be derived from the ideal gas law and standard physics principles. An inherent assumption in the derivation of the equation is that the air temperature between TA-54 and the well is temporally and spatially constant, and that the temperature of the air column in the well is similarly constant.

The corrected barometric pressure data reflecting pressure conditions at the water table were compared with the water-level hydrographs to discern the correlation between the two.

E-3.0 IMPORTANCE OF EARLY DATA

When pumping or recovery first begins, the vertical extent of the cone of depression is limited to approximately the well screen length, the filter-pack length or, the aquifer thickness in relatively thin permeable strata. For many pumping tests on the plateau, the early pumping period is the only time that the effective height of the cone of depression is known with certainty. Thus, the early data often offer the best opportunity to obtain hydraulic conductivity information because conductivity would equal the earliest-time transmissivity divided by the well screen length.

Unfortunately, in many pumping tests, casing storage effects dominate the early-time data, hindering the effort to determine the transmissivity of the screened interval. The duration of casing storage effects can be estimated using the following equation (Schafer 1978, 098240).

Equation 2

$$t_c = \frac{0.6(D^2 - d^2)}{\frac{Q}{s}}$$

Where t_c = duration of casing storage effect in minutes,

D = inside diameter of well casing in inches,

d = outside diameter of column pipe in inches,

Q = discharge rate in gpm

s = drawdown observed in pumped well at time t_c , in feet.

In some instances, it is possible to eliminate casing storage effects by setting an inflatable packer above the tested screen interval before conducting the test. Therefore, this option has been implemented for the R-well testing program, including the R-35 pumping tests. Implementation of the packer was key in obtaining useful data from the R-35 pumping tests.

E-4.0 TIME-DRAWDOWN METHODS

Time-drawdown data can be analyzed using a variety of methods. Among them is the Theis method (1934-1935, 098241). The Theis equation describes drawdown around a well as follows:

Equation 3

$$s = \frac{114.6Q}{T} W(u)$$

Where

Equation 4

$$W(u) = \int_u^{\infty} \frac{e^{-x}}{x} dx$$

and

Equation 5

$$u = \frac{1.87r^2 S}{Tt}$$

and where s = drawdown in feet,

Q = discharge rate in gpm,

T = transmissivity in g/d/ft,

S = storage coefficient (dimensionless),

t = pumping time in days, and

r = distance from center of pumpage in feet.

To use the Theis method of analysis, the time-drawdown data are plotted on log-log graph paper. Then, Theis curve matching is performed using the Theis type curve—a plot of the Theis well function $W(u)$ versus $1/u$. Curve matching is accomplished by overlaying the type curve on the data plot and, while keeping the coordinate axes of the two plots parallel, shifting the data plot to align with the type curve, effecting a match position. An arbitrary point, referred to as the match point, is selected from the overlapping parts of the plots. Match point coordinates are recorded from the two graphs, yielding four values— $W(u)$, $1/u$, s , and t . Using these match point values, transmissivity and storage coefficient are computed as follows:

$$T = \frac{114.6Q}{s} W(u)$$

Equation 6

$$S = \frac{Tut}{2693r^2}$$

Equation 7

Where T = transmissivity in gpd/ft,
 S = storage coefficient,
 Q = discharge rate in gpm,
 $W(u)$ = match point value,
 s = match point value, in feet,
 u = match point value, and
 t = match point value, in minutes.

An alternative solution method applicable to time-drawdown data is the Cooper–Jacob method (1946, 098236), a simplification of the Theis equation that is mathematically equivalent to the Theis equation for most pumped well data. The Cooper–Jacob equation (1946, 098236) describes drawdown around a pumping well as follows:

$$s = \frac{264Q}{T} \log \frac{0.3Tt}{r^2 S}$$

Equation 8

The Cooper–Jacob equation is a simplified approximation of the Theis equation and is valid whenever the u value is less than about 0.05. For small radius values (e.g., corresponding to borehole radii), u is less than 0.05 at very early pumping times and therefore is less than 0.05 for most or all measured drawdown values. Thus, for the pumped well, the Cooper–Jacob equation (1946, 098236) usually can be considered a valid approximation of the Theis equation (1934-1935, 098241).

According to the Cooper–Jacob method, the time-drawdown data are plotted on a semilog graph, with time plotted on the logarithmic scale (1946, 098236). Then a straight line of best fit is constructed through the data points and transmissivity is calculated using:

Equation 9

$$T = \frac{264Q}{\Delta s}$$

Where T = transmissivity in gpd/ft,

Q = discharge rate in gpm, and

Δs = change in head over one log cycle of the graph in feet.

Because the R-wells are severely partially penetrating, an additional solution considered for determining aquifer parameters is the Hantush equation for partially penetrating wells (Hantush 1961, 098237). The Hantush equation is as follows:

Equation 10

$$s = \frac{Q}{4\pi T} \left[W(u) + \frac{2b^2}{\pi^2(l-d)(l'-d')} \sum_{n=1}^{\infty} \frac{1}{n^2} \left(\sin \frac{n\pi l}{b} - \sin \frac{n\pi d}{b} \right) \left(\sin \frac{n\pi l'}{b} - \sin \frac{n\pi d'}{b} \right) W \left(u, \sqrt{\frac{K_z}{K_r} \frac{n\pi r}{b}} \right) \right]$$

Where, in consistent units, s , Q , T , t , r , S , and u are as previously defined and

b = aquifer thickness,

d = distance from top of aquifer to top of well screen in pumped well,

l = distance from top of aquifer to bottom of well screen in pumped well,

d' = distance from top of aquifer to top of well screen in observation well,

l' = distance from top of aquifer to bottom of well screen in observation well,

K_z = vertical hydraulic conductivity, and

K_r = horizontal hydraulic conductivity.

In this equation, $W(u)$ is the Theis well function and $W(u,\beta)$ is the Hantush well function for leaky aquifers where:

Equation 11

$$\beta = \sqrt{\frac{K_z}{K_r} \frac{n\pi r}{b}}$$

Note that for single-well tests, $d = d'$ and $l = l'$.

E-5.0 RECOVERY METHODS

Recovery data were analyzed using the Theis recovery method. This is a semilog analysis method similar to the Cooper–Jacob procedure (1946, 098236).

In this method, residual drawdown is plotted on a semilog graph versus the ratio t/t' where t is the time since pumping began and t' is the time since pumping stopped. A straight line of best fit is constructed through the data points and T is calculated from the slope of the line as follows:

$$T = \frac{264Q}{\Delta s}$$

Equation 12

The recovery data are particularly useful compared with time-drawdown data. Because the pump is not running, spurious data responses associated with dynamic discharge rate fluctuations are eliminated. The result is that the data set is generally “smoother” and easier to analyze.

Other time-drawdown methods, such as the Hantush method, are applicable to recovery data as well (Hantush 1961, 098237). However, they must be used with plots of displacement versus recovery time, rather than residual drawdown versus t/t' . For a valid analysis, the displacement must be the *calculated recovery*—the difference between the observed residual drawdown and the extrapolated drawdown that would have occurred had pumping continued. For wells on the plateau, it is not generally possible to obtain a valid time-drawdown extrapolation because of ongoing flattening of the time-drawdown graph that occurs as a result of vertical growth of the cone of depression with time. As an acceptable alternative, actual recovery, rather than calculated recovery, is plotted versus recovery time, and the analysis is limited to early and middle data. Extending this method of analysis to the late recovery data is not valid.

E-6.0 SPECIFIC-CAPACITY METHOD

The specific capacity of the pumped well can be used to obtain a lower-bound value of hydraulic conductivity. The hydraulic conductivity is computed using formulas that are based on the assumption that the pumped well is 100% efficient. The resulting hydraulic conductivity is the value required to sustain the observed specific capacity. If the actual well is less than 100% efficient, it follows that the actual hydraulic conductivity would have to be greater than the conductivity calculated to compensate for well inefficiency. Thus, because the efficiency is unknown, the computed hydraulic conductivity value represents a lower bound. The actual conductivity is known to be greater than or equal to the computed value.

For fully penetrating wells, the Cooper–Jacob equation can be iterated to solve for the lower-bound hydraulic conductivity. However, the Cooper–Jacob equation (assuming full penetration) ignores the contribution to well yield from permeable sediments above and below the screened interval. To account for this contribution, it is necessary to use a computation algorithm that includes the effects of partial penetration (1946, 098236). One such approach was introduced by Brons and Marting (1961, 098235) and augmented by Bradbury and Rothchild (1985, 098234).

Brons and Marting introduced a dimensionless drawdown correction factor, s_p , (1961, 098235) approximated by Bradbury and Rothschild as follows (1985, 098234):

Equation 13

$$s_p = \frac{1 - \frac{L}{b}}{\frac{L}{b}} \left[\ln \frac{b}{r_w} - 2.948 + 7.363 \frac{L}{b} - 11.447 \left(\frac{L}{b} \right)^2 + 4.675 \left(\frac{L}{b} \right)^3 \right]$$

In this equation, L is the well screen length in feet. Incorporating the dimensionless drawdown parameter, the conductivity is obtained by iterating the following formula:

Equation 14

$$K = \frac{264Q}{sb} \left(\log \frac{0.3Tt}{r_w^2 S} + \frac{2s_p}{\ln 10} \right)$$

To apply this procedure, a storage coefficient value must be assigned. Unconfined conditions were assumed for R-35b, while confined conditions were applied to R-35a. Storage coefficient values for confined conditions can be expected to range from about 10^{-5} to 10^{-3} , depending on aquifer thickness (Driscoll 1986, 098254) while those for unconfined conditions can be expected to range from about 0.01 to 0.25. The calculation result is not particularly sensitive to the choice of storage coefficient value, so a rough estimate of the storage coefficient is generally adequate to support the calculations. A confined value of 5×10^{-4} was used in the calculations for R-35a, while an assumed value of 0.05 was used for R-35b. For PM-3, confined conditions were assumed and a storage coefficient of 0.001 was used because of the substantial aquifer thickness.

The analysis also requires assigning a value for the saturated aquifer thickness, b . Aquifer thickness values of 236 ft and 93 ft were used for R-35a and R-35b, respectively, consistent with the above discussion of the conceptual hydrogeology. The computed result is not particularly sensitive to the exact thickness because sediments far above or below the screen have little effect on yield and drawdown response. Therefore, the calculations based on the assumed aquifer thickness values for R-35a and R-35b were deemed to be adequate. Calculations for PM-3 were based on full penetration.

Computing the lower-bound estimate of hydraulic conductivity can provide a useful frame of reference for evaluating the other pumping test calculations.

E-7.0 BACKGROUND DATA ANALYSIS

Background aquifer pressure data collected during the R-35 test period were plotted along with barometric pressure to determine the barometric effect on water levels and to look for pumping response in the surrounding observation wells. The R-35 well pair, R-5 and R-8, was monitored using nonvented pressure transducers, while the remaining R wells—R-9, R-11, R-13, and R-28—were monitored using vented transducers.

Figure E-1 shows water-level data from R-35a along with barometric pressure data from TA-54 that have been corrected to equivalent barometric pressure at the water table. The R-35a data are referred to in the figure as the “apparent hydrograph” because the measurements reflect the sum of water pressure and barometric pressure, having been recorded using a nonvented pressure transducer. The timing of the pumping periods for the R-35a and R-35b pumping tests are included on the figure for reference.

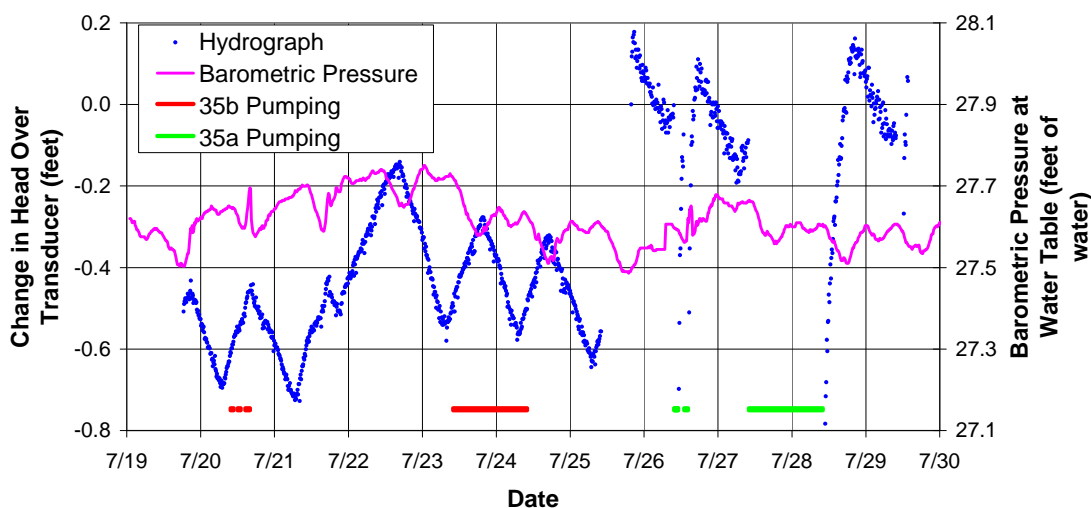


Figure E-1 Comparison of R-35a apparent hydrograph and adjusted TA-54 barometric pressure

The prominent diurnal peaks and valleys shown in the hydrograph signal were caused by the operation of Los Alamos County production well O-4. In addition, however, a subdued barometric pressure signal can be found in the hydrograph. On close inspection, it can be seen that during times of abrupt barometric pressure rise, a rising hydrograph curve segment became slightly steeper, while a falling segment tended to flatten just slightly. Conversely, during rapidly falling barometric pressure, a rising hydrograph segment flattened slightly, while a falling segment became somewhat steeper. The effect was subtle but clearly present.

The data suggest a high barometric efficiency for R-35a, although not 100%. Large changes in barometric pressure cause little change in the apparent hydrograph that reflects the combined water pressure and air pressure. This means that a given change in barometric pressure causes a nearly equal and opposite change in the water level so that the total pressure changes only slightly.

Figure E-2 shows a comparison of the R-35a data and the PM-3 hydrograph. Indicated on the graph are the times of pump startup and shutoff in O-4, showing a clear correlation between the operation of O-4 and the water-level changes in PM-3 and R-35a. The vertical axis for R-35a is expanded relative to that for PM-3. Accounting for the scale difference, the magnitude of the oscillations for R-35a is about 30% of that for PM-3 on average (amplitudes of about 0.3 and 1 ft, respectively). At first glance, it might be

concluded that both wells are responding directly to the pumping of O-4. An alternate explanation is that PM-3 is responding to pumping O-4 and R-35a is responding to the resulting changes in the PM-3 water levels. PM-3 has a specific capacity of about 55 gpf). This means that the foot of water-level change induced in PM-3 is similar to the hydraulic effect of pumping PM-3 at a discharge rate of 55 gpm. It is expected that such an event would cause an observable response in R-35a, located just 343 ft away. In this scenario, the cone of depression/impression caused by operating O-4 would travel rapidly through the most transmissive subsurface sediments to PM-3 and then the water-level change in PM-3 would be transmitted locally to R-35a through the shallow Santa Fe Group sediments. A third possibility is that R-35a is responding to the combined effects of operating O-4 and the induced water-level changes in PM-3.

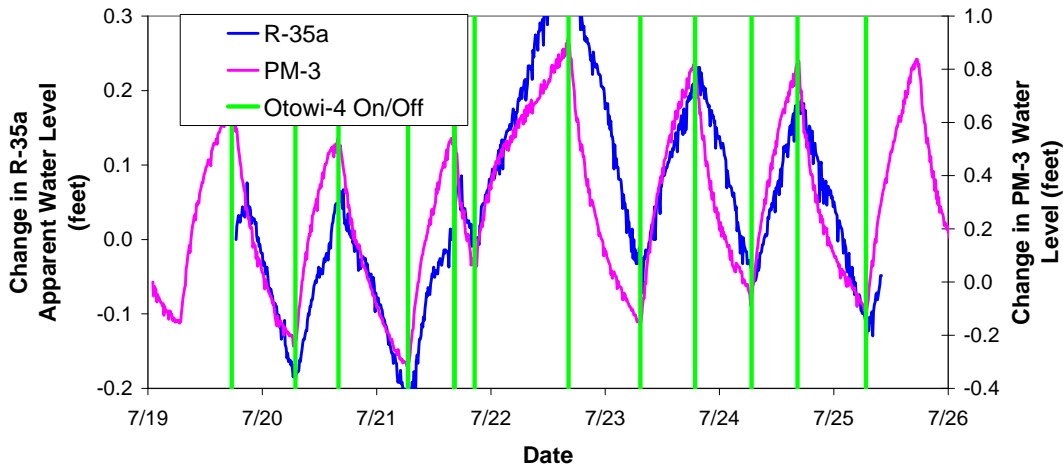


Figure E-2 Comparison of R-35a apparent hydrograph and PM-3 hydrograph

It was hoped that the observed water-level changes in PM-3 could serve as a surrogate for the background fluctuations in R-35a so that the background effects in R-35a could be removed mathematically, based on the PM-3 observations. Unfortunately, the oscillations in the two wells were not sufficiently consistent and regular to correlate them reliably. Because of the large fluctuations in the observed water levels, it was not possible to identify in Figure E-1 discernable drawdown in R-35a attributable to pumping R-35b. Close inspection of the portions of the hydrograph corresponding to pumping and recovery of R-35b revealed no noticeable response.

Figure E-3 shows the apparent hydrograph for R-35b along with the prevailing barometric pressure. The data showed that the aquifer pressure in R-35b was not affected significantly by barometric pressure, PM-3 water-level fluctuations and O-4 operation, or pumping R-35a.

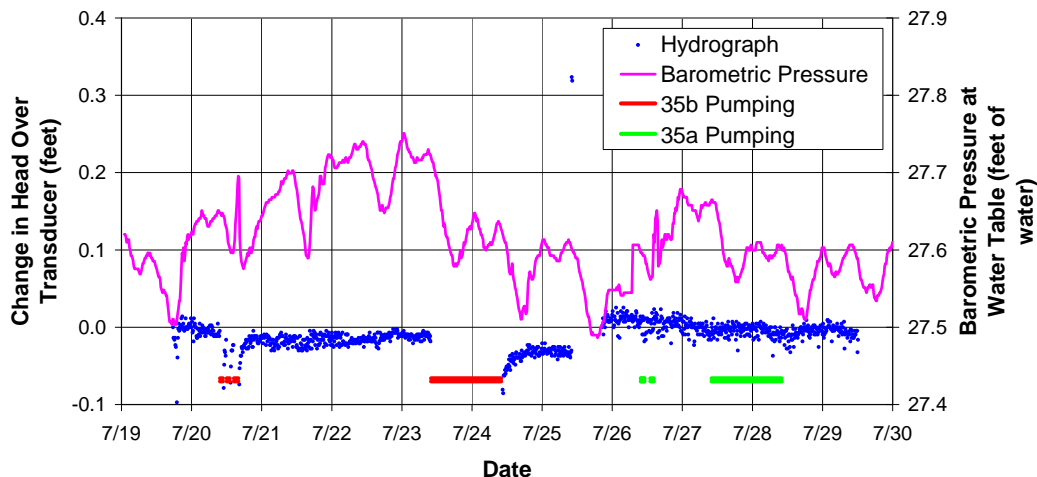


Figure E-3 Comparison of R-35b apparent hydrograph and adjusted TA-54 barometric pressure

The lack of pressure change associated with swings in barometric pressure implied a barometric efficiency of nearly 100% in R-35b. In other words, a given change in barometric pressure caused an equal and opposite change in water level in R-35b, so that the total pressure recorded by the nonvented transducer remained constant. The lack of a discernable response to either pumping R-35a or water-level changes in PM-3 implied that the Puye Formation is fairly well hydraulically separated from the underlying sediments. This observation was consistent with the differing static water levels measured in R-35a and R-35b.

Figure E-4 shows the aquifer pressure recorded in R-5 Screen 3. The nearly flat-line response implied a barometric efficiency of nearly 100% and negligible response to pumping either R-35a or R-35b.

Figure E-5 shows the apparent hydrograph for R-5 Screen 4. Indicated on the graph are the times of pump startup and shutoff in PM-1, showing that operation of this well caused the large water-level fluctuations observed in Screen 4. The magnitude of the PM-1 induced drawdown and recovery was sufficient to mask any possible pumping effect from R-35a or R-35b. It also precluded a determination of barometric efficiency for Screen 4.

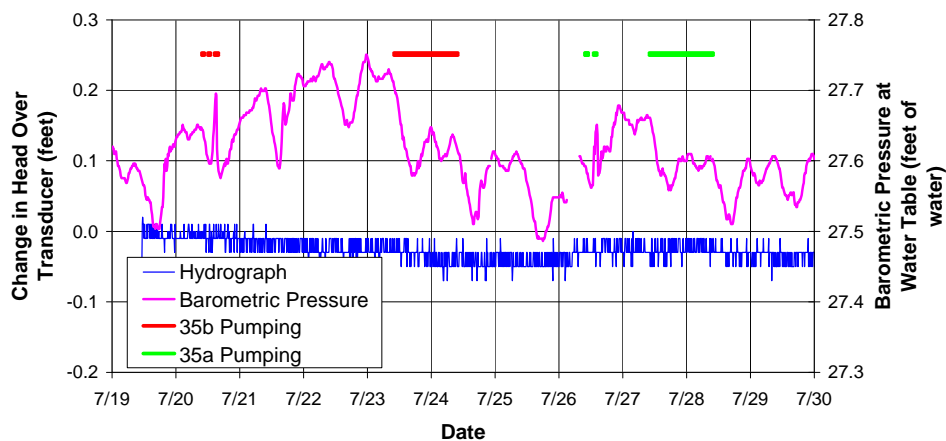


Figure E-4 Comparison of R-5 Screen 3 apparent hydrograph and adjusted TA-54 barometric pressure

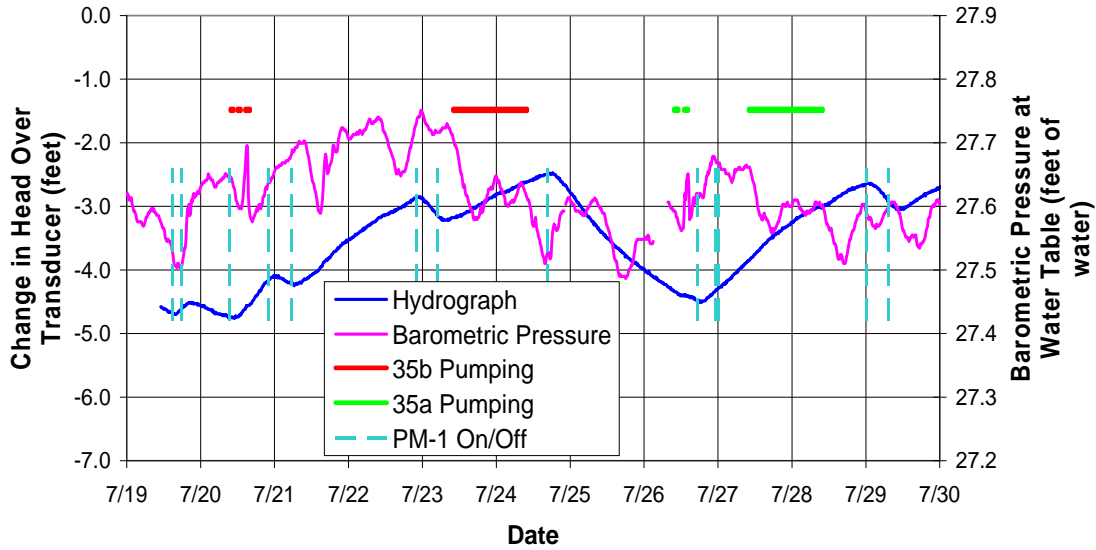


Figure E-5 Comparison of R-5 Screen 4 apparent hydrograph and adjusted TA-54 barometric pressure

Figure E-6 shows the apparent hydrograph for R-8 Screen 1 along with the barometric pressure record for July. The steady rise in the measured water levels was attributable to ongoing recovery associated with the July 2 shutdown of well PM-3.

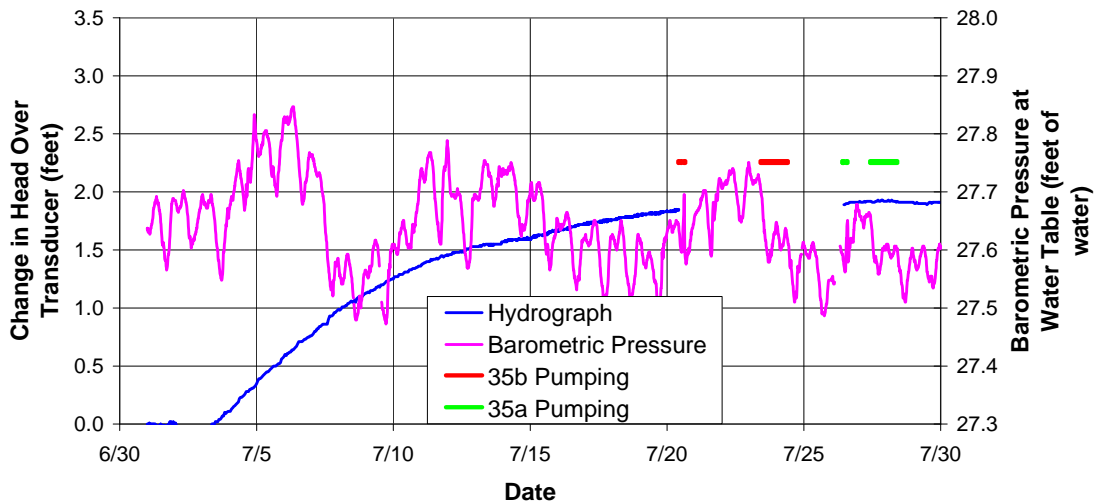


Figure E-6 Comparison of R-8 Screen 1 apparent hydrograph and adjusted TA-54 barometric pressure - full month

Figure E-7 shows an expanded-scale graph of the R-8 Screen 1 data. The data show a high barometric efficiency and belie any discernible response to pumping R-35a. Water levels were not measured in R-8 during the testing of R-35b.

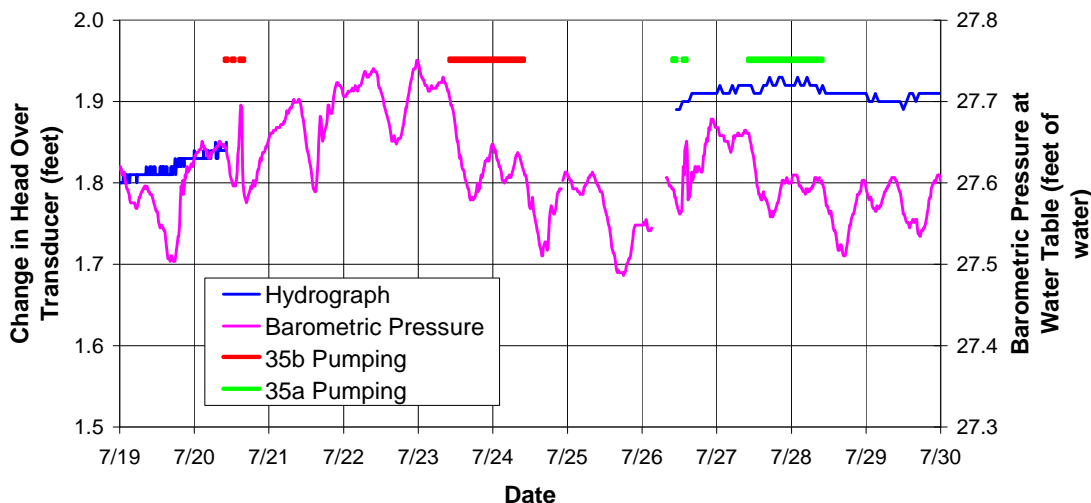


Figure E-7 Comparison of R-8 Screen 1 apparent hydrograph and adjusted TA-54 barometric pressure

Figure E-8 shows the apparent hydrograph for R-8 Screen 2 along with the barometric pressure record for 9 July. The steady rise in the measured water levels was attributable to ongoing recovery associated with the July 2 shutdown of well PM-3. The magnitude of the water-level recovery was substantially greater than that observed in Screen 1, implying the presence of an aquitard between Screens 1 and 2. This is consistent with the observed static water elevations in these two zones, which differ by nearly 20 ft.

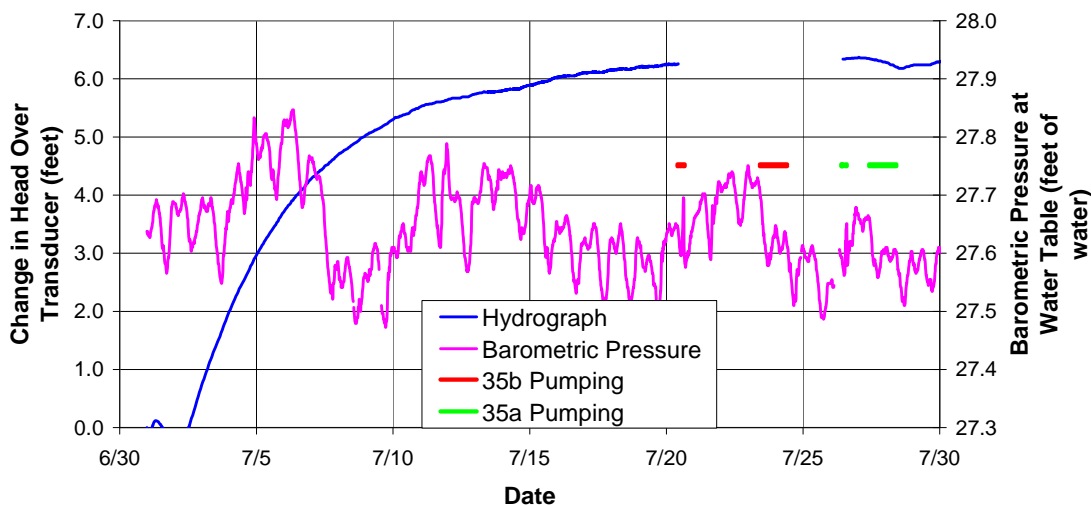


Figure E-8 Comparison of R-8 Screen 2 apparent hydrograph and adjusted TA-54 barometric pressure—full month

Figure E-9 shows an expanded-scale graph of the R-8 Screen 2 data. The measured pressure shown on the right-hand portion of the graph showed changes similar to the barometric pressure changes. At first glance, this appeared to imply a correlation that would have been consistent with a low barometric efficiency for R-8 Screen 2. Recall that a low barometric efficiency means that the total aquifer pressure changes about the same amount as the barometric pressure. That appeared to be the case in Figure E-9 because the R-8 Screen 2 pressure changed by an amount similar to the change in barometric pressure over the last 3 d of data shown on the graph.

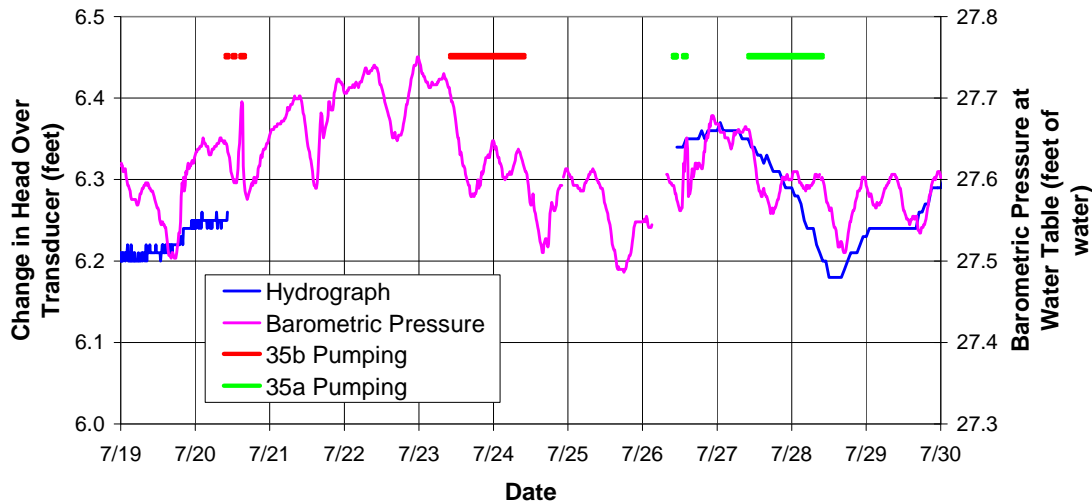


Figure E-9 Comparison of R-8 Screen 2 apparent hydrograph and adjusted TA-54 barometric pressure

However, subsequent data recorded over the next week (not included here) showed no such correlation between R-8 Screen 2 pressures and barometric pressure. This indicated that low barometric efficiency was not the explanation for the observed data in R-8 Screen 2 from July 27 to 30 in Figure E-9. Therefore, there must have been an alternate explanation.

Further examination of Figure E-9 showed that the aquifer pressure in R-8 Screen 2 declined during the R-35a pumping test, as well as for several hours after shutdown, and then recovered slightly over the next day and a half. The resulting hydrograph coincidentally mimicked the general shape of the barometric pressure curve but was probably a result of the R-35a pumping test.

Another observation of the R-8 Screen 2 response in Figure E-9 is that it was not the typical pumping test response in which heads vary logarithmically. The actual head changes appeared to be somewhat sluggish vis-à-vis the start and stop times for the R-35a pumping test. Similar sluggishness was observed in the R-8 response when pumping PM-3, as described below.

Figure E-10 shows the hydrograph recorded in R-9. The data were recorded using a vented transducer as opposed to the nonvented type used to monitor the wells illustrated in the previous figures. In this case, the measured pressure represents the true height of water above the transducer, rather than the sum of the water height and barometric pressure.

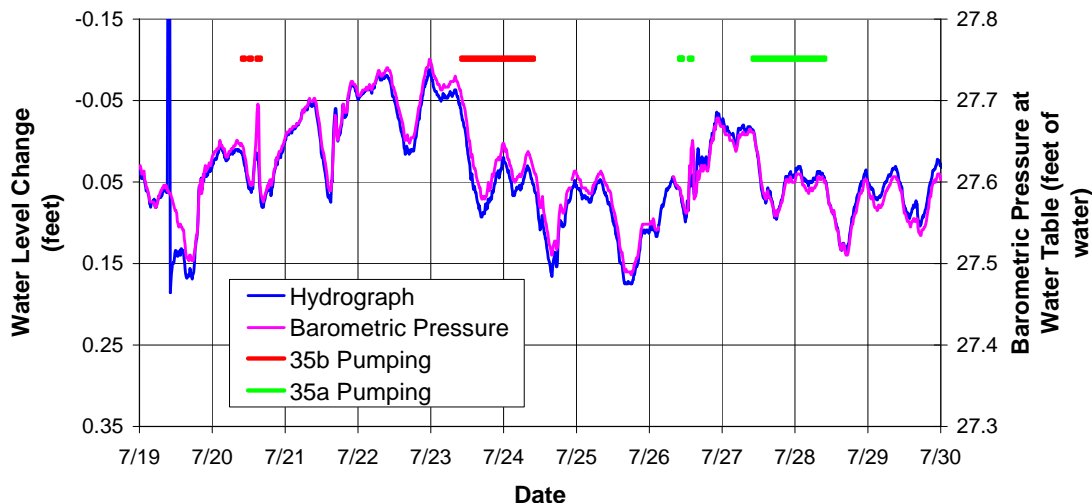


Figure E-10 Comparison of R-9 hydrograph and adjusted TA-54 barometric pressure

In Figure E-10, the relative water levels were plotted on an axis having the same scale as the barometric pressure data axis but inverted. It is evident that a given change in barometric pressure caused an equal and opposite change in water level. This means that R-9 is essentially 100% barometrically efficient. (If the R-9 data were collected using a nonvented transducer, the measured heads would have shown a flat line response, similar to that shown in Figure E-4 for R-5 Screen 3.)

Aside from water-level changes associated with barometric pressure, it was not possible to detect drawdown/recovery caused by either R-35a or R-35b. Additionally, there was no obvious response to the operation of O-4 or PM-1.

Figure E-11 shows the hydrograph measured in R-11 during the R-35 pumping tests. The water-level curve has been plotted inverted, where a rise on the graph corresponds to a decline in water level. Note the similarity between the hydrograph and the barometric pressure record.

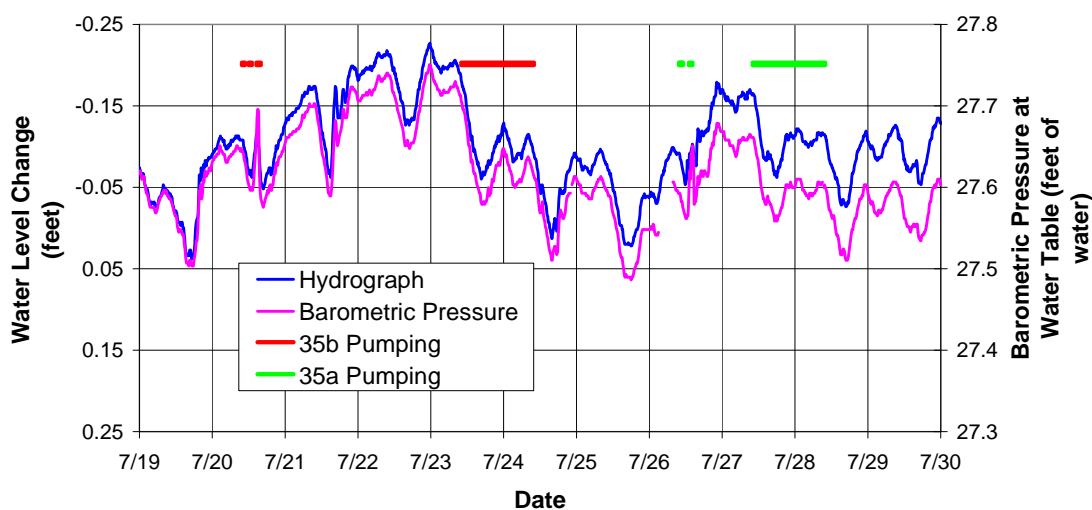


Figure E-11 Comparison of R-11 hydrograph and adjusted TA-54 barometric pressure

Although the shapes of the curves match, they diverge steadily over time. This response may be a result of a steady decline in the regional water levels in R-11. To investigate this possibility, the hydrograph was modified by correcting the data for a presumed uniform background water-level decline. The magnitude of the decline was adjusted to obtain a best fit between the corrected hydrograph and barometric pressure curve. Figure E-12 shows the resulting graphical comparison using a background trend of 0.0064 ft/d.

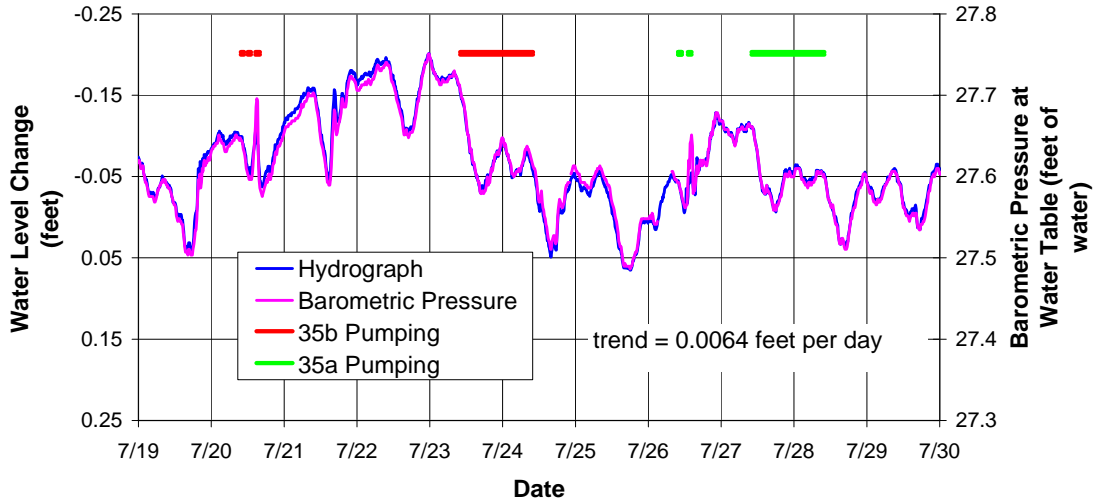


Figure E-12 Comparison of R-11 hydrograph with linear trend and adjusted TA-54 barometric pressure

The good agreement suggests that all of the water-level fluctuation observed in R-11 was attributable to changes in barometric pressure. There appeared to be negligible response to pumping R-35a, R-35b, or any other wells. The results suggested a barometric efficiency near 100%.

Figure E-13 shows the hydrograph measured in R-13 during the R-35 pumping tests. As with R-11, the R-3 data appeared to respond to changes in barometric pressure with a superimposed linear background trend.

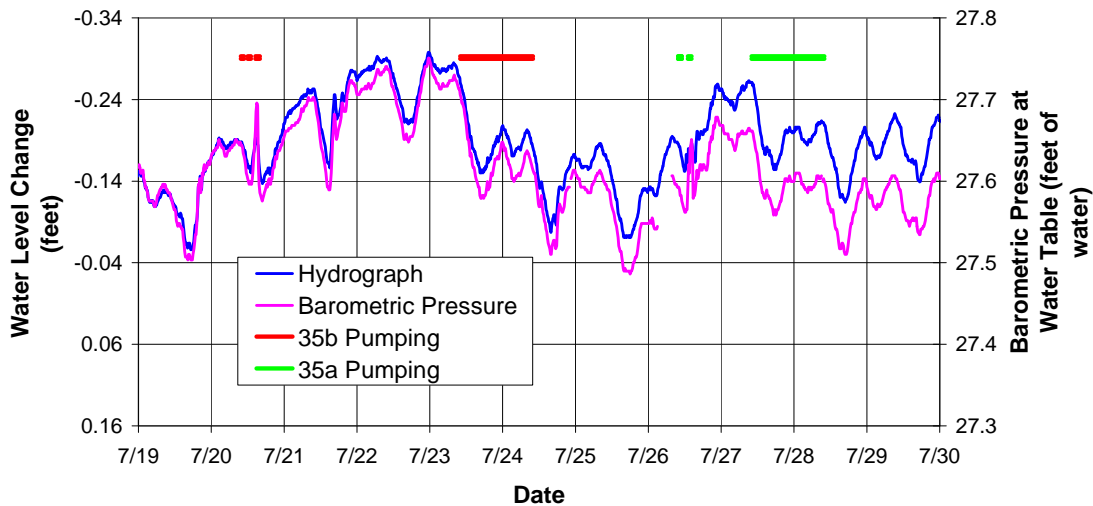


Figure E-13 Comparison of R-13 hydrograph and adjusted TA-54 barometric pressure

Figure E-14 shows a comparison of the barometric pressure curve and the hydrograph adjusted for a background water-level decline of 0.0064 ft/d. The excellent agreement suggested a high barometric efficiency and negligible (nondetectable) response to the pumping tests.

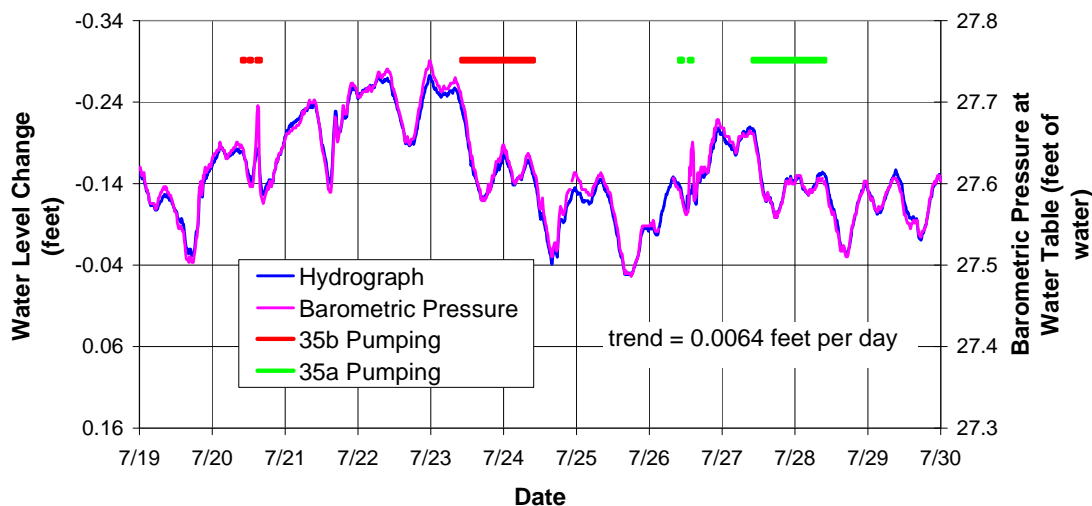


Figure E-14 Comparison of R-13 hydrograph with linear trend and adjusted TA-54 barometric pressure

Figure E-15 shows the hydrograph measured in R-28 during the R-35 pumping tests. As with R-11 and R-13, the R-28 data appeared to respond to changes in barometric pressure with a superimposed linear background trend.

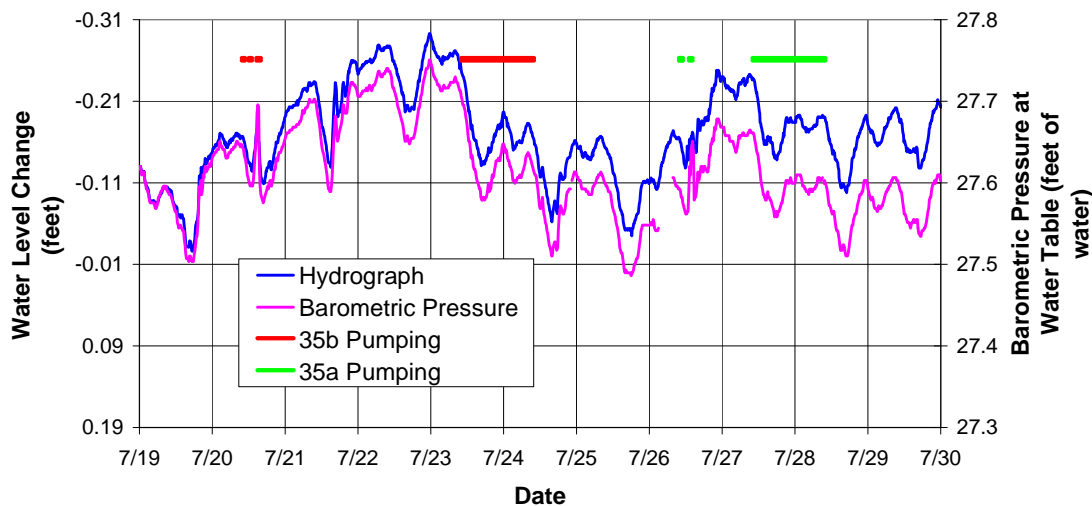


Figure E-15 Comparison of R-28 hydrograph and adjusted TA-54 barometric pressure

Figure E-16 shows a comparison of the barometric pressure curve and the hydrograph adjusted for a background water-level decline of 0.0077 ft/d. The excellent agreement suggested a high barometric efficiency and negligible (nondetectable) response to the pumping tests.

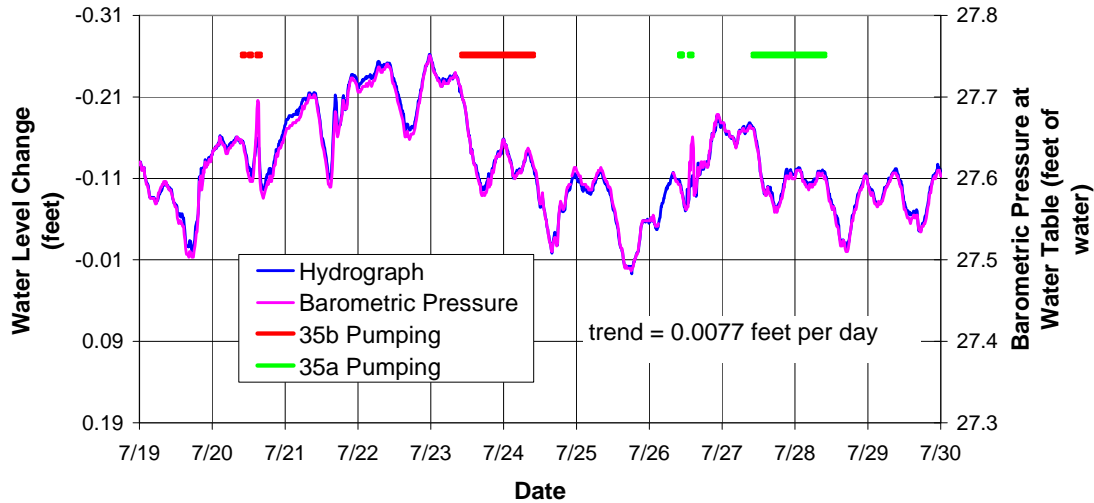


Figure E-16 Comparison of R-28 hydrograph with linear trend and adjusted TA-54 barometric pressure

In summary, the only clear pumping well signals observed in the monitored wells were (a) R-5 Screen 4 response to operation of PM-1, (b) R-8 screens 1 and 2 response to operation of PM-3, (c) sluggish R-8 Screen 2 response to pumping R-35a, and (d) R-35a response to operation of O-4, perhaps indirectly because of the induced water-level changes in PM-3. All other wells showed negligible effects from any of the pumping wells. In other words, with respect to the pumping tests performed on R-35a and R-35b, it was not possible to document a measurable effect in any of the nearby monitored wells.

E-8.0 R-35a DATA ANALYSIS

This section presents the data obtained from the R-35a pumping tests and the results of the analytical interpretations. Analyses were applied to recovery data following trial 1, as well as pumping and recovery data from trials 2 and 3, the 24-h constant-rate pumping test and the final sampling event.

Trial 1

Figure E-17 shows a semilog plot of the trial 1 recovery data. The transmissivity value computed from the very early data (several seconds) was 743 gpft. It was expected that this value represented the transmissivity of a sediment thickness approximately equal to the well screen length because the vertical growth of the cone of impression would have been minimal after such a short time. In other words, the earliest data reflect conditions immediately adjacent to the well screen. Based on a screen length of 49.1 ft, the computed hydraulic conductivity was 15.1 gpd/ft², or 2.0 ft/d.

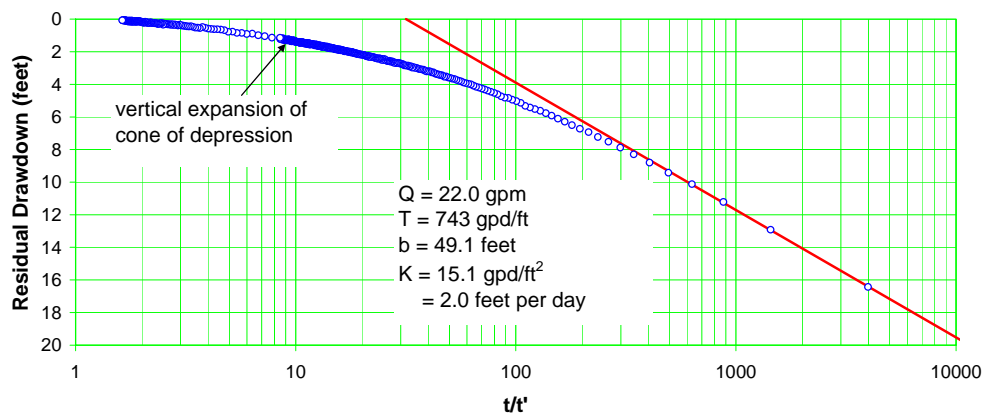


Figure E-17 Well R-35a Trial 1 Recovery

After several seconds of recovery, the data trace began flattening steadily over time as the cone of impression expanded vertically through the thickness of the aquifer (presumably 236 ft as described previously). Figure E-18 shows an expanded-scale graph of the late recovery data, revealing a transmissivity of 4380 gpd/ft. It was expected that this value corresponded to the presumed aquifer thickness of 236 ft, making the calculated hydraulic conductivity 18.6 gpd/ft², or 2.5 ft/d. The hydraulic conductivity value of 2.0 ft/d for the screened interval was considered fairly accurate, whereas the value of 2.5 ft/d average for the thickness of the aquifer was considered approximate because of the uncertainty in the assumed aquifer thickness.

It should be pointed out that for the very early data, it was not possible to know the exact elapsed time since pumping stopped (or started, in the case of time-drawdown graphs). This is because the actual starting and stopping of the pump in the field could not be timed to the nearest split second. Data from the R-35a pumping tests were recorded at 2-s intervals. As a result, the first data point showing measurable drawdown was known to have occurred within 2 s of startup, but the precise duration was not known. Therefore, the elapsed time to the first data point was adjusted between 0 and 2 s until the first few data points on the graph fell on a straight line. The resulting elapsed time was deemed to be a reasonable estimate.

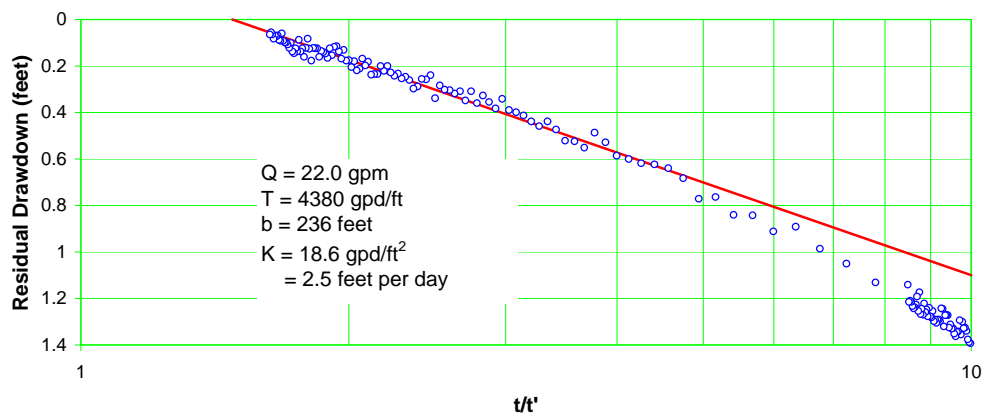


Figure E-18 Well R-35a trial 1 recovery—expanded scale

To illustrate this, the recovery data were replotted in Figure E-19 as feet of recovery versus elapsed time since pumping stopped. The straight-line criterion described above was achieved for an elapsed time of just over 1 s for the first data point on the graph. For this assumption, the first few data points fell in a straight line.

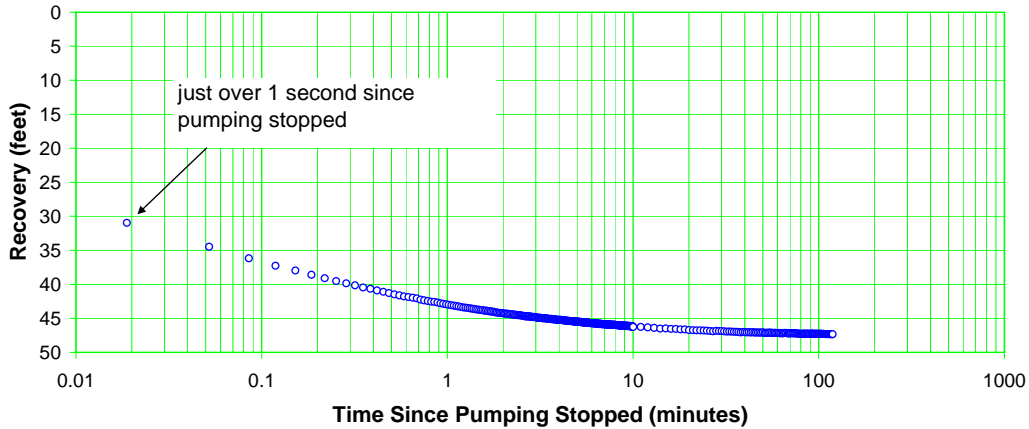


Figure E-19 Well R-35a trial 1 recovery versus time

Note on the graph that the magnitude of the recovery was more than 30 ft in just 1 s. This highlights the advantage of conducting these pumping tests using an inflatable packer, thereby eliminating the sluggish response that occurs when casing storage affects the data. In fact, casing storage calculations showed that casing storage effects would have persisted for 10 to 15 min, eliminating the possibility of obtaining an accurate estimate of the hydraulic conductivity of the screened sediments.

Trial 2

Figure E-20 shows the time-drawdown data from trial 2. The very early data supported a transmissivity calculation of 987 gpd/ft for the screened interval making the hydraulic conductivity of the 49.1-ft screened interval 20.1 gpd/ft², or 2.7 ft/d.

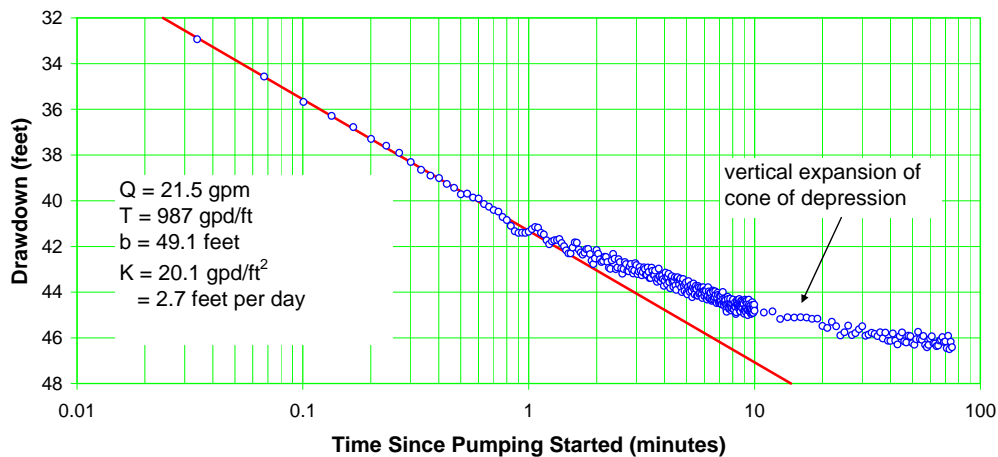


Figure E-20 Well R-35a trial 2 drawdown

Figure E-21 shows an expanded-scale plot of the late drawdown data. It is clear that the data exhibited considerable scatter. Nonavailability of suitable equipment forced the use of a 300 psi pressure transducer for recording water levels in R-35a. The precision of a transducer with such a high-pressure rating is not as good as that of one with a lower pressure rating and is reflected in significant data scatter in the recorded measurements. In addition, some of the scatter was attributable to electrical/magnetic interference from the electric submersible pump cable (as evidenced by reduced scatter in the recovery data set).

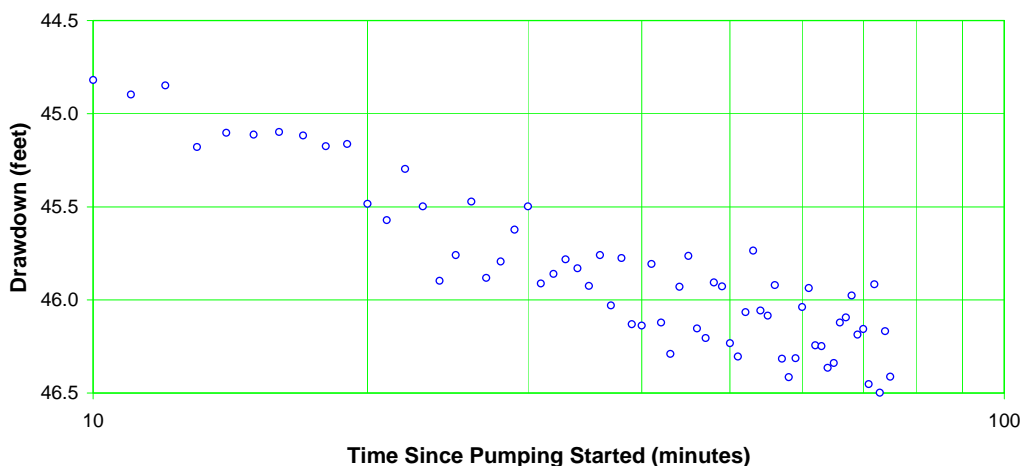


Figure E-21 Well R-35a trial 2 drawdown—expanded scale

To minimize the amount of data scatter, a rolling average of the data was calculated and plotted in Figure E-22. The rolling average included two data points on either side of the plotted point. As shown in the figure, the late data supported a calculated transmissivity of 4370 gpd/ft, making the hydraulic conductivity of the full aquifer thickness 18.5 gpd/ft², or 2.5 ft/d.

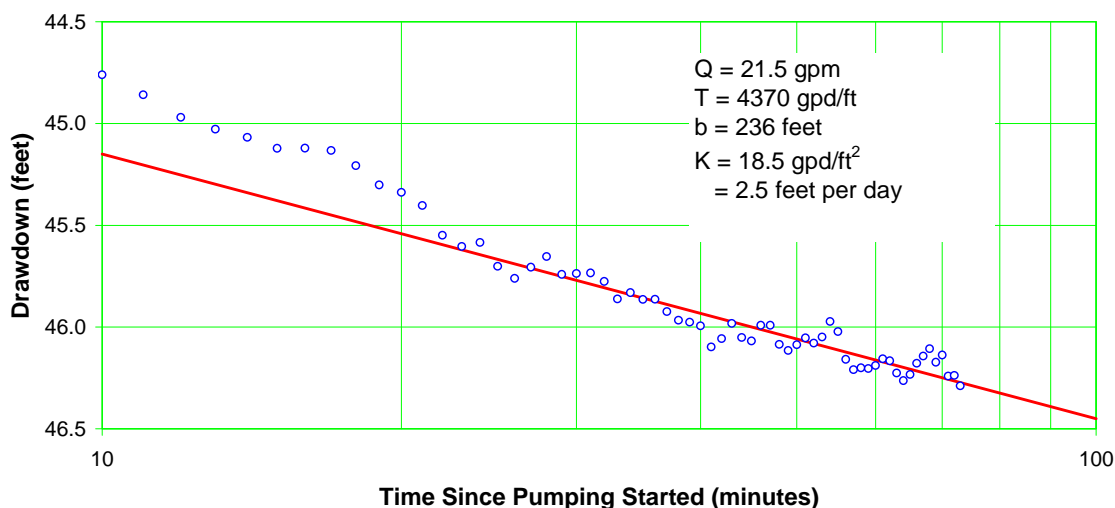


Figure E-22 Well R-35a trial 2 drawdown—rolling average

Figure E-23 shows a semilog plot of the trial 2 recovery data. The transmissivity value computed from the very early data was 800 gpd/ft making the hydraulic conductivity of the screened interval 16.3 gpd/ft², or 2.2 ft/d.

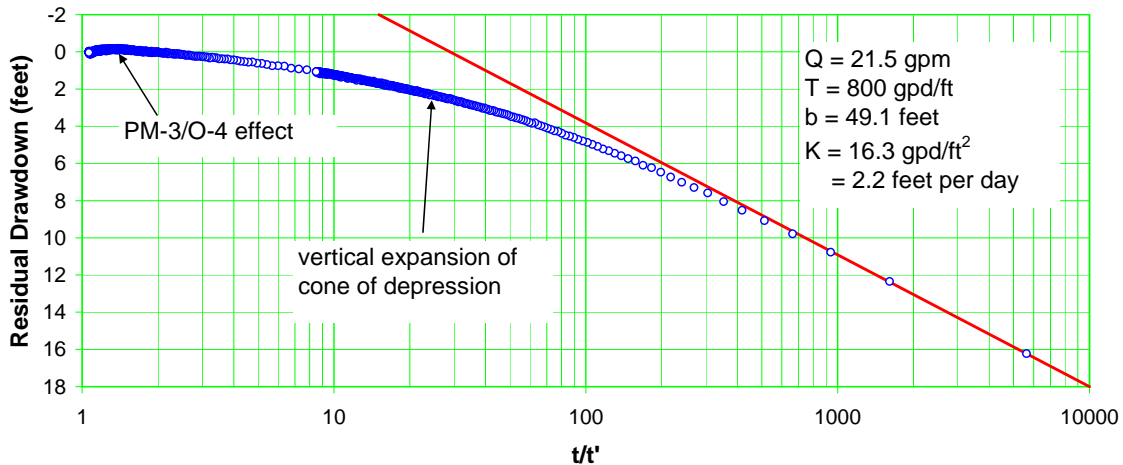


Figure E-23 Well R-35a trial 2 recovery

Figure E-24 shows an expanded-scale plot of the late recovery data. The straight line of fit shown on the graph revealed a transmissivity of 4370 gpd/ft for the 236-ft-thick aquifer, making the hydraulic conductivity 18.5 gpd/ft², or 2.5 ft/d. The line shown utilizes the “middle” data shown in the figure. However, this is analogous to the “late” data shown on previous graphs. The recovery time following trial 2 was much longer (1185 min) than pumping and recovery times (75 to 120 min) shown previously.

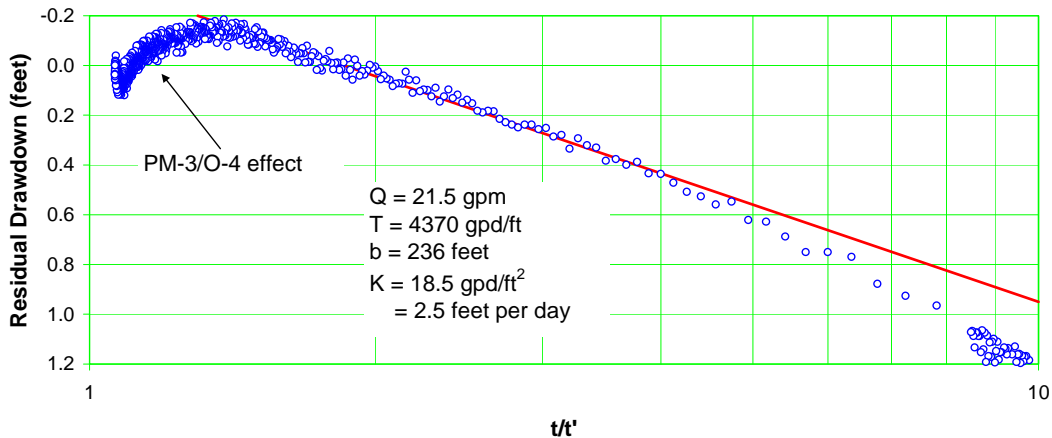


Figure E-24 Well R-35a trial 2 recovery—expanded scale

The effect of O-4/PM-3 is evident in the very late recovery data in Figure E-24. The data trace peaks and then falls a few tenths of a foot in response to the pumping of O-4 and then recovers slightly after O-4 shuts down. As mentioned previously, there was no practical and accurate way to filter out the large water-level fluctuations associated with the operation of O-4.

A third interpretation of the recovery data is shown in E-25. A line of fit was constructed using the very late data, largely ignoring the sinusoidal background water-level fluctuations. In other words, the line connected data from about an hour after shutdown (t/t' of about 2.3) to data from the end of the recovery period nearly a day later. The idea was to remove the 24-h sinusoidal effect of O-4. This would have been a valid analysis if the recovery period had been about 24 h and if the effect of O-4 on the R-35a water

levels were the identical day-to-day. However, the recovery period was less than a full 24-h cycle, and it was known that the O-4 pumping effect varied from day to day. Therefore, the resulting analysis is fairly rough and intended to provide an approximate transmissivity estimate. Understanding these limitations, the line of fit was considered a plausible representation of the approximate path the data points may have taken if the O-4 interference not occurred. The transmissivity value computed from the line of fit was 16,200 gpd/ft. If this value is taken as the true transmissivity of the presumed 236-ft-thick aquifer, the resulting hydraulic conductivity is 68.6 gpd/ft², or 9.2 ft/d.

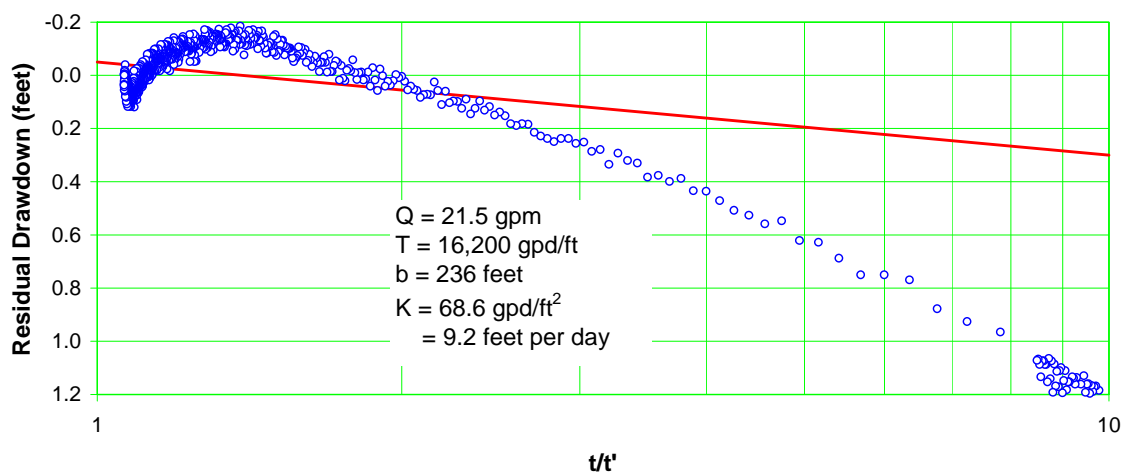


Figure E-25 Well R-35a trial 2 recovery—late data

There are two possible interpretations for the Figure E-25 analysis. One is that the recovery cone of impression was still expanding vertically within the 236-ft-thick zone; thus, the computed hydraulic conductivity represented a realistic average value for the identified thickness. Under this scenario, the late slopes on the previous graphs (corresponding to pumping or recovery times on the order of a couple of hours) would be considered “intermediate” data recorded before full vertical development of the cone of depression/impression. A second interpretation is that the late flat slope in Figure E-25 is a byproduct of leakage from above and/or below the identified subject thickness. This idea is reasonable because, as described later, the overlying permeable zone in which R-35b is completed is highly transmissive and capable of providing a leakage effect. The latter scenario seems more reasonable, but there is no way to distinguish which mechanism is operating here. In this analysis, it was assumed that the intermediate-time data provided valid transmissivity and hydraulic conductivity information while the late data were affected by leakage. Note also that the late-time slope shown in Figure E-25 could only be approximated because of the background fluctuations. In this case, the magnitude of the background noise was several times greater than the likely theoretical change in water level over the last 12 h of recovery.

R-35a 24-H Constant-Rate Pumping Test

Figure E-26 shows drawdown recorded during the 24-h pumping test in R-35a. The transmissivity value computed from Figure E-26 was 900 gpd/ft, making the hydraulic conductivity of the screen zone 18.3 gpd/ft², or 2.5 ft/d.

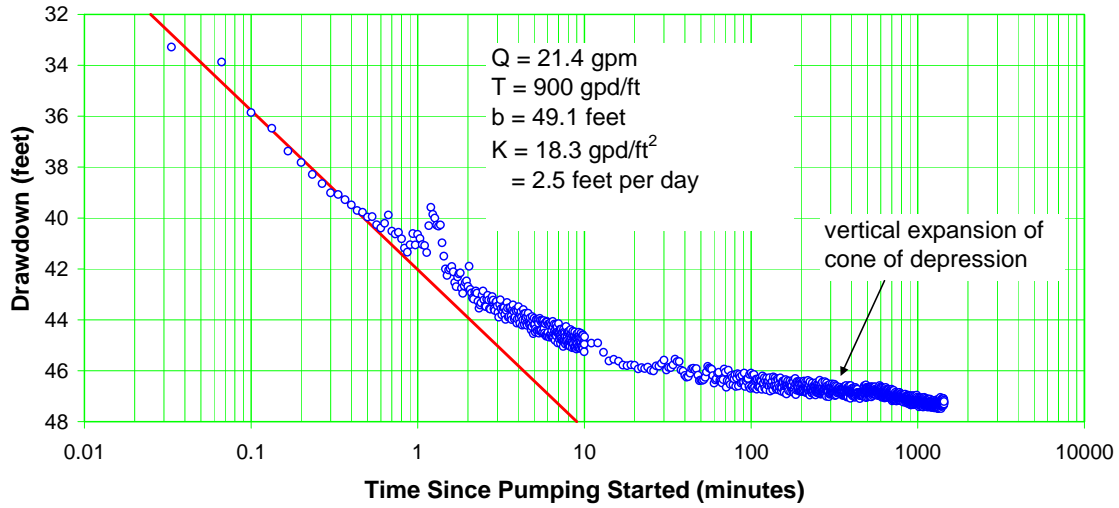


Figure E-26 Well R-35a drawdown

Figure E-27 shows an expanded-scale plot of the drawdown data. The data scatter associated with the 300 psi transducer and interference from the electrical pump cable is evident on the plot. There are, however, some areas where the scatter was noticeably diminished. There was no apparent explanation for this unusual feature of the drawdown values.

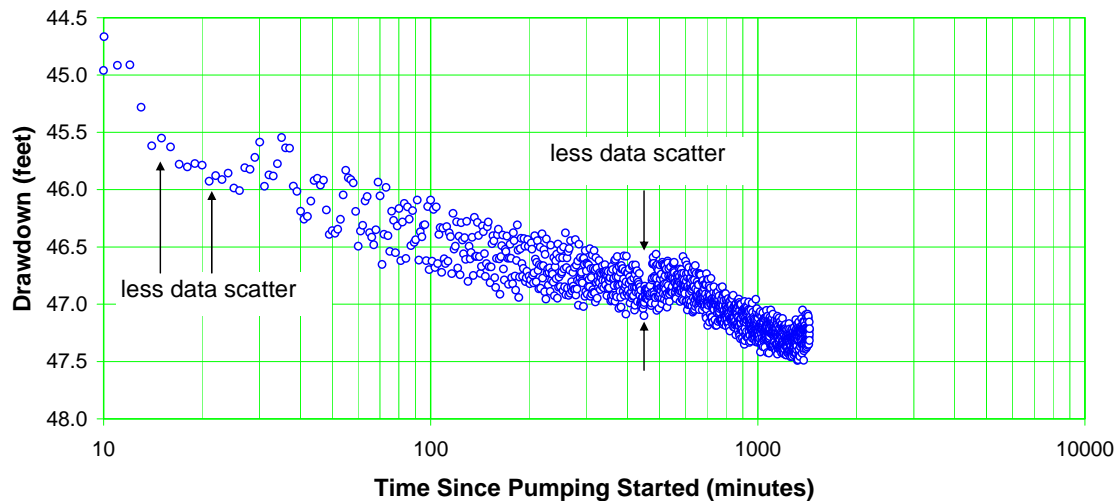


Figure E-27 Well R-35a drawdown—expanded scale

To reduce the data scatter, a rolling average plot (including five data points on either side of the plotted point) was prepared as shown in Figure E-28.

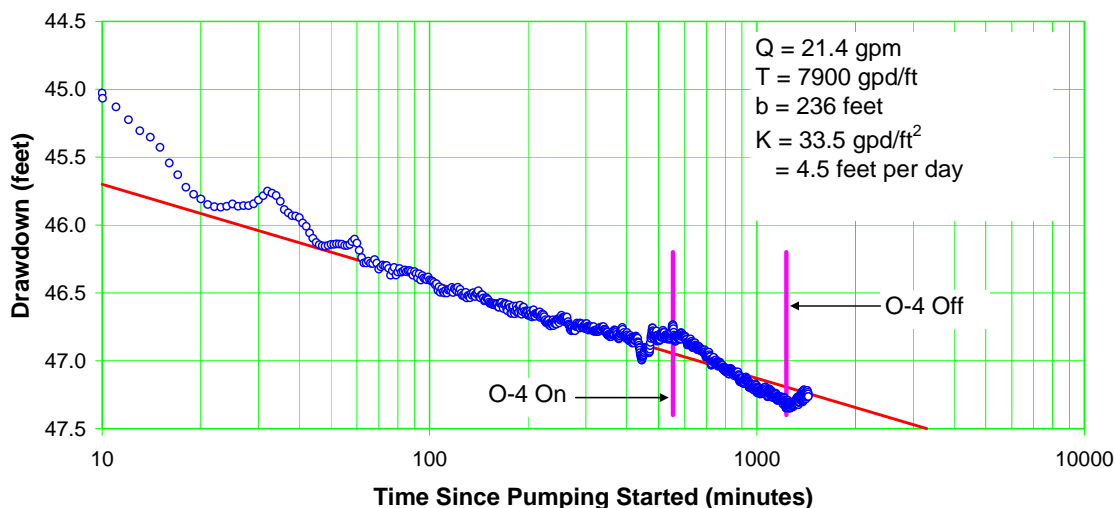


Figure E-28 Well R-35a drawdown—rolling average

The dips (valleys) visible on the figure correspond to periods of reduced data scatter from the original plot. A line of fit constructed through the intermediate and late data supported a transmissivity calculation of 7900 gpd/ft, making the computed hydraulic conductivity 33.5 gpd/ft², or 4.5 ft/d. It is possible that this hydraulic conductivity value was affected by leakage and therefore erroneous. The effects of operation of O-4 are clearly evident in Figure E-28. The apparent noise just preceding the startup of O-4, when the data trace should have been smooth, was an artifact of the unexplained variable amount of data scatter in the original plot.

Figure E-29 shows a semilog plot of the recovery data following pump shutoff. The transmissivity value computed from the very early data was 770 gpd/ft making the hydraulic conductivity of the screened interval 15.7 gpd/ft², or 2.1 ft/d. The first couple of data points showed perturbations that could not be explained readily.

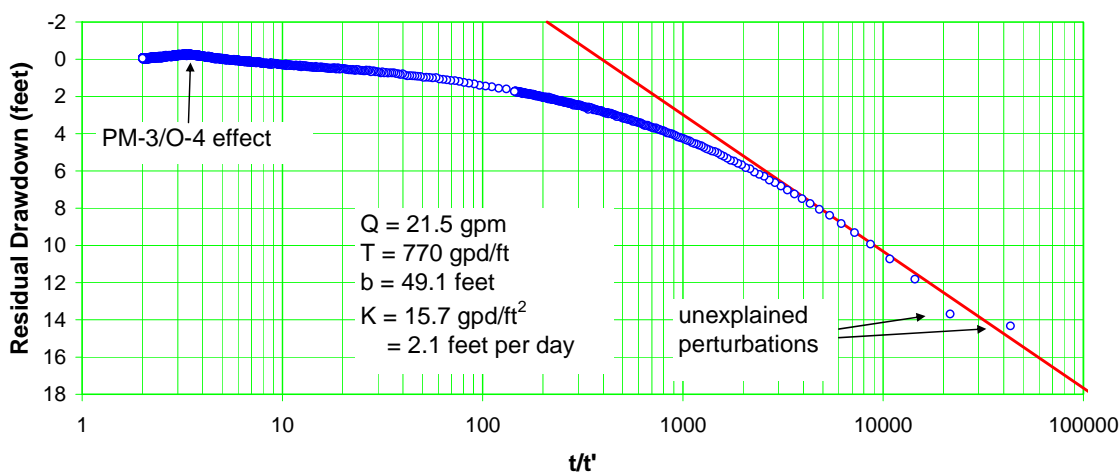


Figure E-29 Well R-35a recovery

Figure E-30 shows an expanded-scale plot of the recovery data. The transmissivity computed from the intermediate data, presumably representative of the full 236-ft thickness, was 6460 gpd/ft, making the average hydraulic conductivity 27.4 gpd/ft², or 3.7 ft/d.

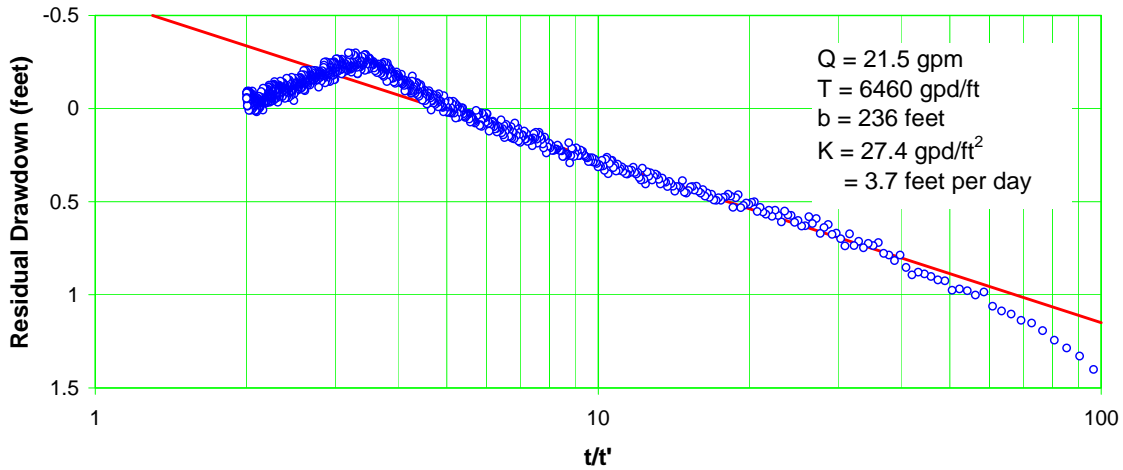


Figure E-30 Well R-35a recovery—expanded scale

Figure E-31 shows an interpretation based on the late data, ignoring the sinusoidal fluctuation caused by the operation of O-4. This line of fit yielded a rough transmissivity estimate of 8630 gpd/ft and a hydraulic conductivity of 36.6 gpd/ft², or 4.9 ft/d. These values could be representative but may likely be affected by leakage.

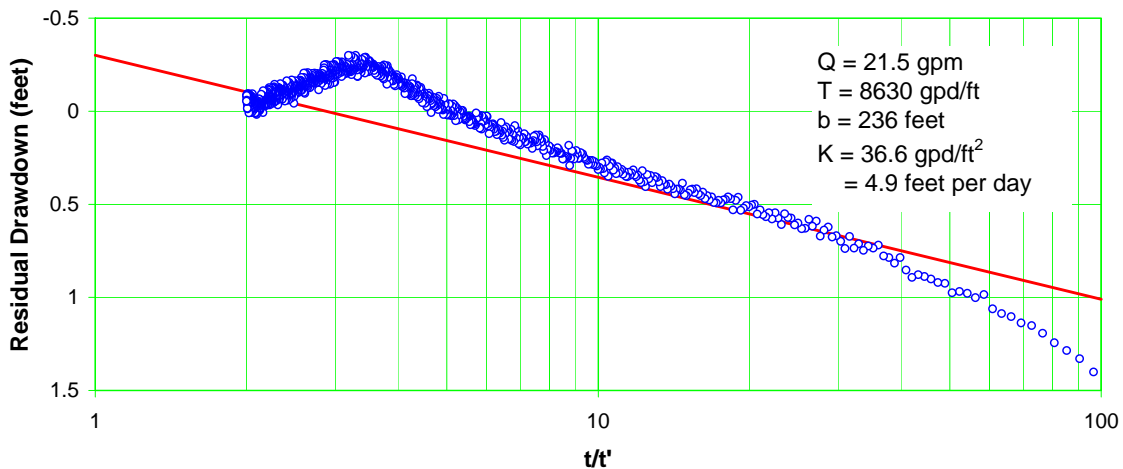


Figure E-31 Well R-35a recovery—late data

To account for the effects of partial penetration, the time-recovery data were analyzed using the Hantush method (1961, 098237). This method helps identify the hydraulic conductivity of the screened interval by using a larger data set than just the very early data points, including data associated with vertical expansion of the cone of depression.

Figures E-32, E-33, and E-34 show curve matching results for assumed vertical anisotropy ratios of 10, 100, and 1000, respectively. A range of assumed vertical anisotropy ratios was used to try to identify an optimum value. Analysis of time-recovery data is only valid for the early to middle data, and cannot be applied to the late data. The curve matches that were applied were consistent with this restriction.

A comparison of the graphs suggested that the curve match obtained for an anisotropy ratio of 100:1 was somewhat better than the others. As indicated in Figure E-33, the resulting hydraulic conductivity value for this anisotropy was 1.8 ft/d, consistent with the early-time values obtained for the screened interval from previous analyses.

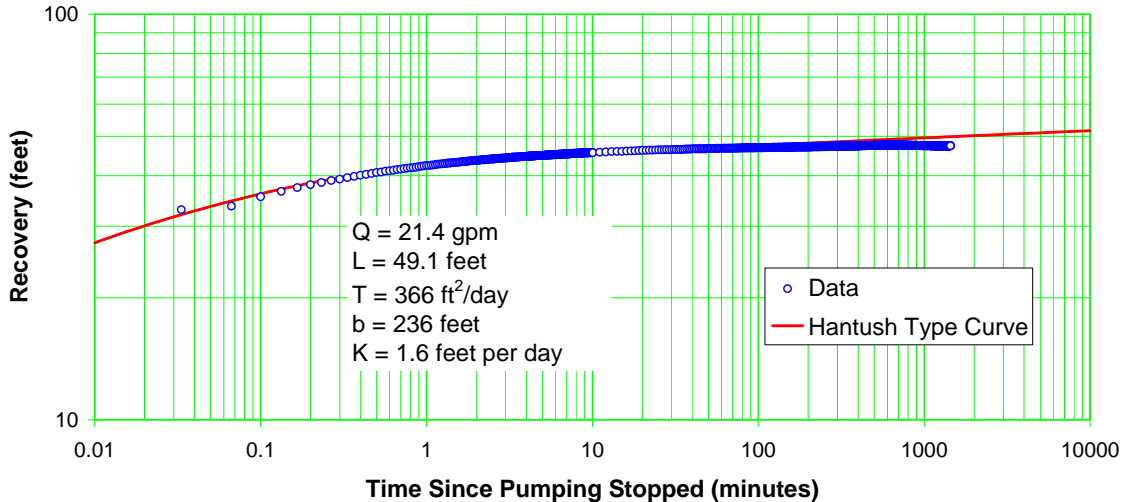


Figure E-32 Well R-35a recovery Hantush solution for anisotropy of 0.1

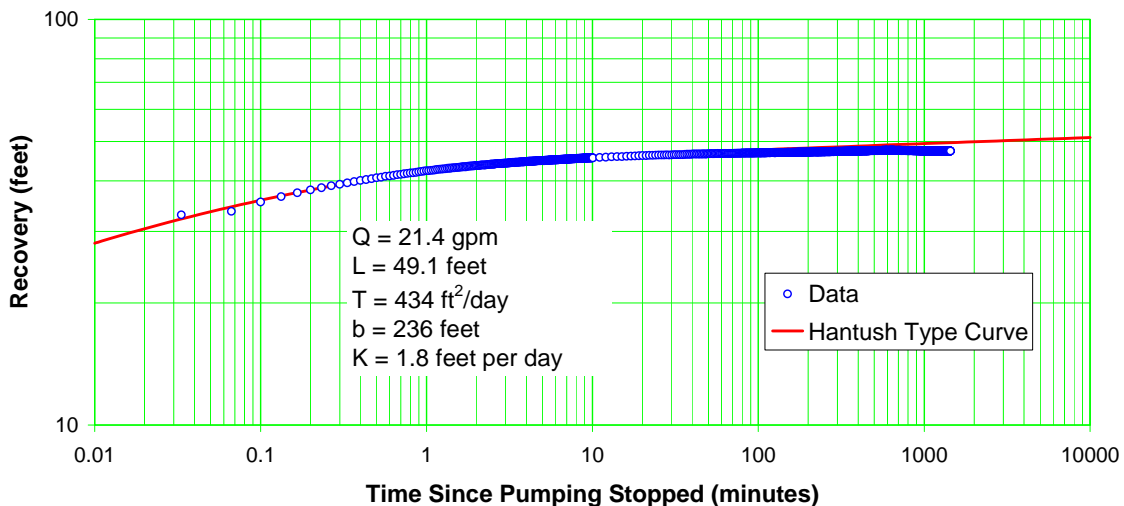


Figure E-33 Well R-35a recovery Hantush solution for anisotropy of 0.01

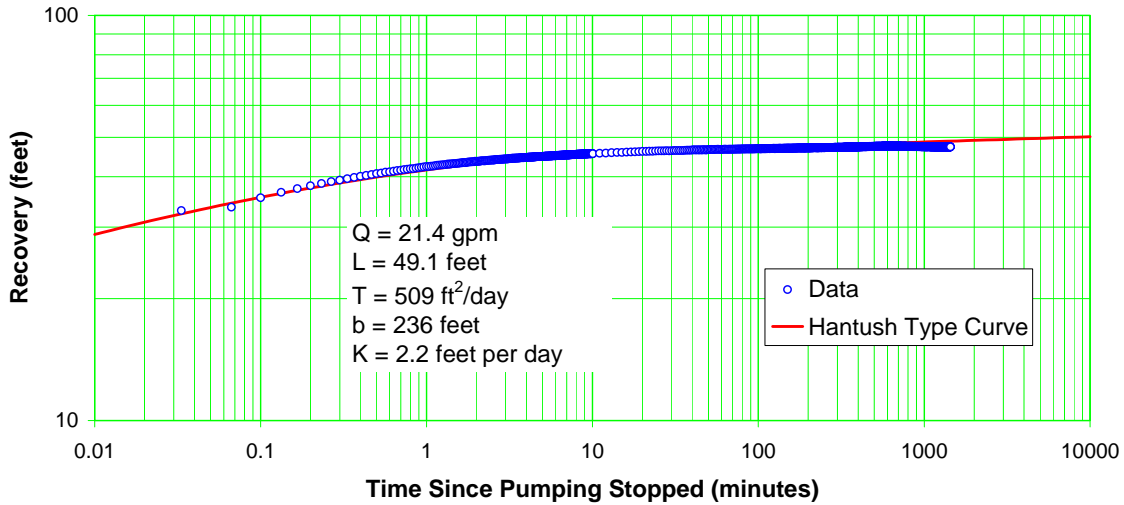


Figure E-34 Well R-35a recovery Hantush solution for anisotropy of 0.001

Water-Sampling Event

Figure E-35 shows recovery data recorded following shutdown from the water-sampling event performed before pulling the test pump from R-35a. The transmissivity value computed from the early data was 835 gpd/ft, making the hydraulic conductivity of the screened interval 17.0 gpd/ft², or 2.3 ft/d. Note that the early data trace is smooth, similar to the trial tests but different from the perturbations seen in the 24-h test.

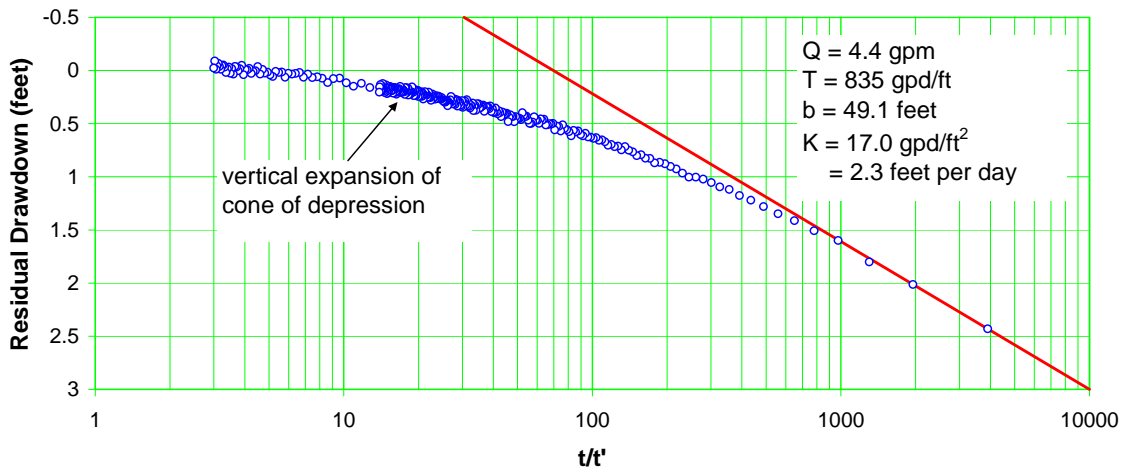


Figure E-35 Well R-35a sampling event recovery

Figure E-36 shows an expanded-scale plot of the late recovery data. The transmissivity value computed from this graph was 5040 gpd/ft, presumably representative of the 236-ft-thick zone, making the hydraulic conductivity 21.4 gpd/ft², or 2.9 ft/d.

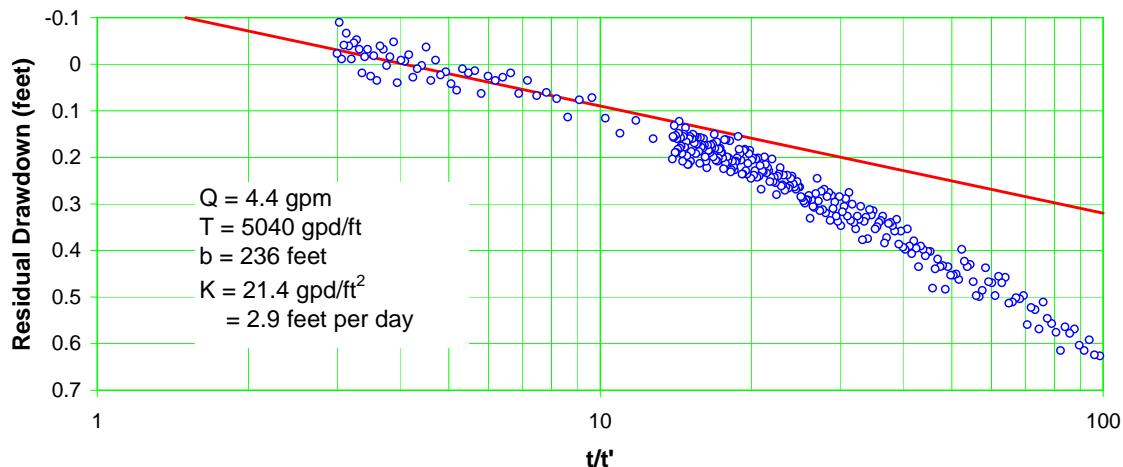


Figure E-36 Well R-35a sampling event recovery—expanded scale

Specific-Capacity Data

Specific-capacity data were used along with well geometry to estimate a lower-bound conductivity value for the R-35a screen zone for comparison to the pumping test values. In addition to specific capacity, other input values used in the calculations included the aquifer thickness of 236 ft, a storage coefficient of 5×10^{-4} and a borehole radius of 0.51 ft. The calculations are somewhat insensitive to the assigned aquifer thickness, as long as the selected value is substantially greater than the screen length.

R-35a produced 21.4 gpm with a drawdown of 47.3 ft after 24 h of pumping for a specific capacity of 0.45 gpm/ft. Applying the Brons and Marting method to these inputs yielded a lower-bound hydraulic conductivity value for the screened interval of 10.6 gpd/ft², or 1.41 ft/d (Brons and Marting 1961, 098235). Table E-2 summarizes the hydraulic conductivity values derived from the pumping tests. As indicated, the average hydraulic conductivity for the screened interval was 2.2 ft/d. The lower-bound value from the specific capacity was consistent with this. The well efficiency can be approximated as the ratio of the lower-bound hydraulic conductivity value to the actual. In this case the computed estimate of efficiency was 1.41/2.1, or 67%—a reasonable value.

This analysis was repeated for the sampling event, which was conducted at a substantially lower discharge rate. During this test, the well produced 4.4 gpm with 8.0 ft of drawdown after 130 min for a specific capacity of 0.55 gpm/ft. Applying the Brons and Marting method to these inputs yielded a lower-bound hydraulic conductivity value for the screened interval of 12.2 gpd/ft², or 1.64 ft/d (1961, 098235). The larger value was attributable the greater specific capacity. It is likely that the turbulent flow related component of drawdown was less at the lower discharge rate. Based on the sampling event data, the estimated well efficiency was 1.64/2.2, or 75%. Again, this value is entirely reasonable for a properly developed well.

Packer Deflation

Following completion of the pumping tests on R-35a, the downhole packer was deflated in preparation for pulling the submersible pump. Figure E-37 shows the head buildup that occurred when the packer was deflated.

The observed response was caused by the release of water suspended above the static water level in the annulus between the well casing and pump drop pipe and above the inflatable packer. Before packer inflation, water in this zone would have been at the same level as the ambient water level in the well. The head buildup of 11 ft shown on the graph corresponded to an annular volume of about 6.6 gal. This represented the volume of water that had leaked through the drop pipe coupling joints during the testing activities.

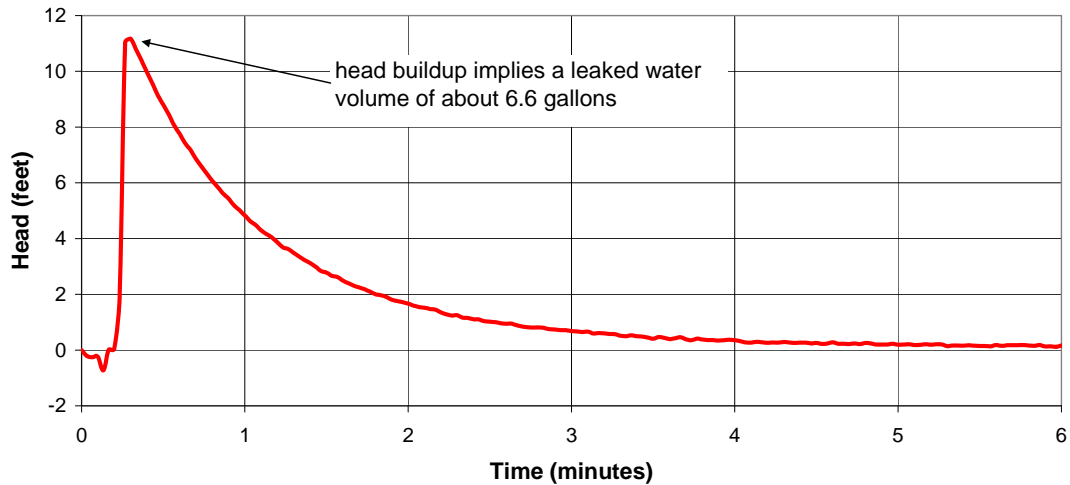


Figure E-37 R-35a head buildup following packer deflation

R-35a Summary

Table E-2 summarizes the hydraulic conductivity values obtained from the R-35a pumping test analyses. The early data revealed an average hydraulic conductivity of 2.2 ft/d for the 49.1-ft-thick screened interval. The lower-bound values computed from specific-capacity data (1.41 to 1.64 ft/d) did not contradict the pumping test result and in fact were entirely consistent with it.

**Table E-2
R-35a Pumping Test Hydraulic Conductivity Values**

Data	Early Data Conductivity b=49.1 ft (ft/d)	Middle/Late Data Conductivity b=236 ft (ft/d)
Trial 1 Recovery	2.0	2.5
Trial 2 Drawdown	2.7	2.5
Trial 2 Recovery	2.2	2.5 9.2 ^a
24-H Drawdown	2.5	4.5 ^a
24-H Recovery	2.1 1.8	3.7 4.9 ^a
Sampling Event	2.3	2.9
Average	2.2	2.8^b

^a Late data, possibly affected by leakage.

^b Middle data average.

The intermediate data yielded an average hydraulic conductivity of 2.8 ft/d, interpreted as applicable to the 236-ft-thick zone between the Puye Formation/Santa Fe interface and the Miocene basalt.

Continuing flattening of the late drawdown and recovery data suggested the possibility of leakage from above and/or below the tested zone.

Operation of Los Alamos County well O-4 and the resulting water-level fluctuations in PM-3 had a large effect on water levels in R-35a, making a precise analysis of the late drawdown and recovery data problematic.

E-9.0 R-35b DATA ANALYSIS

This section presents the data obtained from the R-35b pumping tests and the results of the analytical interpretations. Analyses were applied to pumping and recovery data from trials 1, 2, and 3 as well as the 24-h constant-rate pumping.

Trial 1

Figure E-38 shows the drawdown data recorded during trial 1. The early data could not be evaluated because of the exaggerated drawdown that occurred during the first half minute of pumping. This effect was caused by antecedent drainage of a portion of the drop pipe, as occurred during the R-35a tests described earlier. The resulting void in the drop pipe allowed the pump to operate against reduced head momentarily and thus produce a larger initial pumping rate.

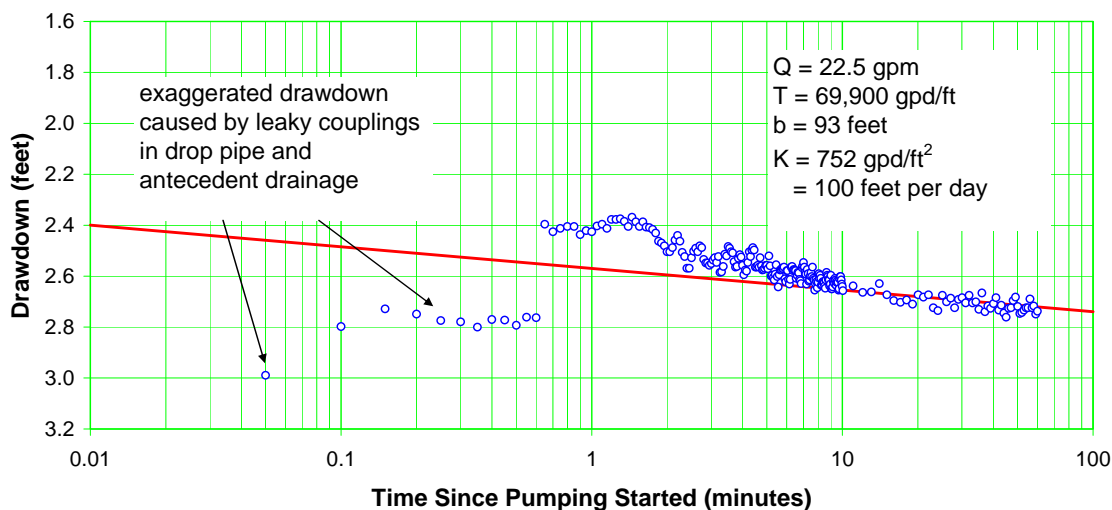


Figure E-38 Well R-35b trial 1 drawdown

The late data from Figure E-38 revealed a transmissivity value of 69,900 gpd/ft, interpreted as reflecting the properties of the full 93 ft thickness of the zone in which R-35b was completed. The corresponding hydraulic conductivity was 752 gpd/ft², or 100 ft/d. Note that although the data used were the latest data from this particular test, they should probably be considered intermediate data because they corresponded to a pumping time of just 10 to 60 min. If the cone of depression had not penetrated the full vertical thickness of the aquifer by this time, the calculated hydraulic conductivity would represent an underestimate of the actual value.

Figure E-39 shows a semilog plot of the trial 1 recovery data. The transmissivity value computed from the early data was 21,800 gpd/ft, making the hydraulic conductivity of the 23.1-ft-thick screened interval 944 gpd/ft², or 126 ft/d.

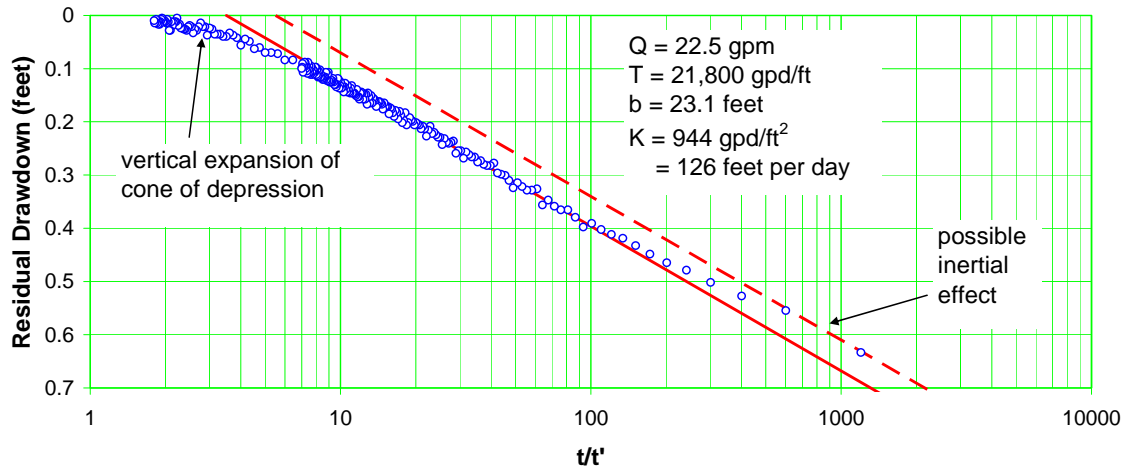


Figure E-39 Well R-35b trial 1 recovery

The first couple of data points in Figure E-39 (corresponding to a recovery time of about 6 s) showed “overrecovery” followed by a transition to the line of fit shown. This unusual response may have been related to inertial effects of water continuing to move toward the well even after pump shutoff. This effect is generally seen only in highly permeable sediments and only at early times. The rapid data collection scheme for the R-35b tests (3-s intervals) apparently allowed detection of this phenomenon.

Figure E-40 shows an expanded-scale plot of the trial 1 recovery data. The line of fit through the late data (corresponding to about 20 to 75 min following pump shutoff) revealed a transmissivity of 63,400 gpd/ft. Dividing this value by the full upper aquifer thickness of 93 ft yielded a hydraulic conductivity of 682 gpd/ft², or 91 ft/d. The drawdown data used in this analysis actually were considered intermediate data because of the short time since pumping stopped (20 to 75 min).

The dashed line in Figure E-40 shows an additional interpretation possibly reflecting late-time response. It is expected that at late recovery time, the recovery curve would trend toward the upper left corner of the graph. The dashed line of fit was selected to run from the latest measured data points to the corner of the graph. The resulting late-time transmissivity was 145,000 gpd/ft, making the hydraulic conductivity 1560 gpd/ft², or 208 ft/d. This value may better represent the average hydraulic conductivity of the full aquifer thickness than values obtained from intermediate time data when the cone of impression may not have been fully developed vertically.

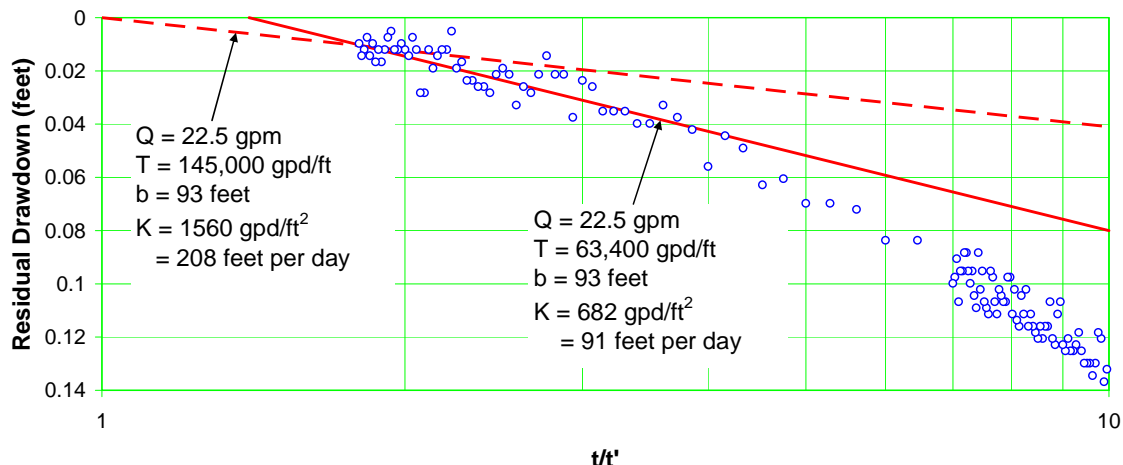


Figure E-40 Well R-35b trial 1 recovery—expanded scale

Trial 2

Figure E-41 shows the drawdown data recorded during trial 2. The early data could not be evaluated because of the exaggerated drawdown that occurred during the first fraction of a minute of pumping. As seen in trial 1, this effect was caused by antecedent drainage of a portion of the drop pipe. The resulting void in the drop pipe allowed the pump to operate against reduced head momentarily and thus produce a larger initial pumping rate with correspondingly greater drawdown.

The late data from Figure E-41 revealed a transmissivity value of 53,500 gpd/ft. If this value is assumed to represent the full 93-ft upper aquifer thickness, the corresponding hydraulic conductivity would be 575 gpd/ft², or 77 ft/d. However, the analyzed data corresponded to pumping times of just 10 to 60 min—essentially intermediate data—and thus the computed transmissivity may represent a thickness less than 93 ft, making the 77 ft/d hydraulic conductivity value an underestimate of the actual value.

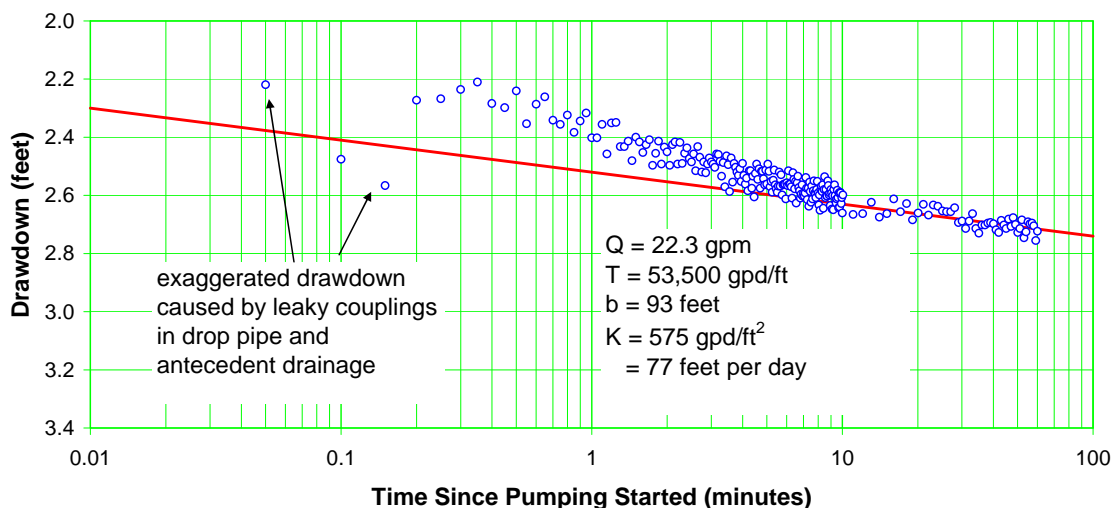


Figure E-41 Well R-35b trial 2 drawdown

Figure E-42 shows a semilog plot of the trial 2 recovery data. The transmissivity value computed from the early data was 23,600 gpd/ft, making the hydraulic conductivity of the 23.1-ft-thick screened interval 1020 gpd/ft², or 137 ft/d.

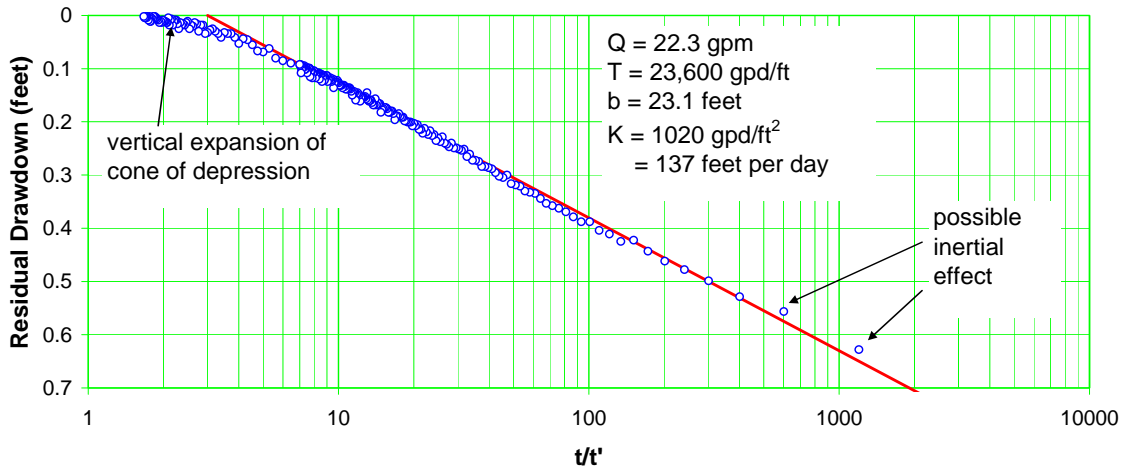


Figure E-42 Well R-35b trial 2 recovery

Figure E-43 shows an expanded-scale plot of the trial 2 recovery data. The line of fit through the late data (corresponding to about 20 to 90 min following pump shutoff) revealed a transmissivity of 60,000 gpd/ft. Dividing this value by the full upper aquifer thickness of 93 ft yielded a hydraulic conductivity of 645 gpd/ft², or 86 ft/d. The drawdown data used in this analysis actually were considered intermediate data because of the short time since pumping stopped (20 to 90 min). Thus, it is possible that the calculated transmissivity represented a sediment thickness less than 93 ft and that the resulting hydraulic conductivity was underestimated.

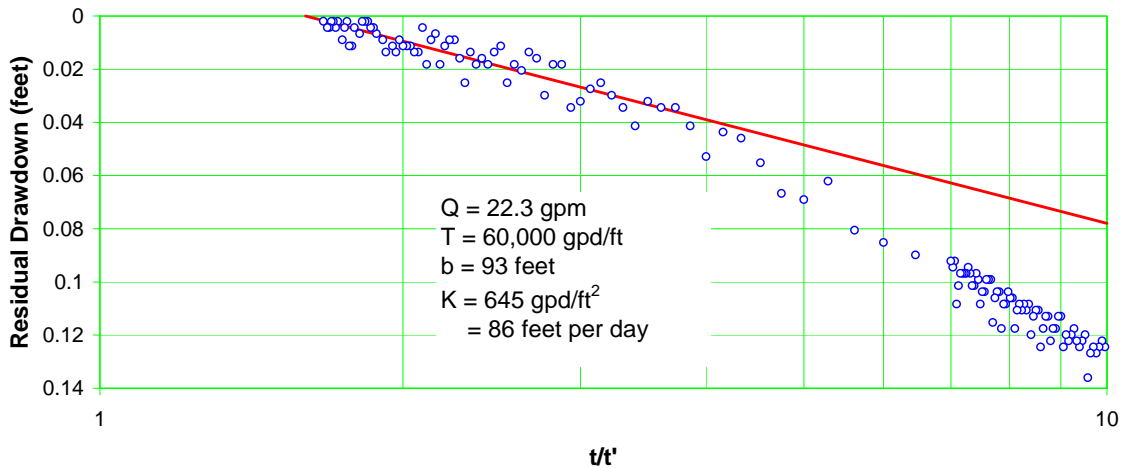


Figure E-43 Well R-35b trial 2 recovery—expanded scale

Trial 3

Figure E-44 shows the drawdown data recorded during trial 3. The early erratic data were possibly related to antecedent drainage of a portion of the drop pipe.

The late data from Figure E-44 revealed a transmissivity value of 69,900 gpd/ft. If this value is assumed to represent the full 93-ft upper aquifer thickness, the corresponding hydraulic conductivity would be 752 gp/ft², or 100 ft/d. However, the analyzed data corresponded to pumping times of just 20 to 90 min—essentially intermediate data—and thus the resulting hydraulic conductivity may be underestimated using the full aquifer thickness.

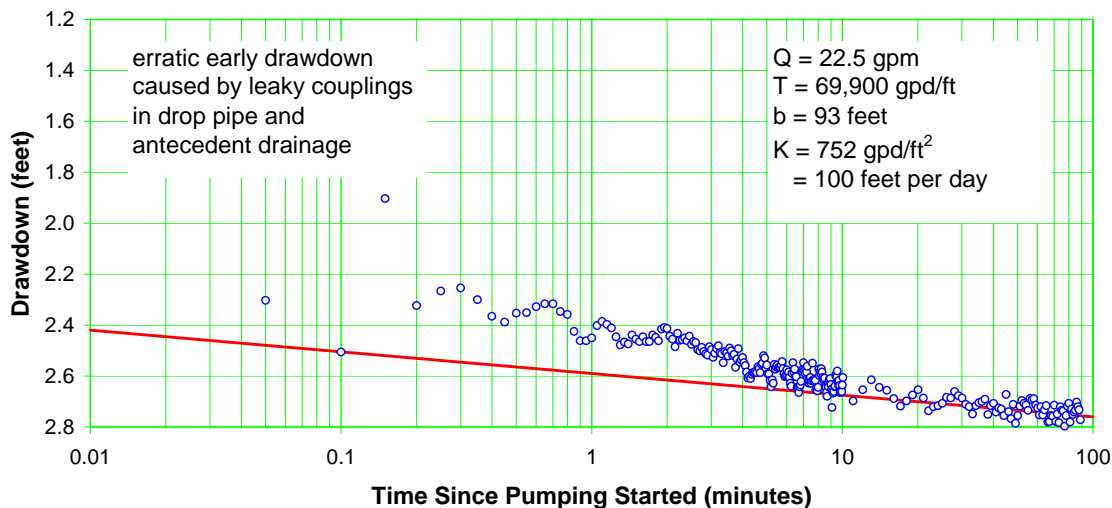


Figure E-44 Well R-35b trial 3 drawdown

Figure E-45 shows a semilog plot of the trial 3 recovery data. The transmissivity value computed from the early data was 23,100 gpd/ft, making the hydraulic conductivity of the 23.1-ft-thick screened interval 1000 gpd/ft², or 134 ft/d.

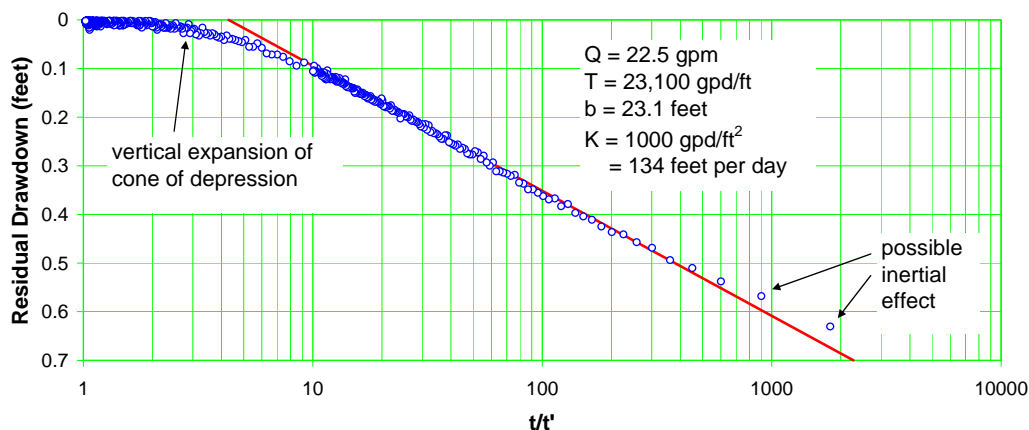


Figure E-45 Well R-35b trial 3 recovery

Figure E-46 shows an expanded-scale plot of the trial 3 recovery data. Note that the recovery period following trial 3 lasted for 3960 min and thus showed late-time response. There were two significant trends indicated by the late-recovery data. First, the data trace was quite flat, suggesting a large transmissivity value. Second, there were fluctuations spanning a magnitude of about three hundredths of a foot over most of the late data. The fluctuations were greater than the magnitude of the head change on any trend line that might be constructed through the data points, precluding accurate analysis of the late data.

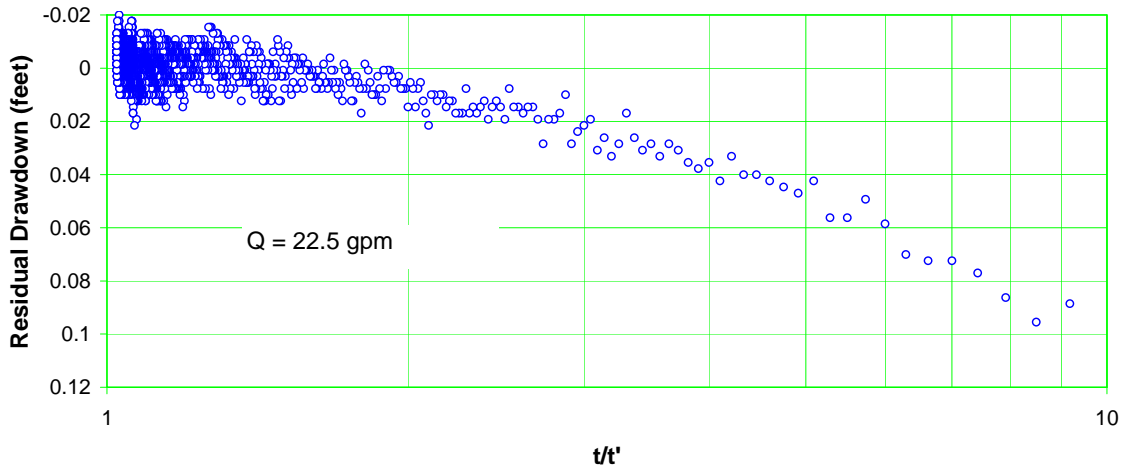


Figure E-46 Well R-35b trial 3 recovery—expanded scale

The trial 3 recovery data were compared with the barometric pressure record to see if a correlation existed. Figure E-47 shows a linear plot of barometric pressure and R-35b water levels for this period. Note on the graph that the vertical axis for the water-level changes has been stretched tenfold compared with that for the barometric pressure. It is clear that the magnitude of water-level fluctuations was an order of magnitude less than the range of barometric pressure changes.

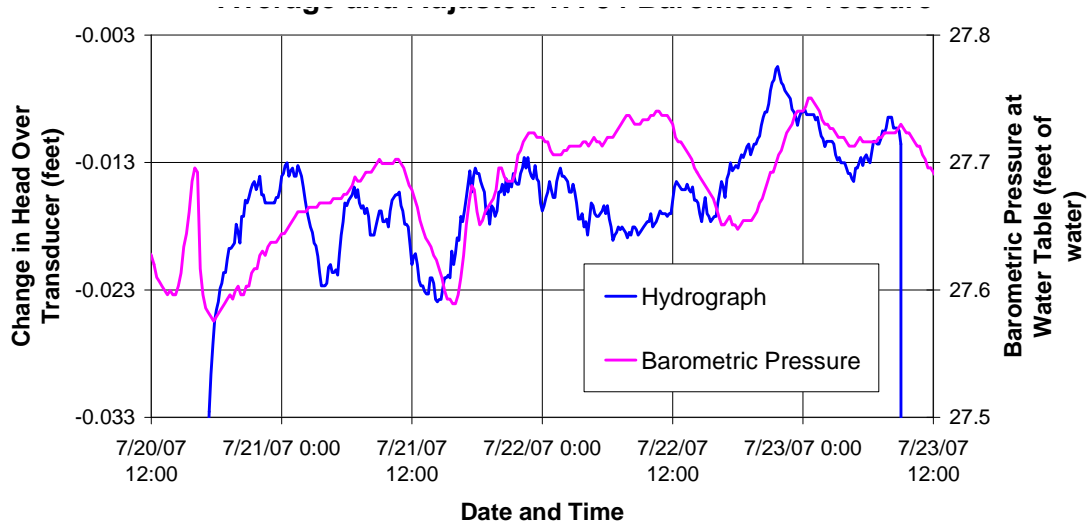


Figure E-47 Comparison of R-35b trial 3 recovery rolling average and adjusted TA-54 barometric pressure

The two curves plotted in Figure E-47 did not correlate particularly well. In fact, on those portions of the graphs that appeared to be similar, the hydrograph changes *preceded* the barometric pressure changes, making it impossible that they could be related. (Water-level response to barometric pressure can lag somewhat but can never precede it.)

A closer examination of the data amazingly revealed a possible *reverse* correlation. To illustrate this, the data were modified and replotted in Figure E-48. On this graph, the scale on the hydrograph vertical axis was inverted. In addition, the hydrograph was delayed by 4 h relative to the barometric pressure data, and the data were corrected for a background water-level *rise* of 0.0075 ft/d. The net water-level rise could have been the difference between ongoing late-time recovery and the overall area-wide gradual decline observed previously in R-11, R-13, and R-28. As shown in Figure E-48, the resulting modified hydrograph mimicked the shape of the barometric pressure graph remarkably well. The hydrograph seemed to have a few more oscillations than the barometric pressure curve, which may be related to Earth tides.

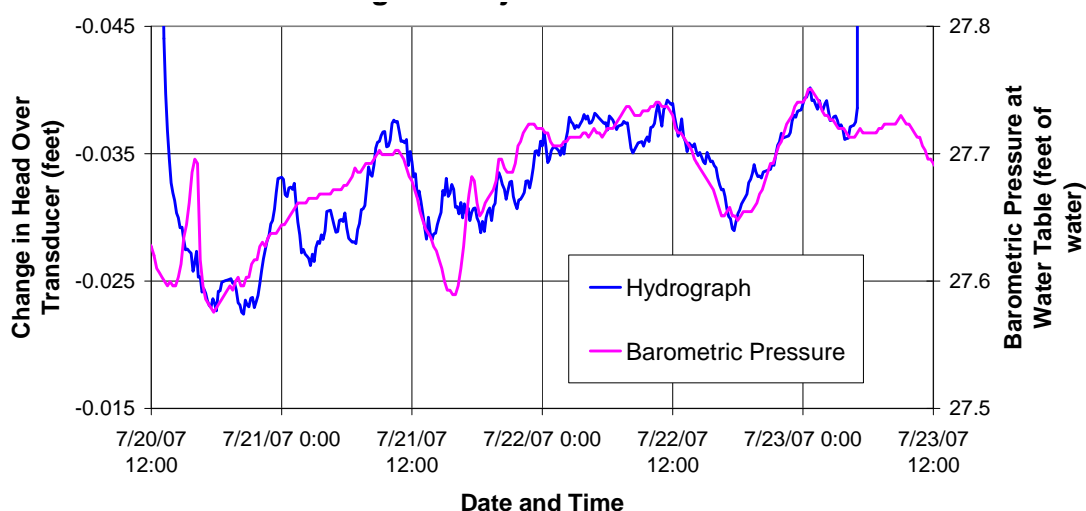


Figure E-48 Comparison of R-35b trial 3 recovery with trend/time lag and adjusted TA-54 barometric pressure

It is not known if the apparent correlation in Figure E-48 is real or just coincidental. It is possible that manipulation of any sinusoidal-varying data can make it look similar to any other sinusoidal curve and that the apparent match is just coincidental. On the other hand, if the correlation is real, it is extremely unusual because it means that an *increase* in barometric pressure caused a corresponding *decrease* in the total pressure in the aquifer—ostensibly impossible.

It is reminiscent of the so-called Noordbergum effect (Wolff 1970, 098242; Rodrigues 1983, 098239; Heish 1996, 098238) in vertical wells in which pumping one well can cause a water-level rise in nearby wells completed in adjacent aquifers or aquitards. Such reverse water-level fluctuations in vertical wells are brought about by poroelastic effects and corresponding pore pressure changes. When the main aquifer is pumped, it undergoes elastic deformation that radiates from the pumped well more rapidly than the cone of depression and causes transient pressure changes, either up or down, in the surrounding sediments. If the apparent correlation in Figure E-48 is real, it may be related to elastic distortion of the subsurface sediments in response to barometric pressure changes.

R-35b 24-H Constant-Rate Pumping Test

Figure E-49 shows drawdown recorded during the 24-h pumping test in R-35b. The first few data points fell below the trend line implied by the subsequent data. This effect was likely caused by a slow leak in the drop pipe that allowed antecedent drainage of a small volume of water from the pipe. On startup, the head against which the pump operated was less than the full column of water until the void caused by the drainage was refilled. This brief period of reduced head resulted in a momentary increased pumping rate and concomitant exaggerated drawdown.

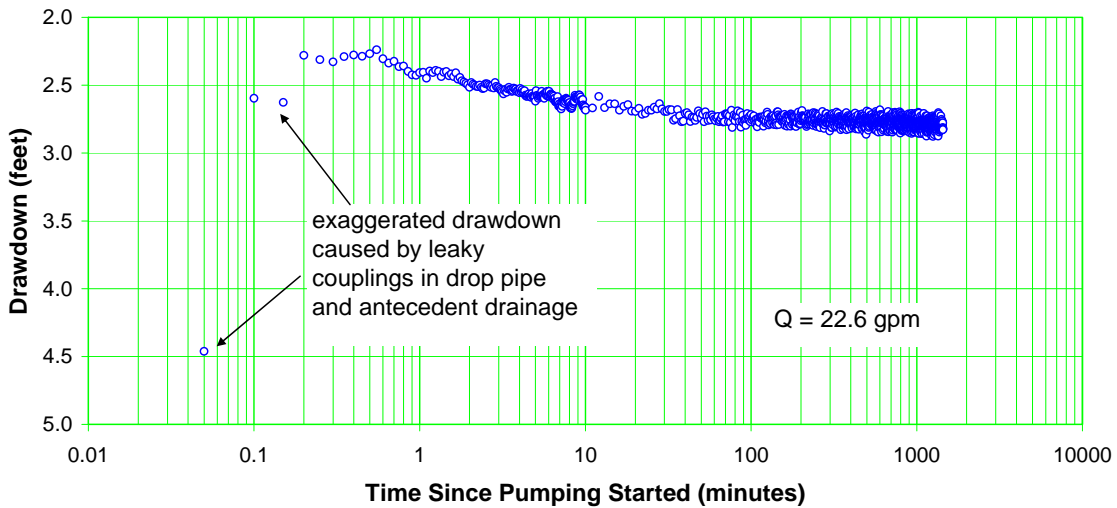


Figure E-49 Well R-35b drawdown

Figure E-50 shows an expanded-scale plot of the drawdown data. The data scatter associated with the 300 psi transducer and interference from the electrical pump cable is evident on the plot.

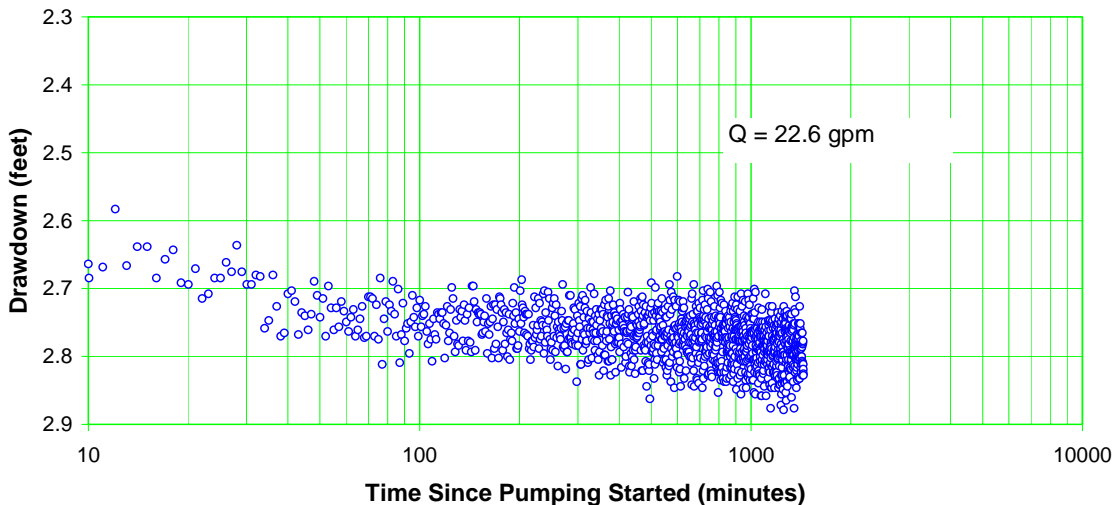


Figure E-50 Well R-35b drawdown—expanded scale

To reduce the data scatter, a rolling average plot (including 10 points on either side of the plotted point) was prepared as shown in Figure E-51. A line of fit constructed through the late data supported a transmissivity calculation of 126,000 gpd/ft, making the computed hydraulic conductivity of the 93-ft- thick upper aquifer 1350 gpd/ft², or 180 ft/d.

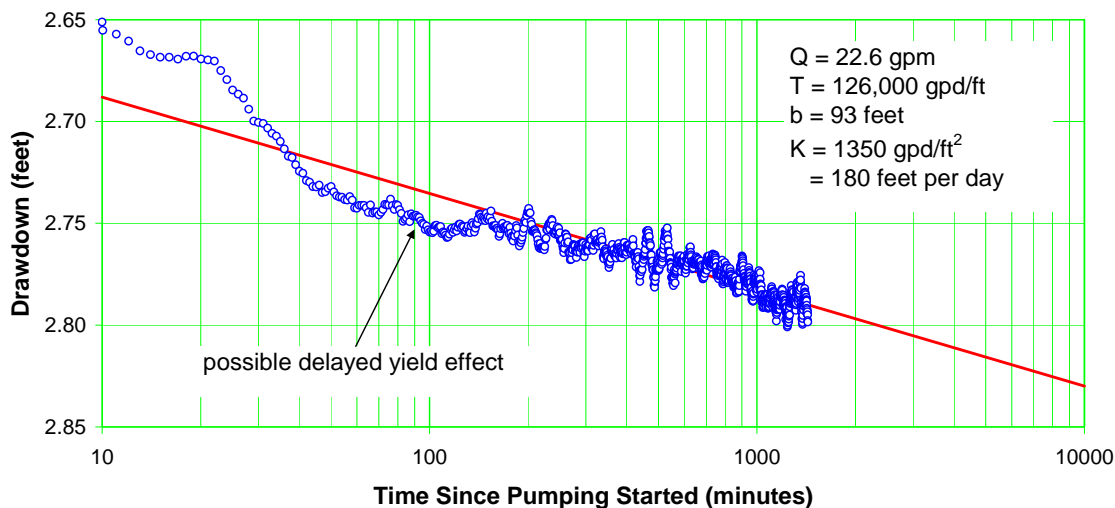


Figure E-51 Well R-35b drawdown—rolling average

Figure E-52 shows a semilog plot of the recovery data following pump shutoff. The transmissivity value computed from the early data was 24,500 gpd/ft making the hydraulic conductivity of the screened interval 1060 gpd/ft², or 142 ft/d.

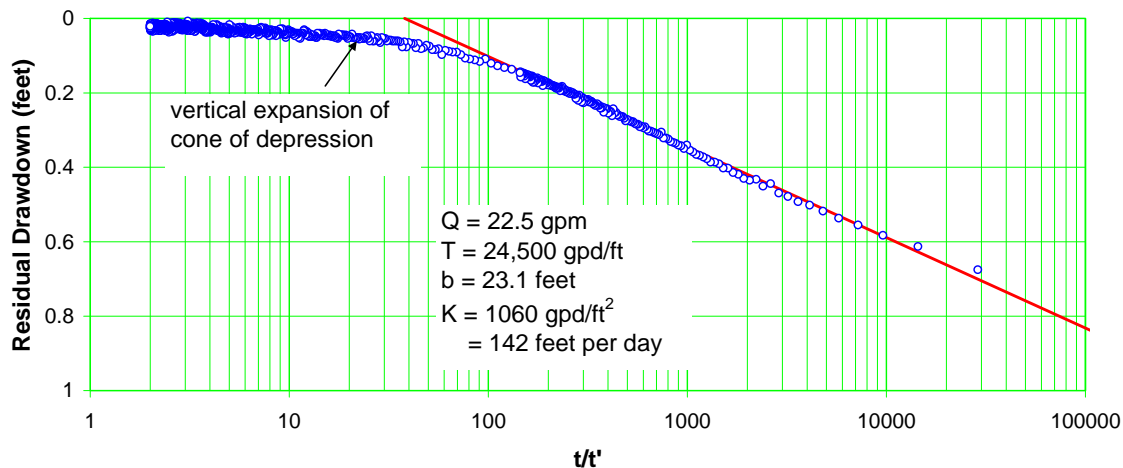


Figure E-52 Well R-35b recovery

Figure E-53 shows an expanded-scale plot of the late recovery data. Two lines of fit are shown on the graph.

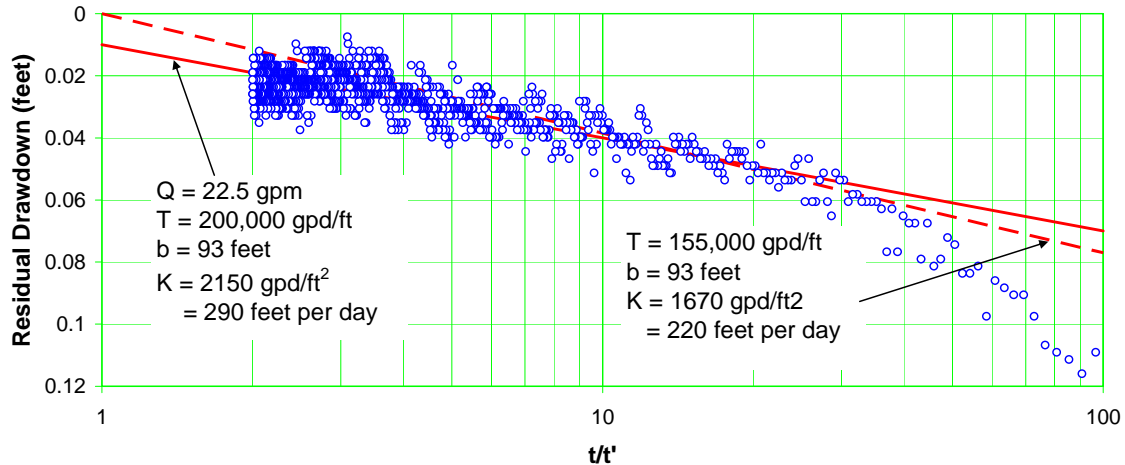


Figure E-53 Well R-35b recovery—expanded scale

The solid line of best fit yielded a transmissivity value of 200,000 gpd/ft and an average hydraulic conductivity 2150 gpd/ft², or 290 ft/d. However, it is apparent that the late data showed a water-level reversal (drop in water level rather than recovery), presumably attributable to background effects. This biased the slope of the line of fit, making it flatter than what would be expected theoretically. Therefore, a second line of fit was constructed using only the data before the water-level reversal. The transmissivity computed from the dashed line of fit was 155,000 gpd/ft, making the average hydraulic conductivity 1670 gpd/ft², or 220 ft/d. This is probably a more realistic estimate of the hydraulic conductivity of the 93-ft-thick upper aquifer.

Specific-Capacity Data

Specific-capacity data were used along with well geometry to estimate a lower-bound conductivity value for the R-35b screen zone for comparison to the pumping test values. In addition to specific capacity, other input values used in the calculations included the aquifer thickness of 93 ft, a storage coefficient of 0.05, and a borehole radius of 0.51 ft. The calculations are somewhat insensitive to the assigned aquifer thickness, as long as the selected value is substantially greater than the screen length.

R-35b produced 22.6 gpm with a drawdown of 2.83 ft after 24 h of pumping for a specific capacity of 8.0 gpm/ft. Applying the Brons and Marting method to these inputs yielded a lower-bound hydraulic conductivity value for the screened interval of 338 gpd/ft², or 45.2 ft/d. Table E-3 summarizes the hydraulic conductivity values derived from the pumping tests. As indicated, the average hydraulic conductivity for the screened interval was 135 ft/d. The lower-bound value from the specific capacity was consistent with this, falling below it rather than exceeding it. The well efficiency can be approximated as the ratio of the lower-bound hydraulic conductivity value to the actual. In this case, the computed estimate of efficiency was 45.2/135, or 33%. This is a relatively low efficiency as a percentage but not out of line for a small-diameter well having a large specific capacity. In this case, the inefficiency drawdown component (well loss) was still less than 2 ft at the measured discharge rate of 22.6 gpm.

Packer Deflation

Following completion of the pumping tests on R-35b, the downhole packer was deflated in preparation for pulling the submersible pump. The pumping test data suggested significant leakage of water from the drop pipe into the annular space above the packer during the test period. Therefore, to avoid overloading and possibly damaging the pressure transducer with a large slug of water applying great head, the packer was bled slowly in hopes of releasing the trapped water gradually. The nitrogen inflation gas was released over a period of more than 20 min. Figure E-54 shows the head buildup that occurred when the packer was deflated.

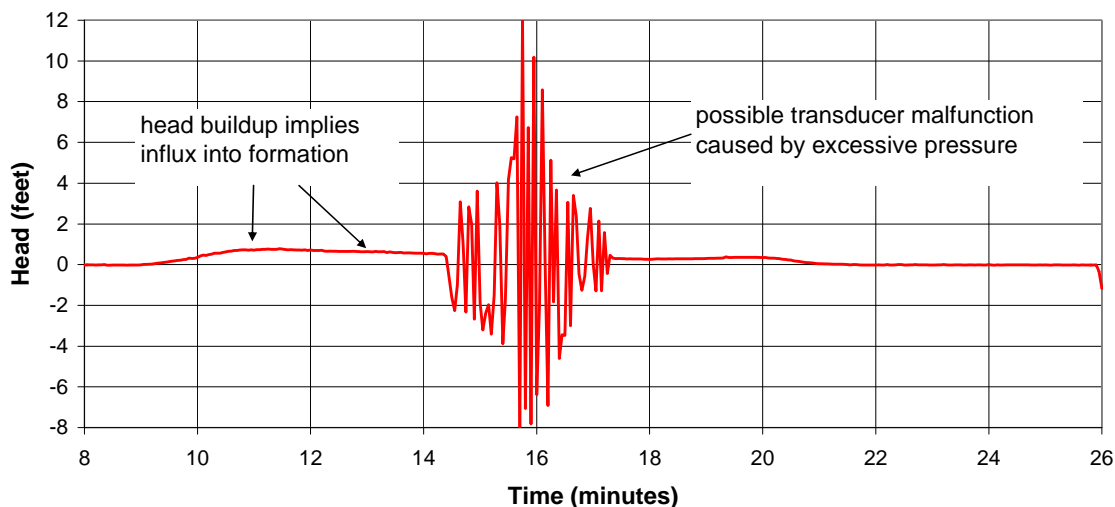


Figure E-54 R-35b head buildup following packer deflation

The observed response represented by the smooth portion of the curve was caused by the release of water suspended above the static water level in the annulus between the well casing and pump drop pipe and above the inflatable packer. Prior to packer inflation, water in this zone would have been at the same level as the ambient water level in the well.

The head buildup of about three quarters of a foot shown on the graph was sustained for several minutes—from about 9.5 to 14.5 min after deflation was initiated. Based on a specific capacity of 8 gpm/ft, it is likely that a sustained influx rate from the casing into the formation of about 6 gpm occurred during this period. This is apparently the rate at which water was able to leak past the gradually deflating packer over this time period.

As is evident in Figure E-54, at about 14.5 min the transducer output became highly erratic. The reason for this response was not known. It is possible that the packer finally deflated sufficiently to expose the transducer to the full height of water above the packer and overpressurized it, causing it to malfunction and output spurious data.

A second possibility is that successive slugs of water were released intermittently. A sudden release of a slug of water would cause a head buildup on the transducer initially. However, the sudden reduction in head above the partially inflated packer would allow the packer to reseal within the casing, based on the remaining internal packer pressure vis-à-vis the remaining head in the water column above it. The reexpansion and resealing of the packer would temporarily relieve the head on the transducer until the next slug of water bypassed the packer as the packer pressure continued to gradually decline.

These explanations of the observed data are merely speculative. The exact cause of the unusual pressure response depicted in Figure 54 is not known.

R-35b Summary

E 3 summarizes the hydraulic conductivity values obtained from the R-35b pumping test analyses. The early data revealed an average hydraulic conductivity of 135 ft/d for the 23.1-ft-thick screened interval. The lower-bound conductivity value of 45.2 ft/d computed from specific-capacity data did not contradict the pumping test result and was reasonable, suggesting a 33% efficient well having less than 2 ft of well loss at a discharge rate of 22.6 gpm.

**Table E-3
R-35b Pumping Test Hydraulic Conductivity Values**

Data	Early Data Conductivity b=49.1 ft (ft/d)	Middle/Late Data Conductivity b=236 ft (ft/d)
Trial 1 Drawdown	n/a ^a	100 ^b
Trial 1 Recovery	126	91 ^a 208
Trial 2 Drawdown	n/a	77 ^b
Trial 2 Recovery	137	86 ^b
Trial 3 Drawdown	n/a	100 ^b
Trial 3 Recovery	134	n/a
24-H Drawdown	n/a	180
24-H Recovery	142	220
Average	135	89^b 203^c

^a n/a = Not applicable.

^b Middle data; may not reflect full thickness of upper aquifer.

^c Late data average.

The intermediate data yielded an average hydraulic conductivity of 89 ft/d, while the late data yielded an average conductivity of 203 ft/d for the full 93-ft thickness of the upper saturated zone. It is possible that the intermediate data occurred before full vertical development of the cone of depression and that the hydraulic conductivity computed from the late data is more accurate.

Background fluctuations in R-35b were only a few hundredths of a foot, belying any significant response to the operation of nearby wells.

E-10.0 PM-3 STARTUP

Following the test program on the R-35 wells, Los Alamos County well PM-3 was restarted and put back on line. The restart was used as an opportunity to monitor pumping and recovery data during the first startup cycle and subsequent shutdown. Water levels were monitored in the same set of wells that was used in the R-35 tests.

PM-3 is a filter packed well completed with 1576 ft of punched pipe set between the depths of 956 and 2532 ft. R-35a and R-35b are located near PM-3 at distances of 343 ft and 411 ft, respectively. The PM-3 perforations overlap the R-35a screen zone (1013 to 1062 ft bgs) but are more than 100 ft beneath the R-35b screen zone (825 to 848 ft).

PM-3 was restarted at 9:30 a.m. on August 6 after 35 d. of inactivity. The well was pumped at a discharge rate of 1450 gpm for 1460 min until 9:50 a.m. on August 7. Following shutdown, recovery was measured in the pumped well for 1346 min. until 8:16 a.m. on August 8, while data were recorded in the nearest observation well—R-35a – for 2011 min until 7:21 p.m. on August 8.

Figure E-55 shows the drawdown data recorded in the pumped well. Because the pump column pipe in PM-3 has no check valve and drains after each pumping cycle, the turbine pump starts against low head initially, as it fills the pipe. This results in an elevated discharge rate initially as evidenced by the great drawdown in the first minute of pumping.

The transmissivity calculated from the line of fit shown on the graph was 189,000 gpd/ft. The effect of operation of Los Alamos County well O-4 is clearly evident on the drawdown plot. The line of best fit was positioned to account for the recovery and subsequent drawdown associated with cycling O-4.

It is important to point out that the computed transmissivity value may overestimate the true value somewhat. While the pump was filling the drop pipe, the discharge rate was greater than 1450 gpm perhaps for several minutes because the pump output is greater when the back pressure (pumping lift) is lower.

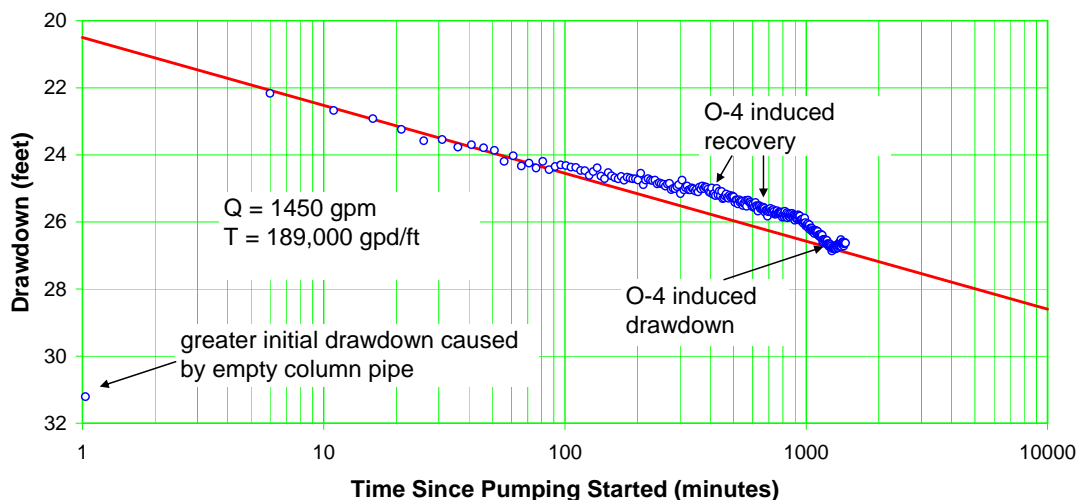


Figure E-55 Well PM-3 draw down

As the pipe filled, the discharge rate gradually declined to the steady rate of 1450 gpm. A gradually declining discharge rate will cause the early portion of the time-drawdown plot to be flatter than what would be observed for a constant pumping rate. The flatter slope results in a greater calculated transmissivity value. For this reason, the computed value of 189,000 gpd/ft should probably be considered an upper-bound value. The combination of variable discharge rate and interference from O-4 lends uncertainty to the analysis.

Figure E-56 shows drawdown data recorded in R-35a. The effect of the O-4 operation can be seen where the data points deviate from the straight line of best fit. The analysis yielded a transmissivity of 120,000 gpd/ft and a storage coefficient of 9.2×10^{-4} . The transmissivity value did not agree with that from the pumped well graph (Figure E-55). It is probable that the observation well data are affected less by the early discharge rate variations than are the pumped well data and that this transmissivity value is more representative of aquifer properties. It also may be in part an artifact of pumping a geologically complex, multilayer system.

During pumping, the cone of depression expands relatively rapidly in high-diffusivity zones and more slowly in low-diffusivity zones. (The diffusivity is the ratio of transmissivity to storage coefficient.) This response can cause small, gradual shifts in the relative contributions of each of the zones to the total discharge rate. Thus, even though the total discharge rate is held constant, the individual discharge rates of the various contributing zones can change slightly. Further complicating the hydraulic response is that low-diffusivity zones may provide leakage into adjacent high-diffusivity zones as the more rapidly expanding drawdown cones in the high-diffusivity strata create drawdown differences among the various zones at a distance from the pumped well. The overall result of these effects is that the observation well drawdown slopes may not all be identical and may not match that of the pumped well. It was expected that these effects would be subtle and that the transmissivity calculated from the R-35a data was reasonably representative of aquifer conditions.

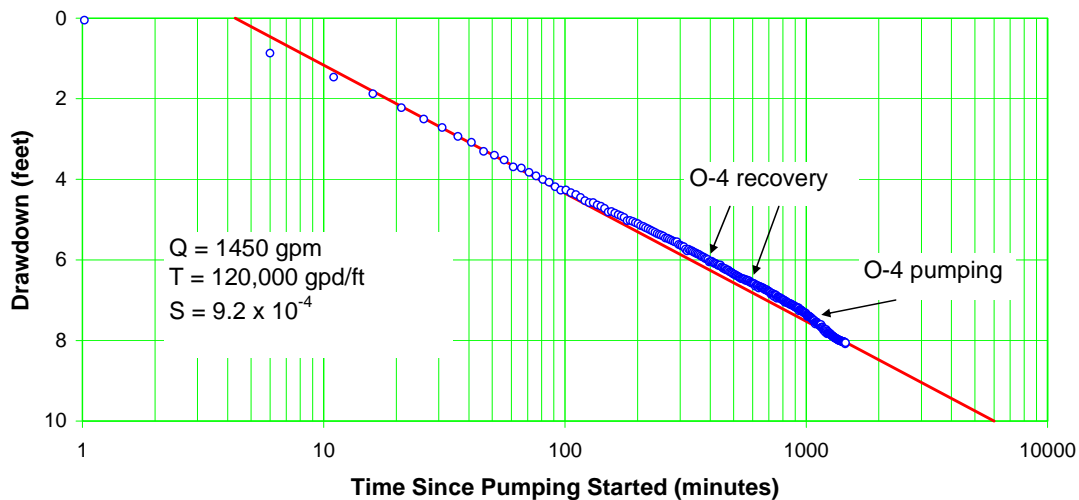


Figure E-56 Well R-35a drawdown—PM-3 test

The early data in Figure E-56 fell below the straight line of best fit. This was because the u value was too large for the logarithm equation (Cooper–Jacob) (1946, 098236) (to be a valid approximation of the Theis equation (1934-1935, 098241)). In order to incorporate the early data points in the analysis, a log-log plot of the data was constructed and analyzed using Theis curve matching.

Figure E-57 shows the resulting Theis curve match. (The drawdown at 1 min of pumping was less than the magnitude of the water-level fluctuations in the prepumping record and thus that data point was excluded from the analysis.) The transmissivity and storage coefficient values computed from the Theis analysis were 118,000 gpd/ft and 9.9×10^{-4} , respectively, in agreement with the semilog analysis.

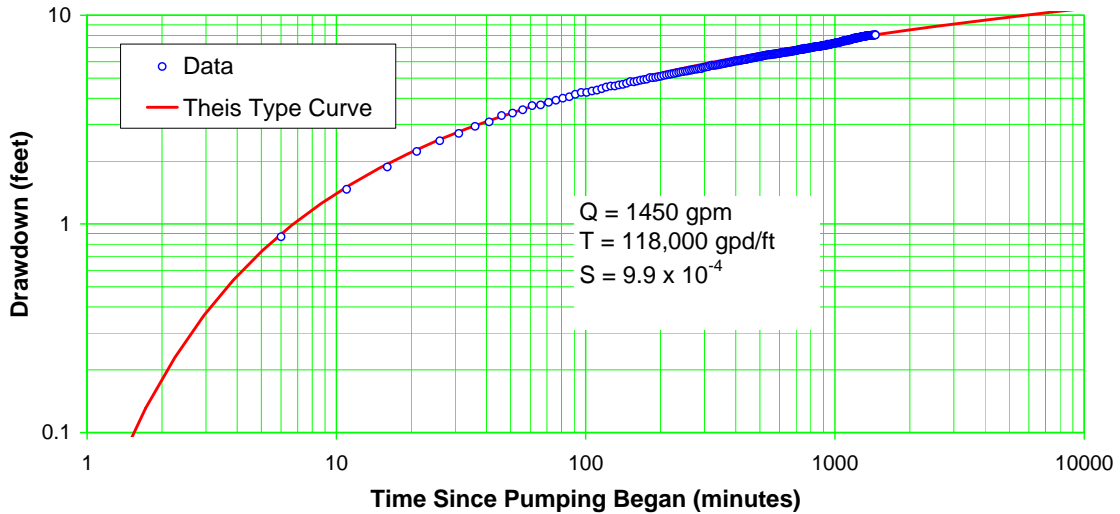


Figure E-57 Thesis analysis of R-35a drawdown

Figure E-58 shows the recovery data recorded in the pumped well following pump shutoff. Because there was no check valve in the pumping string, the water standing in the column pipe, and perhaps some of the surface piping, rushed back into the well when pumping stopped. Note the superrecovery shown by the right-hand data point on the graph. This point corresponded to a recovery time of 1 min and showed that the water level was about 6 ft above the original static level at that time.

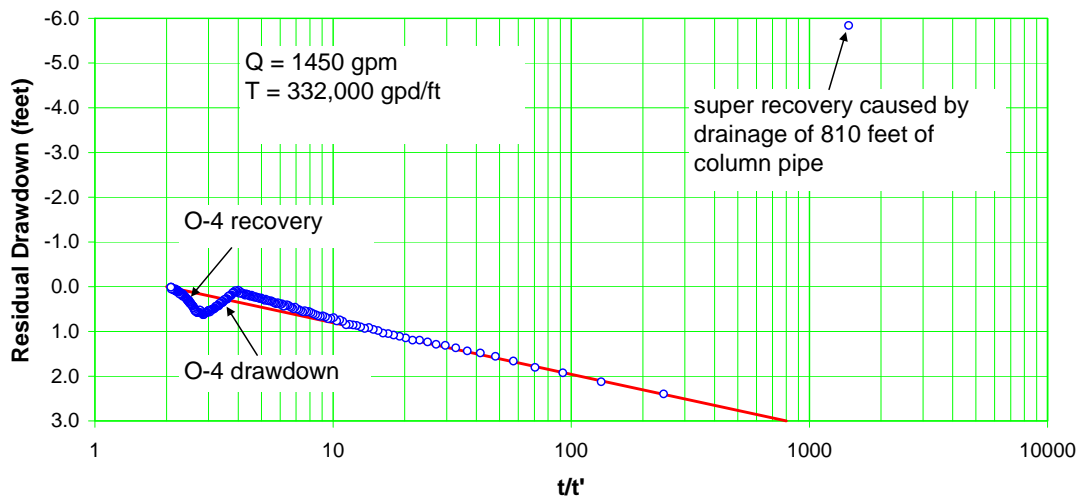


Figure E-58 Well PM-3 recovery

The transmissivity value computed from the line of fit shown on the graph was 332,000 gpd/ft—much greater than values obtained from the drawdown data. This was because drainage of the drop pipe caused a flattening of the recovery graph, that is, the early recovery water levels were higher than they would have been had the column pipe not drained.

This can be illustrated by examining the data measured after 6 min of recovery, corresponding to a t/t' value of 244, and comparing it with the drawdown measured after 6 min of pumping. The residual drawdown shown in Figure E-58 at this time was 2.4 ft. The drawdown when pumping stopped was 26.63 ft. This meant that in the first 6 min of recovery, the water level recovered $26.63 - 2.4 = 24.23$ ft. In contrast, Figure E-55 showed that the drawdown after 6 min of pumping was 22.17 ft. In theory, the recovery response should mimic the drawdown; thus, the recovery should not have exceeded 22.17 ft after 6 min. The recharge associated with draining the column pipe exaggerated the early rate of recovery. (Note that the theoretical recovery probably should have been even less than 22.17 ft. Recall that the 22.17 ft of drawdown observed after 6 min of pumping was in part attributable to the greater pumping rate that occurred at the start of the pumping test, as described earlier.)

To show the possible impact of the exaggerated recovery, the recovery data were replotted with the 6-min data point moved to a residual drawdown value of 4.46 ft (corresponding to 22.17 ft of recovery from the maximum drawdown observed at pump shutoff). Figure E-59 shows the resulting data plot. Extending a straight line from the replotted data point to the late data (which would be essentially unaffected by the one-time recharge of column pipe water) produced a calculated transmissivity of 181,000 gpd/ft in better agreement with the time-drawdown analysis shown in Figure E-55. This reinforced the idea that the transmissivity value of 332,000 gpd/ft was not representative of aquifer conditions but rather was an artifact of the recharge event that occurred when pumping stopped.

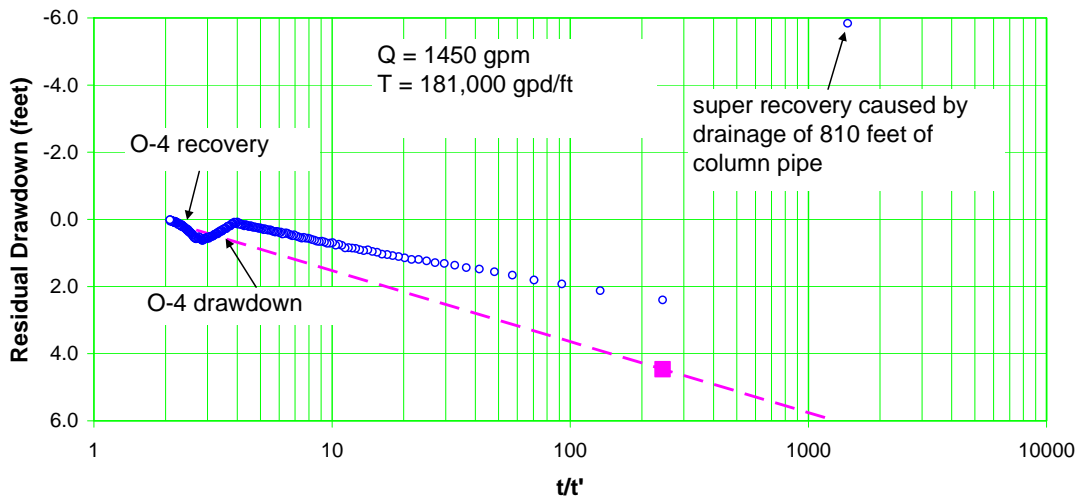


Figure E-59 Adjusted well PM-3 recovery

Figure E-60 shows the recovery data recorded in R-35a following pump shutoff. As with the drawdown graph, the early data (right-hand side of the plot) fell off the straight line of best fit. Also, the effect of the operation of O-4 was evident on the recovery graph.

The transmissivity value computed from the line of fit in Figure E-60 was 115,000 gpd/ft, in agreement with the values obtained from the drawdown data in Figures E-56 and E-57.

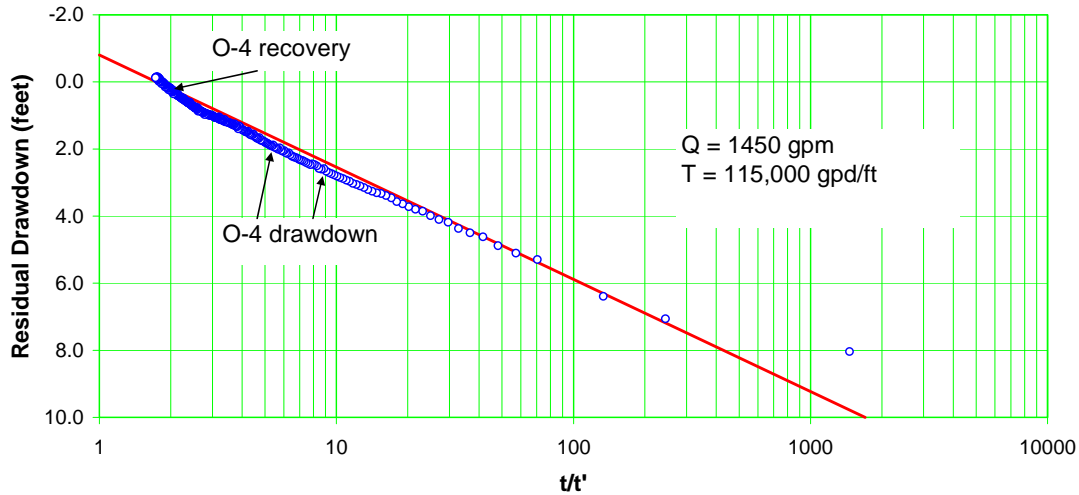


Figure E-60 Well R-35a recovery—PM-3 test

Data from other production wells and observation wells in the area were examined to determine the effect of pumping PM-3. Figure E-61 shows the water-level hydrograph for well R-35b, located 411 ft from PM-3.

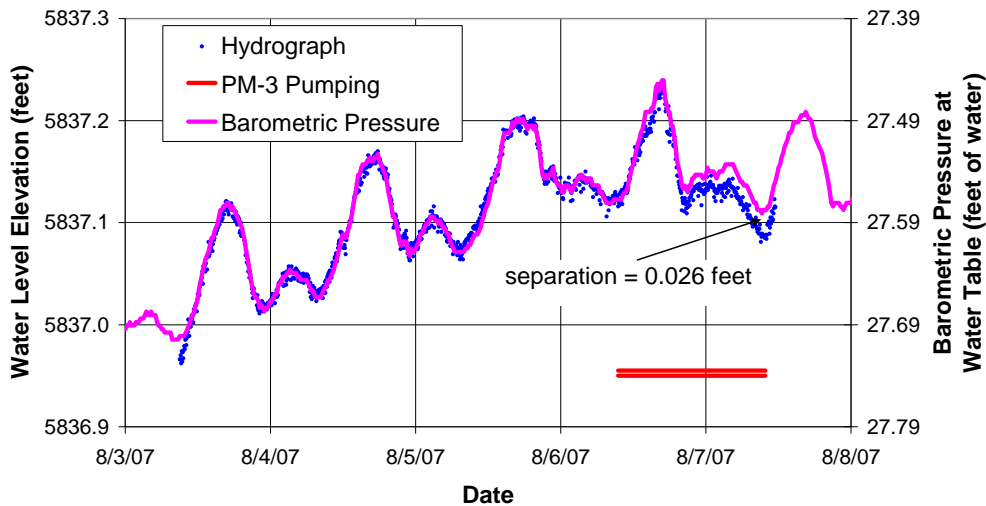


Figure E-61 R-35b water levels

The barometric pressure data are plotted on the same graph for comparison purposes. Also, the time interval during which PM-3 was operated is indicated on the graph for reference. Note that the hydrograph shown in Figure E-61 is very different than the one presented previously in Figure E-3. The former hydrograph was measured with the R-35 pumping test equipment that incorporated nonvented pressure transducers, whereas the hydrograph obtained during the PM-3 pumping test was measured using the permanently installed monitoring equipment that included a vented pressure transducer.

The barometric pressure axis in Figure E-61 was inverted compared with the hydrograph axis so that increasing barometric pressure corresponded to decreasing water levels. The magnitude of the observed changes in water level was about the same as that of the barometric pressure fluctuations, suggesting a barometric efficiency near 100%. For example, a barometric pressure increase of 0.1 ft caused a drop in the water level in the well of about 0.1 ft (leaving the total aquifer pressure unchanged).

As shown in the figure, the hydrograph and barometric pressure curves were nearly identical until PM-3 was pumped. The operation of PM-3 appeared to cause a decline in water levels compared with the position that would have been predicted based on the barometric pressure record. The maximum deviation between the two curves associated with pumping PM-3 was 0.026 ft. This was interpreted as the drawdown caused by the pumping test. *Of note is the fact that the drawdown being sought was an order of magnitude less than the total variation in the hydrograph, making a precise determination of drawdown difficult.* Recall that other R wells indicated a general background water-level decline. It is possible that what is perceived as drawdown could include background trend instead of, or in addition to, actual drawdown.

Figure E-62 shows the hydrograph for Los Alamos County well PM-1, located 1 mi from PM-3. Figure E-63 shows an expanded-scale graph of the PM-1 hydrograph.

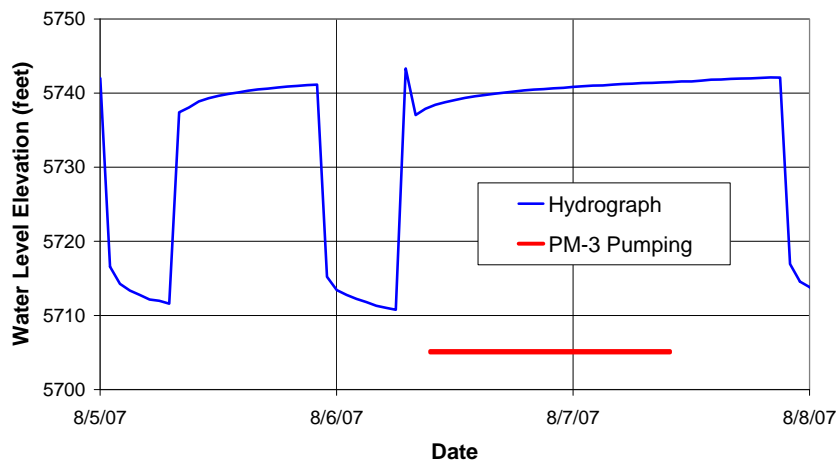


Figure E-62 PM-1 water levels

The water-level fluctuations shown in Figures E-62 and E-63 occurred as a result of pumping PM-1. Examination of the graphs suggested no apparent effect in PM-1 from pumping PM-3. This was consistent with previous information suggesting a lack of hydraulic continuity between PM-1 and PM-3 (Stephen G. McLin, personal communication) and suggests the possibility of a low-permeability barrier separating western wells from eastern wells on the plateau. Another example of this idea has been observed in a pumping test conducted on PM-2 (McLin 2005, 090073). In this test, PM-2 was pumped at 1249 gpm for 25 d. After 19.66 d of pumping, a drawdown of 1.64 ft was observed in R-32 Screen 3 located 4779 ft away; 1.73 ft of drawdown was observed in PM-5 located 8808 ft away yet there was no discernible response in any of the five screened intervals in R-22 located 9234 ft to the east-southeast. Other interactions have been observed between wells separated by about a mile, the approximate distance between PM-1 and PM-3. For example, pumping PM-4 induced drawdown of 13.99 ft and 7.78 ft in PM-2 and PM-5, respectively, after 20 d (McLin 2006, 092218). These two wells are located 4478 ft and 4656 ft, respectively from PM-4. Likewise, as shown previously in Figure E-2, operation of O-4 located 6300 ft from PM-3 induced about a foot of drawdown within half a day. The lack of similar response in PM-1 from pumping PM-3 is unusual and speaks to the geologic complexity of the plateau.

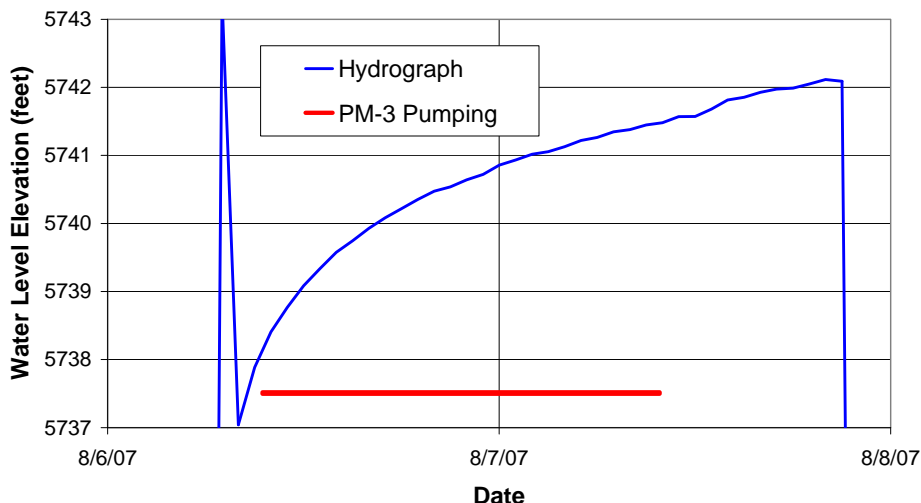


Figure E-63 PM-1 water levels—expanded scale

Figure E-64 shows the hydrograph for PM-4. The well was running during the period shown on the graph except for the brief, off-scale, peak that occurred late on August 6. There was a diurnal sinusoidal effect with a magnitude of about 2 ft evident on August 5 and 6 (as well as several preceding days, not shown). This effect was attributed to operation of either O-4 or PM-2 or perhaps both.

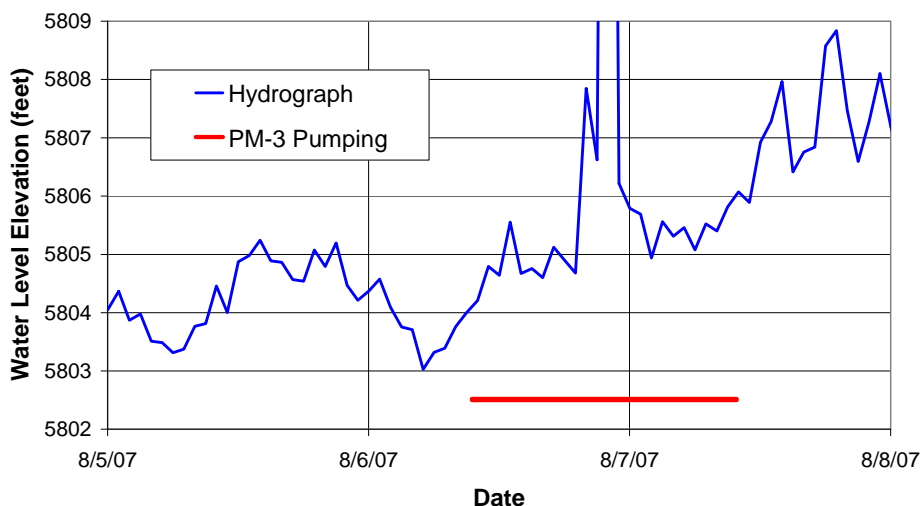


Figure E-64 PM-4 water levels

There was no discernible response to pumping PM-3 in the PM-4 hydrograph. If there was any response, it was obscured by the background signal.

Figure E-65 depicts the hydrograph for PM-5. The large downward spike on the graph corresponds to operation of PM-5 overnight from August 5 to 6.

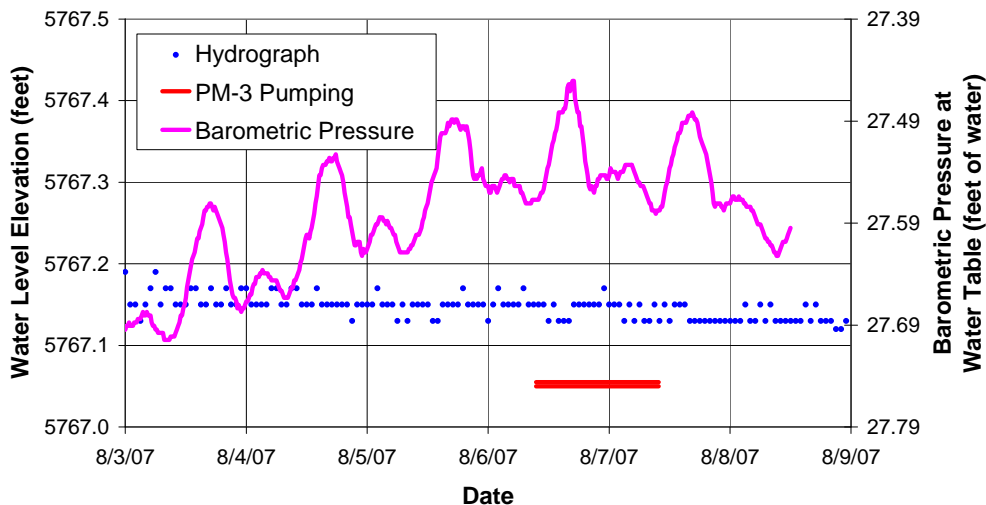


Figure E-67 R-5 Screen 3 aquifer pressure

Figure E-68 shows the corresponding hydrograph for R-5 Screen 4. The peaks and valleys visible on the graph were a response to operation of PM-1. If there was any response to pumping PM-3 (not evident), it was obscured by the fluctuations induced by PM-1.

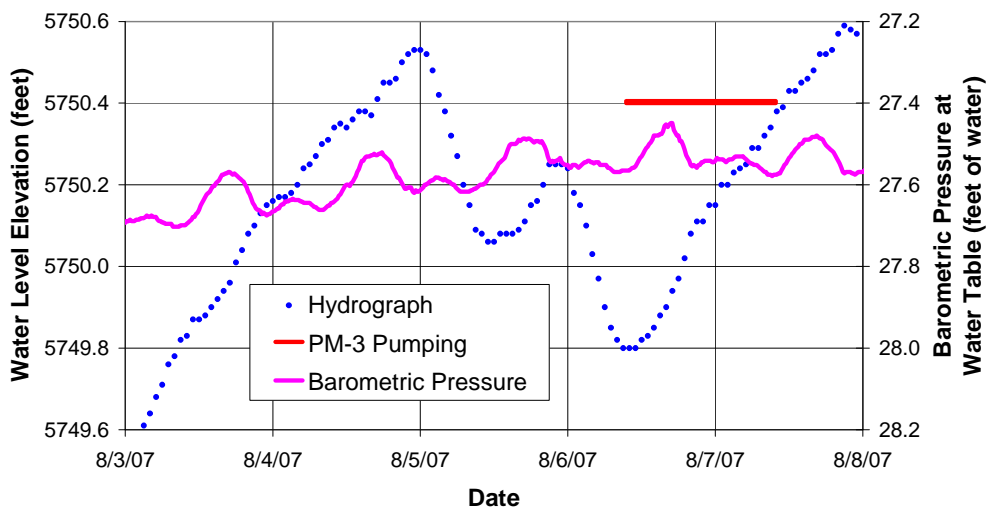


Figure E-68 R-5 Screen 4 aquifer pressure

Figure E-69 shows the water-level record for R-8 Screen 1. There was a clear response to pumping PM-3.

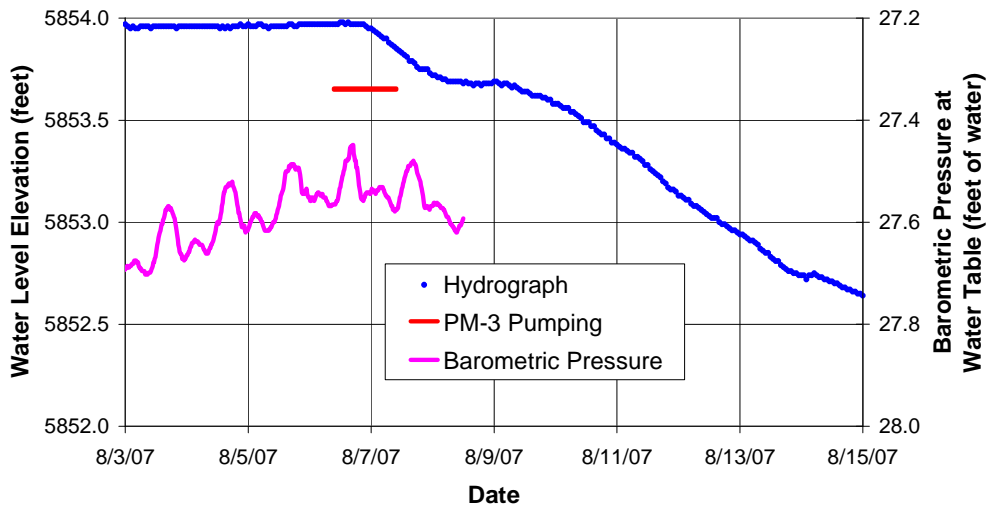


Figure E-69 R-8 Screen 1 aquifer pressure

The figure identifies only the period during which the pumping test was conducted on PM-3. Following the recovery period, PM-3 continued to cycle on a daily basis, inducing increasing drawdown in R-8 Screen 1 over time. These subsequent pumping times were not included on the graph.

The drawdown in Screen 1 at the time of pump shutdown was 0.12 ft. However, the water level continued to decline even when PM-3 was shut off. This suggested a lag between water-level changes in the aquifer surrounding PM-3 and the Screen 1 zone, implying a hydraulic separation between the two hydrologic units. Presumably, an aquitard beneath Screen 1 was the cause of this response.

Figure E-70 shows the water-level record for R-8 Screen 2. As with Screen 1, there was a clear response to pumping PM-3. The magnitude of the drawdown caused by the PM-3 pumping test was 1.8 ft. Unlike the Screen 1 response, the lag in response was diminished sufficiently that water levels in Screen 2 rebounded when PM-3 was shut down. The subsequent operating cycles in PM-3 were clearly visible in the Screen 2 hydrograph.

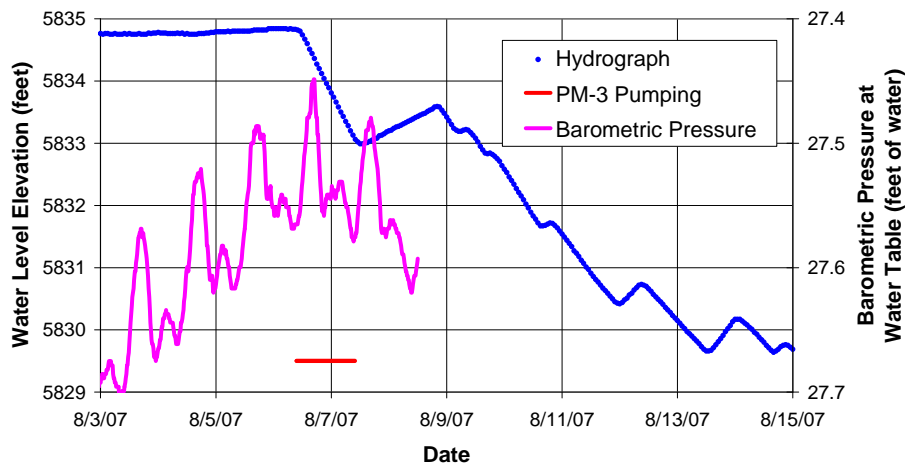


Figure E-70 R-8 Screen 2 aquifer pressure

An unusual feature of the Screen 2 hydrograph was that the water-level changes occurred linearly, or nearly so, rather than logarithmically. The reason for this bizarre response was not apparent. This is the kind of response that could occur in a mostly plugged well screen, although there is no way to determine from the data what the actual cause was. There was no evidence of these kinds of straight line segments on hydrographs recorded earlier from R-8 Screen 2, as shown in Figures E-8 and E-9.

Figure E-71 shows a comparison of the barometric pressure record and hydrograph for R-9. The results were similar to those shown in Figure E-61 for R-35b in that the hydrograph and inverted barometric pressure curves were nearly identical until operation of PM-3 induced minor drawdown in R-9. The data showed a high barometric efficiency—likely near 100%. The separation of the two curves attributable to pumping PM-3 was 0.012 ft. This drawdown value should be considered approximate because of the inherent error in deducing a water-level change that was an order of magnitude smaller than the background fluctuations.

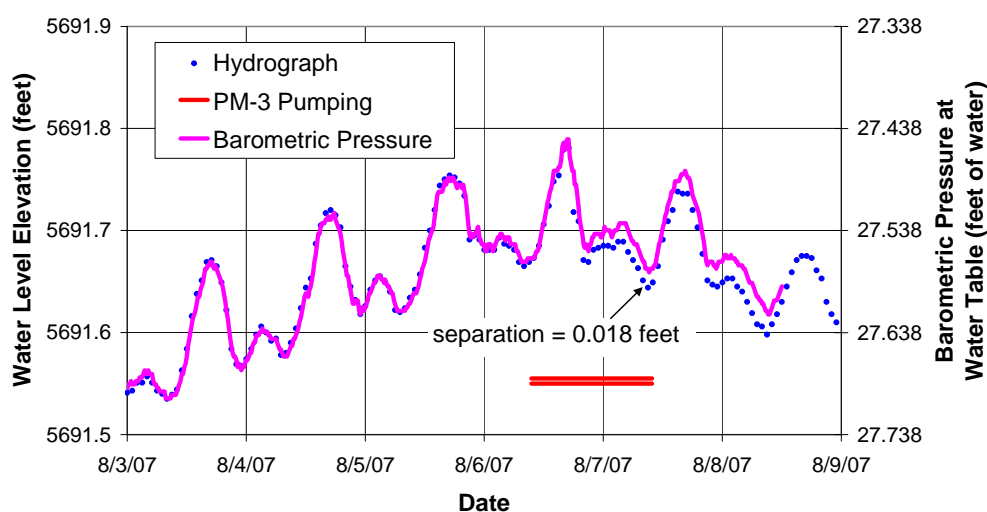


Figure E-71 R-9 water levels

The separation between the two curves continued to increase following pump shutoff. This effect is seen in distant wells or in wells completed in sediments not well connected to the pumped zone. (For example, simple application of the basic Theis equation to predict residual drawdown shows that water levels in very distant wells in a single aquifer will continue to decline for a while after pump shutoff.) In this instance, after PM-3 was shut down, it took an extended period before water levels approached the original static level in the pumped aquifer. The upper aquifer in which R-9 is completed apparently continued to respond to the still depressed water levels. Further, once water levels at PM-3 were restored, there was a lag in seeing the effect in R-9 because of its relative hydraulic isolation from PM-3.

Figure E-72 shows a comparison of the barometric pressure record and hydrograph for R-11. The results were similar to those shown in Figure E-71 for R-9. As shown in the figure, the estimated drawdown in R-11 at the time of pump shutoff in PM-3 was 0.017 ft. Also similar to R-9, there was a sufficient lag in the response that drawdown continued to increase slightly even after pump shutoff.

The similarity between the hydrograph, before the pumping test, and the barometric pressure record suggested a high barometric efficiency—near 100%. Consistent with this idea, the aquifer testing performed on the original R-11 well (the current R-11 is a replacement well) revealed an approximate barometric efficiency of 96%.

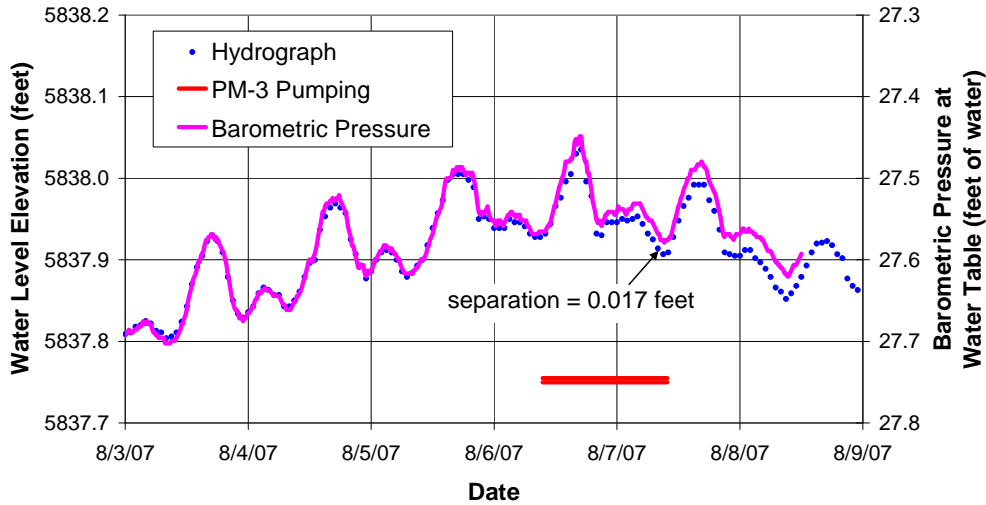


Figure E-72 R-11 water levels

Figure E-73 shows a comparison of the barometric pressure record and a modified hydrograph for R-13. In order to obtain a good match between the barometric pressure and hydrograph, the water-level data were corrected for a barometric efficiency of 90%. The apparent similarity between the two curves shown on the figure supports this estimate of barometric efficiency.

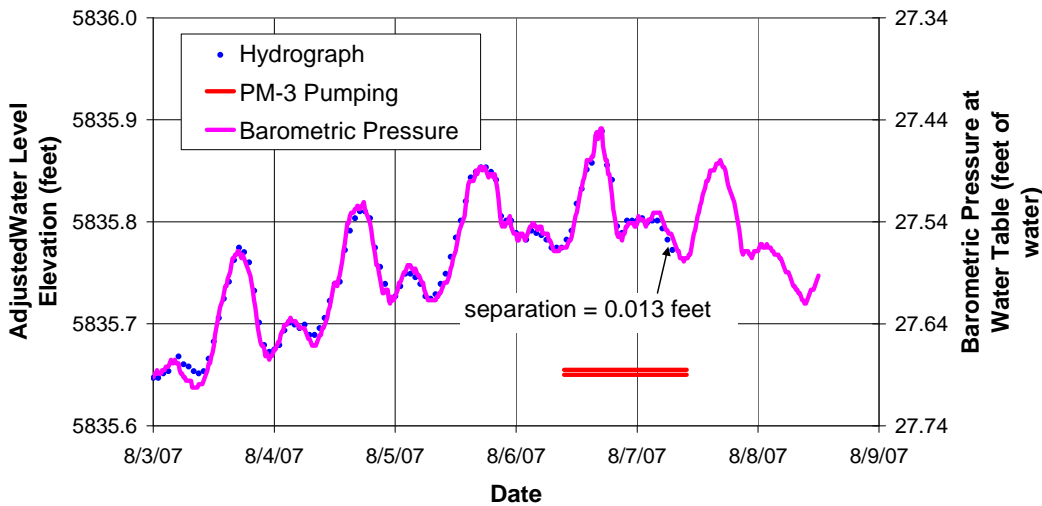


Figure E-73 R-13 water levels corrected for 90% barometric efficiency

The data record collected from R-13 extended only to about 8:00 a.m. on August 7, namely, before pump shutoff in PM-3. The less extensive data record made it more difficult to discern a separation of the barometric pressure curve and modified hydrograph than in the previous wells. However, examination of the data suggested a separation of about 0.013 ft. This estimate should be considered approximate because of the order of magnitude greater background noise, compared with the drawdown and the barometric correction approximation which probably introduced some minor error. It does appear, however, that there was a small response in R-13 to pumping PM-3.

Figure E-74 shows a comparison of the barometric pressure record and a modified hydrograph for R-28. As with R-13, in order to obtain a good match between the barometric pressure and hydrograph, the R-28 water-level data were corrected for a barometric efficiency of 90%. Consistent with this, the original aquifer testing performed on R-28 supported an estimated barometric efficiency of 92%. The good correlation between the two curves shown in the figure supports the estimate of barometric efficiency.

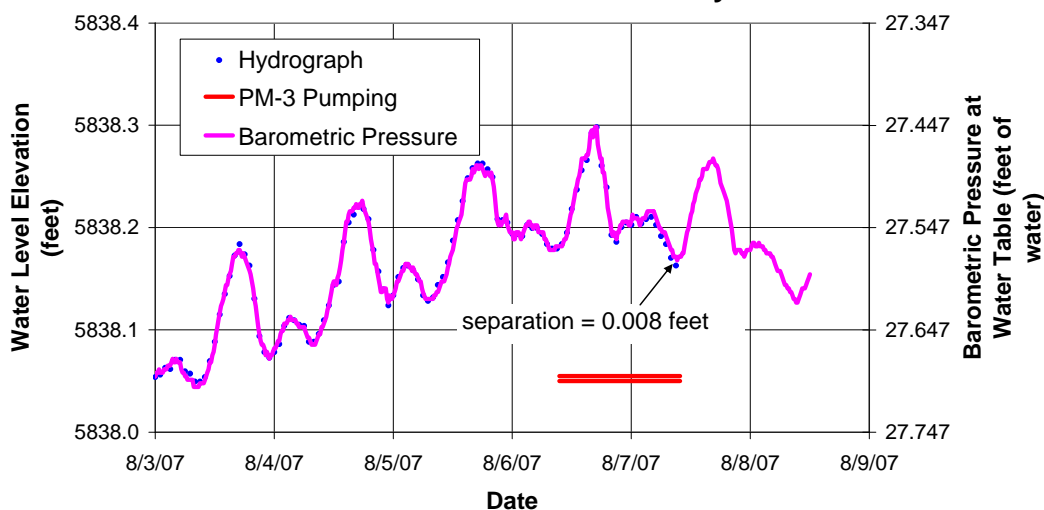


Figure E-74 R-28 water levels corrected for 90% barometric efficiency

The data record collected from R-28 extended only to about 10:00 a.m. on August 7, shortly after pump shutoff in PM-3. The less extensive data record made it difficult to discern a separation of the barometric pressure curve and modified hydrograph. However, examination of the data suggested a separation of about 0.008 ft. This estimate should be considered approximate because of the order of magnitude greater background noise, compared with the drawdown and the barometric correction approximation which probably introduced some minor error. As with R-13, it does appear that there was a small response in R-28 to pumping PM-3.

Table E-4 summarizes the wells that were monitored during the PM-3 pumping test, along with their distances from PM-3 and the observed drawdown. Many of the wells showing non-measurable drawdown actually may have responded to pumping PM-3. It is possible that the drawdown response, if it existed, was too small to detect within the background fluctuations that existed in those particular wells.

Table E-4
Response to Pumping PM-3 at 1450 GPM

Well	Distance from PM-3 (ft)	Drawdown after 1460 Min (ft)
PM-1	5287	Not measurable
PM-3	0.0	26.6
PM-4	8460	Not measurable
PM-5	10623	Not measurable
R-5 Screen 3	5425	Not measurable
R-5 Screen 4	5425	Not measurable
R-8 Screen 1	3355	0.12
R-8 Screen 2	3355	1.8
R-9	5799	0.018
R-11	2562	0.017
R-13	2997	0.013
R-28	3788	0.008
R-35a	343	8.0
R-35b	411	0.026

The drawdown values reported for R-35a and R-8 screens 1 and 2 were reliable. The remaining values for R-35b, R-9, R-11, R-13, and R-28, ranging from 0.008 to 0.026 ft, should be considered only approximate, with the certainty of the observation decreasing with decreasing magnitude. In those cases, the drawdown values were gleaned from data sets containing background fluctuations an order of magnitude greater than the drawdown values being sought.

More important, a number of R wells had shown a general background water-level decline in July. If this trend continued into August, the apparent drawdown values shown in Table E-4 could actually be background effects rather than drawdown or could include a background component. This implies that subject to the general uncertainty in the quantified magnitudes, the values shown might represent upper bounds for the PM-3 pumping effect.

The small drawdown response observed in R-9, R-11, R-13, R-28, and R-35b (or lack of drawdown, if the apparent drawdown is actually a background effect) implied the existence of a significant aquitard separating these screen zones and the pumped zone in PM-3. In the vicinity of R-35b, this was consistent with (1) the difference in static water levels between R-35a and R-35b that suggested an intervening aquitard and (2) the lack of a discernible hydraulic response in R-35b when pumping R-35a.

The response observed in R-8 was in conflict with that observed in the other R wells. The measured drawdown values shown in Table E-4 for R-8 screens 1 and 2 were 1 to 2 orders of magnitude greater than drawdown in the other R wells at similar distances from PM-3. It is possible that the orientation (strike) of geologic strata allow preferential expansion of the cone of depression in the direction of R-8, at least in the shallow portion of the regional aquifer.

The lack of a measurable response in PM-4 and PM-5 was not unusual because of the great distances to these wells—8460 ft and 10,623 ft, respectively. During pumping tests conducted on PM-2 and PM-4, responses at similar distances to these were significant after many days of pumping but small during the first day of pumping.

The lack of measurable response in PM-1, on the other hand, speaks to the complex nature of the makeup of the subsurface materials. PM-1 is only a mile away from PM-3 and would be expected to respond to pumping within 1 d. For example, pumping tests conducted on PM-2 and PM-4 showed responses after 1 d of pumping of a few feet of drawdown at distances of 4478 ft and 4656 ft. Similarly, operation of O-4 located 6300 ft from PM-3 induced drawdown of about 1.5 ft/d of pumping. The lack of hydraulic continuity between PM-3 and PM-1 (and between PM-2 and R-22 as mentioned above) should be investigated in conjunction with a review of the geologic model of the plateau.

Specific-Capacity Data

Specific-capacity data were used along with well geometry to estimate a lower-bound transmissivity value for the PM-3 screen zone for comparison to the pumping test derived values. In addition to specific capacity, other input values used in the calculations included a storage coefficient of 0.001 and an assumed borehole radius of 1 f-t.

PM-3 produced 1450 gpm with a drawdown of 26.6 ft after 1460 min of pumping for a specific capacity of 54.5 gpm/ft. The measured drawdown was reduced to account for the effects of axial pipeline losses within the perforated well casing. The combination of velocity and friction losses reduced the effective drawdown estimate to 25.0 ft, for a revised specific capacity of 58.0 gpm/ft. Applying the Cooper–Jacob equation to these inputs by iteration yielded a lower-bound hydraulic transmissivity value for the screened interval of 115,500 gpd/ft (Cooper and Jacob 1946, 098236).

This result is entirely consistent with the pumping test analysis. The observation well analysis suggested transmissivity values of 118,000 and 115,000 gpd/ft, while the pumped well yielded a value of 189,000 gpd/ft, which was known to be an overestimate.

PM-3 Summary

The PM-3 pumping test yielded transmissivity estimates for the screened interval ranging from about 118,000 to 189,000 gpd/ft. The larger value was known to be an overestimate, making the lower end of the range more likely representative of aquifer conditions. The specific capacity of PM-3 was consistent with these results, revealing a lower-bound transmissivity of 115,500 gpd/ft.

Operation of PM-3 lowered water levels only slightly (a couple hundredths of a foot or less) in most of the shallow R-wells in the vicinity, including R-35b just 411 ft away. This confirmed the presence of an aquitard separating the shallow, high-permeability zone from the underlying sediments at R-35. R-8 was an exception to this, showing more discernible drawdown than the other R-wells. It is expected that this was attributable in part to the orientation (strike and dip) of the various geologic units.

Pumping PM-3 had no measurable effect in PM-1 suggesting the presence of a resistive barrier between the two wells.

E-11.0 AQUITARD LEAKANCE/RESISTANCE

Data from the pumping tests were used to estimate the leakance of the aquitard separating R-35a from R-35b. Two of the tests supported estimation of this parameter.

The pumping test on R-35a produced no apparent drawdown in R-35b, as shown previously in Figure E-3. A detailed examination of the data (plotted at a different scale, not shown here) suggested that a drawdown effect of a hundredth of a foot or even half that would have been noticeable had it occurred. It was possible to use that information to obtain an upper bound value of the leakance of the aquitard by computer modeling the two permeable zones and adjusting the leakance of the intervening aquitard in the model until the modeled drawdown in the upper zone, caused by simulating the pumping of R-35a, equaled the assumed upper-bound drawdown. This approach would produce an *upper bound* for the leakance. The actual leakance would be known to be less than or equal to this value.

The other test that supported a determination of the leakance was the PM-3 test in which the observed drawdown in R-35b, 411 ft from PM-3, was 0.026 ft. Again, model simulation allowed adjusting the leakance of the aquitard until the observed drawdown in R-35b was reproduced in the model.

Early simulations showed that the leakance required to simulate the effects of the PM-3 test was significantly less than the upper-bound leakance predicted by the R-35a test. This made the R-35a analysis superfluous and only the PM-3 analysis was retained.

To simulate the PM-3 pumping test, a multilayer model was constructed, incorporating two productive aquifers separated by an intervening aquitard. The upper aquifer represented the shallow aquifer in which R-35b is completed, while the lower aquifer represented the entire production zone of PM-3. Transient model runs were conducted simulating the PM-3 pumping test. Dozens of simulations were performed for different assumed leakance values of the intervening aquitard between the two aquifers. The leakance value that resulted in an upper aquifer drawdown of 0.026 ft at the location of R-35b was deemed to reasonably reflect the actual aquitard leakance. Keeping in mind that some or all of this apparent drawdown in R-35b might be related to background effects, the actual drawdown might have been less; thus, the leakance solved in the model was considered an upper bound. The actual leakance could be less.

The modeling was performed using MODFLOW implemented under Schlumberger's Visual MODFLOW. A brief summary of the model configuration and input parameters is as follows:

1. Area covered: 20,000 ft × 20,000 ft
2. 116 rows × 116 columns × 10 layers
3. Transmissivity of upper aquifer: 142,000 gpd/ft
4. Transmissivity of pumped aquifer: 120,000 gp/ft
5. Storage coefficient of upper aquifer: 0.01 to 0.05
6. Storage coefficient of pumped aquifer: 0.001
7. Transient simulation of pumping 1450 gpm for 1460 min using four stress periods of 10 time steps each, for a total of 40 time steps.

The range of storage coefficient values of 0.01 to 0.05 for the upper aquifer was on the low side for possible values for unconfined aquifers. This was because the miniscule water-level changes simulated in the model (hundredths of a foot) would probably result in less actual drainage of the sediments than would occur when imposing more substantial drawdown. This idea was conjectural but intuitively reasonable.

The modeling evaluated only the simulated drawdown in R-35b and ignored the remaining

R wells. It was believed that the potential errors in the drawdown estimates in most of the other wells were great enough that it was not worthwhile to try to simulate them. Also, the model was not constructed to try to simulate the larger drawdown observed in R-8. This would have introduced complexities far beyond the intended purpose of the model simulations that was to approximate the effective leakage/resistance between the upper aquifer and deeper sediments at the R-35 site. In other words, the intent of the modeling effort was not to develop a fully calibrated and verified model that faithfully represented all aspects of the hydrogeologic system of the area. Instead, the model was meant to serve simply as a calculation tool to provide insight into the aquitard resistance required to provide the observed muted response between the two R-35 permeable zones, specifically the drawdown of 0.026 ft in response to the high rate of pumping in PM-3.

Figure E-75 shows a graph of the leakage and resistance (reciprocals of one another) determined in the model simulations. Reproducing the observed drawdown in R-35b due to pumping PM-3 required a vertical resistance of about 1500 to 5500 d, depending on the upper aquifer storage coefficient value. This corresponded to a range of leakage values of about 2×10^{-4} to 6×10^{-4} inverse days. These ranges should be viewed as lower-bound resistance values and upper-bound leakage values.

The limitations of this analysis should be reemphasized. First, a simplified two aquifer system with flat-lying strata was assumed in the model, whereas the actual geologic regime includes multiple layers that likely are sloped from horizontal.

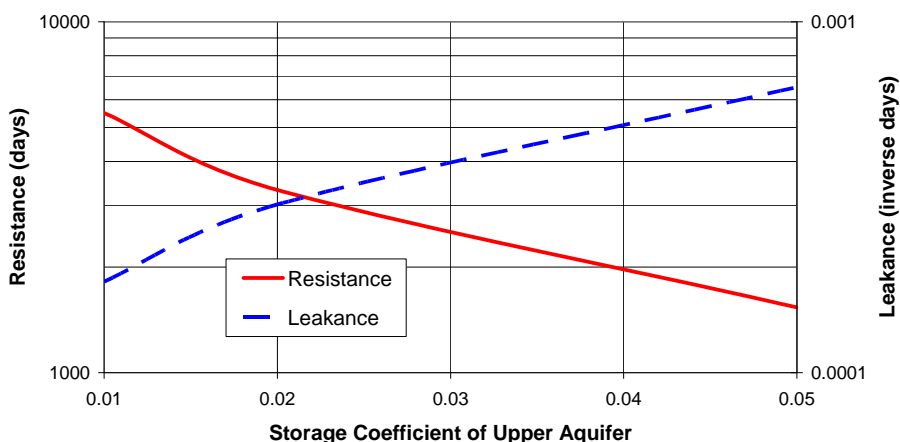


Figure E-75 Aquitard resistance/leakance

Second, there is a chance of significant error in the modeled drawdown in the shallow aquifer at R-35b. The observed/simulated drawdown was only 0.026 ft, gleaned from a hydrograph showing background fluctuations an order of magnitude greater than the estimated drawdown value. The presence of such significant background noise makes it difficult to be certain of the accuracy of the drawdown estimate. Therefore, the computed aquitard properties should be viewed as approximations. Further, that actual drawdown may have been less than the apparent value, because of overall background water-level trends.

E-12.0 SUMMARY

Constant-rate pumping tests were conducted on R-35a, R-35b, and PM-3 in Sandia canyon. The tests were conducted to gain an understanding of the hydraulic characteristics of the aquifers in which the wells were completed as well as the intervening aquitard between R-35a and R-35b. Numerous observations and conclusions were drawn for the tests as summarized below.

1. The static water level in R-35b, completed in the upper aquifer, was 6.2 ft higher than that in R-35a, suggesting the presence of an intervening aquitard.
2. Water-level fluctuations in R-35a (caused by operation of O-4 directly, or by O-4 pumping-induced water-level changes in nearby well PM-3) were too great to allow discerning any drawdown effects from pumping R-35b.
3. Pumping R-35a caused no observable drawdown in R-35b, consistent with the idea of a tight intervening aquitard.
4. Pumping R-35a and R-35b did not create any measurable/discernible responses in the monitored R wells—R-5 screens 3 and 4, R-8 screens 1 and 2, R-9, R-11, R-13, and R-28—with the single exception of a sluggish response in R-8 Screen 2 associated with pumping R-35a.
5. High barometric efficiencies (90% to 100%) were documented for R-5 Screen 3, R-8 Screen 1, R-9, R-11, R-13, and R-28.
6. R-5 Screen 4 showed significant response to pumping PM-1.
7. R-8 screens 1 and 2 showed significant response to pumping PM-3, while Screen 2 showed minor, sluggish response to pumping R-35a.
8. The hydraulic conductivity of the screened interval in R-35a was determined to be about 2.2 ft/d, while the average hydraulic conductivity of the 236 ft of Santa Fe sediments between the Puye Formation and Miocene Basalt was about 2.8 ft/d. Specific-capacity data yielded a lower-bound hydraulic conductivity for the screened interval of 1.64 ft/d, entirely consistent with the pumping test results and suggesting a well efficiency about 75%.
9. Late data from the pumping test suggested leakage from the adjacent aquifers (above and/or below).
10. The hydraulic conductivity of the screened interval in R-35b was determined to be about 135 ft/d, while the average hydraulic conductivity of the 93 ft of Puye sediments was about 203 ft/d. Specific-capacity data yielded a lower-bound hydraulic conductivity for the screened interval of 45.2 ft/d, not in conflict with the pumping test results and suggesting a well efficiency just over 30%. The percentage efficiency was low but corresponded to less than 2 ft of well loss at a discharge rate of more than 20 gpm.
11. Data from both tests confirmed that the coupling joints in the drop pipe leaked during the testing activities. Such leakage interferes with the drawdown signal during pump startup by permitting a momentary elevated discharge rate.

12. The PM-3 pumping test yielded transmissivity estimates of 118,000 to 189,000 gpd/ft. The greater value was known to be an overestimate. It is suspected that the actual transmissivity falls in the lower end of this range. Specific-capacity data yielded a lower-bound transmissivity value of 115,500 gpd/ft, consistent with the pumping test derived values.
13. Pumping PM-3 produced no measurable response in PM-4 and PM-5, likely attributable to a combination of short pumping time (about a day) and great distance to these wells.
14. Pumping PM-3 produced no measurable response in PM-1, which was close enough to PM-3 to show a response. This result suggests an effective hydraulic barrier between PM-1 and PM-3. This result is not unlike the observation of negligible response in R-22 to pumping PM-2 for 25 d.
15. Pumping PM-3 produced little or no drawdown (0 to 0.026 ft) in most of the R-wells within about a mile radius. The lone exception to this was R-8 that showed somewhat greater response possibly related to the complex geology (strike, dip, permeability contrasts) in the area.
16. Groundwater modeling was used to provide an approximation of the leakance/resistance of the aquitard separating the R-35a and R-35b aquifers by simulating the PM-3 pumping test and corresponding drawdown of 0.026 ft in R-35b. Depending on the assumed value of storage coefficient, the estimated aquitard leakance ranged from 2×10^{-4} to 6×10^{-4} inverse days, corresponding to a resistance of about 1500 to 5500 d. Because the actual drawdown might have been less than 0.026 ft (the 0.026 ft may have included some background water-level decline), the resistance and leakance values were considered lower and upper bounds, respectively.
17. Understanding the relatively greater response to pumping PM-3 in R-8 compared with other R wells, as well as the lack of response in PM-1, is important to increasing the understanding of the dynamics of groundwater flow in the area.

E-13.0 REFERENCES

The following list includes all documents cited in this appendix. Parenthetical information following each reference provides the author(s), publication date, and ER ID number. This information is also included in text citations. ER ID numbers are assigned by the Environmental Programs Directorate's Records Processing Facility (RPF) and are used to locate the document at the RPF and, where applicable, in the master reference set.

Copies of the master reference set are maintained at the NMED Hazardous Waste Bureau; the U.S. Department of Energy—Los Alamos Site Office; the U.S. Environmental Protection Agency, Region 6; and the Directorate. The set was developed to ensure that the administrative authority has all material needed to review this document, and it is updated with every document submitted to the administrative authority. Documents previously submitted to the administrative authority are not included.

- Bradbury, K.R., and E.R. Rothschild, March-April 1985. "A Computerized Technique for Estimating the Hydraulic Conductivity of Aquifers from Specific Capacity Data," *Ground Water*, Vol. 23, No. 2, pp. 240-246. (Bradbury and Rothschild 1985, 098234)
- Brons, F., and V.E. Marting, 1961. "The Effect of Restricted Fluid Entry on Well Productivity," *Journal of Petroleum Technology*, Vol. 13, No. 2, pp. 172-174. (Brons and Marting 1961, 098235)
- Cooper, H.H., Jr., and C.E. Jacob, August 1946. "A Generalized Graphical Method for Evaluating Formation Constants and Summarizing Well-Field History," *American Geophysical Union Transactions*, Vol. 27, No. 4, pp. 526-534. (Cooper and Jacob 1946, 098236)

- Driscoll, F.G., 1986. Excerpted pages from *Groundwater and Wells*, 2nd Ed., Johnson Filtration Systems Inc., St. Paul, Minnesota. (Driscoll 1986, 098254)
- Hantush, M.S., July 1961. "Drawdown around a Partially Penetrating Well," *Journal of the Hydraulics Division, Proceedings of the American Society of Civil Engineers*, Vol. 87, No. HY 4, pp. 83-98. (Hantush 1961, 098237)
- Heish, P.A., November-December 1996. "Deformation-Induced Changes in Hydraulic Head During Ground-Water Withdrawal," *Ground Water*, Vol. 34, No. 6, pp. 1082-1089. (Hsieh 1996, 098238)
- McLin, S., July 2005. "Analyses of the PM-2 Aquifer Test Using Multiple Observation Wells," Los Alamos National Laboratory report LA-14225-MS, Los Alamos, New Mexico. (McLin 2005, 090073)
- McLin, S., January 2006. "Analyses of the PM-4 Aquifer Test Using Multiple Observation Wells," Los Alamos National Laboratory report LA-14252-MS, Los Alamos, New Mexico. (McLin 2006, 092218)
- Rodrigues, J.D., 1983. "The Noordbergum Effect and Characterization of Aquitards at the Rio Maior Mining Project," *Ground Water*, Vol. 21, No. 2, pp. 200-207. (Rodrigues 1983, 098239)
- Schafer, D.C., January-February 1978. "Casing Storage Can Affect Pumping Test Data," *The Johnson Drillers Journal*, pp. 1-6, Johnson Division, UOP, Inc., St. Paul, Minnesota. (Schafer 1978, 098240)
- Theis, C.V., 1934-1935. "The Relation Between the Lowering of the Piezometric Surface and the Rate and Duration of Discharge of a Well Using Ground-Water Storage," *American Geophysical Union Transactions*, Vol. 15-16, pp. 519-524. (Theis 1934-1935, 098241)
- Wolff, R.G., December 1970. "Relationship Between Horizontal Strain Near a Well and Reverse Water Level Fluctuation," *Water Resources Research*, Vol. 6, No. 6, pp. 1721-1728. (Wolff 1970, 098242)

Attachment 1

Appendix Data Files and Images (on enclosed CD)

